



THE HONG KONG
POLYTECHNIC UNIVERSITY

香港理工大學

Pao Yue-kong Library

包玉剛圖書館

Copyright Undertaking

This thesis is protected by copyright, with all rights reserved.

By reading and using the thesis, the reader understands and agrees to the following terms:

1. The reader will abide by the rules and legal ordinances governing copyright regarding the use of the thesis.
2. The reader will use the thesis for the purpose of research or private study only and not for distribution or further reproduction or any other purpose.
3. The reader agrees to indemnify and hold the University harmless from and against any loss, damage, cost, liability or expenses arising from copyright infringement or unauthorized usage.

IMPORTANT

If you have reasons to believe that any materials in this thesis are deemed not suitable to be distributed in this form, or a copyright owner having difficulty with the material being included in our database, please contact lbsys@polyu.edu.hk providing details. The Library will look into your claim and consider taking remedial action upon receipt of the written requests.

**INVESTIGATIONS ON DIRECT
ETHYLENE GLYCOL FUEL CELLS
USING HYDROGEN PEROXIDE AS
OXIDANT**

ZHEFEI PAN

PhD

The Hong Kong Polytechnic University

2021

The Hong Kong Polytechnic University
Department of Mechanical Engineering

**Investigations on direct ethylene glycol fuel
cells using hydrogen peroxide as oxidant**

Zhefei PAN

**A thesis submitted in partial fulfilment of the
requirements for the degree of Doctor of Philosophy**

August 2020

CERTIFICATE OF ORIGINALITY

I hereby declare that this thesis is my own work and that, to the best of my knowledge and belief, it reproduces no material previously published or written, nor material that has been accepted for the award of any other degree or diploma, except where due acknowledgement has been made in the text.

Zhefei PAN

Acknowledgements

The three-year PhD study at The Hong Kong Polytechnic University will be a very valuable experience in my life. I would like to thank all who have helped and supported me during my study.

The sincerest gratitude and respect will be expressed to my chief supervisor, Dr. Liang AN, for taking me into this interesting and challenging fuel cell research field. I have received precious guidance and suggestion, as well as adequate lab support from him in implementing my program. His inspiring and encouraging way has guided me to a deep understanding of my work, his novel ideas have given me a broad vision and cutting-edge direction, and his rigorous attitude towards learning and working has set an excellent example for me. His strict and precise standard in pursuing knowledges and good manners, as well as his hardworking impressed me. I also thank my co-supervisor Prof. WEN Chih-yung, who has spent a lot of time revising my paper and providing valuable advice. Special appreciation goes Prof. Zhengtang LUO (Department of Chemical and Biological Engineering, HKUST) and Prof. Jiyun ZHAO (Department of Mechanical Engineering, CityU) for serving as a member of my thesis examination committee and careful reviewing of my thesis.

I want to convey my thanks to technical supporting staff, i.e. Dr. NG Chun and Mr. LEUNG Chi-kuen, administrative staff, i.e., Ms. TAM Lily, Mrs. LAI Michelle, Ms. CHAN Packy and Ms. WONG Merlin, for providing various helps in my study.

I am also grateful to all members of An's Research Group for valuable

discussions, suggestions and concerns to my research work, as well as their kindness and consideration during everyday life at PolyU. They are Dr. Bing HUANG (Guilin university of technology), Dr. Yaoguang YU (Sun Yat-sen University), Mr. Xiangyu SU, Mr. Guangzhe LI, Mr. Xingyi SHI, Mr. Oladapo Christopher ESAN, and all project students worked in our lab. Finally, I want to thank my family and my girlfriend, Miss Fengjia XIE, for their invaluable love and support. I wish them a good health and a happy life in the future. Their love and concerns have been a source of inspiration in my PhD study.

In summary, thanks are expressed to all the people who occurred, inspired, supported, helped and cared me in my study period.

Abstract

Direct ethylene glycol fuel cells (DEGFCs), a clean and efficient power generation technology, have attracted great research interest as a promising power source, primarily because of excellent properties of ethylene glycol (EG), including high energy density and ease of transportation, storage as well as handling. Conventional alkaline fuel cells typically use ambient air as oxidant, but the ambient air containing carbon dioxide will lead to the carbonate issue in alkaline fuel cells, which refers to the reaction between carbon dioxide and hydroxide ions forming carbonates. It has been recently demonstrated that rather than using the ambient air or pure oxygen, using hydrogen peroxide (H_2O_2) as oxidant has attracted ever-increasing attention, primarily due to several unique characteristics of liquid hydrogen peroxide: (1) the use of hydrogen peroxide can substantially increase the theoretical voltage of EG fuel cells from 1.09 V to 2.47 V, potentially boosting the fuel cell performance; (2) the activation loss on the cathode can be lowered due to the two-electron-transfer process for hydrogen peroxide reduction reaction; (3) the serious water flooding problem occurring in air/oxygen-based fuel cells can be alleviated because of the intrinsic liquid state of hydrogen peroxide; and more impressively, (5) the use of hydrogen peroxide can achieve the operation of fuel cells in an oxygen-tight environment, such as outer space and underwater. The primary objective of this thesis is to investigate and understand the performance characteristics of EG fuel cells using hydrogen peroxide as oxidant through experimental and numerical approaches. Firstly, Nafion or polytetrafluoroethylene (PTFE) is typically used as binder in preparing porous electrodes, but the

effective active sites are limited due to the fact that Nafion tends to be clad on the catalyst nanoparticles and PTFE tends to form inaccessible active sites, creating the barrier for mass/ion transport to active sites. A cost-effective poly(vinylidene fluoride-co-hexafluoropropylene) (PVDF-HFP) is adopted as electrode binder, which tends to form a porous structure and adhere the catalyst nanoparticles onto the nickel foam skeleton but not to isolate the catalyst nanoparticles, achieving a higher effective active area. Meanwhile, it contains more amorphous domains capable of trapping a large amount of liquid electrolyte, creating more effective active sites. At the electrode level, the electrochemical surface areas of the three electrodes using PVDF-HFP, Nafion, and PTFE are 24.10, 18.62, and 16.44 m² g⁻¹, respectively. At the cell level, using the PVDF-HFP-based electrode exhibits the best performance with an open-circuit voltage (OCV) of 1.47 V, a maximum current density of 300 mA cm⁻², and a peak power density of 120.0 mW cm⁻² at 60°C, which shows an improvement of 13.7% and 58.1%, respectively, comparing to the fuel cell performance achieved by using Nafion and PTFE as the electrode binder. Secondly, an active fuel cell using EG as fuel and hydrogen peroxide as oxidant is designed, fabricated, and tested, which theoretically offers a theoretical voltage as high as 2.47 V. This active fuel cell can experimentally output an OCV of 1.41V and a peak power density of 80.9 mW cm⁻² at 60°C, which is 20.8% higher than that of using oxygen (67 mW cm⁻²). The performance improvement is mainly attributed to the faster kinetics of the two-electron-transfer hydrogen peroxide reduction reaction. Thirdly, the addition of auxiliary devices, such as liquid pumps and gas compressors, makes the active fuel cell system

bulkier and more complex, reducing not only the volumetric energy density but also the design flexibility. Hence, a passive fuel cell using EG as fuel and hydrogen peroxide as oxidant is demonstrated, which avoids the usage of auxiliary devices. Although the passive fuel cell generates a lower power density than does an active one, it is more structurally compact, no parasitic loss in power, and can be operated under ambient conditions, making it a suitable candidate for powering portable electronic devices. It is found that this passive fuel cell yields an OCV of 1.58 V and peak power densities of 30.3 mW cm⁻² and 65.8 mW cm⁻² at 23°C and 60°C, respectively, showing an impressive improvement comparing to a passive air-based fuel cell, which is more than two times higher in the OCV (0.7 V) and more than five times higher in the peak power density (12 mW cm⁻²). In addition, it is also found that the heat generated by hydrogen peroxide self-decomposition shows a negligible effect on the fuel cell operation over the discharging process. Fourthly, a passive fuel cell stack consisting of two single cells is developed to examine the feasibility of this fuel cell technology in practical applications and then demonstrated to power an electric fan in underwater condition. This passive fuel cell stack exhibits an actual OCV of 3.0 V, a maximum current of 860 mA, and a peak power of 1178 mW at room temperature. The individual cell in the passive stack exhibits a good consistency over the whole current region, indicating a high degree of reproducibility achieved by the appropriate electrode manufacturing and cell assembly processes. Moreover, the running time (per refueling) of an electric fan powered by this passive stack is 2 hours and 36 minutes in underwater condition, demonstrating that this passive fuel cell stack is a

promising power source for airtight situations, such as underwater and outer space. Lastly, a mathematical model is developed to give the in-depth insights of physical and chemical processes occurring in this fuel cell, which incorporates mass/charge transport and electrochemical reactions. Previous models treat the local concentration as the actual reactant concentration participating in the electrochemical reaction, suggesting that EG molecules and OH^- ions are completely adsorbed on active sites. For a specific active site, however, the reactant with a higher local concentration is more likely to be adsorbed, which may lead to active sites fully occupied. The other with a lower local concentration cannot be further adsorbed, hindering the electrochemical reaction. As such, the fuel cell performance is significantly affected by the fuel solution composition and their transport characteristics. By considering the competitive adsorption of reactants on active sites, the present model accurately predicts the voltage losses, electrode potentials, local concentrations, and thus fuel cell performance under various operating and structural design parameters.

Table of Contents

| | |
|--|-------|
| Acknowledgements | iii |
| Abstract | v |
| Table of Contents | ix |
| List of Figures | xv |
| List of Tables | xxi |
| Abbreviations | xxii |
| Nomenclature | xxiii |
| Chapter 1 Introduction | 1 |
| 1.1. Background | 1 |
| 1.2. Direct liquid fuel cells | 2 |
| 1.3. Direct ethylene glycol fuel cells..... | 3 |
| 1.3.1. Features | 3 |
| 1.3.2. Research and development..... | 3 |
| 1.3.3. Working principle..... | 6 |
| 1.3.4. State-of-the-art performance | 7 |
| 1.3.5. Remaining challenges and issues | 7 |
| 1.4. Objectives of this thesis | 8 |
| 1.5. References | 11 |
| Chapter 2 Fuel cell fabrications and characterizations | 21 |
| 2.1. Introduction | 21 |
| 2.2. Fuel cell fabrication and assembly..... | 21 |
| 2.2.1. Flow field plates..... | 21 |
| 2.2.2. Preparation of electrodes..... | 22 |

| | | |
|-----------|--|----|
| 2.2.3. | Preparation of membranes | 24 |
| 2.2.4. | Membrane electrode assembly..... | 25 |
| 2.3. | Characterizations of electrodes | 25 |
| 2.3.1. | Surface morphology..... | 25 |
| 2.3.2. | Electrochemical surface area determination | 25 |
| 2.4. | Characterizations of single cells | 26 |
| 2.4.1. | Testing system..... | 26 |
| 2.4.2. | Fuel supply system..... | 26 |
| 2.4.3. | Oxidant supply system..... | 26 |
| 2.4.4. | Temperature controlling system..... | 26 |
| 2.4.5. | Polarization curves..... | 27 |
| 2.4.6. | Constant-current discharging behavior | 28 |
| 2.4.7. | Long-term durability..... | 28 |
| 2.4.8. | Internal resistance measurement | 28 |
| 2.4.9. | Electrochemical impedance spectra | 29 |
| 2.5. | Summary | 29 |
| 2.6. | References..... | 30 |
| Chapter 3 | Development of three-dimensional porous electrodes..... | 33 |
| 3.1. | Introduction..... | 35 |
| 3.2. | Analysis of transport characteristics | 39 |
| 3.3. | Experiments | 40 |
| 3.3.1. | Preparation of the three-dimensional porous electrode..... | 40 |
| 3.3.2. | Cyclic voltammetry..... | 40 |
| 3.3.3. | Preparation of the membrane electrode assembly . | 41 |

| | | |
|-----------|--|----|
| 3.3.4. | Fuel cell setup and instrumentation | 41 |
| 3.4. | Results and discussion | 42 |
| 3.4.1. | Characterization of as-prepared electrodes | 42 |
| 3.4.2. | Fuel cell performance..... | 46 |
| 3.4.3. | Constant-current discharging behavior | 49 |
| 3.4.4. | Cost estimation..... | 50 |
| 3.5. | Summary | 51 |
| 3.6. | References | 53 |
| Chapter 4 | Performance characteristics of an active fuel cell..... | 71 |
| 4.1. | Introduction..... | 72 |
| 4.2. | Working principle..... | 74 |
| 4.3. | Experiments | 74 |
| 4.3.1. | Preparation of the membrane electrode assembly.. | 74 |
| 4.3.2. | Fuel cell setup and instrumentation | 75 |
| 4.4. | Results and discussion | 76 |
| 4.4.1. | Characterization of catalyst layers | 76 |
| 4.4.2. | General performance..... | 76 |
| 4.4.3. | Effect of the NaOH concentration..... | 77 |
| 4.4.4. | Effect of the EG concentration..... | 79 |
| 4.4.5. | Effect of the H ₂ O ₂ concentration..... | 80 |
| 4.4.6. | Effect of the H ₂ SO ₄ concentration | 82 |
| 4.4.7. | Effect of membrane thickness | 82 |
| 4.4.8. | Effect of the operating temperature..... | 83 |
| 4.5. | Summary | 84 |
| 4.6. | References | 85 |

| | | |
|-----------|--|-----|
| Chapter 5 | Performance characteristics of a passive fuel cell | 105 |
| 5.1. | Introduction..... | 107 |
| 5.2. | Working principle | 109 |
| 5.3. | Experiments | 110 |
| 5.3.1. | Preparation of membrane electrode assembly | 111 |
| 5.3.2. | Fuel cell setup and instrumentation | 111 |
| 5.4. | Results and discussion | 112 |
| 5.4.1. | Advantages of passive fuel cells | 112 |
| 5.4.2. | Characterization of catalyst layers | 113 |
| 5.4.3. | General performance..... | 114 |
| 5.4.4. | Effect of the KOH concentration | 116 |
| 5.4.5. | Effect of the EG concentration..... | 117 |
| 5.4.6. | Effect of the H ₂ O ₂ concentration | 119 |
| 5.4.7. | Effect of the H ₂ SO ₄ concentration | 121 |
| 5.4.8. | Effect of the membrane thickness..... | 122 |
| 5.4.9. | Effect of the operating temperature | 122 |
| 5.4.10. | Effect of the H ₂ O ₂ self-decomposition | 123 |
| 5.5. | Summary | 124 |
| 5.6. | References..... | 126 |
| Chapter 6 | Lab-scale demonstration of a stack..... | 151 |
| 6.1. | Introduction..... | 153 |
| 6.2. | Working principle | 158 |
| 6.3. | Experiments | 159 |
| 6.3.1. | Preparation of membrane electrode assembly | 159 |

| | | |
|-----------|---|-----|
| 6.3.2. | Fuel cell setup and instrumentation | 159 |
| 6.4. | Results and discussion | 160 |
| 6.4.1. | General performance..... | 160 |
| 6.4.2. | Effect of the EG concentration..... | 163 |
| 6.4.3. | Effect of the KOH concentration | 165 |
| 6.4.4. | Effect of the H ₂ O ₂ concentration..... | 166 |
| 6.4.5. | Effect of the H ₂ SO ₄ concentration | 168 |
| 6.4.6. | Demonstration of the stack to power an underwater fan | 169 |
| 6.5. | Summary | 171 |
| 6.6. | References | 172 |
| Chapter 7 | Mathematical modeling of direct ethylene glycol fuel cells | 195 |
| 7.1. | Introduction..... | 198 |
| 7.2. | Model development..... | 201 |
| 7.2.1. | Anode | 202 |
| 7.2.1.1. | Mass transport | 202 |
| 7.2.1.2. | Electrochemical kinetics | 204 |
| 7.2.2. | Cathode | 204 |
| 7.2.3. | Boundary conditions | 206 |
| 7.2.4. | Cell voltage | 206 |
| 7.3. | Experiments | 207 |
| 7.4. | Results and discussion | 207 |
| 7.4.1. | Model validation | 207 |
| 7.4.2. | Voltage loss | 208 |

| | |
|--|-----|
| 7.4.3. Effect of the EG concentration..... | 208 |
| 7.4.4. Effect of the NaOH concentration | 210 |
| 7.4.5. Effect of the H ₂ O ₂ concentration | 212 |
| 7.4.6. Effect of the H ₂ SO ₄ concentration | 212 |
| 7.4.7. Effect of the exchange current density..... | 213 |
| 7.4.8. Effect of the diffusion layer thickness | 214 |
| 7.5. Summary | 215 |
| 7.6. References..... | 217 |
| Chapter 8 Conclusions and future work | 247 |
| 8.1. Conclusions..... | 247 |
| 8.2. Future work..... | 250 |
| Appendix I Publications during PhD study at The Hong Kong Polytechnic University..... | 251 |

List of Figures

| | |
|---|----|
| Figure 1.1 Schematic of a conventional DEGFC using oxygen as oxidant..... | 19 |
| Figure 1.2 Schematic of a DEGFC using hydrogen peroxide as oxidant. | 20 |
| Figure 2.1 Testing system of an active DEGFC..... | 31 |
| Figure 2.2 A typical polarization curve of a PEM fuel cell [2]..... | 32 |
| Figure 3.1 Schematic of the an active alkaline-acid direct ethylene glycol fuel cell using a three-dimensional electrode..... | 59 |
| Figure 3.2 Fuel cell performances achieved by using different binders at room temperature. | 60 |
| Figure 3.3 CV curves in 1.0 M KOH at a scan rate of 50 mV s ⁻¹ | 61 |
| Figure 3.4 SEM image of the PVDF-HFP at dry state..... | 62 |
| Figure 3.5 SEM image of the Nafion at dry state. | 63 |
| Figure 3.6 SEM image of the PTFE at dry state. | 64 |
| Figure 3.7 Nyquist plots of three different electrodes at room temperature..... | 65 |
| Figure 3.8 Polarization and power density curves achieved by using three different electrodes at room temperature. | 66 |
| Figure 3.9 Polarization and power density curves achieved by using three different electrodes at 60°C..... | 67 |
| Figure 3.10 Polarization and power density curves achieved by using three different electrodes at 60°C..... | 68 |
| Figure 3.11 Constant-current discharging behavior of the fuel cell fabricated with the PVDF-HFP-based and Nafion-based | |

| | |
|--|-----|
| electrodes at 60°C. | 69 |
| Figure 4.1 Schematic of the active DEGFC..... | 90 |
| Figure 4.2 SEM image of the cathode catalyst layer. | 91 |
| Figure 4.3 The polarization and power density curves. | 92 |
| Figure 4.4 Constant-current discharging behavior. | 93 |
| Figure 4.5 General performance of the passive DEGFC. | 94 |
| Figure 4.6 Effect of the NaOH concentration on the OCV and internal resistance. | 95 |
| Figure 4.7 Effect of the EG concentration on the fuel cell performance. | 96 |
| Figure 4.8 Effect of the EG concentration on the OCV and internal resistance. | 97 |
| Figure 4.9 Effect of the H ₂ O ₂ concentration on the fuel cell performance. | 98 |
| Figure 4.10 Effect of the H ₂ O ₂ concentration on the OCV and internal resistance. | 99 |
| Figure 4.11 Effect of the H ₂ SO ₄ concentration on the cell performance. | 100 |
| Figure 4.12 Effect of the H ₂ SO ₄ concentration on the OCV and internal resistance. | 101 |
| Figure 4.13 Effect of the membrane thickness on the OCV and cell performance. | 102 |
| Figure 4.14 Effect of the membrane thickness on the OCV and internal resistance. | 103 |
| Figure 4.15 Effect of the operating temperature on the cell | |

| | |
|---|-----|
| performance. | 104 |
| Figure 5.1 Working principle of a passive DEGFC. | 132 |
| Figure 5.2 Schematic illustration of a passive DEGFC. | 133 |
| Figure 5.3 SEM images of the catalyst layer of anode. | 134 |
| Figure 5.4 SEM images of the catalyst layer of cathode. | 135 |
| Figure 5.5 General performance of the passive DEGFC. | 136 |
| Figure 5.6 Long-term durability of the passive fuel cell..... | 137 |
| Figure 5.7 Effect of the KOH concentration on the cell performance. | 138 |
| Figure 5.8 Effect of the KOH concentration on the OCV and internal resistance..... | 139 |
| Figure 5.9 Effect of the EG concentration on the cell performance. | 140 |
| Figure 5.10 Effect of the EG concentration on the OCV and internal resistance..... | 141 |
| Figure 5.11 Effect of the H ₂ O ₂ concentration on the cell performance. | 142 |
| Figure 5.12 Effect of the H ₂ O ₂ concentration on the OCV and internal resistance..... | 143 |
| Figure 5.13 Effect of the H ₂ SO ₄ concentration on the cell performance. | 144 |
| Figure 5.14 Effect of the H ₂ SO ₄ concentration on the OCV and internal resistance..... | 145 |
| Figure 5.15 Effect of the membrane thickness on the cell performance. | 146 |

| | |
|---|-----|
| Figure 5.16 Effect of the membrane thickness on the OCV and internal resistance..... | 147 |
| Figure 5.17 Effect of the operating temperature on the cell performance. | 148 |
| Figure 5.18 Transient cell temperature behaviors with constant current discharging..... | 149 |
| Figure 6.1 Working principle of a passive DEGFC stack..... | 179 |
| Figure 6.2 Schematic illustration of a passive DEGFC stack. | 180 |
| Figure 6.3 General Performance of the passive stack..... | 181 |
| Figure 6.4 The consistency of the individual cell. | 182 |
| Figure 6.5 Transient OCV behavior of the passive stack..... | 183 |
| Figure 6.6 Transient discharging behavior of the passive stack. | 184 |
| Figure 6.7 Effect of the EG concentration on the stack performance. | 185 |
| Figure 6.8 Effect of the EG concentration on the OCV and internal resistance..... | 186 |
| Figure 6.9 Effect of the KOH concentration on the stack performance. | 187 |
| Figure 6.10 Effect of the KOH concentration on the OCV and internal resistance..... | 188 |
| Figure 6.11 Effect of the H ₂ O ₂ concentration on the stack performance. | 189 |
| Figure 6.12 Effect of the H ₂ O ₂ concentration on the OCV and internal resistance..... | 190 |
| Figure 6.13 Effect of the H ₂ SO ₄ concentration on the stack | |

| | |
|--|-----|
| performance. | 191 |
| Figure 6.14 Effect of the H ₂ SO ₄ concentration on the OCV and internal resistance. | 192 |
| Figure 6.15 Running time of the fan powered by the passive stack under the ambient environment. | 193 |
| Figure 6.16 Running time of the fan powered by the passive stack under the imitated underwater environment. | 194 |
| Figure 7.1 Schematic of a DEGFC and the coordinate system. | 223 |
| Figure 7.2 Validation made between numerical results and experimental data. | 224 |
| Figure 7.3 Specific polarizations and overall voltage loss with the current density. | 225 |
| Figure 7.4 Effect of the EG concentration on the polarization curves. | 226 |
| Figure 7.5 Effect of the EG concentration on the anode overpotentials. | 227 |
| Figure 7.6 Effect of the EG concentration on the concentration on the active sites. | 228 |
| Figure 7.7 Effect of the hydroxyl ion concentration on the polarization curves. | 229 |
| Figure 7.8 Effect of the hydroxyl ion concentration on the anode overpotentials. | 230 |
| Figure 7.9 Effect of the hydroxyl ion concentration on the concentration on the active sites. | 231 |
| Figure 7.10 Effect of the hydrogen peroxide concentration on the | |

| | |
|--|-----|
| polarization curves. | 232 |
| Figure 7.11 Effect of the hydrogen peroxide concentration on the cathode overpotentials. | 233 |
| Figure 7.12 Effect of the H^+ concentration on the polarization curves. | 234 |
| Figure 7.13 Effect of the H^+ concentration on the cathode overpotentials. | 235 |
| Figure 7.14 Effect of the anode exchange current density on the polarization curves. | 236 |
| Figure 7.15 Effect of the anode exchange current density on the anode overpotentials. | 237 |
| Figure 7.16 Effect of the cathode exchange current density on the polarization curves. | 238 |
| Figure 7.17 Effect of the cathode exchange current density on the cathode overpotentials. | 239 |
| Figure 7.18 Effect of the anode DL thickness on the polarization curves. | 240 |
| Figure 7.19 Effect of the anode DL thickness on the anode overpotentials. | 241 |
| Figure 7.20 Effect of the cathode DL thickness on the polarization curves. | 242 |
| Figure 7.21 Effect of the cathode DL thickness on the cathode overpotentials. | 243 |

List of Tables

| | |
|---|-----|
| Table 3-1 Cost estimation of three electrode binders..... | 70 |
| Table 7-1 Physicochemical parameters..... | 244 |
| Table 7-2 Operating parameters..... | 245 |
| Table 7-3 Structural parameters..... | 245 |
| Table 7-4 Mass/charge transport parameters..... | 246 |

Abbreviations

| | |
|--------------|--------------------------------------|
| ACL | Anode catalyst layer |
| ADL | Anode diffusion layer |
| AEM | Anion exchange membrane |
| AFC | Alkaline fuel cell |
| AFF | Anode flow field |
| CCL | Cathode catalyst layer |
| CDL | Cathode diffusion layer |
| CEM | Cation exchange membrane |
| CFF | Cathode flow field |
| CL | Catalyst layer |
| CV | Cyclic voltammetry |
| DEFC | Direct ethanol fuel cell |
| DEGFC | Direct ethylene glycol fuel cell |
| DFFC | Direct formate fuel cell |
| DLFC | Direct liquid fuel cell |
| DMFC | Direct methanol fuel cell |
| ECSA | Electrochemical surface area |
| EGOR | Ethylene glycol oxidation reaction |
| IR | Internal resistance |
| MEA | Membrane electrode assembly |
| OCV | Open-circuit voltage |
| ORR | Oxygen reduction reaction |
| PEM | Proton exchange membrane |
| PEMFC | Proton exchange membrane fuel cell |
| PTFE | Polytetrafluoroethylene |
| SCCM | Standard cubic centimetre per minute |
| SEM | Scanning electron microscope |

Nomenclature

List of Symbols

| | |
|----------------|---|
| c | Concentration, mol m ⁻³ |
| D | Diffusivity, m ² s ⁻¹ |
| E ⁰ | Theoretical potential, V |
| F | Faraday's constant, A s mol ⁻¹ |
| i | Current density, A m ⁻² |
| i ₀ | Exchange current density, A m ⁻² |
| N | Flux, mol m ⁻² s ⁻¹ |
| P | Gas pressure, Pa |
| T | Operating temperature, K |
| x | Coordinate |
| z | Valence of ion |
| u | Mobility, m ² V ⁻¹ s ⁻¹ |
| R | Universal gas constant, J mol ⁻¹ K ⁻¹ |
| j | Local current density, A m ⁻² |
| n | Participating electron number, 1 |
| V | Fuel cell voltage, V |

Greeks

| | |
|---|---|
| α | Electron transfer coefficient, 1 |
| γ | Reaction order, 1 |
| η | Overpotential, V |
| σ | Conductivity, Ω ⁻¹ m ⁻¹ |
| ε | Porosity, 1 |
| δ | Thickness, m |

Superscripts

| | |
|------|--------------------|
| feed | Feeding |
| eff | Effective |
| A | Anode |
| C | Cathode |
| i | Chemical species i |
| FF | Flow field |
| DL | Diffusion layer |
| CL | Catalyst layer |

Subscripts

| | |
|---|---------|
| a | Anode |
| c | Cathode |
| l | Liquid |

Chapter 1 Introduction

1.1. Background

The global energy demand, the modern society heavily relying on, has reached 14×10^9 TOE (ton of oil equivalent) per year to maintain sustainable development of the society. Over 80% of the energy, however, comes from the use of the oil, coal and natural gases. The massive use of fossil fuels leads to the fuel overexploitation resulting in the energy crisis and the increasing CO₂ emission resulting in the climate change. We have to adopt new energy supply technologies that utilize renewable energy sources, due to the current energy and environmental issues we are facing today [1-8].

Fuel cells have been considered as one of the most promising clean and efficient power generation technologies for a sustainable future [9-15]. Hence, tremendous efforts have been made on the development of fuel cells [16-22]. Alkaline fuel cells (AFCs) that use potassium hydroxide (KOH) solution as the liquid electrolyte have shown much success since the 1960s, particularly working as the energy supply devices powering the Gemini and Apollo spacecraft, due to the fact that the electrochemical kinetics of the oxygen reduction reaction (ORR) is much enhanced resulting from the alkaline environment, allowing the absence of expensive noble metals in preparing the electrocatalysts and thus reducing the cost of the fuel cell system [23-25]. Despite its compelling merits, however, this fuel cell technology has not made sufficient progress in market presence yet. One significant factor preventing widespread commercialization is the use of the alkaline liquid electrolyte, which may cause two problems [26]. One is the carbonate, the product of the side reaction between hydroxide ions in the

liquid electrolyte and carbon dioxide in the air, reducing the concentration of hydroxide ions and potentially blocking the pores of the porous electrode via the precipitation of the metal carbonate [27-29]. The other is electrode flooding and drying problems, which are more likely to arise if the liquid electrolyte is not well controlled [30, 31].

To address the issues caused by involving the liquid electrolyte, ion exchange membrane fuel cells that employ solid electrolyte have received ever-increasing attention [32-36]. The use of solid electrolyte membranes in fuel cells can remove the carbonate problem and avoid the liquid electrolyte management. A typical example is the proton exchange membrane fuel cell (PEMFC) employing the proton exchange membrane (PEM) to transport protons from the anode to cathode. Together with the PEM, the anode and the cathode, generally using carbon supported Pt electrocatalysts, form the membrane electrode assembly (MEA), which is the core component of PEMFCs. The compact layer-by-layer structure provides higher specific and volumetric energy densities. As a result, the PEMFC is a suitable candidate for portable, transportation, and stationary applications.

1.2. Direct liquid fuel cells

In PEMFCs, the gas hydrogen is used as the fuel, so the only product is water, which is environmentally friendly and causes minimal corrosion of the system. However, the green and sustainable production of hydrogen needs further development. As hydrogen is the lightest gas, its storage and transportation require compressing gas hydrogen into liquid hydrogen at high pressure, which leads to potential explosion issue when the hydrogen

is not properly handled. For this reason, direct liquid fuel cells (DLFCs) using liquid alcohol fuels have attracted increasing research attention, primarily due to liquid fuels processing much higher energy densities and being easier to store, transport, and handle.

1.3. Direct ethylene glycol fuel cells

1.3.1. Features

Currently, methanol, ethanol, and ethylene glycol (EG) are three most common liquid fuels utilized in fuel cells. As for methanol, severe fuel crossover can result in dramatic performance degradation [37]. As for ethanol, the C-C bond is hardly broken in fuel cells running at low temperatures (generally $< 60^{\circ}\text{C}$), leading to a low electron transfer rate (i.e., 33%) [20, 38]. EG, an alcohol with 2 hydroxyl groups, has received considerable interest for mobile, stationary, and portable applications, resulting from its promising theoretical energy capacity of 4.8 Ah mL^{-1} , high boiling point of 198°C , and outstanding efficiency of electric power conversion [39]. Hence, direct ethylene glycol fuel cells (DEGFCs) using liquid EG not only avoids the poisoning and safety problems, but also possesses an electron transfer rate as high as 80% [24]. In addition, EG has a well-established supply chain producing more than 7 million tons annually. Figure 1.1 shows a conventional DEGFC using oxygen as oxidant.

1.3.2. Research and development

Due to the above-mentioned advantages, DEGFCs have attracted ever-increasing attention, particularly these fuel cells using anion exchange membranes (AEMs) due to the both enhanced anodic and cathodic kinetics [38, 40-42]. AEMs and cation exchange membranes (CEMs) are classified

by the charge type of fixed functional groups, which can selectively allow the passage of oppositely charged ions (counter-ions), while obstruct similarly charged ions (co-ions) [43]. An et al. [44] compared the AEM and CEM in direct ethanol fuel cells (DEFCs). It was found that the AEM possessed the higher ionic conductivity and mechanical property, but the worse thermal stability. In addition, the CEM showed the lower ionic conductivity, but acceptable thermal stability, mechanical property, and species permeability. There is no significant difference in the fuel cell performance between the AEM and CEM at low operating temperatures (<60°C), but the CEM-DEFC can operate stably at high operating temperatures (typically 90°C).

In the past decade, numerous effects have been made on performance improvement, catalyst development, and system innovations [24, 45-51]. An et al. [45] developed and tested an alkaline DEGFC using an AEM, which exhibited a peak power density of 67 mW cm⁻² at 60°C. The outstanding performance was ascribed to the alkaline environment, which much enhances the kinetics of both the ORR and ethylene glycol oxidation reaction (EGOR). Considering the poor stability of AEM at high temperatures, generally over 60°C, they replaced the AEM with an alkali-doped polybenzimidazole in an alkaline DEGFC, which allows the operation of the fuel cell at higher temperatures (90°C). As a result, it was found that a higher peak power density of 112 mW cm⁻² was achieved at 90°C [24]. To improve the activity of the catalyst toward EGOR, Feng et al. [46] reported networked Pt-Pb nanowires (NWs), which was synthesized via a large-scalable wet-chemical approach. The electrocatalyst showed a

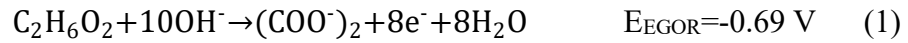
3D networked structure with rich defects/steps. Using the acidified hydrogen peroxide rather than the oxygen or air in the cathode as the oxidant has been tested in fuel cells running on various fuels such as formate [52], propanol, and glycerol [53]. Li [52] found that the AEM direct formate-peroxide fuel cell showed a more stable cell voltage than the AEM direct ethanol fuel cell in a conceptual half-hour constant-current discharge. Chino et al. [53] reported that the split pH environment improved the thermodynamics of the fuel cell by creating a large potential difference between electrodes. However, the decomposition of H_2O_2 and thus generation of O_2 may form a two-phase flow in the cathode flow channel, resulting in the voltage fluctuation, which is not desirable in the practical applications. Meanwhile, it creates a large transport resistance of H_2O_2 from the cathode flow channel to the cathode catalyst layer (CL), which may lead to the H_2O_2 in the cathode CL at a starving state, thus the cathodic reaction kinetics is sluggish [54].

Moreover, to meet the voltage requirement of electronics in practice, a fuel cell stack rather than a single cell is used, which is constituted by cells connected in series. Cremers et al. [55] developed an active AEM-DEGFC stack using the air as oxidant. When the feeding rates were 12 mL min^{-1} on the anode and 800 sccm on the cathode, the fuel cell stack showed a peak power density of 44 mW cm^{-2} at 50°C . Although the performance is promising, the active operation mode needs auxiliary equipment such as liquid pumps and gas compressors, leading to a more complicated and heavier system [56, 57]. To meet the demand for portable electronic devices, the active operation mode can be replaced by a passive way, which makes

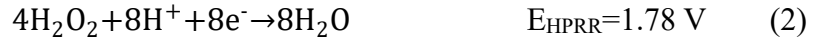
the reactants store in the reservoirs and transport to the catalyst layer mainly via diffusion, driven by the concentration gradient [58]. It should be mentioned that the delivery of reactants at the passive operation mode in the porous electrode is slower than the active one does, which is attributed to the fact that an additional driving force of convection for the delivery of reactants exists at the active operation mode. Hence, the passive fuel cell performance is generally lower than the active fuel cell does at the same operation conditions. Marchionni et al. [59] synthesized Pd-(Ni-Zn)/C catalyst, which was Pd nanoparticles supported on a Ni-Zn phase, and adopted it as the anode catalyst in a passive DEGFC. It was found that the peak power density increased from 12 mW cm⁻² to 24 mW cm⁻² for passive mode at 25°C and 65 mW cm⁻² to 95 mW cm⁻² for active mode at 80°C when the Pd-(Ni-Zn)/C replaced the Pd/C. Fashedemi et al. [42] prepared Pd-based ternary core-shell (FeCo@Fe@Pd) nanocatalyst using multi-walled carbon nanotubes bearing carboxylic (MWCNT-COOH) as supporting platform and compared its performance with the Pd/MWCNT-COOH in a passive DEGFC. It was reported that the running time of the fuel cell using the FeCo@Fe@Pd/MWCNT-COOH-based anode was around 4.7 h at a discharging current density of 20 mA cm⁻², which was higher than the Pd/MWCNT-COOH-based anode did (3.3 h).

1.3.3. Working principle

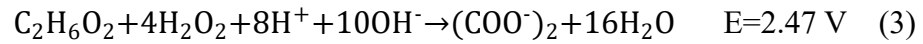
As shown in Figure ??, the hybrid DEGFC consists of an anode diffusion layer (DL), an anode CL, a CEM, a cathode CL, and a cathode DL. In the anode where EGOR takes place, the EG reacts with OH⁻ to produce oxalate, electrons, and water according to [20]:



Then the produced electrons transport from the external circuit and reach the cathode CL, participating in the hydrogen peroxide reduction reaction (HPRR), to react with hydrogen peroxide and protons to generate water according to [60]:



The sodium ions transport through the CEM from the anode to the cathode to form the ionic current. Therefore, combining the Eqs. (1) and (2), the overall reaction of the hybrid DEGFC can be obtained as follows:



Although the theoretical voltage of this hybrid DEGFC is so high, the practical voltage exhibits a severe degradation due to the activation loss, ohmic loss, as well as concentration loss. In addition, the mixed potential in the cathode, lowering the cell voltage, needs to be paid special attention to.

1.3.4. State-of-the-art performance

From the literature review in section 1.3.3, the performance of DEGFCs increases from 12 mW cm⁻² to 112 mW cm⁻². The reasons for the performance difference can be concluded as follows: i) the highly active electrocatalyst will enhance the reaction kinetics and lowers the activation loss, ii) the highly conductive membrane will facilitate the ion transport and lowers the ohmic loss, and iii) the higher operating temperature will enhance the reaction kinetics and mass transport.

1.3.5. Remaining challenges and issues

Although significant progress has been made in DEGFCs, there are still

some remaining challenges and issues, which can be concluded as follows: i) the conventional layer-by-layer electrode design has large mass transport resistance in CL, and generates tremendous inaccessible active sites, ii) the water flooding on cathode, water transporting from the anode to cathode, limits the gas oxygen transport to the cathode CL, iii) the complicated design and bulky auxiliary equipment reduce the specific and volumetric energy densities of fuel cell system, and iv) few demonstration of DEGFC applications is reported. Before the worldwide commercialization of this technology, it is expected that the performance should be substantially improved. To achieve this goal, a better understanding on the mass transport characteristics of DEGFCs and innovative electrode designs are needed.

1.4. Objectives of this thesis

The primary objective of this thesis is to investigate and understand the performance characteristics of EG fuel cells using hydrogen peroxide as oxidant through experimental and numerical approaches. Firstly, a cost-effective poly(vinylidene fluoride-co-hexafluoropropylene) (PVDF-HFP) is adopted as electrode binder, which tends to form a porous structure and adhere the catalyst nanoparticles onto the nickel foam skeleton but not to isolate the catalyst nanoparticles, achieving a higher effective active area. Meanwhile, it contains more amorphous domains capable of trapping a large amount of liquid electrolyte, creating more effective active sites. At the electrode level, the electrochemical surface areas of the three electrodes using PVDF-HFP, Nafion, and PTFE are 24.10, 18.62, and 16.44 m² g⁻¹, respectively. At the cell level, using the PVDF-HFP-based electrode exhibits the best performance with an open-circuit voltage (OCV) of 1.47

V, a maximum current density of 300 mA cm^{-2} , and a peak power density of 120.0 mW cm^{-2} at 60°C , which shows an improvement of 13.7% and 58.1%, respectively, comparing to the fuel cell performance achieved by using Nafion and PTFE as the electrode binder. Secondly, an active fuel cell using EG as fuel and hydrogen peroxide as oxidant is designed, fabricated, and tested, which theoretically offers a theoretical voltage as high as 2.47 V. This active fuel cell can experimentally output an OCV of 1.41 V and a peak power density of 80.9 mW cm^{-2} at 60°C , which is 20.8% higher than that of using oxygen (67 mW cm^{-2}). The performance improvement is mainly attributed to the faster kinetics of the two-electron-transfer hydrogen peroxide reduction reaction. Thirdly, a passive fuel cell using EG as fuel and hydrogen peroxide as oxidant is demonstrated, which avoids the usage of auxiliary devices. Although the passive fuel cell generates a lower power density than does an active one, it is more structurally compact, no parasitic loss in power, and can be operated under ambient conditions, making it a suitable candidate for powering portable electronic devices. It is found that this passive fuel cell yields an OCV of 1.58 V and peak power densities of 30.3 mW cm^{-2} and 65.8 mW cm^{-2} at 23°C and 60°C , respectively, showing an impressive improvement comparing to a passive air-based fuel cell, which is more than two times higher in the OCV (0.7 V) and more than five times higher in the peak power density (12 mW cm^{-2}). Fourthly, a passive fuel cell stack consisting of two single cells is developed to examine the feasibility of this fuel cell technology in practical applications and then demonstrated to power an electric fan in underwater condition. This passive fuel cell stack exhibits an actual OCV of 3.0 V, a maximum current of 860

mA, and a peak power of 1178 mW at room temperature. The individual cell in the passive stack exhibits a good consistency over the whole current region, indicating a high degree of reproducibility achieved by the appropriate electrode manufacturing and cell assembly processes. Moreover, the running time (per refueling) of an electric fan powered by this passive stack is 2 hours and 36 minutes in underwater condition, demonstrating that this passive fuel cell stack is a promising power source for airtight situations, such as underwater and outer space. Lastly, a mathematical model is developed to give the in-depth insights of physical and chemical processes occurring in this fuel cell, which incorporates mass/charge transport and electrochemical reactions. Previous models treat the local concentration as the actual reactant concentration participating in the electrochemical reaction, suggesting that EG molecules and OH⁻ ions are completely adsorbed on active sites. For a specific active site, however, the reactant with a higher local concentration is more likely to be adsorbed, which may lead to active sites fully occupied. The other with a lower local concentration cannot be further adsorbed, hindering the electrochemical reaction. As such, the fuel cell performance is significantly affected by the fuel solution composition and their transport characteristics. By considering the competitive adsorption of reactants on active sites, the present model accurately predicts the voltage losses, electrode potentials, local concentrations, and thus fuel cell performance under various operating and structural design parameters. The obtained results are applicable for other DLFCs and can provide guidance for electrode fabrication, fuel composition, as well as system design.

1.5. References

- [1] L. An, T.S. Zhao, J.B. Xu, A bi-functional cathode structure for alkaline-acid direct ethanol fuel cells, *International Journal of Hydrogen Energy* 36 (2011) 13089-13095.
- [2] L. An, T.S. Zhao, S.Y. Shen, Q.X. Wu, R. Chen, Alkaline direct oxidation fuel cell with non-platinum catalysts capable of converting glucose to electricity at high power output, *Journal of Power Sources* 196 (2011) 186-190.
- [3] M. Mamlouk, J.A. Horsfall, C. Williams, K. Scott, Radiation grafted membranes for superior anion exchange polymer membrane fuel cells performance, *International Journal of Hydrogen Energy* 37 (2012) 11912-11920.
- [4] L. An, T.S. Zhao, X.L. Zhou, X.H. Yan, C.Y. Jung, A low-cost, high-performance zinc-hydrogen peroxide fuel cell, *Journal of Power Sources* 275 (2015) 831-834.
- [5] L. An, T.S. Zhao, X.L. Zhou, L. Wei, X.H. Yan, A high-performance ethanol-hydrogen peroxide fuel cell, *RSC Advances* 4 (2014) 65031-65034.
- [6] J.R. Varcoe, P. Atanassov, D.R. Deke, A.M. Herring, M.A. Hickner, P.A. Kohl, A.R. Kucernak, W.E. Mustain, K. Nijmeijer, K. Scott, T. Xu, L. Zhuang, Anion-exchange membranes in electrochemical energy systems, *Energy & Environmental Science* 7 (2014) 3135-3191.
- [7] L. An, R. Chen, Mathematical modeling of direct formate fuel cells, *Applied Thermal Engineering* 124 (2017) 232-240.
- [8] Y.S. Li, T.S. Zhao, Ultra-low catalyst loading cathode electrode for anion-exchange membrane fuel cells, *International Journal of Hydrogen*

Energy 37 (2012) 15334-15338.

[9] J.R. Varcoe, M. Beillard, D.M. Halepoto, J.P. Kizewski, S. Poynton, R.C.T. Slade, Membrane and Electrode Materials for Alkaline Membrane Fuel Cells, ECS Transactions 16 (2019) 1819-1834.

[10] E.H. Yu, X. Wang, U. Krewer, L. Li, K. Scott, Direct oxidation alkaline fuel cells: from materials to systems, Energy & Environmental Science 5 (2012) 5668-5680.

[11] L. An, T.S. Zhao, Z.H. Chai, L. Zeng, P. Tan, Modeling of the mixed potential in hydrogen peroxide-based fuel cells, International Journal of Hydrogen Energy 39 (2014) 7407-7416.

[12] Y. Li, Y. He, Layer reduction method for fabricating Pd-coated Ni foams as high-performance ethanol electrode for anion-exchange membrane fuel cells, RSC Advances 4 (2014) 16879-16884.

[13] C. Duan, D. Hook, Y. Chen, J. Tong, R. O'Hayre, Zr and Y co-doped perovskite as a stable, high performance cathode for solid oxide fuel cells operating below 500 °C, Energy & Environmental Science 10 (2017) 176-182.

[14] L. An, T.S. Zhao, L. Zeng, X.H. Yan, Performance of an alkaline direct ethanol fuel cell with hydrogen peroxide as oxidant, International Journal of Hydrogen Energy 39 (2014) 2320-2324.

[15] L. An, T.S. Zhao, Performance of an alkaline-acid direct ethanol fuel cell, International Journal of Hydrogen Energy 36 (2011) 9994-9999.

[16] H. Zhang, H. Ohashi, T. Tamaki, T. Yamaguchi, Direction and Management of Water Movement in Solid-State Alkaline Fuel Cells, The Journal of Physical Chemistry C 116 (2012) 7650-7657.

- [17] L. An, T.S. Zhao, L. Zeng, Agar chemical hydrogel electrode binder for fuel-electrolyte-fed fuel cells, *Applied Energy* 109 (2013) 67-71.
- [18] L. An, C.Y. Jung, Transport phenomena in direct borohydride fuel cells, *Applied Energy* 205 (2017) 1270-1282.
- [19] I. Gunasekara, M. Lee, D. Abbott, S. Mukerjee, Mass Transport and Oxygen Reduction Kinetics at an Anion Exchange Membrane Interface: Microelectrode Studies on Effect of Carbonate Exchange, *ECS Electrochemistry Letters* 1 (2012) F16-F19.
- [20] L. An, R. Chen, Recent progress in alkaline direct ethylene glycol fuel cells for sustainable energy production, *Journal of Power Sources* 329 (2016) 484-501.
- [21] L. An, T. Zhao, X. Yan, X. Zhou, P. Tan, The dual role of hydrogen peroxide in fuel cells, *Science Bulletin* 60 (2015) 55-64.
- [22] Y. Li, J. Lv, Y. He, A Monolithic Carbon Foam-Supported Pd-Based Catalyst towards Ethanol Electro-Oxidation in Alkaline Media, *Journal of The Electrochemical Society* 163 (2016) F424-F427.
- [23] H.Y. Hou, Recent Research Progress in Alkaline Polymer Electrolyte Membranes for Alkaline Solid Fuel Cells, *Acta Physico-Chimica Sinica* 30 (2014) 1393-1407.
- [24] L. An, L. Zeng, T.S. Zhao, An alkaline direct ethylene glycol fuel cell with an alkali-doped polybenzimidazole membrane, *International Journal of Hydrogen Energy* 38 (2013) 10602-10606.
- [25] L. An, T.S. Zhao, An alkaline direct ethanol fuel cell with a cation exchange membrane, *Energy & Environmental Science* 4 (2011) 2213-2217.
- [26] G. Merle, M. Wessling, K. Nijmeijer, Anion exchange membranes for

alkaline fuel cells: A review, *Journal of Membrane Science* 377 (2011) 1-35.

[27] E. Gülzow, M. Schulze, Long-term operation of AFC electrodes with CO₂ containing gases, *Journal of Power Sources* 127 (2004) 243-251.

[28] G.F. McLean, T. Niet, S. Prince-Richard, N. Djilali, An assessment of alkaline fuel cell technology, *International Journal of Hydrogen Energy* 27 (2002) 507-526.

[29] P. Gouérec, L. Poletto, J. Denizot, E. Sanchez-Cortezon, J.H. Miners, The evolution of the performance of alkaline fuel cells with circulating electrolyte, *Journal of Power Sources* 129 (2004) 193-204.

[30] Y.-J. Wang, J. Qiao, R. Baker, J. Zhang, Alkaline polymer electrolyte membranes for fuel cell applications, *Chemical Society Reviews* 42 (2013) 5768-5787.

[31] Y.S. Li, T.S. Zhao, R. Chen, Cathode flooding behaviour in alkaline direct ethanol fuel cells, *Journal of Power Sources* 196 (2011) 133-139.

[32] L. An, T.S. Zhao, Y.S. Li, Carbon-neutral sustainable energy technology: Direct ethanol fuel cells, *Renewable and Sustainable Energy Reviews* 50 (2015) 1462-1468.

[33] L. An, T.S. Zhao, Y. Li, Q. Wu, Charge carriers in alkaline direct oxidation fuel cells, *Energy & Environmental Science* 5 (2012) 7536-7538.

[34] L. An, T.S. Zhao, Transport phenomena in alkaline direct ethanol fuel cells for sustainable energy production, *Journal of Power Sources* 341 (2017) 199-211.

[35] D. Yang, H. Yu, G. Li, W. Song, Y. Liu, Z. Shao, Effect of gas diffusion electrode parameters on anion exchange membrane fuel cell performance,

Chinese Journal of Catalysis 35 (2014) 1091-1097.

[36] Y.S. Li, Y.L. He, W.W. Yang, Performance characteristics of air-breathing anion-exchange membrane direct ethanol fuel cells, *International Journal of Hydrogen Energy* 38 (2013) 13427-13433.

[37] X. Chen, T. Li, J. Shen, Z. Hu, From structures, packaging to application: A system-level review for micro direct methanol fuel cell, *Renewable and Sustainable Energy Reviews* 80 (2017) 669-678.

[38] Z.F. Pan, R. Chen, L. An, Y.S. Li, Alkaline anion exchange membrane fuel cells for cogeneration of electricity and valuable chemicals, *Journal of Power Sources* 365 (2017) 430-445.

[39] H. Yue, Y. Zhao, X. Ma, J. Gong, Ethylene glycol: properties, synthesis, and applications, *Chemical Society Reviews* 41 (2012) 4218-4244.

[40] J. Qi, N. Benipal, C. Liang, W. Li, PdAg/CNT catalyzed alcohol oxidation reaction for high-performance anion exchange membrane direct alcohol fuel cell (alcohol=methanol, ethanol, ethylene glycol and glycerol), *Applied Catalysis B: Environmental* 199 (2016) 494-503.

[41] R. Kannan, A.R. Kim, J.S. Kim, D.J. Yoo, 3D graphene-mixed metal oxide-supported carbonpalladium quantum dot nanoarchitectures – A facile bifunctional electrocatalyst for direct ethylene glycol fuel cells and oxygen evolution reactions, *International Journal of Hydrogen Energy* 41 (2016) 18033-18043.

[42] O.O. Fashedemi, H.A. Miller, A. Marchionni, F. Vizza, K.I. Ozoemena, Electro-oxidation of ethylene glycol and glycerol at palladium-decorated FeCo@Fe core-shell nanocatalysts for alkaline direct alcohol fuel cells: functionalized MWCNT supports and impact on product selectivity, *Journal*

of Materials Chemistry A 3 (2015) 7145-7156.

[43] T. Luo, S. Abdu, M. Wessling, Selectivity of ion exchange membranes: A review, *Journal of Membrane Science* 555 (2018) 429-454.

[44] L. An, T.S. Zhao, Q.X. Wu, L. Zeng, Comparison of different types of membrane in alkaline direct ethanol fuel cells, *International Journal of Hydrogen Energy* 37 (2012) 14536-14542.

[45] L. An, T.S. Zhao, S.Y. Shen, Q.X. Wu, R. Chen, Performance of a direct ethylene glycol fuel cell with an anion-exchange membrane, *International Journal of Hydrogen Energy* 35 (2010) 4329-4335.

[46] Y. Feng, L. Bu, S. Guo, J. Guo, X. Huang, 3D Platinum–Lead Nanowire Networks as Highly Efficient Ethylene Glycol Oxidation Electrocatalysts, *Small* 12 (2016) 4464-4470.

[47] Z. Pan, Y. Bi, L. An, Mathematical modeling of direct ethylene glycol fuel cells incorporating the effect of the competitive adsorption, *Applied Thermal Engineering* 147 (2019) 1115-1124.

[48] E. Peled, V. Livshits, T. Duvdevani, High-power direct ethylene glycol fuel cell (DEGFC) based on nanoporous proton-conducting membrane (NP-PCM), *Journal of Power Sources* 106 (2002) 245-248.

[49] Y.-C. Shi, J.-J. Feng, X.-X. Lin, L. Zhang, J. Yuan, Q.-L. Zhang, A.-J. Wang, One-step hydrothermal synthesis of three-dimensional nitrogen-doped reduced graphene oxide hydrogels anchored PtPd alloyed nanoparticles for ethylene glycol oxidation and hydrogen evolution reactions, *Electrochimica Acta* 293 (2019) 504-513.

[50] Z.-N. Yu, Z. Zhang, Z.-S. Lv, M.-T. Liu, L. Zhang, A.-J. Wang, L.-Y. Jiang, J.-J. Feng, Platinum₆₉-cobalt₃₁ alloyed nanosheet nanoassemblies

as advanced bifunctional electrocatalysts for boosting ethylene glycol oxidation and oxygen reduction, *Journal of Colloid and Interface Science* 525 (2018) 216-224.

[51] X.-Y. Huang, A.-J. Wang, X.-F. Zhang, L. Zhang, J.-J. Feng, One-Step Synthesis of PtCu Alloyed Nanocages with Highly Open Structures as Bifunctional Electrocatalysts for Oxygen Reduction and Polyhydric Alcohol Oxidation, *ACS Applied Energy Materials* 1 (2018) 5779-5786.

[52] Y. Li, A liquid-electrolyte-free anion-exchange membrane direct formate-peroxide fuel cell, *International Journal of Hydrogen Energy* 41 (2016) 3600-3604.

[53] I. Chino, K. Hendrix, A. Keramati, O. Muneeb, J.L. Haan, A split pH direct liquid fuel cell powered by propanol or glycerol, *Applied Energy* 251 (2019) 113323.

[54] T.S. Zhao, C. Xu, R. Chen, W.W. Yang, Mass transport phenomena in direct methanol fuel cells, *Progress in Energy and Combustion Science* 35 (2009) 275-292.

[55] C. Cremers, A. Niedergesäß, F. Jung, D. Müller, J. Tübke, Development of an Alkaline Anion Exchange Membrane Direct Ethylene Glycol Fuel Cell Stack, *ECS Transactions* 41 (2019) 1987-1996.

[56] J.P. Pereira, D.S. Falcão, V.B. Oliveira, A.M.F.R. Pinto, Performance of a passive direct ethanol fuel cell, *Journal of Power Sources* 256 (2014) 14-19.

[57] Y.S. Li, T.S. Zhao, A passive anion-exchange membrane direct ethanol fuel cell stack and its applications, *International Journal of Hydrogen Energy* 41 (2016) 20336-20342.

[58] S.S. Munjewar, S.B. Thombre, R.K. Mallick, Approaches to overcome the barrier issues of passive direct methanol fuel cell – Review, *Renewable and Sustainable Energy Reviews* 67 (2017) 1087-1104.

[59] A. Marchionni, M. Bevilacqua, C. Bianchini, Y.-X. Chen, J. Filippi, P. Fornasiero, A. Lavacchi, H. Miller, L. Wang, F. Vizza, Electrooxidation of Ethylene Glycol and Glycerol on Pd-(Ni-Zn)/C Anodes in Direct Alcohol Fuel Cells, *ChemSusChem* 6 (2013) 518-528.

[60] L. An, T.S. Zhao, R. Chen, Q.X. Wu, A novel direct ethanol fuel cell with high power density, *Journal of Power Sources* 196 (2011) 6219-6222.

Figures

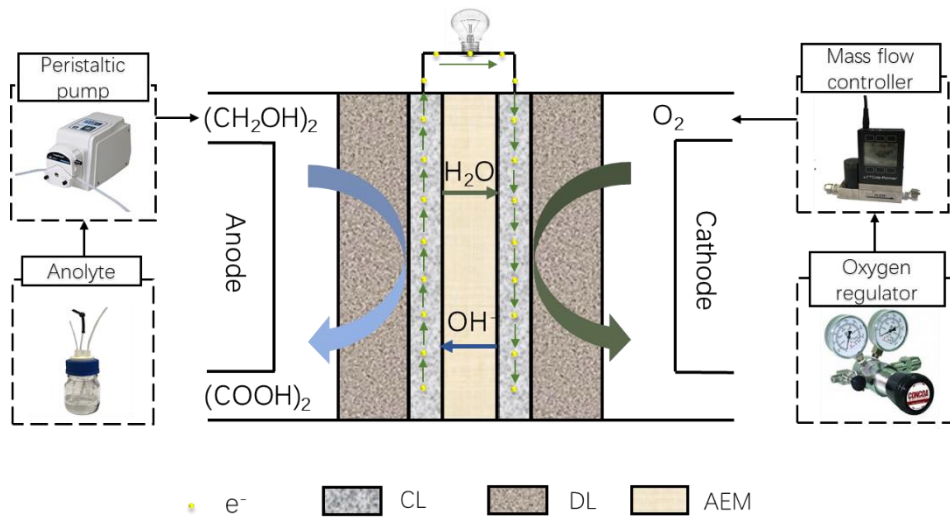


Figure 1.1 Schematic of a conventional DEGFC using oxygen as oxidant.

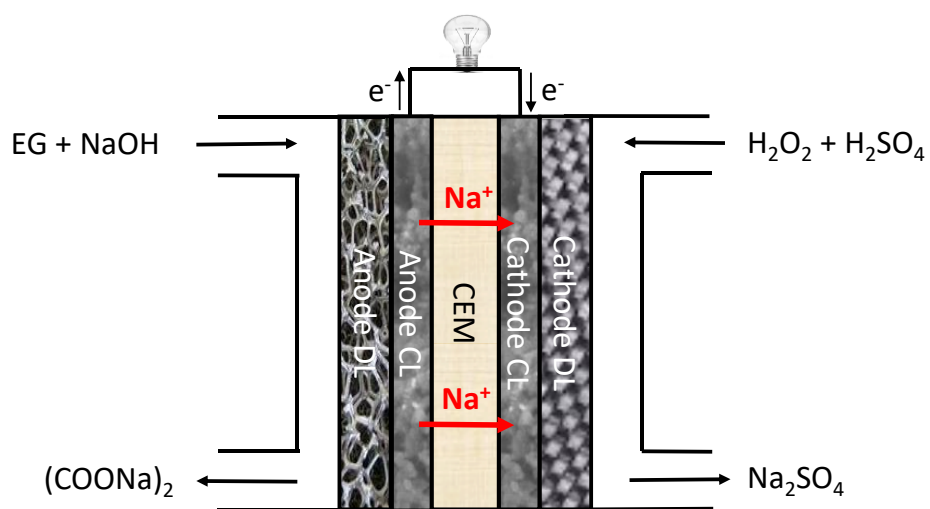


Figure 1.2 Schematic of a DEGFC using hydrogen peroxide as oxidant.

Chapter 2 Fuel cell fabrications and characterizations

2.1. Introduction

This chapter is to introduce the procedures of fuel cell fabrications and characterizations of electrodes and fuel cells: i) section 2.2 is to introduce the preparation procedures of flow field plates, electrodes, membranes, membrane electrode assembly (MEA), single-cell setup, and fuel cell stack setup; ii) section 2.3 is to introduce the characterizations of electrodes including surface morphology and electrochemical surface area (ECSA) determination; and iii) section 2.4 is to introduce the characterizations of single cells including testing system, fuel supply system, oxygen supply system, temperature controlling system, polarization curves, constant-current discharging behaviour, long-term durability, internal resistance measurement, and electrochemical impedance spectra (EIS).

2.2. Fuel cell fabrication and assembly

Each MEA is fixed between an anode plate and a cathode plate, both of which were made of 316 L stainless steel plates with flow fields. Four bolts and nuts are used to compress the anode plate and cathode plate tightly. Wooden insulators are put between plates and bolts to prevent short circuit.

2.2.1. Flow field plates

The anode and cathode plates are made of 316 L stainless steel plates with flow fields. The flow field is a single serpentine flow channel grooved by the wire-cut technique, which was 0.5 mm deep and 1.0 mm wide. A larger

hole is drilled for heating rods, and a smaller hole is drilled for thermocouples.

2.2.2. Preparation of electrodes

The widely used electrode structure is a layer by layer structure constructed by coating a catalyst layer (CL), which is usually a dense layer consisting of pure electrocatalyst or carbon supported electrocatalyst and electrode binder, onto a backing layer (BL), which is usually a porous material, e.g. carbon cloth, carbon paper, and metal foam. Three methods are used in this thesis to coat the CL on the BL, which are brushing, spraying, and dip-coating. The procedures to fabricate the nickel foam-based electrode with an area of 1.0 cm × 1.0 cm via brushing method are given as follows:

- i) A piece of nickel foam with an area of 2.0 cm × 2.0 cm is cut off, whose weight is recorded for calculating the catalyst loading.
- ii) The nickel foam is fixed onto a heating plate with tapes, exposing an area of 1.5 cm × 1.5 cm.
- iii) The electrocatalyst nanoparticles are mixed with 5 wt.% Nafion solution (Fuel Cell Store, USA) as the binder and an appropriate amount of ethanol as the solvent.
- iv) The electrocatalyst ink is stirred continuously in an ultrasonic bath for 20 min, making it well dispersed.
- v) The prepared electrocatalyst ink is brushed onto the nickel foam using a painting brush.
- vi) Wait for a few minutes until the catalyst layer is dried.
- vii) Repeat the procedures v) and vi) for several times, until the desired catalyst loading is achieved.

-
- viii) Cut off the electrode with an area of $1.0\text{ cm} \times 1.0\text{ cm}$ in the middle of the brushed nickel foam.

The procedures to fabricate the carbon cloth-based electrode with an area of $1.0\text{ cm} \times 1.0\text{ cm}$ via spraying method are given as follows:

- i) A piece of carbon cloth with an area of $1.5\text{ cm} \times 1.5\text{ cm}$ is cut off, whose weight is recorded for calculating the catalyst loading.
- ii) The carbon cloth is fixed onto a heating plate with tapes, exposing an area of $1.0\text{ cm} \times 1.0\text{ cm}$.
- iii) The electrocatalyst nanoparticles are mixed with 5 wt.% Nafion solution as the binder and an appropriate amount of ethanol as the solvent.
- iv) The electrocatalyst ink is stirred continuously in an ultrasonic bath for 20 min, making it well dispersed.
- v) The prepared electrocatalyst ink is sprayed onto the carbon cloth using a spray gun.
- vi) Wait for a few minutes until the catalyst layer is dried.
- vii) Repeat the procedures v) and vi) for several times, until the desired catalyst loading is achieved.
- viii) Cut off the electrode with an area of $1.0\text{ cm} \times 1.0\text{ cm}$ in the central of the sprayed carbon cloth.

The procedures to fabricate the nickel foam-based electrode with an area of $1.0\text{ cm} \times 1.0\text{ cm}$ via dip-coating method are given as follows:

- i) A piece of nickel foam with an area of $1.0\text{ cm} \times 1.0\text{ cm}$ is cut off, whose weight is recorded for calculating the catalyst loading.

-
- ii) The electrocatalyst nanoparticles are mixed with 5 wt.% Nafion solution as the binder and an appropriate amount of ethanol as the solvent.
 - iii) The electrocatalyst ink is stirred continuously in an ultrasonic bath for 20 min, making it well dispersed.
 - iv) The prepared nickel foam is dipped in the catalyst ink for 1 min before withdrawing it from the ink.
 - v) Wait for a few minutes until the catalyst layer is dried by a blower.
 - vi) Repeat the procedures iv) and v) for several times, until the desired catalyst loading is achieved.

The method to control the catalyst loading is same for brushing, painting, and spraying. The original weight of substrate will be obtained first. Then the catalyst ink with specific catalyst/binder ratio will be coated onto substrate. Finally, the catalyst loading is determined by the mass difference between the original substrate and the fabricated electrode and the ink ratio.

2.2.3. Preparation of membranes

The membrane in fuel cells is to conduct the charge carrier and separate the fuel and oxidant. In this thesis, a cation exchange membrane conducting Na^+ is used, which can be obtained by treating commercial Nafion membranes. The procedures are given as follows:

- i) Cut off a piece of Nafion membrane with the desire area.
- ii) Immerse the membranes into 2.5 M NaOH solution.
- iii) Heat up the solution to 80°C for 1 h.
- iv) Wash the membranes with DI water for several times.

Before assembling the fuel cell, the CEM can be stored in DI water.

2.2.4. Membrane electrode assembly

MEAs are synthesized using the as prepared anode, membrane, and cathode with an active area of 1.0 cm × 1.0 cm and 2.0 cm × 2.0 cm for active fuel cells and passive fuel cells, respectively.

2.3. Characterizations of electrodes

2.3.1. Surface morphology

The surface morphology of the prepared electrodes can be observed by conducting scanning electron microscopy (SEM) tests. The SEM image provides the information about pore sizes and electrocatalyst distribution. The working principle of the SEM test can be briefly described that an electron beam produced by an electron gun of SEM machine is applied to the sample surface and interacts with the surficial atoms of the sample, generating various signals that contain the information of the surface morphology.

2.3.2. Electrochemical surface area determination

Electrochemical surface area (ECSA) is an important parameter to describe the electrochemical surface of the prepared electrode, where the electrochemical reaction can occur. The technique for determining the ECSA of electrodes by cyclic voltammetry (CV) tests has been used for several decades. The procedures are given as follows: CV tests are conducted in a three-electrode electrochemical cell, where the fabricated electrode, the Pt foil, and the Hg-HgO (MMO, 1.0 M KOH) are used as the working electrode, the counter electrode and the reference electrode, respectively. The CV curves are recorded by an electrochemical workstation (PGSTAT302N). The potential window for the CV tests is from

–1.126 to 0.074 V at a scan rate of 50 mV s⁻¹. The ECSA can be calculated by the PdO reduction charge in the CV curves as shown in Equation (1):

$$\text{ECSA} = \frac{Q}{qm} \quad (1)$$

where Q is the coulombic charge, q is the charge value of 405 μC cm⁻² for the reduction of PdO monolayer, and m is the Pd loading on the electrode [1].

2.4. Characterizations of single cells

2.4.1. Testing system

The fuel cell testing system consists of the core component of single fuel cell and other auxiliary systems, including fuel and oxidant supply system, operating temperature controlling system, and testing equipment, as shown in Figure 2.1.

2.4.2. Fuel supply system

The fresh fuel solution is stored in a reservoir, which will be fed into the single cell via a peristaltic pump (BT100-2J, Longer Pump Co., China). The flow rate can be adjusted by the revolutions per minute (RPM) of the pump. Another reservoir is used to store the exhausted solution running out from the outlet.

2.4.3. Oxidant supply system

The fresh oxidant solution is stored in a reservoir, which will be fed into the single cell via a peristaltic pump. The flow rate can be adjusted by the RPM of the pump. Another reservoir is used to store the exhausted solution running out from the outlet.

2.4.4. Temperature controlling system

Two electrical heating rods are installed in the larger holes on the anode plate and cathode plate to heat up the cell. Two thermocouples are installed in the larger holes on the anode plate and cathode plate to detect the temperature of the single cell. A temperature controller is used to maintain the temperature of the single cell at a set value.

2.4.5. Polarization curves

A polarization curve is a critical method to evaluate the fuel cell performance, which contains three crucial performance indicators, i.e., open-circuit voltage, peak power density, and maximum current density. A typical polarization curve is illustrated in Figure 2.2 [2]. In general, the fuel cell voltage decreases with the increase of current density. The relationship can be expressed as equation (2):

$$V_{cell} = E^0 - \eta_{activation} - \eta_{concentration} - iR_{resistance} \quad (2)$$

where E^0 is the theoretical voltage, $\eta_{activation}$ and $\eta_{concentration}$ are the activation and concentration overpotentials of two electrodes, and $R_{resistance}$ is the internal resistance of the fuel cell.

- i) Activation overpotential, caused by the slowness of the reactions taking place on electrode surface, drives the electrons transferring to or from the electrode.
- ii) Concentration overpotential, caused by the insufficient reactant concentration on the electrode surface to support the fast reaction, changes the equilibrium potentials and reduces the exchange current density of the electrode. In general, it occurs at high current density region.

-
- iii) Internal resistance is caused by the electronic and ionic resistance in the conductive fixture, electrodes, and membrane and contact interfaces between the electronic conductors.

To measure the polarization curve, a testing equipment (BT-2000, Arbin Instruments, USA) is used. The fuel cell is discharging from 0 mA cm⁻², and the discharging current density increases with a same step. At each current density, it takes 30 seconds for voltage stabilization. The polarization curve can be obtained after the voltage reduces to zero.

2.4.6. Constant-current discharging behavior

The polarization test is basically a short-term test, because it only lasts for tens of minutes. In practical applications, however, the fuel cell is required to work for tens or hundreds of hours. To test its long-term stability, constant-current discharging is adopted. The fuel cell is discharging at a set and constant current density, and the voltage is recorded for hours or days, so the long-term stability can be tested.

2.4.7. Long-term durability

Apart from the long-term stability, the long-term durability of the passive fuel cell is examined. A long-term stability is conducted first, then the used fuel and oxidant are extracted, and the fuel cell is washed with DI water several times and dried in an oven. Fresh fuel and oxidant are injected into the cell and the long-term stability is tested again. The procedures are repeated to examine the long-term durability of the fuel cell.

2.4.8. Internal resistance measurement

The ohmic loss is determined by the internal resistance of fuel cell, which is measured by a current interrupt method. A small current pulse is induced

by the testing equipment and the transient voltage change is recorded. The internal resistance is calculated by the sudden voltage drop and the disrupt current.

2.4.9. Electrochemical impedance spectra

Electrochemical impedance spectra (EIS) is used to test the reaction kinetics, ohmic resistance, and mass transport efficiency of fuel cells. During the test, an electrochemical workstation applies sinusoidal voltages with small amplitude and different frequencies (1~100000 Hz) to a fuel cell and records the current response. The ohmic resistance and charge transfer resistance dominate in the high-frequency region, while the mass transport resistance dominates in the low-frequency region.

2.5. Summary

In this chapter, the fabrications of fuel cell are introduced, including the flow field plates, preparation of electrodes, preparation of membranes, and membrane electrode assembly. The techniques for the characterizations of fuel cells both in electrode scale and single cell scale are reviewed.

2.6. References

- [1] Y. Li, J. Lv, Y. He, A Monolithic Carbon Foam-Supported Pd-Based Catalyst towards Ethanol Electro-Oxidation in Alkaline Media, *Journal of The Electrochemical Society* 163 (2016) F424-F427.
- [2] X. Huang, Z. Zhang, J. Jiang, in: 2006 IEEE International Symposium on Industrial Electronics, 2006, pp. 1613-1618.

Figures

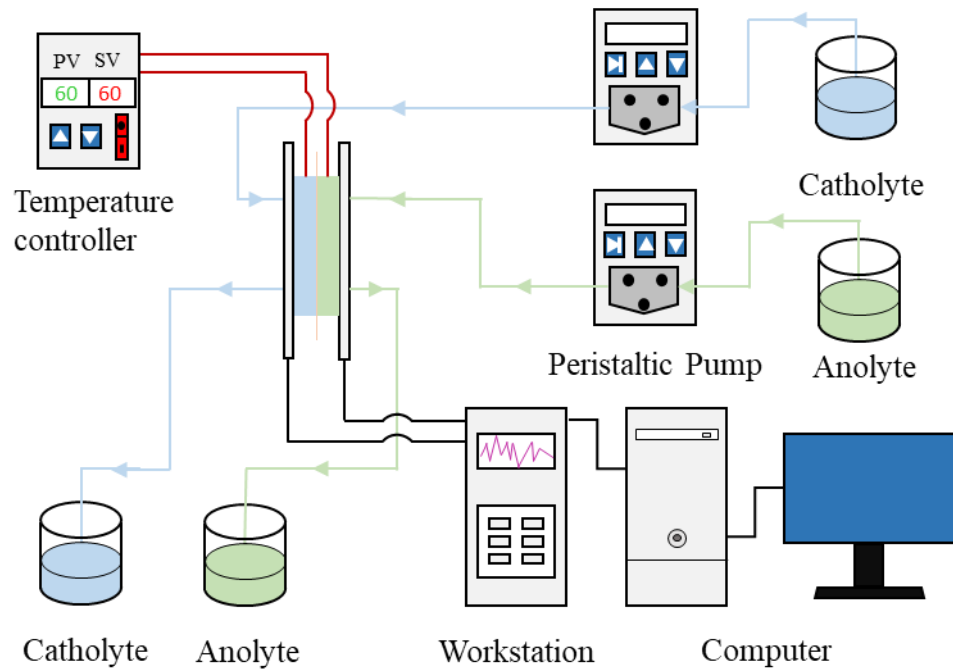


Figure 2.1 Testing system of an active DEGFC.

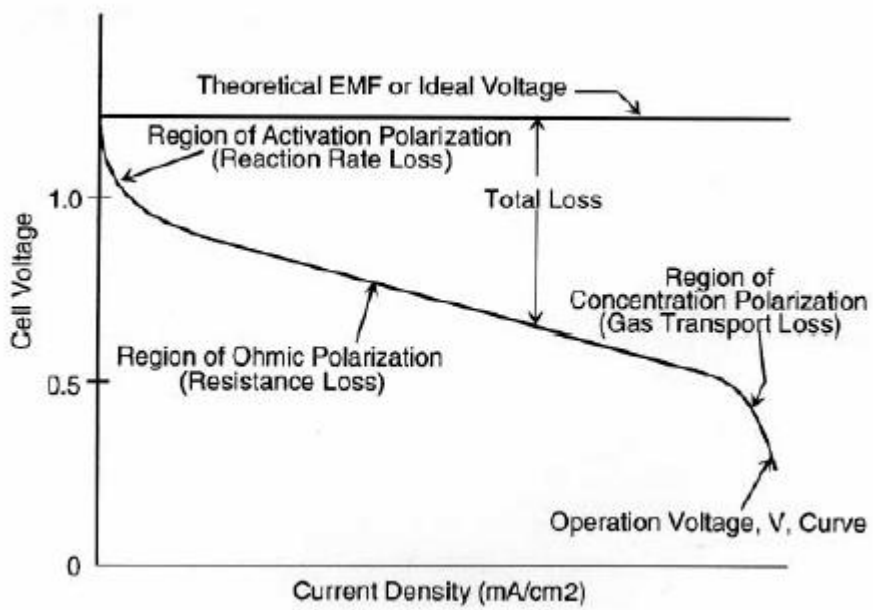


Figure 2.2 A typical polarization curve of a PEM fuel cell [2].

Chapter 3 Development of three-dimensional porous electrodes

Abstract

In preparing direct liquid fuel cell electrodes, an ionomer is necessary, whose functions are not only to bind the discrete catalyst nanoparticles onto the substrate materials to build the porous catalyst layer, but also to construct the triple phase boundaries to provide continuous pathways for reactant delivery. In this work, a cost-effective and chemically stable poly(vinylidene fluoride-co-hexafluoropropylene) electrode binder is adopted and compared with the conventional Nafion and polytetrafluoroethylene in terms of the electrode morphology and the fuel cell performance. It is found that the fuel cell using the poly(vinylidene fluoride-co-hexafluoropropylene)-based electrode exhibits the best performance in terms of an open-circuit voltage of 1.47 V, a maximum current density of 300 mA cm^{-2} , and a peak power density of 120.0 mW cm^{-2} . Comparing to the fuel cell performances fabricated with the conventional Nafion and polytetrafluoroethylene as electrode binder, the peak power density achieved by using the new type of electrode binder shows an improvement of 13.7% and 58.1%, respectively. Poly(vinylidene fluoride-co-hexafluoropropylene) shows the lowest cost of $\$0.18 \text{ kW}^{-1}$, while polytetrafluoroethylene and Nafion possess the higher cost of $\$0.80 \text{ kW}^{-1}$ and $\$145.59 \text{ kW}^{-1}$, respectively. The impressive improvement is attributed to the fact that the poly(vinylidene fluoride-co-hexafluoropropylene)-based electrode has a higher electrochemical surface area due to its intrinsic

porous property, enhancing the anodic reaction kinetics. It is found that the best cell performance is achieved with 1.0 M EG and 5.0 M KOH in the anolyte and 1.0 M H₂O₂ and 4.0 M H₂SO₄ in the catholyte at 60°C.

Keywords: Direct ethylene glycol fuel cells; Electrode binder; Hydrogen peroxide; Operating parameters; Power density

3.1. Introduction

As two global issues of climate change and energy crisis are becoming severer, proton exchange membrane fuel cells (PEMFCs) that use hydrogen as fuel and oxygen/air as oxidant have received ever-increasing attention as an alternative energy production technology in the last several decades [1, 2], which is primarily due to their intrinsic superiorities such as high efficiency [3, 4], simple design [5, 6], low emissions [7, 8], and quick refueling [9, 10]. Apart from the great achievements made in PEMFCs that use proton exchange membranes (PEMs) as ion exchange membranes (IEMs) [11, 12], anion exchange membrane fuel cells (AEMFCs) using anion exchange membranes (AEMs) as IEMs have attracted worldwide research interest, which is mainly ascribed to the fact that non-precious metal nanocatalysts can be used in AEMFCs due to the enhanced reaction kinetics rendered from the alkaline environment, thus the cost of the fuel cell is significantly reduced [13, 14]. However, the production, storage, and transport of hydrogen are still the critical issues in the commercialization of hydrogen fuel cells, which need to be addressed [15]. Recently, direct liquid fuel cells (DLFCs) using liquid alcohols and soluble organics instead of gaseous hydrogen as the fuel have obtained tremendous development, which is regarded as one of the most promising power sources for portable electronics [16, 17]. In addition to the above-mentioned advantages, the DLFCs possesses a broader range of advantages including mature production, easy transportation, and convenient handling of liquid fuels comparing to gaseous hydrogen [18, 19]. Among the widely used alcohols such as methanol, ethanol, and ethylene glycol (EG), EG has received

considerable interests because of the electron transfer rate as high as 80%, the boiling point of 198°C, and the theoretical energy capacity of 4.8 Ah mL⁻¹, which is a promising fuel for portable electronic devices [20, 21]. The term of electron transfer rate is similar to Faradaic efficiency, because EG cannot be completely oxidized to CO₂ using common catalysts under low temperature (<80°C). The main product of the ethylene glycol oxidation reaction in alkaline media could be oxalate, releasing 8 electrons per EG molecular. When EG is completely oxidized to CO₂, it will release 10 electrons per EG molecular, so the electron transfer rate of EG is 80%. Hence, direct ethylene glycol fuel cells (DEGFCs) become one of the research hotspots in DLFCs [22]. An et al. [23] developed and tested an alkaline DEGFC using an AEM, which yielded a peak power density of 67 mW cm⁻² at 60°C. The excellent performance was attributed to the alkaline environment, which much promotes the kinetics of both the oxygen reduction reaction (ORR) and ethylene glycol oxidation reaction (EGOR). Considering the poor stability of the AEM at high temperatures, generally over 60°C, they replaced the AEM with an alkali-doped polybenzimidazole in an alkaline DEGFC, which allows the operation of the fuel cell at higher temperatures (90°C). As a result, it was found that a higher peak power density of 112 mW cm⁻² was achieved at 90°C [24]. To further promote the cell performance, Pan et al. [25] reported that an open-circuit voltage (OCV) of 1.41 V and a peak power density of 80.9 mW cm⁻² at 60°C were achieved by replacing the oxygen with hydrogen peroxide in an alkaline DEGFC. This type of DEGFC boosted the OCV by 62.1% and the peak power density by 20.8%, as well as eliminated the requirement of the air from the

ambient environment. To improve the specific energy density and volumetric energy density, as well as extend the application situations to underwater and outer space, they developed a passive DEGFC with hydrogen peroxide as oxidant. This fuel cell exhibited peak power densities of 30.3 and 65.8 mW cm⁻² at 23 and 60°C, respectively [26]. They further developed and tested a passive DEGFC stack, which yielded an OCV of 3.0 V, a maximum current of 860 mA, and a peak power of 1178 mW at room temperature [27]. The passive stack was applied to power an electric fan for around 3 hours under the mimetic underwater circumstance, indicating that this passive stack can be air-independent power sources for underwater and outer space applications.

Similar to hydrogen fuel cells, in the preparation of the DLFC electrodes, an ionomer is necessary and plays an important role in the electrode fabrication. The ionomer possesses two functions. One is to bind the discrete catalyst nanoparticles onto the substrate materials to build the porous catalyst layer (CL), and the other is to construct the triple phase boundaries (TPBs) providing pathways for ion transport [28]. Generally, Nafion and polytetrafluoroethylene (PTFE) are two ionomers that have been widely used in fuel cells [29]. Although Nafion has proved to be a promising ionomer in forming the CL, the cost is the main concern hindering its wide applications [30]. The price of the 5 wt. % Nafion dispersion is as high as \$4 mL⁻¹ [31]. Choudhury et al. [32] prepared polyvinyl alcohol chemical hydrogel (PCH) and chitosan chemical hydrogel (CCH) as electrode binder for direct borohydride fuel cells (DBFCs) a chemical cross-linking reaction. Because of the hydrophilic

property and thus high water-retention capability, the CCH performed better than the Nafion binder, and the PCH showed similar performance comparing to the Nafion binder. An et al. [29] synthesized agar chemical hydrogel (ACH) as electrode binder in a fuel-electrolyte-fed fuel cell. It yielded a peak power density of 380 mW cm^{-2} at 90°C . PTFE is a cheaper binder comparing to Nafion. The price of the 60 wt. % PTFE dispersion is $\$0.312 \text{ mL}^{-1}$ [33]. However, one disadvantage of using PTFE as the electrode binder is that the reactants are not able to penetrate the PTFE binder [29]. For this reason, once the active sites in the catalyst layer, which are essential for electrochemical reactions, are covered by PTFE, the covered part would be not accessible and cannot catalyze the electrochemical reactions, resulting in the decrease in the electrochemical surface area (ECSA) [29].

Poly(vinylidene fluoride-co-hexafluoropropylene) (PVDF-HFP), an emerging fluorocopolymer, has been solely used or composited with other polymers to act as the membrane electrolyte in Li-ion batteries [34, 35]. Because of the copolymerization effect, PVDF-HFP has relatively low crystallinity. Hence, it contains more amorphous domains capable of trapping a large amount of liquid electrolytes [34]. For this reason, its superiority comparing to PTFE is that even though the active sites in the catalyst layer may be covered by PVDF-HFP, they are still capable to catalyze the electrochemical reactions, leading to a higher ECSA. In addition, the price of PVDF-HFP powder is $\$0.12 \text{ g}^{-1}$ [36], which is much cheaper than Nafion. Therefore, the cost of the fuel cell can be substantially reduced when used in the electrode fabrication. In this work, three

electrodes with different binders including PTFE, Nafion, and PVDF-HFP are prepared and then assembled into a DEGFC using acidified hydrogen peroxide as oxidant. It is found that the peak power densities achieved by PTFE, Nafion, and PVDF-HFP are 75.9, 105.5, and 120.0 mW cm⁻² at 60°C, respectively. Impressively, the fuel cell performance achieved by using the PVDF-HFP-based electrode as anode is even higher than that using the Nafion-based one. In addition, PVDF-HFP shows the lowest cost of \$0.18 kW⁻¹, while PTFE and Nafion possess the higher cost of \$0.80 kW⁻¹ and \$145.59 kW⁻¹, respectively. Considering the practical applications of DLFCs in portable electronics, electric vehicles, and stationary stations, PVDF-HFP can be the candidate to replace expensive Nafion functioning as the electrode binder, which meets the crucial requirement of low cost for worldwide commercialization.

3.2. Analysis of transport characteristics

In a DEGFC as shown in Figure 3.1, the mass transport of reactants, from the fuel reservoir through the flow field and then the porous diffusion layer to the porous catalyst layer, is mainly driven by the concentration gradient and pressure difference, in which the oxidation/reduction reaction will take place to consume the reactants, while the remaining will transport through the membrane reach the other electrode, wasting the utilization efficiency of reactants and even causing the mixed potential problem. In order to achieve the optimal fuel cell performance, therefore, the local concentrations of reactants in the catalyst layer should be at an appropriate level. For the conventional layer-by-layer electrode design, the CL formed by randomly stacking nanoparticles has smaller pore sizes, and thus a larger

transport resistance for reactant. Meanwhile, the removal of products is also a problem. As a result, the local concentration of reactants in the CL might be at an inadequate level, and the limited active sites might be covered by products, resulting in much lower performance. For the nickel foam-based three-dimensional electrode, the transport resistance for reactants and products are effectively reduced due to the large pores. Therefore, the performance can be improved, and the long-term stability can be enhanced.

3.3. Experiments

3.3.1. Preparation of the three-dimensional porous electrode

To prepare the Pd/C anodes, dip-coating method was applied, which has been reported in previous publication [41]. When Nafion was used as the binder, the catalyst ink was prepared by mixing 30 wt. % Pd/C (Sigma-Aldrich Co., USA) with 5 wt.% Nafion (Fuel Cell Store, USA) and ethanol, which serves as the binder and solvent, respectively. Then, the catalyst ink was stirred in an ultrasonic bath for 20 minutes to disperse it uniformly. Subsequently, the nickel foam (Hohsen Co., Japan) with designed shape was dipped in the catalyst ink for 1 min before withdrawing it from the ink. Afterwards, the nickel foam was dried in the air by a blower. These two steps were repeated continuously until reaching the required catalyst coating, which is $1.0 \text{ mg}_{\text{Pd}} \text{ cm}^{-2}$ for the anode. The preparation of the anode with 60 wt. % PTFE (Fuel Cell Store, USA) and PVDF-HFP (Solvay S. A., France) as binders adopted the same method except that acetone was used as the solvent for PVDF-HFP.

3.3.2. Cyclic voltammetry

Cyclic voltammetry (CV) tests were conducted in a three-electrode

electrochemical cell, where the fabricated electrode, the Pt foil, and the Hg-HgO (MMO, 1.0 M KOH) were used as the working electrode, the counter electrode and the reference electrode, respectively. The CV curves were recorded by an electrochemical workstation (PGSTAT302N). The potential window for the CV tests was from -1.126 to 0.074 V at a scan rate of 50 mV s^{-1} .

3.3.3. Preparation of the membrane electrode assembly

Three membrane electrode assemblies (MEAs) were prepared in this work with different binder materials on the anodes, including Nafion, PTFE and PVDF-HFP. The MEAs consist of three components: an anode, a cathode and a CEM with a thickness of 30 μm (Nafion 211). Both electrodes were in-house fabricated with the same active area of 1.0 $\text{cm} \times 1.0$ cm . The Au/C cathode was prepared by the spray method, which has been reported previously [42]. Firstly, 60 wt. % Au/C (Permetek Co., USA) was mixed with 15 wt. % Nafion and ethanol for the preparation of the catalyst ink. Subsequently, it was placed in an ultrasonic bath for 20 minutes. Lastly, the ink was sprayed onto the carbon cloth (Hesen, China), until a catalyst loading of 2.66 $\text{mg}_{\text{Au}} \text{cm}^{-2}$ on the cathode was achieved. The CEMs used in the MEAs were obtained by the following treatments [42]: (1) cut the original Nafion 211 membranes to the designed shape of 1.5 $\text{cm} \times 1.5$ cm , (2) immerse the membranes into an aqueous solution of 2.5 M KOH, (3) heat up the solution to 80°C for 1 h, and (4) use DI water to rinse the membranes for several times and store them in DI water before the fuel cell assembly.

3.3.4. Fuel cell setup and instrumentation

The whole fuel cell was assembled by fixing the MEA in between an anode plate and a cathode plate. The material of the plates is 316L stainless steel to avoid the corrosion problem caused by the anolyte and catholyte. In addition, flow fields were grooved on both plates with a single serpentine shape. The flow fields have a width of 1.0 mm and a depth of 0.5 mm. The electrolytes on anode and cathode were fed into the flow fields by utilizing two peristaltic pumps with a flow rate of 2 mL min⁻¹. The electrochemical impedance spectra (EIS) test was conducted with a CHI 605C (CH Instruments, China). Moreover, to examine the effects of the operating temperatures on the cell performance, two electrical heating rods were used to heat up the cell, and the temperature was measured and controlled by a thermocouple and a temperature controller, respectively. To evaluate the fuel cell performance, an Arbin BT2000 (Arbin Instrument Inc.) was utilized to measure the polarization curves.

3.4. Results and discussion

3.4.1. Characterization of as-prepared electrodes

Figure 3.2 shows the general performance of the fuel cell fed with anolyte containing 1.0 M EG and 1.0 M KOH and catholyte containing 1.0 M H₂O₂ and 1.0 M H₂SO₄, both of which are at a flow rate of 2 mL min⁻¹, running with three home-made electrodes using different binders at room temperature with pretreated Nafion 211 membrane as the CEM. It is seen that the fuel cell using PVDF-HFP as the electrode binder showed the highest voltage over the whole current density region, followed by the Nafion binder, and the fuel cell using the PTFE binder output the worst cell voltage. The OCVs of PVDF-HFP and Nafion were similar at around 1.18

V, while the OCV of PTFE was a little lower at around 1.14 V. In addition, the peak power densities achieved by the PVDF-HFP, Nafion, and PTFE were 31.9, 27.5, and 20.8 mW cm⁻², respectively. Therefore, among three electrode binders, PVDF-HFP is the best choice to be applied in alkaline-acid DEGFCs as an electrode binder, which is not only due to the highest power output, but also the lowest price as compared previously.

To find the reasons why PVDF-HFP performs better than Nafion and PTFE, CV tests and scanning electron microscope (SEM) characterizations are implemented for the fabricated electrodes and SEM tests are conducted for the binders at dry state as well. Pd on carbon system exhibits a poor definition of the hydrogen region, so the adsorption and desorption of hydrogen to determine the ECSA is not an appropriate method. Therefore, the quantity of electricity used in the reduction of palladium oxide formed over the top layer of the Pd particles, probably as a form of PdO, is employed in calculating the ECSA. A charge value of 405 μC cm⁻² is assumed for the reduction of PdO monolayer. Figure 3.3 shows the CV curves of three electrodes in 1.0 M KOH solution at a scan rate of 50 mV s⁻¹. It can be seen that the electrode with PVDF-HFP as the binder possessed the highest peak area of the reduction of PdO ranging from -0.8 to -0.2 V, indicating that the electrode with PVDF-HFP yielded the largest ECSA. The ECSA can be calculated by the PdO reduction charge in the CV curves as shown in Equation (4):

$$\text{ECSA} = \frac{Q}{q_m} \quad (4)$$

where Q is the coulombic charge, q is the charge value of 405 μC cm⁻² for

the reduction of PdO monolayer, and m is the Pd loading on the electrode [43, 44]. Based on the equation, the ECSAs of the three electrodes with PVDF-HFP, Nafion, and PTFE are 24.10, 18.62, and 16.44 $\text{m}^2 \text{g}^{-1}$, respectively. Hence, the remarkable performance of PVDF-HFP is attributed to the higher ECSA, which provides more active sites for the EGOR. Figures 3.4, 3.5, and 3.6 show the SEM images of the PVDF-HFP, Nafion, and PTFE at dry state, respectively. It is found that the PVDF-HFP tends to form a porous structure with small particles accumulation together. In contrast, the Nafion tends to form a film structure with a smooth surface. The roughness of the PTFE is in between the PVDF-HFP and Nafion. Therefore, it can be inferred from the structures that Nafion tends to be clad on the catalyst nanoparticles when used as the binder in the electrode fabrication, thus the ECSA is decreased significantly. When PVDF-HFP is employed as the binder, it tends to adhere the catalyst nanoparticles onto the nickel foam skeleton but not to cover the catalyst nanoparticles, so that the PVDF-HFP-based electrode has the highest ECSA [28]. Although the PTFE-based electrode is supposed to have the higher ECSA than the Nafion-based electrode according to the morphology of the binders at dry state, the Nafion-based electrode actually possesses the higher ECSA. This abnormal phenomenon can be explained as follows. As Nafion is permeable to reactants [29], the active sites covered by Nafion are still accessible to the reactants, indicating that the total active sites of the Nafion-based electrode having the catalytic ability include not only the uncovered active sites but also a number of active sites covered by the binder. In addition, the reactants are not able to penetrate the PTFE binder, so the total active sites

of the PTFE-based electrode are merely the uncovered active sites. As a result, the additional active sites of the Nafion-based electrode compensate the disparity between the Nafion-based electrode and the PTFE-based electrode, leading to the higher ECSA of the Nafion-based electrode.

EIS is a widely used method to quantify the different processes in the fuel cell, such as ohmic resistance, charge transfer resistance, and mass-transport resistance. When the frequency is in high region, the change of input current signal is so quick that mass transport cannot occur in time, so the faster charge transport is dominated. When the frequency is decreasing, the change of input current signal is slow, so the mass-transport resistance will occur due to the long relaxation time of the mass-transport being met. The total resistance combines the R_{Ω} , R_{ct} and Z_w . The R_{Ω} and R_{ct} will be fixed as the half circle shows, while the mass transport resistance will increase with decreasing frequency, so mass transport dominates in low frequency region. Figure 3.7 shows Nyquist plots of the present fuel cell using three different electrodes at room temperature. The ohmic resistance and charge transfer resistance dominate in the high-frequency region, while the mass transport resistance dominates in the low-frequency region [45].

It is found that the arcs of the impedance spectra in high-frequency region are similar, suggesting that the charge transfer resistances of fuel cells using these three electrodes are near. It also can be seen from the intersections of the curves and horizontal axis that the PVDF-HFP-based electrode possesses the lowest ohmic resistance, followed by the Nafion-based electrode, and the PTFE-based electrode results in the largest ohmic

resistance. This observation also accounts for the fuel cell performance variations. Due to the lowest ohmic resistance, the PVDF-HFP-based electrode yields the best fuel cell performance.

3.4.2. Fuel cell performance

Figure 3.8 shows the polarization and power density curves of fuel cells with three different electrodes at the previously optimized reactant-feeding concentrations, *i.e.* 1.0 M EG and 5.0 M KOH in the anolyte and 4.0 M H₂O₂ and 1.0 M H₂SO₄ in the catholyte, at room temperature. Comparing to the cell performance fed with 1.0 M EG and 1.0 M KOH in the anolyte and 1.0 M H₂O₂ and 1.0 M H₂SO₄ in the catholyte, the cell performance with three binders all shows great improvements in OCVs, maximum current densities, and peak power densities. It is seen that the OCV of the cell using PTFE binder increases from 1.14 V to 1.31 V and the OCVs of the cells with PVDF-HFP and Nafion increase from 1.18 V to 1.39 V and 1.18 V to 1.38 V, respectively. In addition, the increases in maximum current densities of the PVDF-HFP, Nafion, and PTFE are 25, 10, and 30 mA cm⁻², respectively. Due to the elevations in both the cell voltage and current densities, the peak power densities boost significantly from 31.9 to 57.0 mW cm⁻² with PVDF-HFP binder, from 27.4 to 46.1 mW cm⁻² with Nafion binder, and from 20.8 to 39.9 mW cm⁻² with PTFE binder. This performance improvement can be explained as follows. For the specific anode and cathode, the concentrations of reactants in the CLs have the dominant effect on the reaction kinetics. As the reactant-feeding concentrations are low, the reactant concentrations in the CLs are at starvation state, thus the reaction kinetics is sluggish. When the reactant

concentrations increase, the delivery of the reactants from the flow field through the DL to the CL is enhanced, which is derived from the higher concentration gradient. As a result, the reactant concentrations in the CLs transfer from the starvation state to the saturation state, hence the reaction kinetics is enhanced.

Figure 3.9 shows the polarization and power density curves of fuel cells with three different electrodes fed with 1.0 M EG and 1.0 M KOH in the anolyte and 1.0 M H₂O₂ and 1.0 M H₂SO₄ in the catholyte at 60°C. It is found that the cell performance with three binders all has conspicuous enhancement in OCVs, maximum current densities, as well as peak power densities. It is seen that the OCV of the cell using PTFE binder increases from 1.14 V to 1.23 V and the OCVs of the cells with PVDF-HFP and Nafion increase from 1.18 V to 1.24 V and 1.18 V to 1.22 V, respectively. Meanwhile, the increases in maximum current densities of the PVDF-HFP, Nafion, and PTFE are 25, 15, and 25 mA cm⁻², respectively. In addition, the peak power densities increase dramatically from 31.9 to 56.3 mW cm⁻² with PVDF-HFP binder, from 27.4 to 42.1 mW cm⁻² with Nafion binder, and from 20.8 to 28.5 mW cm⁻² with PTFE binder. The impressive improvement in the fuel cell performance is attributed to the elevated operating temperature, which can be illustrated by three reasons Firstly, increasing the operating temperature enhances the reaction kinetics of the EGOR in the anode and the HPRR in the cathode simultaneously, which lowers the activation loss. Secondly, the mobility of electrons and diffusivity of reactants are promoted with at higher operating temperatures, leading to the fact that the reactants can reach the active sites on the CLs more efficiently,

thus the concentration loss is reduced. Lastly, as the operating temperature increases, the viscosity of the anolyte and catholyte decreases and the conductivity of CEMs increases, which reduces the ohmic loss. Therefore, the fuel cell yields a better performance at higher operating temperatures due to the decreases in activation loss, concentration loss, and ohmic loss. Figure 3.10 shows the polarization and power density curves of fuel cells with three different electrodes at the reactant-feeding concentrations of 1.0 M EG and 5.0 M KOH in the anolyte and 1.0 M H₂O₂ and 4.0 M H₂SO₄ in the catholyte at 60°C. It is found that the best cell performance in OCVs, maximum current densities, and peak power densities is achieved combining the increased reactant-feeding concentrations and higher operating temperature. It is shown that the OCVs of the cell using PVDF-HFP, Nafion, and PTFE are 1.47 V, 1.46 V, and 1.45 V, respectively. Meanwhile, the maximum current densities of the PVDF-HFP, Nafion, and PTFE show great improvements, which are 300, 220, and 195 mA cm⁻², respectively. In addition, comparing to the fuel cell performance fed with 1.0 M EG and 1.0 M KOH in the anolyte and 1.0 M H₂O₂ and 1.0 M H₂SO₄ in the catholyte at room temperature, the peak power densities increase dramatically from 31.9 to 120.0 mW cm⁻² with PVDF-HFP binder, from 27.4 to 105.5 mW cm⁻² with Nafion binder, and from 20.8 to 75.9 mW cm⁻² with PTFE binder. The tremendous enhancement in power densities is attributed to the positive effects brought by increasing reactant-feeding concentrations and operating temperature. The maximum peak power density of 120.0 mW cm⁻² is 48.3% higher than that achieved in our previous publication (80.9 mW cm⁻²) [25]. The only difference is the

fabrication method of the electrode, which is dip-coating method rather than the brushing method, suggesting that the dip-coating method is superior than the brushing method when nickel foam is used as the backing layer. The reasons can be summarized as follows. For the same catalyst loading, the CL formed on the surface of nickel foam by the brushing method is much thicker and denser, which may result in large agglomerates lowering the catalyst utilization efficiency. Conversely, the CL formed on the skeleton of nickel foam by the dip-coating method is much thinner and sparser, which improves the catalyst utilization efficiency, thus the ECSA of the electrode using the dip-coating method is higher than that using the brushing method [41]. Moreover, the dense CL formed by the brushing method has the low porosity and small pore size, resulting in a low permeability and high transport resistance, while the electrode using the dip-coating method has the higher porosity and larger open pores, thus the permeability is higher. Hence, mass transport is enhanced through the porous electrode using the dip-coating method, reducing the fuel cell resistance [44].

3.4.3. Constant-current discharging behavior

Figure 3.11 demonstrates the transient discharging behavior of the fuel cell using the PVDF-HFP-based and Nafion-based electrodes fed with 1.0 M EG and 5.0 M KOH in the anolyte and 1.0 M H₂O₂ and 4.0 M H₂SO₄ in the catholyte at 60°C. It is indicated that the fuel cell using PVDF-HFP-based electrode exhibits a stable output voltage around 0.8 V with acceptable fluctuations for 100 h at a discharging current density of 100 mA cm⁻². The voltage fluctuation may be attributed to the decomposition of H₂O₂ and thus

generation of O₂, forming a two-phase flow in the cathode flow channel. It creates a large transport resistance of H₂O₂ from the cathode flow channel to the cathode CL [46]. The stable running time of the fuel cell is twenty times as long as the fuel cell using the sprayed electrode (5 h) [25], which is attributed to the dip-coated electrode having the higher porosity and larger open pores, thus the efficient reactant-feeding and product-removing are achieved, contributing to stabilizing the cell voltage. The outstanding stability indicates that this DEGFC with the PVDF-HFP-based electrode fabricated using the dip-coating method possesses the potential for future practical applications. Although the voltage of Nafion electrode is higher than the PVDF-HFP-based electrode at the initial 20 h, the Nafion-based electrode experiences an obvious voltage degradation at the rest 80h, while the PVDF-HFP-based electrode shows a rather stable voltage at the same discharging current density. It implies that PVDF-HFP-based electrode has a longer life-time in this fuel cell.

3.4.4. Cost estimation

Table 3-1 shows the cost estimation and comparison of three electrode binders in the fuel cell and the cost is evaluated according to the equation (5):

$$C = \frac{1000 \times 1000 \times UP \times m}{PP} \quad (5)$$

where C is the cost of the electrode binder in the fuel cell normalized by power output, UP is the unite price of the binder, m is the mass of the used binder, and PP is the peak power generated by the fuel cell with the electrode binder obtained previously. It is seen that PVDF-HFP shows the

lowest cost of \$0.18 kW⁻¹, while PTFE and Nafion possess the higher cost of \$0.80 kW⁻¹ and \$145.59 kW⁻¹, respectively. The significant reduction in cost is attributed the lower unit price of PVDF-HFP and the higher peak power achieved by the fuel cell using PVDF-HFP as the electrode binder.

3.5. Summary

In this work, the cost-effective poly(vinylidene fluoride-co-hexafluoropropylene) is used to replace the conventional and expensive Nafion and polytetrafluoroethylene as the binder in the electrode fabrication. The home-made electrodes using these binders are characterized via cyclic voltammetry and scanning electron microscope. In addition, they are assembled into an alkaline-acid direct ethylene glycol fuel cell and evaluated in terms of the fuel cell performance. The results show that the ECSAs of the electrodes with PVDF-HFP, Nafion, and PTFE are 24.10, 18.62, and 16.44 m² g⁻¹, respectively. It is because PVDF-HFP tends to adhere the catalyst nanoparticles onto the nickel foam skeleton but not to cover the catalyst nanoparticles, thus the PVDF-HFP-based electrode has the highest ECSA. In performance tests, the fuel cell using the PVDF-HFP-based electrode exhibits the best performance of an open-circuit voltage of 1.47 V, a maximum current density of 300 mA cm⁻², and a peak power density of 120.0 mW cm⁻² with 1.0 M EG and 5.0 M KOH in the anolyte and 4.0 M H₂O₂ and 1.0 M H₂SO₄ in the catholyte at 60°C. Comparing to the cell performance with conventional Nafion and polytetrafluoroethylene as the electrode binder, the peak power density shows an improvement of 13.7% and 58.1%, respectively. The impressive improvement is attributed to the higher ECSA due to its intrinsic porous property, contributing to the

enhancement in the reaction kinetics. It is found that PVDF-HFP shows the lowest cost of \$0.18 kW⁻¹, while PTFE and Nafion possess the higher cost of \$0.80 kW⁻¹ and \$145.59 kW⁻¹, respectively. The significant reduction in cost is attributed the lower unit price of PVDF-HFP and the higher peak power achieved by the fuel cell using PVDF-HFP as electrode binder.

3.6. References

- [1] Z.F. Pan, L. An, T.S. Zhao, Z.K. Tang, Advances and challenges in alkaline anion exchange membrane fuel cells, *Progress in Energy and Combustion Science* 66 (2018) 141-175.
- [2] L. An, T. Zhao, *Anion Exchange Membrane Fuel Cells*, (2018).
- [3] Z.F. Pan, L. An, C.Y. Wen, Recent advances in fuel cells based propulsion systems for unmanned aerial vehicles, *Applied Energy* 240 (2019) 473-485.
- [4] X. Sun, Y. Li, Understanding mass and charge transports to create anion-ionomer-free high-performance alkaline direct formate fuel cells, *International Journal of Hydrogen Energy* 44 (2019) 7538-7543.
- [5] J. Larminie, A. Dicks, M.S. McDonald, *Fuel cell systems explained*, J. Wiley Chichester, UK, 2003.
- [6] Y. Li, Y. Feng, X. Sun, Insight into Interface Behaviors to Build Phase-Boundary-Matched Na-Ion Direct Liquid Fuel Cells, *ACS Sustainable Chemistry & Engineering* 6 (2018) 12827-12834.
- [7] Q.X. Wu, Z.F. Pan, L. An, Recent advances in alkali-doped polybenzimidazole membranes for fuel cell applications, *Renewable and Sustainable Energy Reviews* 89 (2018) 168-183.
- [8] X. Sun, Y. Li, M.-J. Li, Highly Dispersed Palladium Nanoparticles on Carbon-Decorated Porous Nickel Electrode: An Effective Strategy to Boost Direct Ethanol Fuel Cell up to 202 mW cm⁻², *ACS Sustainable Chemistry & Engineering* 7 (2019) 11186-11193.
- [9] D.R. Dekel, Review of cell performance in anion exchange membrane fuel cells, *Journal of Power Sources* 375 (2018) 158-169.

-
- [10] Q. Wu, H. Li, W. Yuan, Z. Luo, F. Wang, H. Sun, X. Zhao, H. Fu, Performance evaluation of an air-breathing high-temperature proton exchange membrane fuel cell, *Applied Energy* 160 (2015) 146-152.
- [11] N. Mahato, A. Banerjee, A. Gupta, S. Omar, K. Balani, Progress in material selection for solid oxide fuel cell technology: A review, *Progress in Materials Science* 72 (2015) 141-337.
- [12] X. Zhao, W. Yuan, Q. Wu, H. Sun, Z. Luo, H. Fu, High-temperature passive direct methanol fuel cells operating with concentrated fuels, *Journal of Power Sources* 273 (2015) 517-521.
- [13] A. Kulkarni, S. Siahrostami, A. Patel, J.K. Nørskov, Understanding Catalytic Activity Trends in the Oxygen Reduction Reaction, *Chemical Reviews* 118 (2018) 2302-2312.
- [14] A.A. Gewirth, J.A. Varnell, A.M. DiAscro, Nonprecious Metal Catalysts for Oxygen Reduction in Heterogeneous Aqueous Systems, *Chemical Reviews* 118 (2018) 2313-2339.
- [15] J.A. Turner, Sustainable Hydrogen Production, *Science* 305 (2004) 972.
- [16] U.B. Demirci, Direct liquid-feed fuel cells: Thermodynamic and environmental concerns, *Journal of Power Sources* 169 (2007) 239-246.
- [17] Q.X. Wu, T.S. Zhao, R. Chen, L. An, A sandwich structured membrane for direct methanol fuel cells operating with neat methanol, *Applied Energy* 106 (2013) 301-306.
- [18] Z.F. Pan, R. Chen, L. An, Y.S. Li, Alkaline anion exchange membrane fuel cells for cogeneration of electricity and valuable chemicals, *Journal of Power Sources* 365 (2017) 430-445.

-
- [19] J. Jiang, Y. Li, J. Liang, W. Yang, X. Li, Modeling of high-efficient direct methanol fuel cells with order-structured catalyst layer, *Applied Energy* 252 (2019) 113431.
- [20] H. Yue, Y. Zhao, X. Ma, J. Gong, Ethylene glycol: properties, synthesis, and applications, *Chemical Society Reviews* 41 (2012) 4218-4244.
- [21] Z. Pan, Y. Bi, L. An, Mathematical modeling of direct ethylene glycol fuel cells incorporating the effect of the competitive adsorption, *Applied Thermal Engineering* 147 (2019) 1115-1124.
- [22] L. An, R. Chen, Recent progress in alkaline direct ethylene glycol fuel cells for sustainable energy production, *Journal of Power Sources* 329 (2016) 484-501.
- [23] L. An, T.S. Zhao, S.Y. Shen, Q.X. Wu, R. Chen, Performance of a direct ethylene glycol fuel cell with an anion-exchange membrane, *International Journal of Hydrogen Energy* 35 (2010) 4329-4335.
- [24] L. An, L. Zeng, T.S. Zhao, An alkaline direct ethylene glycol fuel cell with an alkali-doped polybenzimidazole membrane, *International Journal of Hydrogen Energy* 38 (2013) 10602-10606.
- [25] Z. Pan, B. Huang, L. An, Performance of a hybrid direct ethylene glycol fuel cell, *International Journal of Energy Research* 43 (2019) 2583-2591.
- [26] Z. Pan, Y. Bi, L. An, Performance characteristics of a passive direct ethylene glycol fuel cell with hydrogen peroxide as oxidant, *Applied Energy* 250 (2019) 846-854.

-
- [27] Z. Pan, H. Zhuang, Y. Bi, L. An, A direct ethylene glycol fuel cell stack as air-independent power sources for underwater and outer space applications, *Journal of Power Sources* 437 (2019) 226944.
- [28] Y.S. Li, T.S. Zhao, Z.X. Liang, Effect of polymer binders in anode catalyst layer on performance of alkaline direct ethanol fuel cells, *Journal of Power Sources* 190 (2009) 223-229.
- [29] L. An, T.S. Zhao, L. Zeng, Agar chemical hydrogel electrode binder for fuel-electrolyte-fed fuel cells, *Applied Energy* 109 (2013) 67-71.
- [30] F. Zhang, G. Chen, M.A. Hickner, B.E. Logan, Novel anti-flooding poly(dimethylsiloxane) (PDMS) catalyst binder for microbial fuel cell cathodes, *Journal of Power Sources* 218 (2012) 100-105.
- [31] L.J.I.J.E.S. Fang, The Preparation and Electrochemical Properties of Perovskite $\text{La}_{0.6}\text{Sr}_{0.4}\text{CoO}_3$ -d for Catalytic Reduction of Oxygen, 12 (2017) 218-229.
- [32] N.A. Choudhury, J. Ma, Y. Sahai, R.G. Buchheit, High performance polymer chemical hydrogel-based electrode binder materials for direct borohydride fuel cells, *Journal of Power Sources* 196 (2011) 5817-5822.
- [33] Y. Luo, C. Jin, Z. Wang, M. Wei, C. Yang, R. Yang, Y. Chen, M. Liu, A high-performance oxygen electrode for Li-O₂ batteries: Mo₂C nanoparticles grown on carbon fibers, *Journal of Materials Chemistry A* 5 (2017) 5690-5695.
- [34] W. Pu, X. He, L. Wang, C. Jiang, C. Wan, Preparation of PVDF-HFP microporous membrane for Li-ion batteries by phase inversion, *Journal of Membrane Science* 272 (2006) 11-14.

-
- [35] R. Miao, B. Liu, Z. Zhu, Y. Liu, J. Li, X. Wang, Q. Li, PVDF-HFP-based porous polymer electrolyte membranes for lithium-ion batteries, *Journal of Power Sources* 184 (2008) 420-426.
- [36] H. Beyer, M. Metzger, J. Sicklinger, X. Wu, K.U. Schwenke, H.A. Gasteiger, Antimony Doped Tin Oxide–Synthesis, Characterization and Application as Cathode Material in Li-O₂Cells: Implications on the Prospect of Carbon-Free Cathodes for Rechargeable Lithium-Air Batteries, *Journal of The Electrochemical Society* 164 (2017) A1026-A1036.
- [37] L. An, T.S. Zhao, R. Chen, Q.X. Wu, A novel direct ethanol fuel cell with high power density, *Journal of Power Sources* 196 (2011) 6219-6222.
- [38] S.S. Munjewar, S.B. Thombre, R.K. Mallick, Approaches to overcome the barrier issues of passive direct methanol fuel cell – Review, *Renewable and Sustainable Energy Reviews* 67 (2017) 1087-1104.
- [39] S.P.S. Badwal, S. Giddey, A. Kulkarni, J. Goel, S. Basu, Direct ethanol fuel cells for transport and stationary applications – A comprehensive review, *Applied Energy* 145 (2015) 80-103.
- [40] L. An, R. Chen, Direct formate fuel cells: A review, *Journal of Power Sources* 320 (2016) 127-139.
- [41] Y.S. Li, T.S. Zhao, A high-performance integrated electrode for anion-exchange membrane direct ethanol fuel cells, *International Journal of Hydrogen Energy* 36 (2011) 7707-7713.
- [42] L. An, T.S. Zhao, Performance of an alkaline-acid direct ethanol fuel cell, *International Journal of Hydrogen Energy* 36 (2011) 9994-9999.

-
- [43] Y. Li, J. Lv, Y. He, A Monolithic Carbon Foam-Supported Pd-Based Catalyst towards Ethanol Electro-Oxidation in Alkaline Media, *Journal of The Electrochemical Society* 163 (2016) F424-F427.
- [44] Y. Li, Y. He, An All-in-One Electrode for High-Performance Liquid-Feed Micro Polymer Electrolyte Membrane Fuel Cells, *Journal of The Electrochemical Society* 163 (2016) F663-F667.
- [45] M.E. Orazem, B.J.N.J. Tribollet, *Electrochemical impedance spectroscopy*, (2008).
- [46] T.S. Zhao, C. Xu, R. Chen, W.W. Yang, Mass transport phenomena in direct methanol fuel cells, *Progress in Energy and Combustion Science* 35 (2009) 275-292.

Figures

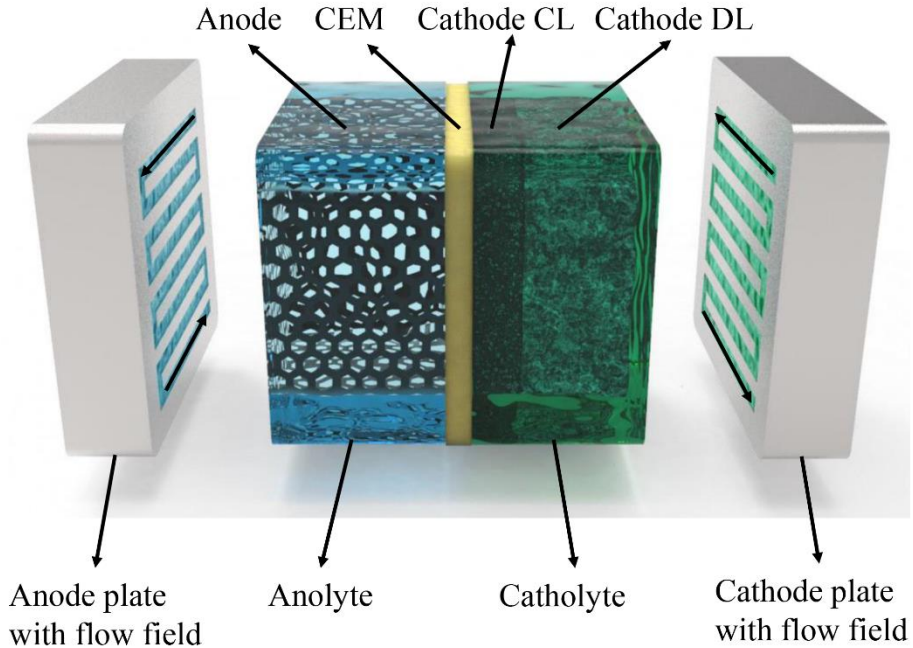


Figure 3.1 Schematic of the an active alkaline-acid direct ethylene glycol fuel cell using a three-dimensional electrode.

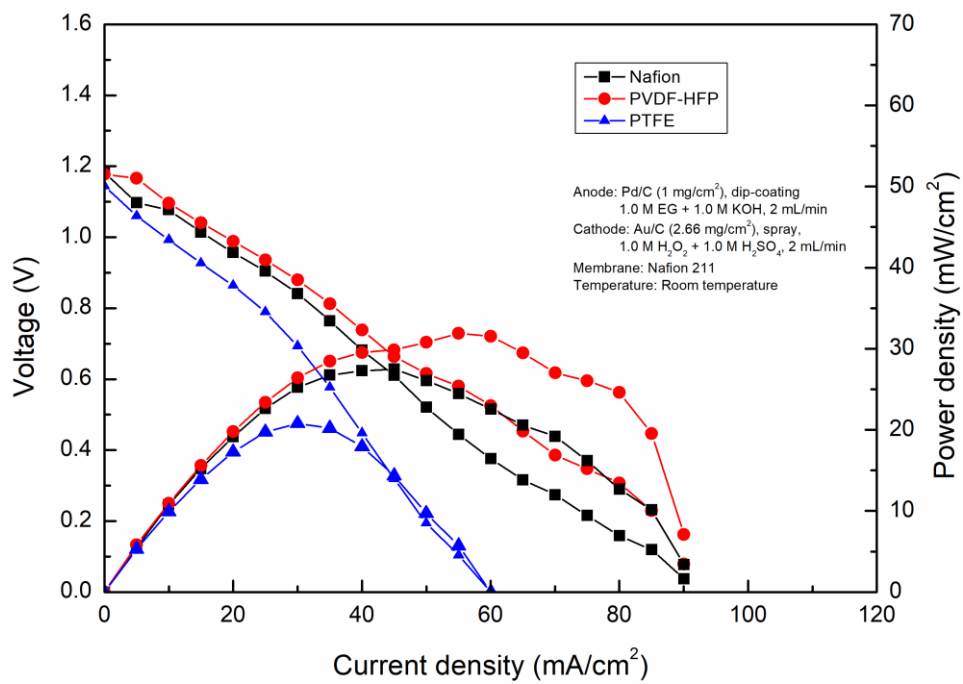


Figure 3.2 Fuel cell performances achieved by using different binders at room temperature.

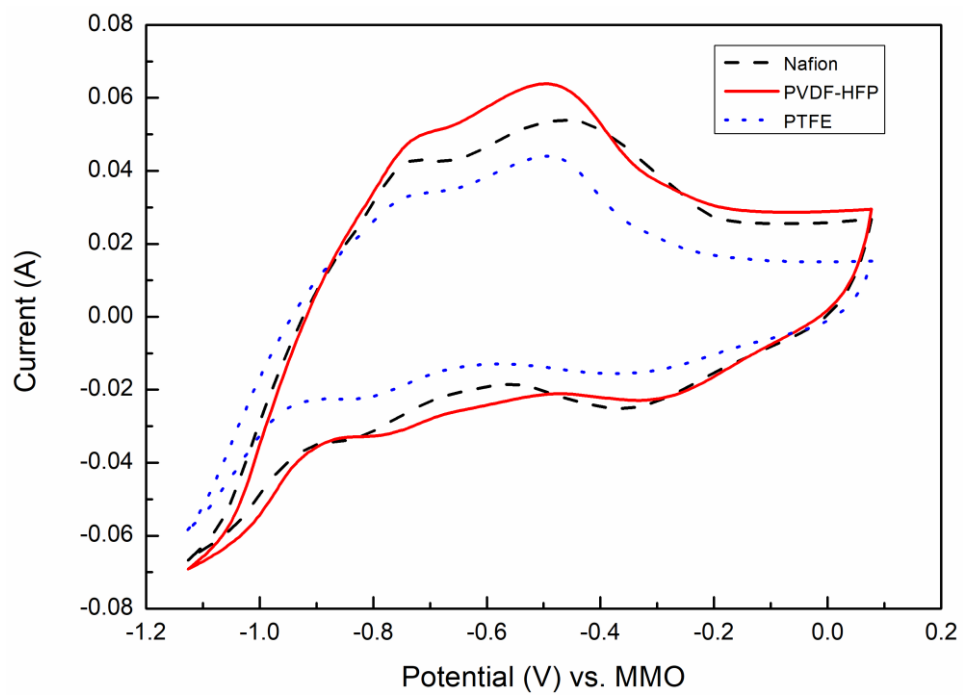


Figure 3.3 CV curves in 1.0 M KOH at a scan rate of 50 mV s⁻¹.

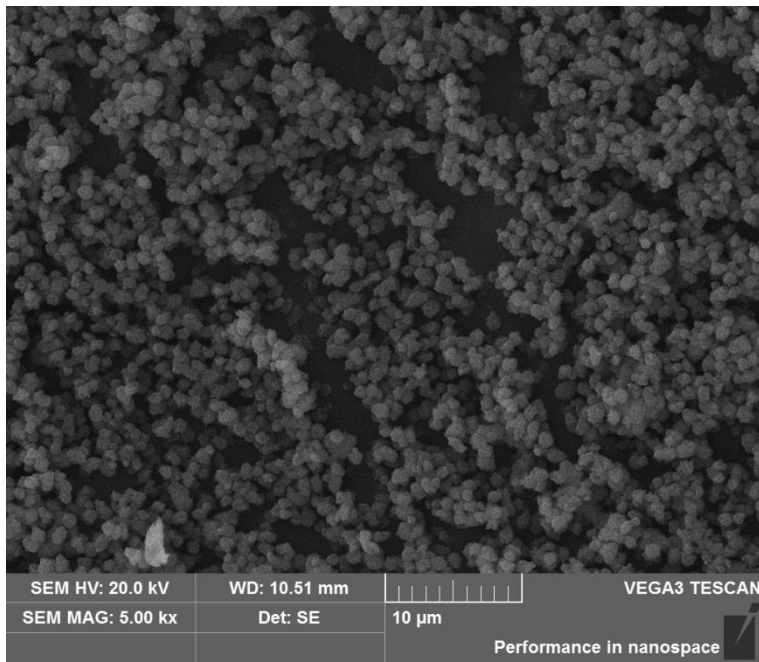


Figure 3.4 SEM image of the PVDF-HFP at dry state.

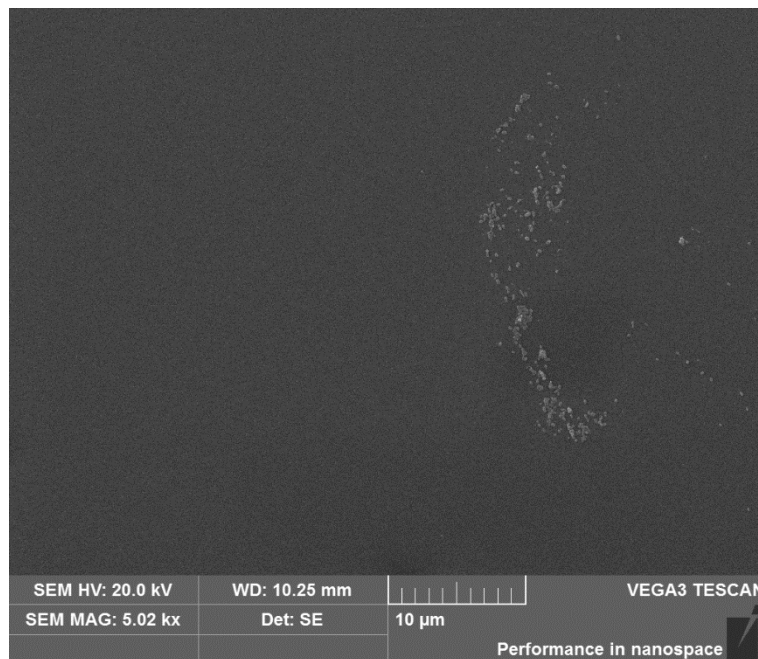


Figure 3.5 SEM image of the Nafion at dry state.

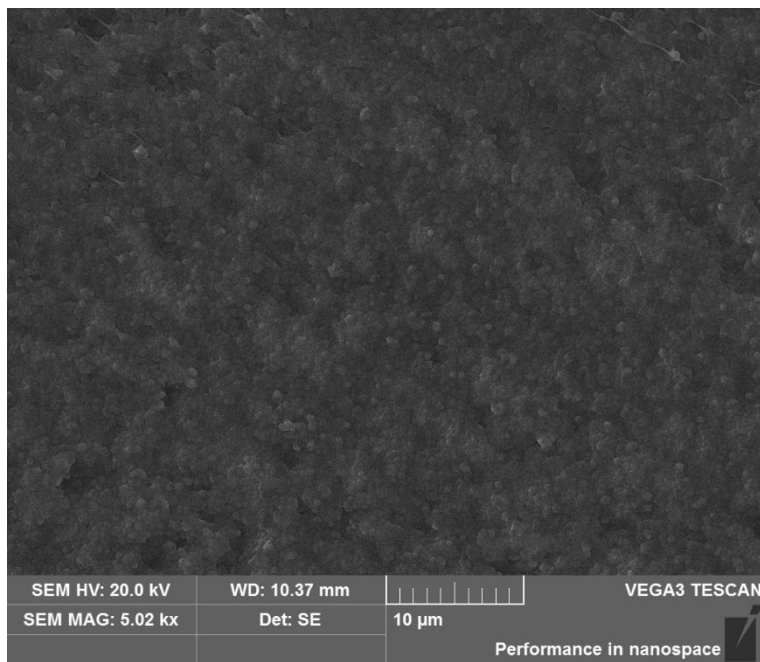


Figure 3.6 SEM image of the PTFE at dry state.

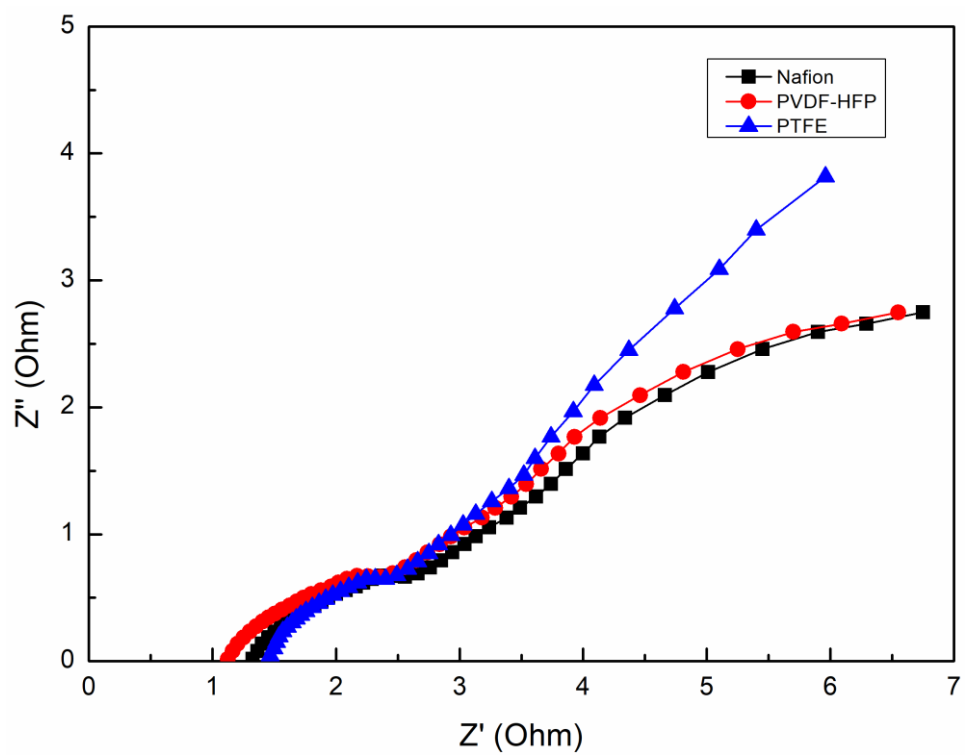


Figure 3.7 Nyquist plots of three different electrodes at room temperature.

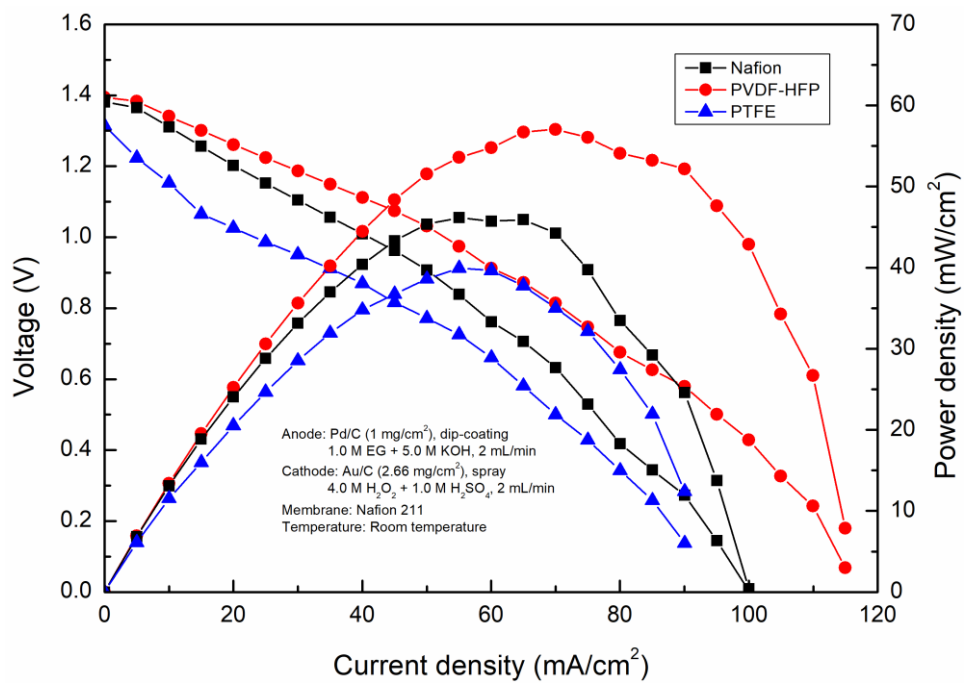


Figure 3.8 Polarization and power density curves achieved by using three different electrodes at room temperature.

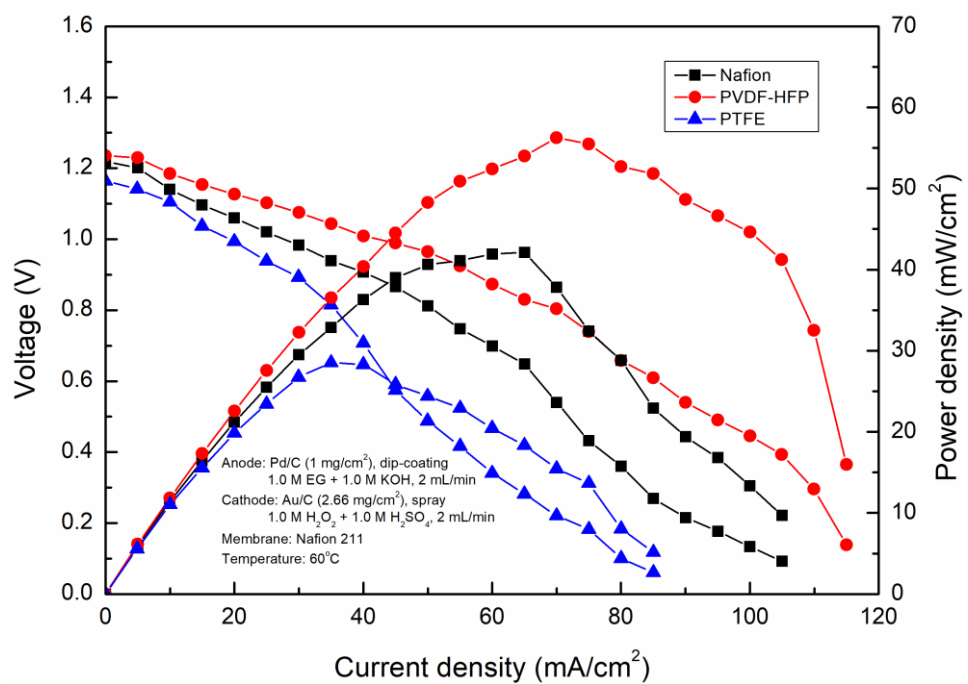


Figure 3.9 Polarization and power density curves achieved by using three different electrodes at 60°C.

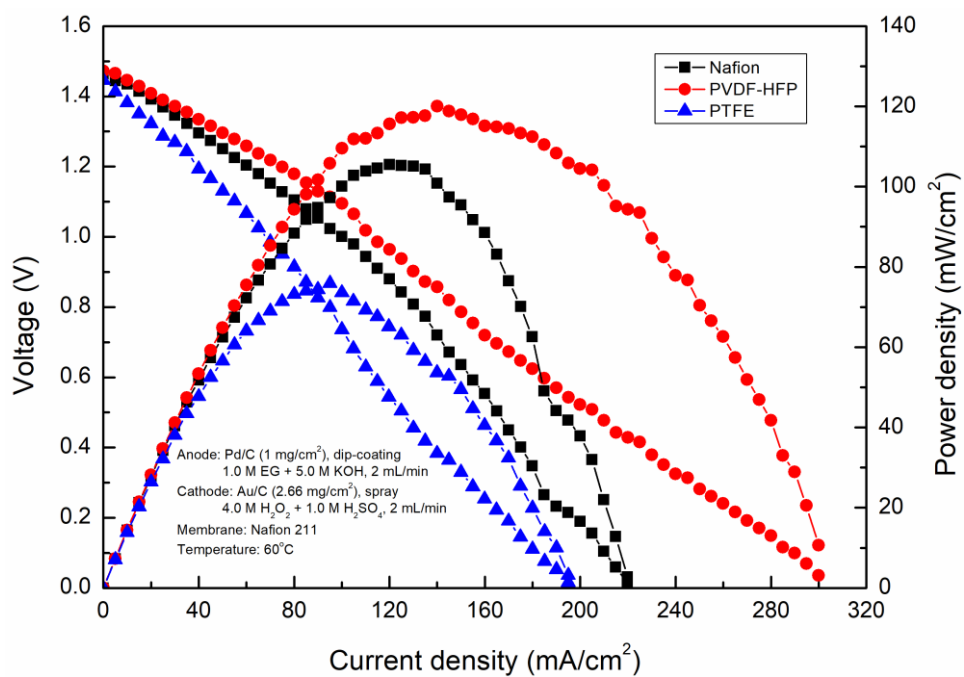


Figure 3.10 Polarization and power density curves achieved by using three different electrodes at 60°C.

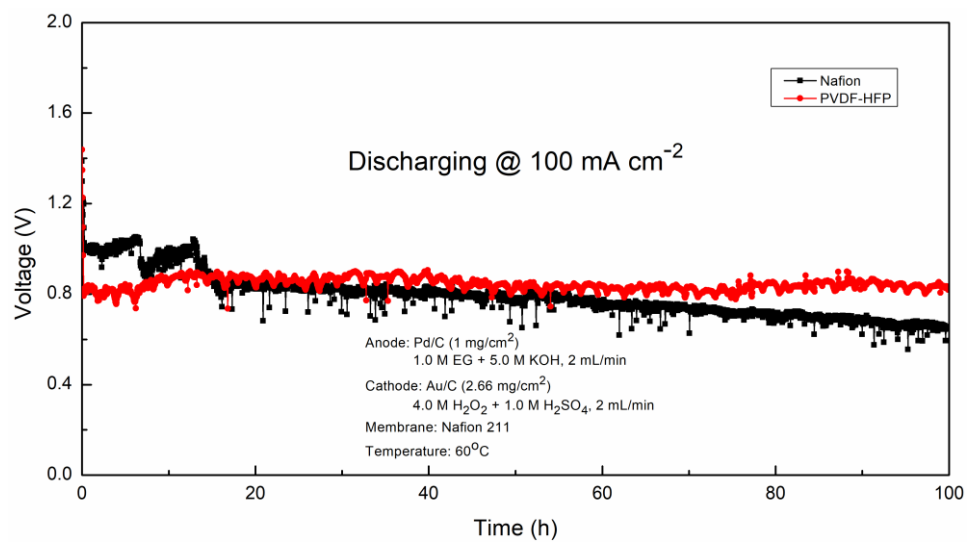


Figure 3.11 Constant-current discharging behavior of the fuel cell fabricated with the PVDF-HFP-based and Nafion-based electrodes at 60°C .

Table

Table 3-1 Cost estimation of three electrode binders.

| Binder | Unit price | Mass | Peak power | Cost |
|-----------------------------|---------------------------------|-----------------------------|-------------|---------------------------|
| PVDF-HFP (Powder) | \$0.12 g ⁻¹ [29] | 1.75×10^{-4} g | 120.0 mW | \$0.18 kW ⁻¹ |
| 5 wt.% Nafion (Solution) | \$4 mL ⁻¹ [24] | 3.84×10^{-3} mL | 105.5 mW | \$145.59 kW ⁻¹ |
| 60 wt.% PTFE (Solution) | \$0.31 mL ⁻¹ [26] | 1.95×10^{-4} mL | 75.9 mW | \$0.80 kW ⁻¹ |

Chapter 4 Performance characteristics of an active fuel cell

Abstract

In this work, a hybrid direct ethylene glycol fuel cell is developed and tested, which is composed of an alkaline anode, an acid cathode, and a cation exchange membrane. In this fuel cell, ethylene glycol and hydrogen peroxide serve as fuel and oxidant, respectively. Theoretically, this fuel cell exhibits a theoretical voltage reaching 2.47 V, whereas it is experimentally demonstrated that the hybrid fuel cell delivers an open-circuit voltage of 1.41 V at 60°C. More impressively, this fuel cell yields a peak power density of 80.9 mW cm⁻² (115.3 mW cm⁻² at 80°C). Comparing to an open-circuit voltage of 0.86 V and a peak power density of 67 mW cm⁻² previously achieved by an ethylene glycol fuel cell operating with oxygen, this hybrid ethylene glycol fuel cell boosts the open-circuit voltage by 62.1% and the peak power density by 20.8%. This significant improvement is mainly attributed not only to the high-voltage output of this hybrid system design, but also to the faster kinetics rendered by the reduction reaction of hydrogen peroxide.

Keywords: Fuel cells; Direct ethylene glycol fuel cell; Hydrogen peroxide; Operation parameters; Power density

4.1. Introduction

Fuel cells, which are alternative choices for power supply sources, have attracted extensive research interest due to its potential to be an efficient and clean energy conversion technology [1-8]. Currently, hydrogen, methanol, ethanol, and formate are four of the most common fuels utilized in fuel cells [9-15]. Among them, the source, transport, and storage of hydrogen are still remaining to be solved for widespread application. In addition, since the gaseous hydrogen has to be compressed into liquid phase to reduce the device volume, the high pressure may lead to a potential safety problem [16]. As for methanol, severe fuel crossover can result in dramatic performance degradation [17]. As for ethanol, the C-C bond is hardly broken in fuel cells running at low temperatures (generally $< 60^{\circ}\text{C}$), leading to a low electron transfer rate (i.e., 33%) [16, 18]. Ethylene glycol (EG), an alternative choice for fuel, has received considerable interest for mobile, stationary, and portable applications, resulting from its promising theoretical energy capacity of 4.8 Ah mL^{-1} , high boiling point of 198°C , and outstanding efficiency of electric power conversion [19]. Hence, the use of liquid EG not only avoids the poisoning and safety problems, but also possesses an electron transfer rate as high as 80% [20].

On the cathode, pure oxygen and air are used as oxidant in most cases [20, 21]. On one hand, the pure oxygen needs to be compressed and stored in a tank particularly, which not only makes the fuel cell system bulkier, but also increases the system design complexity. On the other hand, ambient environment can provide adequate air to sustain the fuel cell operation, which makes the fuel cell system more compact and cost-effective [22].

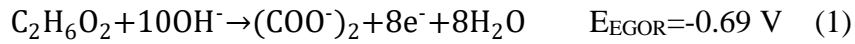
Hence, the utilization of the air in fuel cells is more attractive. Although promising, one major issue impeding the commercialization of this fuel cell running on the air is the carbonate issue in alkaline fuel cells, which refers to the behavior that CO_2 in the air reacts with OH^- to form carbonate [1]. Two undesired phenomena will occur when the carbonate is formed. One is that the carbonate precipitation in the cathode may cover the active sites for the reaction, resulting in the sluggish oxygen reduction reaction (ORR) kinetics [23]. The other is that the pores and channels in the cathode may be blocked when the precipitation gets larger, which elevates the transport resistance of oxygen [24]. Recently, the use of hydrogen peroxide acting as oxidant to replace the air or pure oxygen has been extensively investigated [25, 26]. As the supply of air and oxygen are insufficient in special cases, e.g. outer space and underwater, the fuel cells running on hydrogen peroxide are still able to operate under these conditions. In addition, the use of liquid hydrogen peroxide provides the several advantages: (1) a substantial increase in the theoretical voltage; (2) low activation loss on the cathode due to two-electron transfer; and (3) negligible effects of water flooding issue [27].

In this work, a hybrid fuel cell running on ethylene glycol as fuel and hydrogen peroxide as oxidant is proposed. This hybrid ethylene glycol fuel cell is composed of a non-platinum anode, a non-platinum cathode, and a cation exchange membrane (CEM). The theoretical voltage of this hybrid ethylene glycol fuel cell reaches 2.47 V and experimentally, the practical open-circuit voltage (OCV) is as high as 1.41 V. The developed fuel cell can output a peak power density of 80.9 mW cm^{-2} at 60°C , which is 20.8%

higher than that of using oxygen (67 mW cm^{-2}) [28]. In addition, the effects of operating conditions on the cell performance were studied.

4.2. Working principle

As shown in Figure 4.1, the hybrid DEGFC consists of an anode diffusion layer (DL), an anode catalyst layer (CL), a CEM, a cathode CL, and a cathode DL. In the anode where ethylene glycol oxidation reaction (EGOR) takes place, the EG reacts with OH^- to produce oxalate, electrons, and water according to [18]:



Then the produced electrons transport from the external circuit and reach the cathode CL, participating in the hydrogen peroxide reduction reaction (HPRR), to react with hydrogen peroxide and protons to generate water according to [29]:



The sodium ions transport through the CEM from the anode to the cathode to form the ionic current. Therefore, combining the Eqs. (1) and (2), the overall reaction of the hybrid DEGFC can be obtained as follows:



Although the theoretical voltage of this hybrid DEGFC is so high, the practical voltage exhibits a severe degradation due to the activation loss, ohmic loss, as well as concentration loss. In addition, the mixed potential in the cathode, lowering the cell voltage, needs to be paid special attention to.

4.3. Experiments

4.3.1. Preparation of the membrane electrode assembly

The membrane electrode assembly (MEA) consists of a pair of home-made electrodes that serve as the anode and the cathode, as well as CEMs with different thicknesses, including 30 μm (N211), 60 μm (N212), and 120 μm (N115). The thicknesses of the dry CEMs were measured by a vernier caliper. The electrodes have an active area of 2.0 cm \times 2.0 cm. The Pd/C anode was prepared based on the method reported somewhere else [36]. Firstly, the catalyst ink was prepared. 30 wt.% Pd/C (Sigma-Aldrich Co., USA) was mixed with 5 wt.% Nafion (Fuel Cell Store, USA), which serves as the binder, and ethanol, which serves as the solvent. The ink was then dispersed in ultrasonic bath for 20 minutes. Subsequently, it was sprayed onto the backing layer, i.e., carbon cloth (Hesen, China). The catalyst loading on the anode was 1.0 $\text{mg}_{\text{Pd}} \text{cm}^{-2}$. The Au/C cathode was prepared by the same method except that the ink used in the cathode was made by 60 wt.% Au/C (Premetek Co., USA) with 15 wt.% Nafion and ethanol. The catalyst loading of cathode was 2.66 $\text{mg}_{\text{Au}} \text{cm}^{-2}$. To obtain the CEMs, original Nafion membranes were cut to the designed shape (3.00 cm \times 3.00 cm) and immersed in 2.5 M KOH solution at 80°C for 1h [36]. Then, the treated membranes were rinsed by washing it in DI water for several times and stored in DI water before the assembly of this fuel cell.

4.3.2. Fuel cell setup and instrumentation

Each MEA was fixed between an anode plate and a cathode plate, both of which were made of 316 L stainless steel plates with flow fields. The flow field was a single serpentine flow channel grooved by the wire-cut technique, which was 0.5 mm deep and 1.0 mm wide. Two peristaltic pumps were used to feed a solution containing EG and NaOH and a solution

containing H_2O_2 and H_2SO_4 to the anode and the cathode, respectively. Both of the flow rates of anode and cathode were 2.0 mL min^{-1} . Two electrical heating rods were installed to heat up the cell, and the temperature was measured by a thermocouple and controlled by a temperature controller. The polarization curves were measured by an Arbin BT2000 (Arbin Instrument Inc.) and the internal resistance was measured by the built-in function of the Arbin BT2000.

4.4. Results and discussion

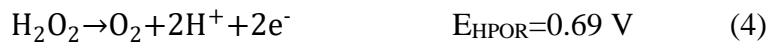
4.4.1. Characterization of catalyst layers

Figure 4.2 shows the SEM image of the cathode CL. It can be seen that the carbon supported Au nanoparticles were uniformly distributed on the carbon cloth. Tremendous pores were formed in the CL. The porous structure provides not only large specific surface area for the electrochemical reactions, but also sufficient pathway for the mass transport. It is also shown that the distribution of Au/C nanoparticles was uniform as well, and no obvious agglomeration was observed, which is advantageous to supply numerous active sites for electrochemical reactions.

4.4.2. General performance

Figure 4.3 presents the polarization and power density curves of the hybrid DEGFC with n solution containing 1.0 M EG and 7.0 M NaOH at a flow rate of 2.0 mL min^{-1} fed into anode as well as a solution containing 1.0 M H_2SO_4 and 4.0 M H_2O_2 at a flow rate of 2.0 mL min^{-1} fed into cathode at 80°C . It demonstrates that a peak power density of 115.3 mW cm^{-2} and an OCV of 1.43 V were achieved. The performance shows significant improvements both in peak power density and OCV when comparing with

the results of previous work (67 mW cm⁻² and 0.86 V at 60°C) [28]. The main reason accounting for the phenomenon is that the HPRR goes through a two-electron transfer process, which is more favorable due to the faster electrochemical kinetics comparing with the four-electron-transfer ORR process [31]. In spite of the performance improvement, the actual voltage (1.41 V) is much less than the theoretical voltage (2.47 V). The reason why the practical voltage is relatively low is explained as follows. As H₂O₂ is not stable and is more likely to be oxidized to produce oxygen, protons, and electrons at a high potential [32], this oxidation reaction together with HPRR can spontaneously establish a hydrogen peroxide-based fuel cells at the cathode.



Hence, the cathode potential decreases as a result of the mixed potential. Additionally, the produced oxygen is probable to be reduced in the cathode according to:



The ORR potential is not as high as the HPRR potential, which is another possible reason for the unexpected voltage. The constant-current discharging behavior of this hybrid DEGFC is presented in Figure 4.4. The constant current was set to be 50 mA cm⁻². It can be seen that the fuel cell exhibits a rather stable performance in 4-hour continuous operation, indicating that this DEGFC possesses the potential for future applications.

4.4.3. Effect of the NaOH concentration

Figure 4.5 shows the effect of the NaOH concentration on the cell performance with EG concentration fixed at 1.0 M. It is shown that the cell

voltage increased with the NaOH concentration initially, and decreased subsequently over the whole current density range. And the OCV increased when the OH⁻ concentration increased from 1.0 M to 7.0 M. This phenomenon can be explained that for a specific electrocatalyst, the kinetics of EGOR primarily depends on the local concentration of EG and OH⁻ in the anode CL. As the concentration of EG is fixed at 1.0 M, the increase in OH⁻ concentration leads to the OH⁻ concentration in the anode CL transferring from starving state to sufficient state, which is beneficial for enhancing the EGOR kinetics. However, further increasing the OH⁻ concentration from 7.0 M to 9.0 M did not contribute to higher OCV. The reason for this behavior is that high OH⁻ concentration leads to more active sites being covered by OH⁻, which may hinder the EG adsorption on the active sites. The adsorption competition between EG and OH⁻ may cause the EG concentration in a starving state [33], resulting in the voltage degradation as shown in Figure 4.6. It is seen that the highest peak power density of 80.9 mW cm⁻² was achieved at 7.0 M, while either higher or lower OH⁻ concentration would result in the performance decline. In general, the alkalinity of the anode not only affects the electrochemical kinetics, but also influences the transport of species in the anode, including EG, OH⁻, and Na⁺. Figure 4.6 shows that the internal resistance increased from 408 mOhm to 931 mOhm with the NaOH concentration increasing from 1.0 M to 9.0 M, suggesting that the mass/charge transport is impeded and the ohmic loss is enhanced. On one hand, although the ohmic loss increases with increasing the OH⁻ concentration, resulting in the performance degradation, the performance promotion that is attributed to

the facilitated EGOR kinetics can compensate the negative performance decline to achieve the positive overall effect from 1.0 M to 7.0 M. Therefore, the overall performance increases with the NaOH concentration increasing from 1.0 M to 7.0 M. On the other hand, too high OH⁻ concentration will occupy the active sites and suppress the EG adsorption, leading to higher concentration loss. The combination of the reduced EGOR kinetics and undesirable ohmic loss causes the inferior performance at 9.0 M.

4.4.4. Effect of the EG concentration

The effect of EG concentration on the cell performance was also studied when the NaOH concentration was fixed at 7.0 M, as shown in Figure 4.7. It is seen that the cell voltage increased with the EG concentration initially, and decreased subsequently over the whole current density range. The reasons for this behavior can be explained as follows. As the EG concentration increases from 0.5 M to 1.0 M, the transport of EG to active sites is accelerated, lowering the concentration loss and improving the OCV, as shown in Figure 4.8. This is evidenced by the fact that the performance experienced a severe degradation from 150 mA cm⁻² to 160 mA cm⁻², which is attributed to significant concentration loss due to the lack of EG in the anode CL. In contrast, no obvious concentration loss was observed in high current density region under 1.0 M operation. As the EG concentration further increased from 1.0 M to 2.0 M, the cell voltage exhibited a small degradation. One reason for the decline is the presence of adsorption competition between EG and OH⁻. A higher EG concentration may arrogate the active sites, preventing the OH⁻ from participating in the EGOR. In addition, the EG crossover from the anode to the cathode is enhanced with

the increased EG concentration. As the mixed potential increases resulting from more EG reaching the cathode, the cathode potential will degrade, leading to a lower OCV. The fuel crossover from the anode through the membrane to the cathode will cause mixed potential, lowering the fuel cell voltage and performance. One way to combat the fuel crossover is developing highly selective ion exchange membranes, preventing the fuel crossover. The other way is using inactive cathode catalyst towards fuel oxidation, such Fe-Co-Ni alloy, which can catalyze ORR but cannot catalyze EGOR. In our work, we use Au, which is less sensitive to EG than Pt, as the cathode catalyst. As a result, the OCV decreases derived from the increased concentration loss of OH^- and the subdued electrochemical kinetics. The other is that the increasing viscosity of anolyte due to the higher EG concentration restricts the mass/charge transport in the anode, which is verified by Figure 4.8. The internal resistance increases with the EG concentration, thus the ohmic loss boosts simultaneously, declining the cell performance.

4.4.5. Effect of the H_2O_2 concentration

Figure 4.9 shows the effect of hydrogen peroxide concentration on the cell performance when the sulfuric acid concentration was fixed at 1.0 M. It is seen that the cell voltage first decreased in the low current density region and then increased, finally followed by a voltage drop when the hydrogen peroxide concentration increased from 1.0 M to 6.0 M as depicted in Figure 4.10. The cell voltage first increased and then decreased with increasing hydrogen peroxide concentration in the high current density region. At the low current density region, the decreased voltage with the H_2O_2

concentration increasing from 1.0 M to 2.0 M is mainly ascribed to the H₂O₂ crossover from the cathode to the anode [34]. The permeated H₂O₂ will react with EG in the anode and produce a mixed potential, lowering the anode potential and thus the overall voltage. Afterwards, the voltage increased with the H₂O₂ concentration increasing from 2.0 M to 4.0 M. The reason for this phenomenon is that although the crossover becomes more serious with higher H₂O₂ concentration, the higher H₂O₂ concentration also transfers the starving state to sufficient state in the cathode CL, enhancing the HPRR kinetics. As a consequence, the positive effect on the cell voltage exceeds the negative effect, exhibiting an improved performance. However, further increasing the H₂O₂ concentration did not present a continuous enhancement. It can be explained that the H₂O₂ in the CL is sufficient at 4.0 M, so further increasing the H₂O₂ concentration to 6.0 M brings out the adsorption competition between H₂O₂ and H⁺. Therefore, the concentration loss of H⁺ is elevated. Meanwhile, accompanying with the negative effect derived from the severer H₂O₂ crossover, the cell voltage showed a degradation when the H₂O₂ concentration increases from 4.0 M to 6.0 M. At a high current density region, the reason for the voltage increasing with the H₂O₂ concentration from 1.0 M to 4.0 M is attributed to the sufficient supply of H₂O₂ in the cathode CL, reducing the cathode concentration loss of H₂O₂ and thus promoting the cell voltage. While the H₂O₂ concentration increased to 6.0 M, the performance degraded. because the reason is that the internal resistance increases with H₂O₂ concentration, which is evidenced by the Figure 4.10. A higher internal resistance results in a high ohmic loss, leading to the voltage degradation. Moreover, the mixed

potential in the anode is enhanced due to the severer H_2O_2 crossover, elevating the anode potential and thus lowering the overall cell voltage.

4.4.6. Effect of the H_2SO_4 concentration

The effect of sulfuric acid concentration on the cell performance was investigated with the hydrogen peroxide concentration fixed at 4.0 M, and the results were shown in Figure 4.11. It is seen that the cell voltage increased with the H_2SO_4 concentration initially, and decreased subsequently over the whole current density range. The explanation for the increased voltage from 0.5 M to 1.0 M is that the transport of H^+ to active sites is enhanced, which reduces the concentration loss of H^+ and promotes the cell voltage as shown in Figure 4.12 [35]. However, a higher H_2SO_4 concentration exceeding 1.0 M did not contribute to a higher cell performance. This behavior is mainly attributed to two reasons. One is that numerous active sites are covered by the redundant H_2SO_4 , resulting in the shortage of H^+ in the CL and higher concentration loss of H^+ , so that the cell voltage degrades. The other is that the viscosity of catholyte increases with the H_2SO_4 concentration, leading to the linear rise in the internal resistance as depicted in Figure 4.12, which causes the enhanced ohmic loss. Therefore, the cell performance underwent a significant degradation at 2.0 M due to the synergetic negative effect.

4.4.7. Effect of membrane thickness

The effect of membrane thickness on the cell performance was studied and the results were shown in Figure 4.13. It is seen that the cell with a thinner membrane yielded a superior performance over almost the whole current density range, whereas the cell with a thicker membrane exhibited a

superior OCV. As shown in Figure 4.14, both of the OCV and internal resistance were increasing with the membrane thickness. Since the membrane becomes thicker, the EG crossover from the anode to cathode is suppressed. As a result, the EG crossover from the anode to the cathode is hindered, lowering the mixed potential in the cathode so that both the cathode potential and the OCV increases. However, when the cell was discharging, the ohmic loss needed to be taken into consideration. Over the whole current density range, the cell with a thicker membrane experienced a rapider voltage degradation due to the higher ohmic loss. It is indicated that the positive effect derived from the reduced mixed potential in the cathode is too deficient to compensate the negative effect owing to the substantial internal resistance, suggesting that the internal resistance plays the predominant role in the cell performance.

4.4.8. Effect of the operating temperature

Figure 4.15 shows the effect of operating temperature on the cell performance. It is seen that the cell performance increased with the operating temperature. The peak power densities were 49.3, 80.9, and 115.3 mW cm^{-2} when the cell was operated at 40°C, 60°C, and 80°C, respectively. The reasons for this remarkable improvement with the operating temperature can be concluded as follows. On one hand, both the kinetics of the EGOR in the anode and the HPRR in the cathode will be facilitated at higher operating temperatures, resulting in the decreased activation loss [36]. On the other hand, increasing operating temperature is beneficial for accelerating the reactants transport in both of the anode and the cathode as well as the ion transport through the membrane. As the reactants deliver to

the active sites more easily, the concentration loss of both anode and cathode due to the reactant shortage is reduced. In addition, the conductivity of the membrane increases and thus the internal resistance decreases, which lowers the ohmic loss. The fuel cell performance is determined by electrochemical reaction and mass transport. The higher temperature will enhance the reaction kinetics and improve the mass transport, and thus the fuel cell performance will be improved. Therefore, the cell performance upgrades with operating temperature.

4.5. Summary

In this work, a hybrid direct ethylene glycol fuel cell has been developed and tested. The effects of operation conditions on the cell performance have been also examined. It is demonstrated that the peak power densities were 80.9 mW cm^{-2} and 115.3 mW cm^{-2} with an aqueous solution containing 1.0 M EG and 7.0 M NaOH at a flow rate of 2.0 mL min^{-1} fed into anode as well as an aqueous solution containing 1.0 M H_2SO_4 and 4.0 M H_2O_2 at a flow rate of 2.0 mL min^{-1} fed into cathode at 60°C and 80°C , respectively. The hybrid DEGFC exhibits a 20.8% increase in the peak power density at 60°C than that in a DEGFC with oxygen as oxidant (67 mW cm^{-2}), which is ascribed to the faster kinetics of two-electron-transfer HPRR and the reduced ohmic loss. It is also shown that the operation conditions, including species concentrations both in anode and cathode, the thickness of membrane, and the operating temperature, possessed significant effects on the cell performance.

4.6. References

- [1] Z.F. Pan, L. An, T.S. Zhao, Z.K. Tang, Advances and challenges in alkaline anion exchange membrane fuel cells, *Progress in Energy and Combustion Science* 66 (2018) 141-175.
- [2] L. An, T.S. Zhao, *Anion exchange membrane fuel cells: Principles, Materials and Systems*, Springer International Publishing, Cham, Switzerland, 2018.
- [3] Q.X. Wu, Z.F. Pan, L. An, Recent advances in alkali-doped polybenzimidazole membranes for fuel cell applications, *Renewable & Sustainable Energy Reviews* 89 (2018) 168-183.
- [4] C.Y. Wen, G.W. Huang, Application of a thermally conductive pyrolytic graphite sheet to thermal management of a PEM fuel cell, *Journal of Power Sources* 178 (2008) 132-140.
- [5] C.Y. Wen, Y.S. Lin, C.H. Lu, Experimental study of clamping effects on the performances of a single proton exchange membrane fuel cell and a 10-cell stack, *Journal of Power Sources* 192 (2009) 475-485.
- [6] L. An, R. Chen, Direct formate fuel cells: A review, *Journal of Power Sources* 320 (2016) 127-139.
- [7] Y.S. Li, Y. Feng, X.D. Sun, Y.L. He, A sodium-ion-conducting direct formate fuel cell: generating electricity and producing base, *Angewandte Chemie International Edition* 129 (2017) 5828-5831.
- [8] Y.S. Li, X.D. Sun, Y. Feng, Hydroxide self-feeding high-temperature alkaline direct formate fuel cells, *ChemSusChem* 10 (2017) 2135-2139.
- [9] C.Y. Wen, Y.S. Lin, C.H. Lu, Performance of a proton exchange membrane fuel cell stack with thermally conductive pyrolytic graphite

sheets for thermal management, *Journal of Power Sources* 189 (2009) 1100-1105.

[10] T.S. Zhao, C. Xu, R. Chen, W.W. Yang, Mass transport phenomena in direct methanol fuel cells, *Progress in Energy and Combustion Science* 35 (2009) 275-292.

[11] L. An, T.S. Zhao, Transport phenomena in alkaline direct ethanol fuel cells for sustainable energy production, *Journal of Power Sources* 341 (2017) 199-211.

[12] L. An, T.S. Zhao, Y.S. Li, Carbon-neutral sustainable energy technology: Direct ethanol fuel cells, *Renewable & Sustainable Energy Reviews* 50 (2015) 1462-1468.

[13] L. An, R. Chen, Mathematical modeling of direct formate fuel cells, *Applied Thermal Engineering* 124 (2017) 232-240.

[14] Y.S. Li, T.S. Zhao, A passive anion-exchange membrane direct ethanol fuel cell stack and its applications, *International Journal of Hydrogen Energy* 41 (2016) 20336-20342.

[15] Y.S. Li, Y.L. He, W.W. Yang, A high-performance direct formate-peroxide fuel cell with palladium-gold alloy coated foam electrodes, *Journal of Power Sources* 278 (2015) 569-573.

[16] Z.F. Pan, R. Chen, L. An, Y.S. Li, Alkaline anion exchange membrane fuel cells for cogeneration of electricity and valuable chemicals, *Journal of Power Sources* 365 (2017) 430-445.

[17] X.Y. Chen, T.C. Li, J.N. Shen, Z.L. Hu, From structures, packaging to application: A system-level review for micro direct methanol fuel cell, *Renewable & Sustainable Energy Reviews* 80 (2017) 669-678

-
- [18] L. An, R. Chen, Recent progress in alkaline direct ethylene glycol fuel cells for sustainable energy production, *Journal of Power Sources* 329 (2016) 484-501.
- [19] H.R. Yue, Y.J. Zhao, X.B. Ma, J.L. Gong, Ethylene glycol: properties, synthesis, and applications, *Chemical Society Reviews* 41 (2012) 4218-4244.
- [20] L. An, L. Zeng, T.S. Zhao, An alkaline direct ethylene glycol fuel cell with an alkali-doped polybenzimidazole membrane, *International Journal of Hydrogen Energy* 38 (2013) 10602-10606.
- [21] C.Y. Wen, Y.S. Lin, C.H. Lu, T.W. Luo, Thermal management of a proton exchange membrane fuel cell stack with pyrolytic graphite sheets and fans combined, *International Journal of Hydrogen Energy* 36 (2011) 6082-6089.
- [22] L. An, T.S. Zhao, X.H. Yan, X.L. Zhou, P. Tan, The dual role of hydrogen peroxide in fuel cells, *Science Bulletin* 60 (2015) 55-64.
- [23] E.H. Yu, U. Krewer, K. Scott, Principles and materials aspects of direct alkaline alcohol fuel cells, *Energies* 3 (2010) 1499-1528.
- [24] G.F. McLean, T. Niet, S. Prince-Richard, N. Djilali, An assessment of alkaline fuel cell technology, *International Journal of Hydrogen Energy* 27 (2002) 507-526.
- [25] L. An, T.S. Zhao, Z.H. Chai, L. Zeng, P. Tan, Modeling of the mixed potential in hydrogen peroxide-based fuel cells, *International Journal of Hydrogen Energy* 39 (2014) 7407-7416.
- [26] L. An, C.Y. Jung, Transport phenomena in direct borohydride fuel cells, *Applied Energy* 205 (2017) 1270-1282.

-
- [27] S. Fukuzumi, Y. Yamada, Hydrogen peroxide used as a solar fuel in one-compartment fuel cells, *ChemElectroChem* 3 (2016) 1978-1989.
- [28] L. An, T.S. Zhao, S.Y. Shen, Q.X. Wu, R. Chen, Performance of a direct ethylene glycol fuel cell with an anion-exchange membrane, *International Journal of Hydrogen Energy* 35 (2010) 4329-4335.
- [29] L. An, T.S. Zhao, R. Chen, Q.X. Wu, A novel direct ethanol fuel cell with high power density, *Journal of Power Sources* 196 (2011) 6219-6222.
- [30] L. An, T.S. Zhao, Performance of an alkaline-acid direct ethanol fuel cell, *International Journal of Hydrogen Energy* 36 (2011) 9994-9999.
- [31] G.H. Miley, N. Luo, J. Mather, R. Burton, G. Hawkins, L.F. Gu, E. Byrd, R. Gimlin, P.J. Shrestha, G. Benavides, J. Laystrom, D. Carroll, Direct $\text{NaBH}_4/\text{H}_2\text{O}_2$ fuel cells, *Journal of Power Sources* 165 (2007) 509-516.
- [32] X. Jing, D.X. Cao, Y. Liu, G.L. Wang, J.L. Yin, Q. Wen, Y.Y. Gao, The open circuit potential of hydrogen peroxide at noble and glassy carbon electrodes in acidic and basic electrolytes, *Journal of Electroanalytical Chemistry* 658 (2011) 46-51.
- [33] Y.S. Li, T.S. Zhao, Z.X. Liang, Performance of alkaline electrolyte-membrane based direct ethanol fuel cells, *Journal of Power Sources* 187 (2009) 387-392.
- [34] Integrated electrochemical/chemical oxygen generating system. US 4,488,951; Dec. 18, 1984.
- [35] R.K. Raman, N.A Choudhury, A.K. Shukla, A high output voltage direct borohydride fuel cell, *Electrochem Solid-State Lett.* 7 (2004) A488-491.

[36] Y.S. Li, T.S. Zhao, A high-performance integrated electrode for anion-exchange membrane direct ethanol fuel cells, *International Journal of Hydrogen Energy* 36 (2011) 7707-7713.

Figures

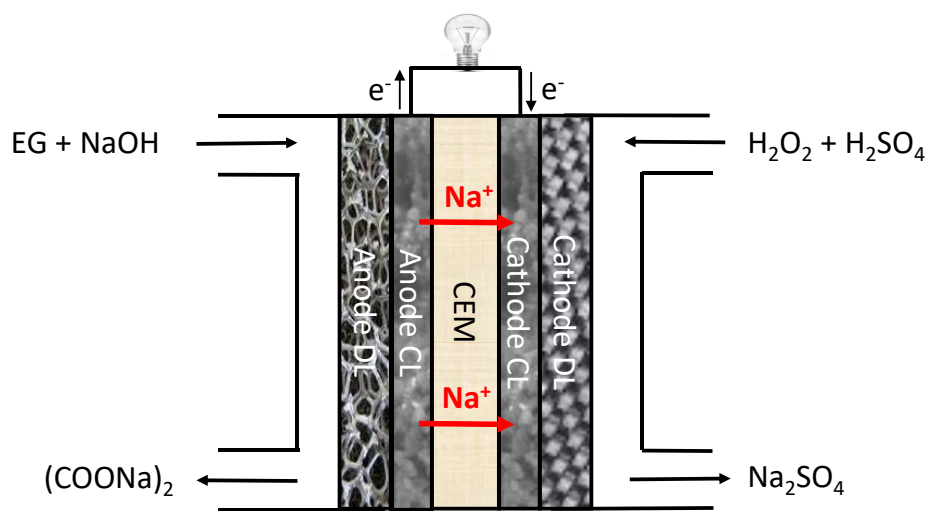


Figure 4.1 Schematic of the active DEGFC.

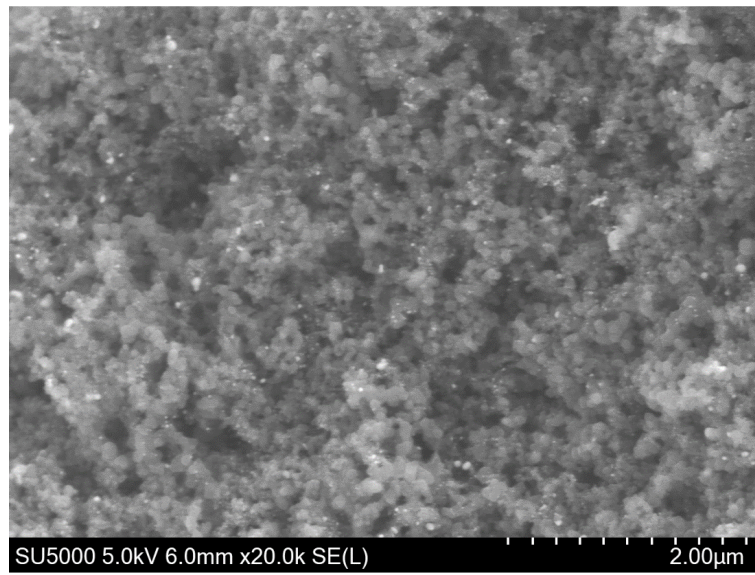


Figure 4.2 SEM image of the cathode catalyst layer.

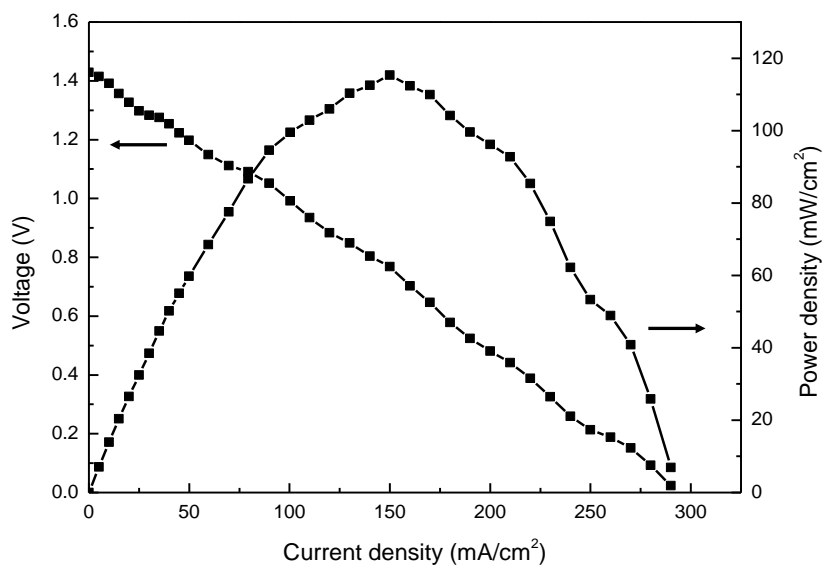


Figure 4.3 The polarization and power density curves.

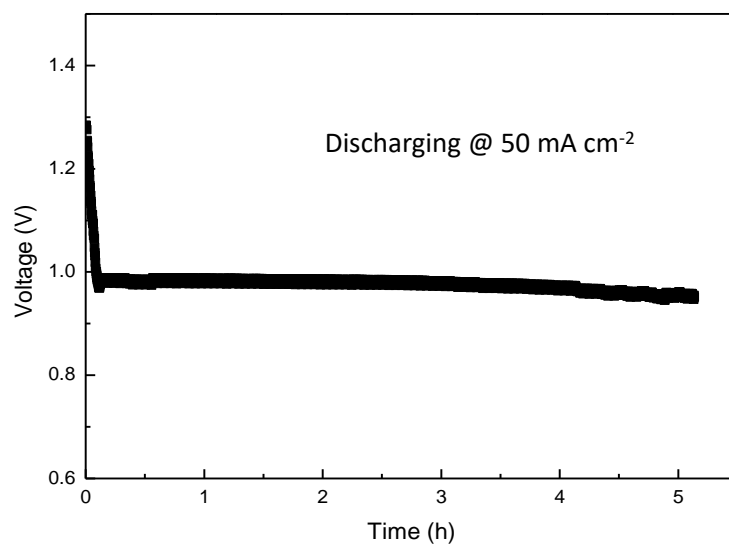


Figure 4.4 Constant-current discharging behavior.

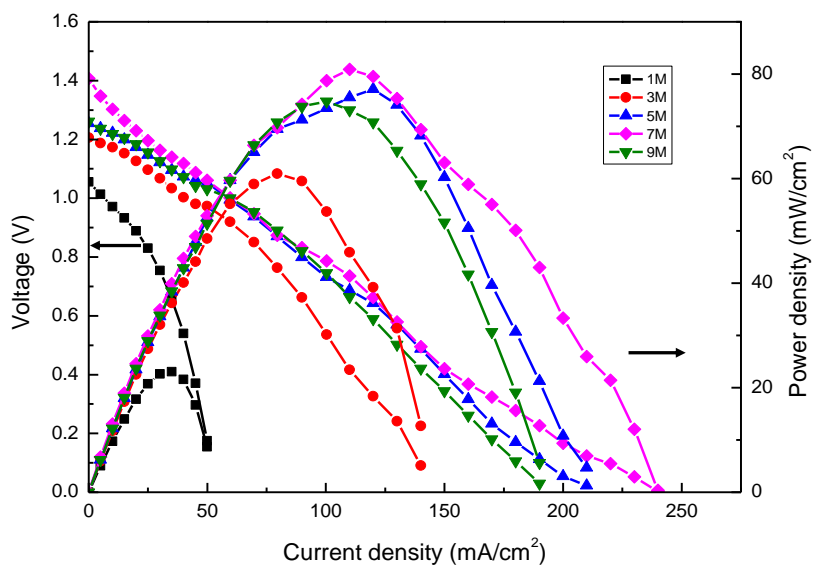


Figure 4.5 General performance of the passive DEGFC.

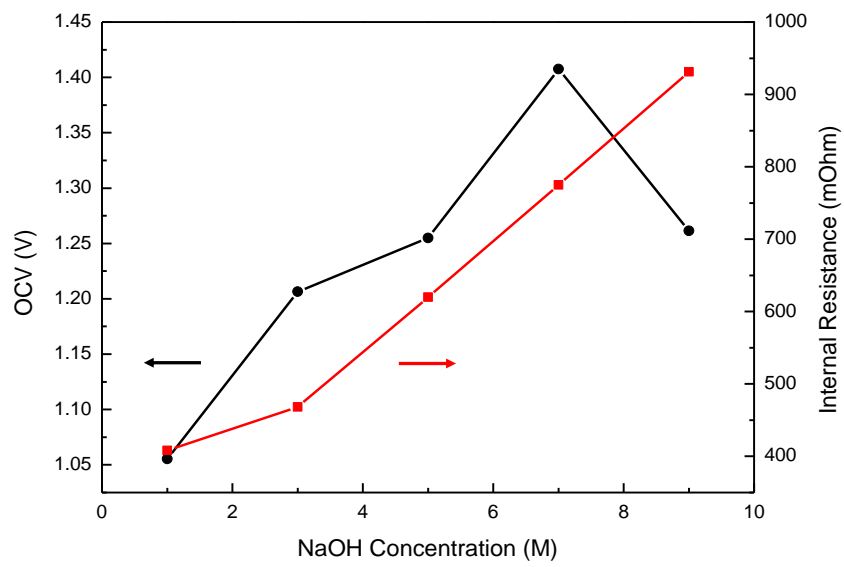


Figure 4.6 Effect of the NaOH concentration on the OCV and internal resistance.

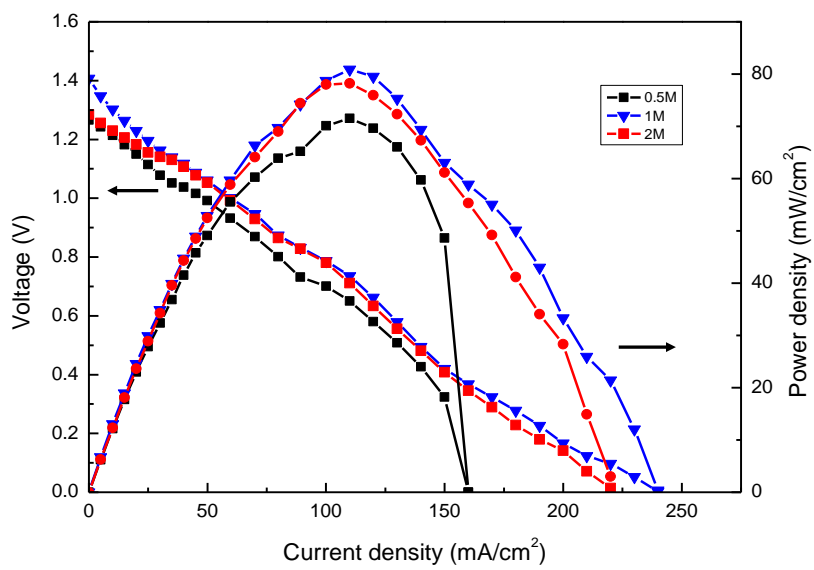


Figure 4.7 Effect of the EG concentration on the fuel cell performance.

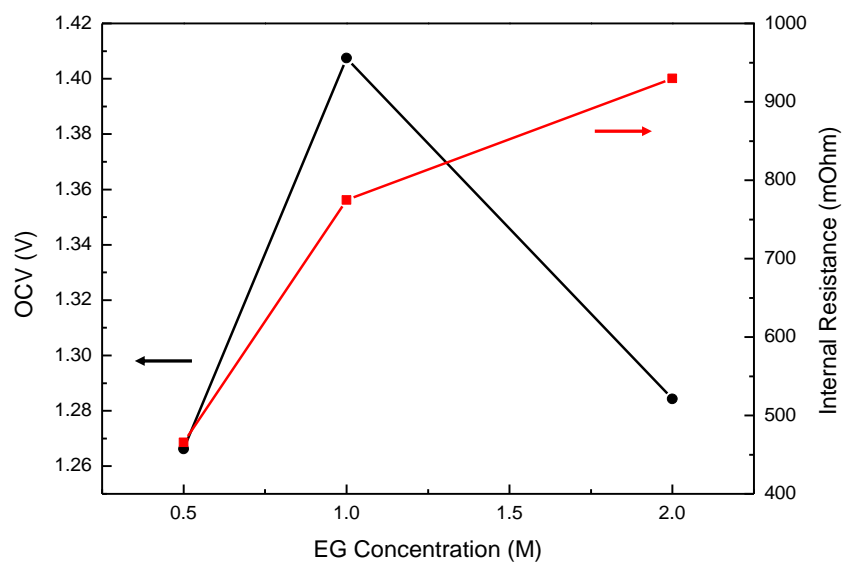


Figure 4.8 Effect of the EG concentration on the OCV and internal resistance.

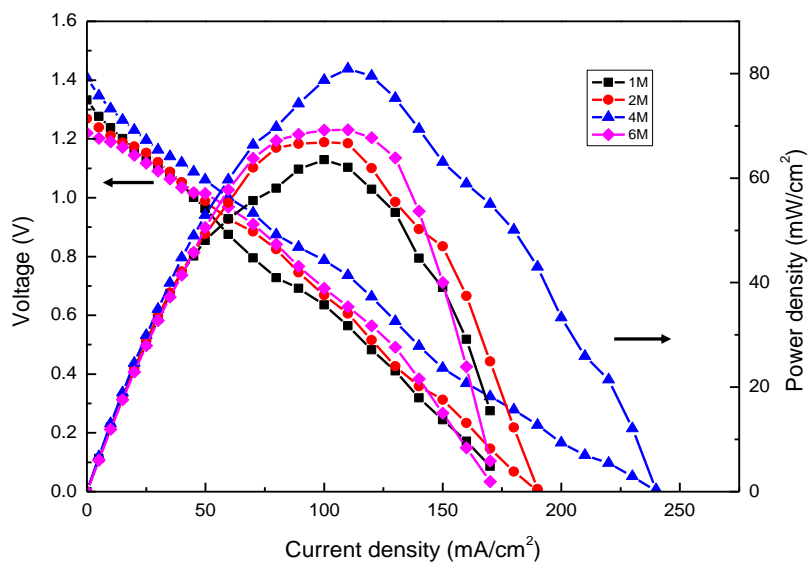


Figure 4.9 Effect of the H₂O₂ concentration on the fuel cell performance.

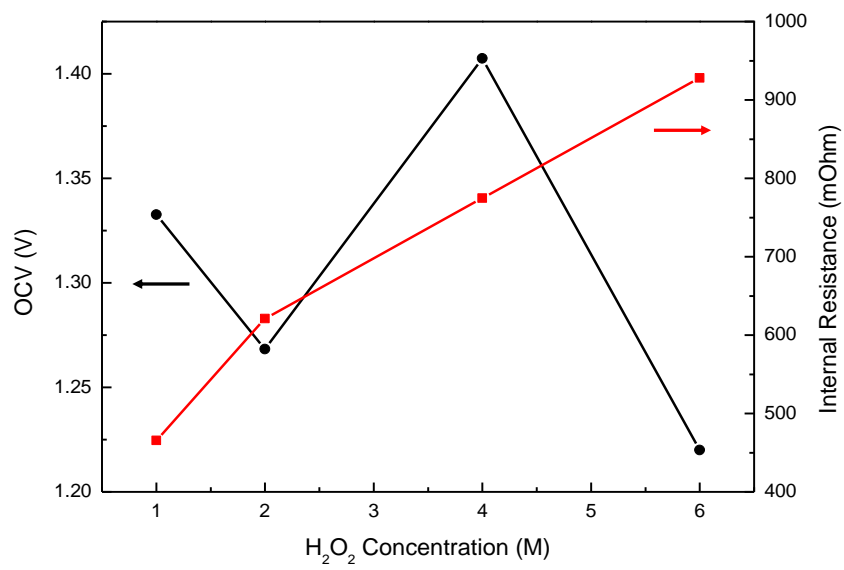


Figure 4.10 Effect of the H₂O₂ concentration on the OCV and internal resistance.

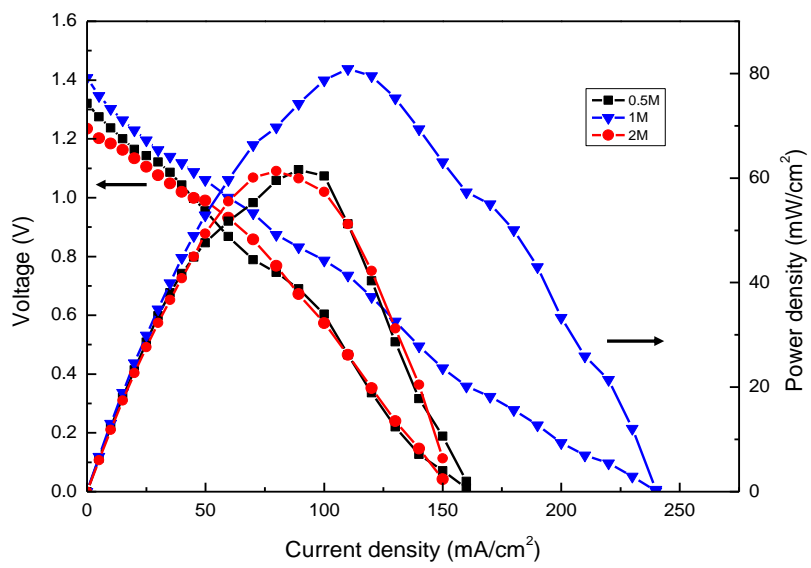


Figure 4.11 Effect of the H₂SO₄ concentration on the cell performance.

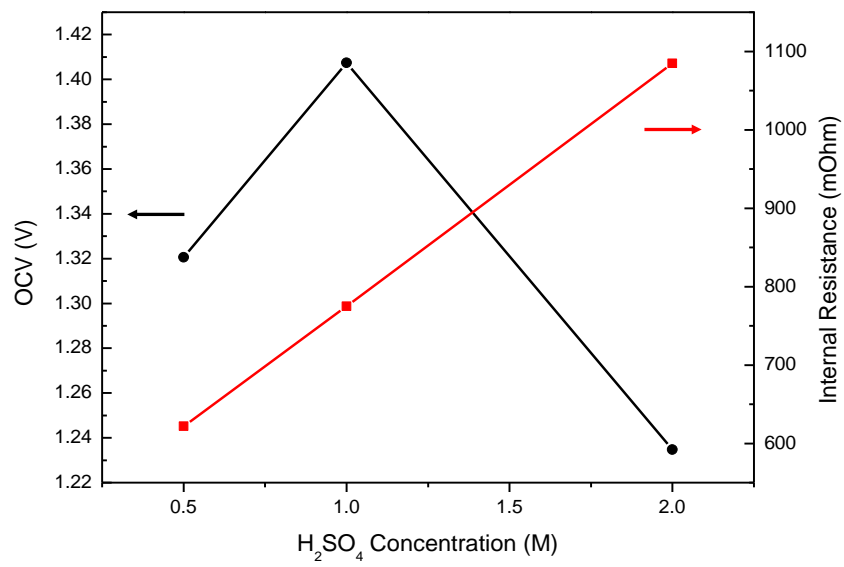


Figure 4.12 Effect of the H₂SO₄ concentration on the OCV and internal resistance.

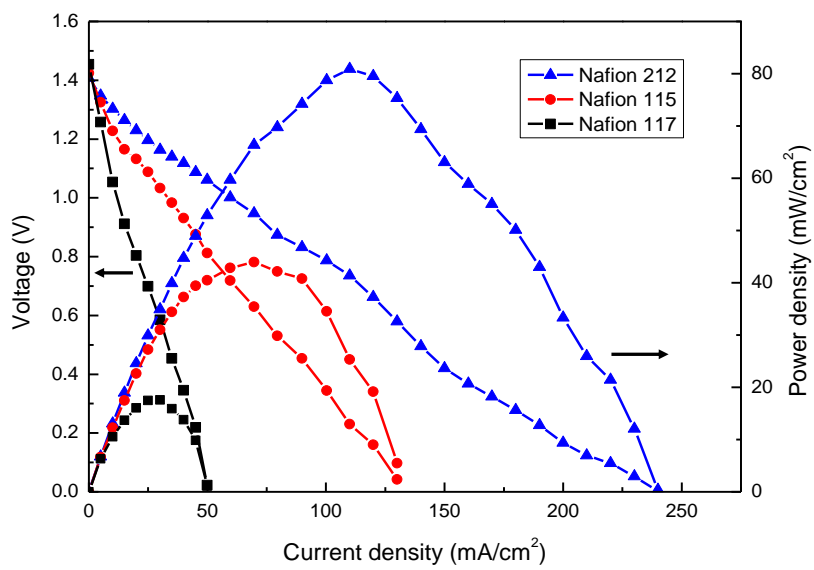


Figure 4.13 Effect of the membrane thickness on the OCV and cell performance.

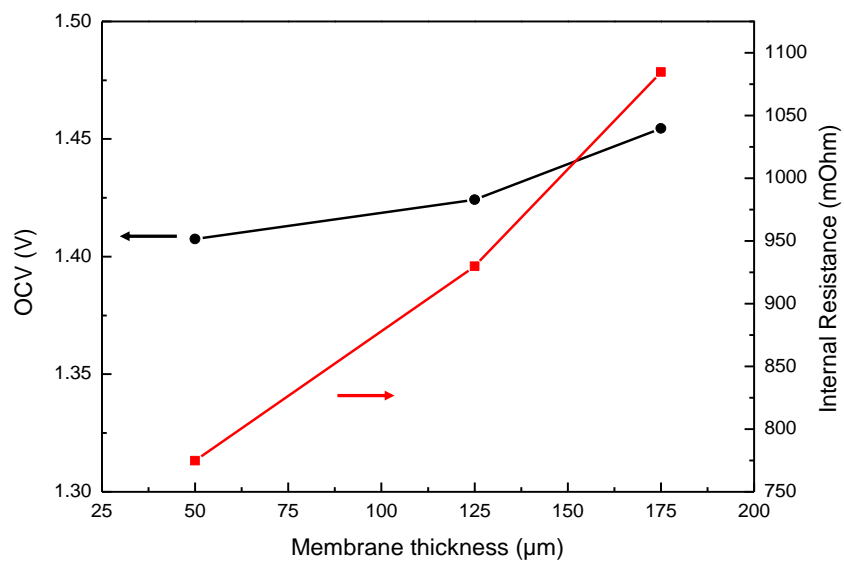


Figure 4.14 Effect of the membrane thickness on the OCV and internal resistance.

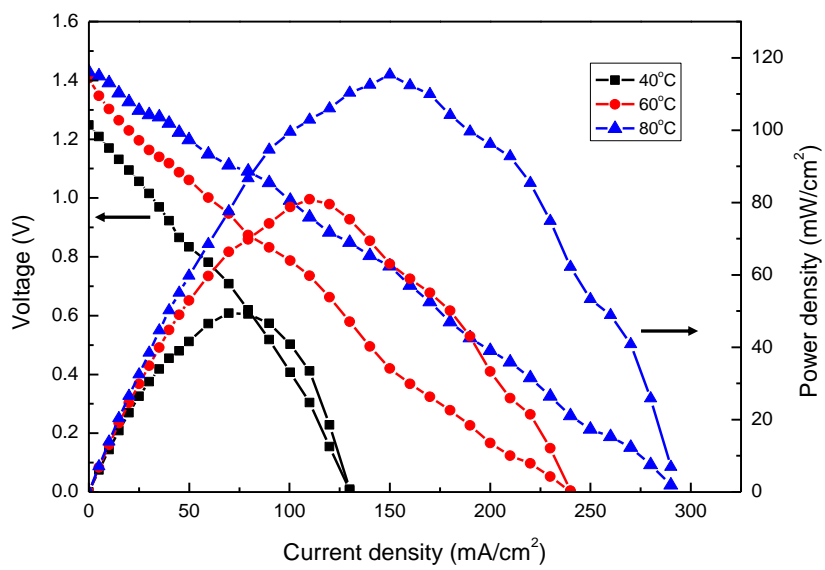


Figure 4.15 Effect of the operating temperature on the cell performance.

Chapter 5 Performance characteristics of a passive fuel cell

Abstract

A passive direct ethylene glycol fuel cell is proposed and tested, which does not contain external liquid pumps, gas blowers/compressors or any other auxiliary device. Therefore, comparing to the active fuel cells, the volumetric energy density is improved. In this work, ethylene glycol in alkaline solution is employed as fuel in this fuel cell, while hydrogen peroxide in acid solution is employed as oxidant, and a cation exchange membrane is employed to transport cations. The theoretical voltage of this type of fuel cell is as high as 2.47 V, which exhibits a promising potential in practical applications. The operating conditions can influence the performance of this fuel cell system, including species concentrations in both fuel and oxidant, thicknesses of membranes, and operating temperatures. In addition, the open-circuit voltage and the peak power density of this fuel cell are as high as 1.58 V and 65.8 mW cm⁻² at 60°C, respectively. Comparing to a fuel cell system with a similar setting but using oxygen as oxidant, the higher voltage output and power output are attributed to the easier and faster reduction reaction of hydrogen peroxide, which makes contributions to the impressive performance improvement of this fuel cell. Moreover, the effect of the released heat caused by the hydrogen peroxide self-decomposition to the cell performance is studied as well.

Keywords: Passive fuel cells; Direct ethylene glycol fuel cell; Hydrogen peroxide; Operating parameters; Power density; Hydrogen peroxide self-decomposition

5.1. Introduction

Fuel cells have attracted great research interest as a promising power source in the last decades, which is mainly attributed to their simple design [1,2], high efficiency [3,4], low emissions [5,6] as well as quick refueling [7,8]. Three common fuels, i.e., hydrogen [9], methanol [10], and ethanol [11], are widely used in proton exchange membrane fuel cells (PEMFCs) [12] as well as anion exchange membrane fuel cells (AEMFCs) [13,14]. Among them, the widespread application of hydrogen is required to address the production, transport, and storage of hydrogen [15,16]. As for methanol, the fuel cell performance is severely degraded under long-term operation due to the severe crossover of methanol and the poisonousness of catalyst derivatives [17]. Ethanol, a C₂ fuel, has a main final oxidation product of acetic acid. When the system works at a temperature lower than 60°C, the electron transfer rate is low (33%) [16,18]. Recently, another fuel option, ethylene glycol (EG), has attracted wide attention due to its excellent properties [19,20], including the theoretical energy capacity of 4.8 Ah mL⁻¹, the boiling point of 198°C [21], and the electron transfer rate of 80%, which is suitable for mobile, stationary and portable devices [22,23]. Zhu et al. [20] synthesized hollow Ag₄₄Pt₅₆ nanotube bundles for ethylene glycol oxidation reaction (EGOR). To improve the electrocatalytic activity, Shi et al. [21] and Huang et al. [22] prepared three-dimensional nitrogen-doped reduced graphene oxide hydrogels anchored PtPd alloyed nanoparticles and PtCu alloyed nanocages with highly open structures via one-pot solvothermal method, respectively. Pan et al. [23] developed a mathematical modeling of direct ethylene glycol fuel cells using hydrogen

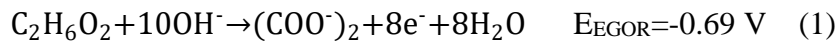
peroxide as oxidant incorporating the effect of the competitive adsorption. An et al. [24] reported an alkaline direct ethylene glycol fuel cell (DEGFC) with a maximum peak power density of 67 mW cm^{-2} at 60°C , which was attributed to the alkaline media enhancing the kinetics of both the EGOR and oxygen reduction reaction (ORR). The anion exchange membrane (AEM) and non-platinum catalysts are adopted in this fuel cell. Afterwards, an alkali-doped polybenzimidazole membrane was used to replace the AEM, which allows the system to be operated at high temperatures [25]. As a result, the maximum peak power densities of this fuel cell were 80 mW cm^{-2} at 60°C and 112 mW cm^{-2} at 90°C , respectively. Air or pure oxygen is usually used as oxidant on the cathode [25, 26]. It is necessary to compress the pure oxygen to store it in tanks. However, by doing so, the system becomes bulkier, and the complexity and potential risks are increased [27]. In addition, although the air breathing design is compact and light, one major issue is the carbonate problem in alkaline fuel cells, referring to the phenomenon that CO_2 in the ambient air reacts with hydroxide ions to produce carbonates [1]. The active sites in the cathode are covered by the precipitated carbonates, which causes the sluggish ORR kinetics [28]. At the same time, the pores and channels are blocked in the cathode, which increases the mass transport resistance of oxygen [29]. In addition, the air breathing design is not applicable with the absence of air, such as underwater and outer space. Recently, extensive research has been conducted on replacing air or pure oxygen with hydrogen peroxide as oxidant [30,31]. There are three intrinsic superiorities by using hydrogen peroxide: (1) the theoretical voltage will experience a substantial increase;

(2) comparing to the four-electron transfer process of ORR, only two electrons are transferred in the hydrogen peroxide reduction reaction (HPRR), which reduces the activation loss; and (3) the water flooding will be avoided due to the aqueous state of hydrogen peroxide [32]. Pan et al. [33] designed and tested an active DEGFC using hydrogen peroxide as oxidant. Comparing to the DEGFC using oxygen as oxidant, the cell performance is elevated significantly. The open-circuit voltage (OCV) is improved by 62.1% to 1.41 V, while the peak power density is elevated by 20.8% to 80.9 mW cm⁻² at 60°C. However, the active electrolyte delivery system requires auxiliary equipment, making the system more complicated and heavier.

In this work, a passive DEGFC using hydrogen peroxide as oxidant is developed, which avoids the usage of auxiliary devices. The proposed fuel cell system is structurally compact, no parasitic loss in power, and can operate under low-temperature, which makes it a suitable choice for portable electronic devices [34]. Because of the simpler and more compact structures, the volumetric energy density and the design flexibility are elevated significantly. This fuel cell consists of a palladium-based anode, a cation exchange membrane (CEM), and a gold-based cathode. The theoretical voltage of this system is 2.47 V. When operating at 60°C, it exhibits a practical OCV of 1.58V, and a peak power density of 65.8 mW cm⁻². In addition, the effect of operating conditions and the heat released from the H₂O₂ self-decomposition on the cell performance are also investigated.

5.2. Working principle

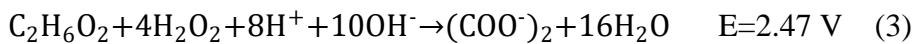
As demonstrated in Figure 5.1, the passive fuel cell is formed in a symmetric manner, which consists a diffusion layer (DL) and a catalyst layer (CL) in both anode and cathode, and a CEM between the two electrodes. The anolyte is injected into the anode reservoir. Under the driving force of the concentration gradient, it transports through the DL to the CL in the anode. The EGOR occurs on the anode CL where EG reacts with hydroxide ions to produce electrons, oxalate and water as shown below [18]:



Through the external circuit, the electrons produced by the EGOR are transferred from the anode to the cathode. In the cathode, the hydrogen peroxide, protons, and electrons participate in the hydrogen peroxide reduction reaction (HPRR) and water is produced as shown in the following equation [35]:



At the same time, the internal ionic circuit is formed by the potassium ions transferring from the anode to cathode. Therefore, the EGOR and HPRR reactions can be combined to form the overall reaction of this fuel cell, which is shown as follows:



As shown in Equation (3), the theoretical voltage of this passive fuel cell is as high as 2.47 V. However, due to the presence of activation loss, ohmic loss, and concentration loss, the actual voltage will experience a huge decrease.

5.3. Experiments

5.3.1. Preparation of membrane electrode assembly

The membrane electrode assembly (MEA) consists of a pair of home-made electrodes that serve as the anode and the cathode, as well as CEMs with different thicknesses, including 30 μm (N211), 60 μm (N212), and 120 μm (N115). The thicknesses of the dry CEMs were measured by a vernier caliper. The electrodes have an active area of 2.0 cm \times 2.0 cm. The Pd/C anode was prepared based on the method reported somewhere else [36]. Firstly, the catalyst ink was prepared. 30 wt.% Pd/C (Sigma-Aldrich Co., USA) was mixed with 5 wt.% Nafion (Fuel Cell Store, USA), which serves as the binder, and ethanol, which serves as the solvent. The ink was then dispersed in ultrasonic bath for 20 minutes. Subsequently, it was sprayed onto the backing layer, i.e., carbon cloth (Hesen, China). The catalyst loading on the anode was 1.0 $\text{mg}_{\text{Pd}} \text{cm}^{-2}$. The Au/C cathode was prepared by the same method except that the ink used in the cathode was made by 60 wt.% Au/C (Premetek Co., USA) with 15 wt.% Nafion and ethanol. The catalyst loading of cathode was 2.66 $\text{mg}_{\text{Au}} \text{cm}^{-2}$. To obtain the CEMs, original Nafion membranes were cut to the designed shape (3.00 cm \times 3.00 cm) and immersed in 2.5 M KOH solution at 80°C for 1h [36]. Then, the treated membranes were rinsed by washing it in DI water for several times and stored in DI water before the assembly of this fuel cell.

5.3.2. Fuel cell setup and instrumentation

As shown in Figure 5.2, an end plate, a heating plate and a current collector are added to both sides of the MEA to form the whole fuel cell system, in which end plates and heating plates are made of 1Cr18Ni9Ti stainless steel and current collectors are made of 316L stainless steel. Several

polytetrafluoroethylene (PTFE) gaskets are placed between each component of the fuel cell to avoid the leakage. The heating plates serve as the solution reservoir as well. As shown in Figure 5.2, two holes are drilled on the top surface of the heating plate. One is a perforative hole designed for injecting the anolyte or catholyte, and the other is not perforative and designed for placing the heating rod. The current collectors are manufactured by laser cutting with 25 holes in the center part with a diameter of 3.2 mm. The holes allow the fuel and oxidant to diffuse from the reservoir to the anode and cathode.

An Arbin BT2000 (Arbin instrument Inc.) is utilized to control the discharging process of this passive fuel cell and measure the polarization curves. Meanwhile, the built-in function of the Arbin BT2000 is utilized to measure the internal resistance of this fuel cell. In addition, to examine the fuel cell performance with specific operating temperatures, two electrical heating rods are inserted into the holes on the heating plates and two thermocouples and a dual-channel temperature controller are used to control the anode and cathode temperatures.

5.4. Results and discussion

5.4.1. Advantages of passive fuel cells

Compared to active fuel cells using external pumps or other auxiliary devices for fuel and oxidant supply, the advantages of passive fuel cells can be concluded as follows: (1) The passive fuel cells have much simpler and more compact structures, which increases both the volumetric energy density and the design flexibility of the fuel cell system [37]; (2) The passive fuel cells eliminate the electricity consumed by the added pumps,

blowers, and compressors, which can be regarded as parasitic energy losses [38]; and (3) Especially for portable and mobile electrical devices, using passive fuel cells is more favorable than the active fuel cells due to the simplicity of diffusion and natural-convection reactant delivery [39]. Although the passive fuel cells yield lower power output than dose the active fuel cells, they are still considered as a promising power source for applications in future electronic devices. For instance, the research and development of passive fuel cells have been conducted by several giant electronic companies, including Toshiba, Samsung, NEC, etc. [40]. Radically different from our previous work, hence, we develop and demonstrate a passive fuel cell using EG and hydrogen peroxide as fuel and oxidant, respectively. It is a promising power source to be applied underwater and outer space where oxygen is insufficient.

5.4.2. Characterization of catalyst layers

Figures 5.3 and 5.4 show the scanning electron microscope (SEM) images of the anode CL and the cathode CL, respectively. It is seen from Figure 5.3 that the carbon fibers were decorated with carbon supported Pd nanoparticles. Since the loading is as low as 1.0 mg cm^{-2} , partial carbon fibers are bare, indicating that further increasing the catalyst loading may promote the fuel cell performance. As shown in Figure 5.4, the carbon supported Au nanoparticles entirely covered the carbon fibers and were uniformly distributed on the carbon cloth. As the porous structure was formed in the CLs, the specific surface area is large, which is beneficial for the electrochemical reactions. In addition, sufficient pathways make contribution to mass transport. There is no obvious agglomeration of

nanoparticles, providing tremendous active sites for electrochemical reactions.

5.4.3. General performance

Figure 5.5 shows the performance of the passive fuel cell with a 4.0 mL of aqueous solution containing 5.0 M EG and 9.0 M KOH in the anode reservoir and a 4.0 mL of aqueous solution containing 4.0 M H₂O₂ and 1.0 M H₂SO₄ in the cathode reservoir at 60°C with pretreated Nafion 211 as the membrane. It is shown that the peak power density was 65.8 mW cm⁻² and the OCV was 1.58 V. A significant improvement can be observed that both of the peak power density and OCV increase remarkably compared to the results shown in a previous work using oxygen as oxidant (12 mW cm⁻² and 0.7 V) [41]. This improvement is mainly attributed to the enhanced cathode reaction kinetics, because the HPOR is a two-electron rather than four-electron transfer process [42]. Although the practical voltage is as high as 1.58 V, it is still far below the theoretical voltage (2.47 V). A general explanation was proposed by Pan et al. [33]. As the H₂O₂ can be either reduced or oxidized, a hydrogen peroxide-based fuel cell will be spontaneously established in the cathode, resulting in the mixed potential. Figure 5.6 shows the transient discharging behavior of this passive fuel cell at a constant current density of 5 mA cm⁻² under the same feeding concentrations but a different temperature of 23°C. When the cell was discharging, the voltage gradually decreased because the consumption of the reactants resulted in a lower concentration gradient, thus the diffusion of the reactants to the CLs was weaker. After the voltage plateau, the voltage dramatically decreased due to the continuous drop of concentration gradient

as well as the accumulation of products on the active sites. When the voltage was lower than 0.6 V, the cell was refueled with fresh anolyte and catholyte and the constant current discharging was repeated. Clearly, this fuel cell system can be stably operated for around 150 h in constant-current discharging, indicating that the potential of this passive fuel cell for practical applications.

In a passive DEGFC, the mass transport of reactants, from the fuel reservoir through the current collector holes and then the porous diffusion layer to the porous catalyst layer, is mainly driven by the concentration gradient, i.e., diffusion [43], in which the oxidation/reduction reaction will take place to consume the reactants, while the remaining will transport through the membrane reach the other electrode, wasting the utilization efficiency of reactants and even causing the mixed potential problem [44]. In order to achieve the optimal fuel cell performance, therefore, the local concentrations of reactants in the catalyst layer should be at an appropriate level [39]. For a given design of a passive DEGFC, the reactant-feeding concentrations in the fuel reservoir are the key factor that affects the local concentrations in the catalyst layer, which means that there is an optimal reactant-feeding concentration in the fuel reservoir. Too low reactant-feeding concentration of each reactant in the fuel reservoir leads to the local concentration in the catalyst layer at an inadequate level. Too high reactant-feeding concentration of each reactant causes the high reactant crossover rate and severe competitive adsorption between two reactants on active sites, leading to the other reactant at a starvation level. Therefore, it is critically important to study the effect of the reactant-feeding concentration of each

reactant in the fuel reservoir on the fuel cell performance.

5.4.4. Effect of the KOH concentration

Figure 5.7 demonstrates the performance of the DEGFC running on various KOH concentrations with EG, H₂O₂, and H₂SO₄ concentrations fixed at 5.0, 4.0, and 1.0 M, respectively. Both anolyte and catholyte were of 4.0 mL, while the pretreated Nafion 211 was utilized as the membrane and the operating temperature was at 23°C. It is seen that the OCV boosted from 1.27 V to 1.54 V with the OH⁻ concentration increasing from 3.0 M to 9.0 M. This improvement can be elucidated as follows. Although the performance of catalyst can be substantially improved via modification [45], for a specific catalyst of anode, the concentrations of EG and OH⁻ in the CL have the major effect on the kinetics of EGOR. As the EG has a constant concentration of 1.0 M, a higher KOH feeding concentration is beneficial to the hydroxide ion transport from the fuel reservoir to the anode CL, transferring it from starvation state to sufficient state. The enhanced hydroxide ion transport is derived from the higher concentration gradient of hydroxide ions, as the main driving force for reactants to transport in passive fuel cell is diffusion. As a result, the EGOR kinetics are enhanced, which can be confirmed by the increased OCV, as shown in Figure 5.8. However, when the concentration of OH⁻ was increased from 7.0 M to 9.0 M, the OCVs were similar, indicating that further increasing the OH⁻ concentration did not bring about higher OCV. The explanation for this phenomenon is that the adsorption of OH⁻ on active sites is already saturated when the OH⁻ concentration is 7.0 M, so the positive effect on the OCV is negligible when the OH⁻ concentration is 9.0 M. It is worth

mentioning that the adsorption competition between OH^- and EG on active sites may lead to the starvation state of EG [46], resulting in the declined voltage. It can be seen that under 9.0 M OH^- operation, the highest peak power density was as high as 30.3 mW cm^{-2} , whereas either higher or lower OH^- concentration would cause the performance degradation. The reasons can be described as follows. In general, the electrochemical kinetics as well as the transport of species in the anode will be heavily affected by the alkalinity of the anode. On one hand, when the OH^- concentration raises from 3.0 M to 9.0 M, the internal resistance increases from 620 mOhm to 927 mOhm, as shown in Figure 5.8. Although the ohmic loss is enhanced, the EGOR kinetics is improved, which can compensate the promoted ohmic loss, resulting in the improved performance. On the other hand, when the OH^- concentration increases from 9.0 M to 11.0 M, the internal resistance further increases to 1077 mOhm, resulting in a severer ohmic loss. It is because when the KOH concentration exceeds the optimal level, the undesired competitive adsorption between EG and OH^- occurs, resulting in the lack of EG reversely. Therefore, the active sites will be occupied and the EG adsorption will be suppressed due to too high OH^- concentration, resulting in reduced EGOR kinetics and higher concentration loss. In addition, the KOH concentration in the CL will be so high that it transports through the CEM reaching the cathode and covering the cathode active sites, thus the HPRR is hindered due to the loss of active sites. As a result, the performance declines with OH^- concentration increasing from 9.0 M to 11.0 M.

5.4.5. Effect of the EG concentration

As shown in Figure 5.9, the effect of the concentration of EG on the cell performance was tested, where the concentrations of KOH, H₂O₂ and H₂SO₄ were fixed at 9.0 M, 4.0 M and 1.0 M, respectively. The concentration of EG was increasing from 1.0 M to 7.0 M, while the voltage of this cell over the whole range of current density exhibited an increasing trend firstly when the concentration of EG was increased from 1.0 M to 5.0 M, and then went through a decline when further increasing the concentration of EG from 5.0 M to 7.0 M. The former increasing trend of the cell voltage is attributed to the following reasons. As the concentration of EG becomes higher from 1.0 M to 5.0 M, the diffusion of EG to the active sites on anode CL is improved, which reduces the concentration loss of EG. In Figure 5.10, it can be seen that the OCV is elevated as the concentration of EG is increased from 1.0 M to 5.0 M as well. Meanwhile, the cell performance with the 1.0 M EG concentration exhibited a severe decline when the current density is in the range of 36 mA cm⁻² to 37 mA cm⁻². With 3.0 M EG concentration, a similar decline of cell performance occurred in the current density range of 41 mA cm⁻² to 43 mA cm⁻². However, no such kind of performance decline was found with higher concentration of EG, such as 5.0 M and 7.0 M. The severe decline of cell performance is attributed to the vast concentration loss as the EG concentration is low and the transport of EG to the active sites is not sufficient to support the need for the electrochemical reactions on the anode. As it is seen from Figure 5.9, the OCV of this cell and the power output experienced a drop when increasing the concentration of EG from 5.0 M to 7.0 M. Three reasons make contributions to this noticeable drop of the cell

performance. Firstly, as mentioned before, the transport of EG to the active sites is boosted with higher EG concentration. However, when its concentration reaches 7.0 M, it is actually superfluous and brings the problem of competitive adsorption between EG and OH⁻. With a high concentration of EG, the active sites on anode CL are taken up by EG, and the OH⁻ will be insufficient in the EGOR. Secondly, as the concentration of EG is increasing, the crossover problem of EG from the anode to cathode becomes severer. As a result, the crossover of EG enhances the mixed potential and reduces the cathode potential. The subdued electrochemical kinetics and the increased concentration loss of OH⁻ function together and lower the OCV of this cell. Lastly, the mass/charge transport is hindered by the increasing viscosity of anode solution with high EG concentration, which is proved by the elevated internal resistance, as shown in Figure 5.10. The ohmic loss is enhanced due to the higher internal resistance, and thus, the cell performance is degraded.

5.4.6. Effect of the H₂O₂ concentration

As shown in Figure 5.11, the effect of the concentration of hydrogen peroxide on the performance of this fuel cell was studied. Meanwhile, the Figure 5.12 shows the OCVs and internal resistances of this fuel cell with different concentrations of H₂O₂, which were 2.0 M, 4.0 M, and 6.0 M. The concentrations of KOH, EG and H₂SO₄ were fixed at 9.0 M, 5.0 M and 1.0 M, respectively. The OCV decreased continuously with increasing concentration of H₂O₂. This reduction in OCV is mainly attributed to the severer crossover problem of the H₂O₂ from the cathode to anode when the H₂O₂ concentration is increased. The permeated H₂O₂ will not react with

EG, producing a mixed potential, however, the H_2O_2 self-decomposition will produce gaseous oxygen, which may hinder the transport of EG and OH^- in the anode. Therefore, a lower H_2O_2 concentration results in a higher OCV. Three methods that can improve H_2O_2 self-decomposition are operating fuel cell at room temperature, developing cathode catalyst that can suppress H_2O_2 oxidation, and designing the cathode structure that can quickly remove generated O_2 . In spite of the OCV, as the concentration of H_2O_2 increased from 2.0 M to 4.0 M, the cell voltage increased over the whole range of current density and decreased subsequently when the concentration of H_2O_2 was further elevated from 4.0 M to 6.0 M, which can be explained by the following reason. From 2.0 M to 4.0 M, although the crossover problem of H_2O_2 is severer with a higher H_2O_2 concentration, the H_2O_2 has a better transportation to the active sites on the cathode CL, which changes it to sufficient state from the starvation state. This positive effect brought by the enhanced transport of H_2O_2 compensates the negative effect brought by the crossover of H_2O_2 , so that both the cell voltage and the power output are improved. However, when the concentration of H_2O_2 was increased from 4.0 M to 6.0 M, the cell voltage and power output were degraded. The reasons can be concluded as follows. Firstly, as mentioned above, the crossover problem becomes severer with higher concentration of H_2O_2 , which lowers the OCV. Secondly, the competitive adsorption occurs between hydrogen peroxide and protons on the active sites in cathode CL, which is brought by the superfluous H_2O_2 . As a result, this problem increases the concentration loss of H^+ . Lastly, the internal resistance becomes larger with higher H_2O_2 concentration, as shown in Figure 5.12,

which brings a larger ohmic loss. It can also be seen from the Figure 5.11 that the cell performance with 6.0 M H₂O₂ exceeded that of 2.0 M H₂O₂ when the current density was high. The cell performance in this region is promoted with a higher concentration of H₂O₂, which is attributed to the reduced concentration loss of H₂O₂ in cathode.

5.4.7. Effect of the H₂SO₄ concentration

As shown in Figure 5.13, the effect of the concentration of sulfuric acid on the performance of this fuel cell was investigated, and the concentrations of KOH, EG and H₂O₂ were fixed at 9.0 M, 5.0 M and 4.0 M, respectively. The OCVs with different H₂SO₄ concentration were similar, as shown in Figure 5.14. In spite of the OCV, as the concentration of H₂SO₄ increased from 0.5 M to 1.0 M, the cell voltage over the whole range of current density increased firstly. Then, further increasing the concentration of H₂SO₄ from 1.0 M to 2.0 M results in a decrease in the cell voltage. The rise of the cell voltage as the concentration of H₂SO₄ increased from 0.5 M to 1.0 M is attributed to the reduction in concentration loss of H⁺, because the H⁺ has an enhanced transport to the active sites on CL [47]. However, when the H₂SO₄ concentration increased from 1.0 M to 2.0 M, the cell performance degraded, which is mainly ascribed to two reasons. On one hand, the shortage of H₂O₂ occurs because the superfluous H₂SO₄ covered the active sites on the cathode CL. The concentration loss increases because of the deficiency of H₂O₂ on the active sites, and the cell voltage decreases as a result of that. On the other hand, the ohmic loss increases due to the high concentration of H₂SO₄. The increasing concentration of H₂SO₄ gives rise to a higher viscosity of the catholyte, which increases the internal resistance

in a linear manner and the ohmic loss as well. Due to these two reasons, the cell performance with 2.0 M H₂SO₄ had a serious degradation comparing to the performance with 1.0 M H₂SO₄.

5.4.8. Effect of the membrane thickness

The effect of membrane thickness on cell performance was studied by using different CEMs (N211, N212, and N115) at 23°C, where 4 mL aqueous solution of 5.0 M EG and 9.0 M KOH was contained in anode reservoir and 4 mL aqueous solution of 1.0 M H₂SO₄ and 4.0 M H₂O₂ was contained in cathode reservoir, and the results are shown in Figure 5.15. When the current density was low, a thicker membrane yielded a superior cell performance, which can be confirmed by the OCVs shown in Figure 5.16. However, the performance of this passive fuel cell was better with a thinner CEM at medium and high current densities. This phenomenon can be explained as follows. A thicker membrane suppresses the crossover of both EG from the anode to cathode and H₂O₂ from the cathode to anode. As a result, the negative effects derived from species crossover are hindered and the cell voltage increases at low current density region. However, the ohmic loss plays an important role during the discharging process, especially at medium and high current densities. As shown in Figure 5.16, as the membrane thickness increased, the internal resistance also increased considerably, which led to a rapider degradation of the cell voltage during the whole discharging process. As a result, the cell had a worse performance with thicker membrane due to the increasing ohmic loss at both medium and high current densities.

5.4.9. Effect of the operating temperature

The operating temperature of this passive fuel cell has a considerable effect on the cell performance. When the operating temperature increased, the cell performance also had an obvious improvement. The cell performance was studied with different operating temperatures as shown in Figure 5.17, where 4 mL aqueous solution of 5.0 M EG and 9.0 M KOH was contained in anode reservoir and 4 mL aqueous solution of 1.0 M H₂SO₄ and 4.0 M H₂O₂ was contained in cathode reservoir, and the pretreated Nafion 211 was utilized as the membrane. When the operating temperatures of this fuel cell were at 23°C, 40°C, and 60°C, the peak power densities reached 30.3, 39.6 and 65.8 mW cm⁻², respectively. The impressive enhancement in cell performance is attributed to three reasons. Firstly, the increasing temperature promotes the kinetics of both anode and cathode reactions, including the EGOR and HPRR, which decreases the activation loss during the discharging process [48]. Secondly, the concentration loss decreases with increasing operating temperature. The transport of the reactants in both anolyte and catholyte is improved with higher temperature. The transport of cations through the membrane is boosted as well. As a result of this enhanced transport, the reactants reach the active sites on the CLs more easily, thus the concentration loss decreases because of the alleviative reactant shortage. Lastly, as the operating temperature increases, the CEMs will have a better conductivity, which brings a reduction in ohmic loss. The three improvements result in a better performance of this fuel cell.

5.4.10. Effect of the H₂O₂ self-decomposition

As mentioned, the H₂O₂ self-decomposition will take place in the cathode, and it is an exothermic reaction according to:



Meanwhile, both the electrochemical reactions on the anode and the cathode are exothermic reactions as well, so the cell temperature will increase during discharging. Therefore, it is critical to determine whether the heat released from the H_2O_2 self-decomposition plays an important role in the cell temperature. If the cell temperature increases rapidly due to the H_2O_2 self-decomposition, it is necessary to adopt heat management methods to control the cell temperature at a reasonable range. Figure 5.18 shows the transient temperature behaviors of the passive fuel cell under 20, 40, and 80 mA constant current discharging operation, where 4 mL aqueous solution of 5.0 M EG and 9.0 M KOH was contained in anode reservoir and 4 mL aqueous solution of 1.0 M H_2SO_4 and 4.0 M H_2O_2 was contained in cathode reservoir, and the pretreated Nafion 211 was utilized as the membrane at 23°C. It can be seen that the cell temperature first increased from the room temperature, 23°C, with the discharging time, and finally reached a stable temperature, indicating the heat balance between the cell and external environment. The increased temperatures were 0.5, 1.1, and 2.0°C under 20, 40, and 80 mA current discharging operation, respectively. It can be inferred from the linear temperature increase with the discharging current that the increased temperature is caused by the electrochemical reactions rather than the H_2O_2 self-decomposition. Otherwise, the increased temperature at three different discharging currents should be similar rather than the linear increase. Therefore, both the electrochemical reactions on the anode and the cathode play the dominant role in the cell temperature.

5.5. Summary

A passive direct ethylene glycol fuel cell is proposed and tested in this work. Different operating conditions are tested to investigate the effects of different feeding concentrations of reactants, different thicknesses of the cation exchange membranes, and different operating temperatures on the cell performance. The results exhibit that the peak power densities of this fuel cell are 30.3 and 65.8 mW cm⁻² at 23 and 60°C, respectively, with optimal aqueous anolyte containing 5.0 M EG and 9.0 M KOH, and optimal aqueous catholyte containing 1.0 M H₂SO₄ and 4.0 M H₂O₂. In addition, the results show that the thickness of the CEMs has a significant effect on cell performance. Although a thicker membrane reduces the crossover problem, a thinner one shows a significant reduction in ohmic loss, resulting in a superior cell performance. As a result, the cation exchange membrane prepared from N211 exhibits the best performance. The performance of this fuel cell under the optimal operating conditions (1.58 V and 65.8 mW cm⁻²) has an impressive improvement comparing to a passive direct ethylene glycol fuel cell with oxygen as oxidant, which is more than 2 times in the open circuit voltage and more than 5 times in the peak power density. The excellent performance is mainly attributed to the faster kinetics of hydrogen peroxide reduction reaction due to the two-electron-transfer process. Moreover, the effect of the heat released by the self-decomposition of hydrogen peroxide is also investigated. The results indicate that the hydrogen peroxide self-decomposition shows a negligible effect on the total heat released over the discharging process, during which both the electrochemical reactions on the anode and cathode play the dominant role.

5.6. References

- [1] Z.F. Pan, L. An, T.S. Zhao, Z.K. Tang, Advances and challenges in alkaline anion exchange membrane fuel cells, *Progress in Energy and Combustion Science* 66 (2018) 141-175.
- [2] L. An, T. Zhao, *Anion Exchange Membrane Fuel Cells*, (2018).
- [3] Q.X. Wu, Z.F. Pan, L. An, Recent advances in alkali-doped polybenzimidazole membranes for fuel cell applications, *Renewable and Sustainable Energy Reviews* 89 (2018) 168-183.
- [4] Z.F. Pan, L. An, C.Y. Wen, Recent advances in fuel cells based propulsion systems for unmanned aerial vehicles, *Applied Energy* 240 (2019) 473-485.
- [5] N. Mahato, A. Banerjee, A. Gupta, S. Omar, K. Balani, Progress in material selection for solid oxide fuel cell technology: A review, *Progress in Materials Science* 72 (2015) 141-337.
- [6] A. Kulkarni, S. Siahrostami, A. Patel, J.K. Nørskov, Understanding Catalytic Activity Trends in the Oxygen Reduction Reaction, *Chemical Reviews* 118 (2018) 2302-2312.
- [7] A.A. Gewirth, J.A. Varnell, A.M. DiAscro, Nonprecious Metal Catalysts for Oxygen Reduction in Heterogeneous Aqueous Systems, *Chemical Reviews* 118 (2018) 2313-2339.
- [8] Y. Li, X. Sun, Y. Feng, Hydroxide Self-Feeding High-Temperature Alkaline Direct Formate Fuel Cells, *ChemSusChem* 10 (2017) 2135-2139.
- [9] C.-Y. Wen, Y.-S. Lin, C.-H. Lu, Performance of a proton exchange membrane fuel cell stack with thermally conductive pyrolytic graphite sheets for thermal management, *Journal of Power Sources* 189 (2009) 1100-

1105.

[10] T.S. Zhao, C. Xu, R. Chen, W.W. Yang, Mass transport phenomena in direct methanol fuel cells, *Progress in Energy and Combustion Science* 35 (2009) 275-292.

[11] L. An, T.S. Zhao, Transport phenomena in alkaline direct ethanol fuel cells for sustainable energy production, *Journal of Power Sources* 341 (2017) 199-211.

[12] C. Wang, B. Mo, Z. He, Q. Shao, D. Pan, E. Wujick, J. Guo, X. Xie, X. Xie, Z. Guo, Crosslinked norbornene copolymer anion exchange membrane for fuel cells, *Journal of Membrane Science* 556 (2018) 118-125.

[13] L. An, R. Chen, Mathematical modeling of direct formate fuel cells, *Applied Thermal Engineering* 124 (2017) 232-240.

[14] T.J. Omasta, L. Wang, X. Peng, C.A. Lewis, J.R. Varcoe, W.E. Mustain, Importance of balancing membrane and electrode water in anion exchange membrane fuel cells, *Journal of Power Sources* 375 (2018) 205-213.

[15] Y. Li, Y. He, W. Yang, A high-performance direct formate-peroxide fuel cell with palladium–gold alloy coated foam electrodes, *Journal of Power Sources* 278 (2015) 569-573.

[16] Z.F. Pan, R. Chen, L. An, Y.S. Li, Alkaline anion exchange membrane fuel cells for cogeneration of electricity and valuable chemicals, *Journal of Power Sources* 365 (2017) 430-445.

[17] X. Chen, T. Li, J. Shen, Z. Hu, From structures, packaging to application: A system-level review for micro direct methanol fuel cell, *Renewable and Sustainable Energy Reviews* 80 (2017) 669-678.

[18] L. An, R. Chen, Recent progress in alkaline direct ethylene glycol fuel

cells for sustainable energy production, *Journal of Power Sources* 329 (2016) 484-501.

[19] H. Yue, Y. Zhao, X. Ma, J. Gong, Ethylene glycol: properties, synthesis, and applications, *Chemical Society Reviews* 41 (2012) 4218-4244.

[20] X.-Y. Zhu, L. Zhang, P.-X. Yuan, J.-J. Feng, J. Yuan, Q.-L. Zhang, A.-J. Wang, Hollow Ag₄₄Pt₅₆ nanotube bundles with high electrocatalytic performances for hydrogen evolution and ethylene glycol oxidation reactions, *Journal of Colloid and Interface Science* 532 (2018) 571-578.

[21] Y.-C. Shi, J.-J. Feng, X.-X. Lin, L. Zhang, J. Yuan, Q.-L. Zhang, A.-J. Wang, One-step hydrothermal synthesis of three-dimensional nitrogen-doped reduced graphene oxide hydrogels anchored PtPd alloyed nanoparticles for ethylene glycol oxidation and hydrogen evolution reactions, *Electrochimica Acta* 293 (2019) 504-513.

[22] X.-Y. Huang, A.-J. Wang, X.-F. Zhang, L. Zhang, J.-J. Feng, One-Step Synthesis of PtCu Alloyed Nanocages with Highly Open Structures as Bifunctional Electrocatalysts for Oxygen Reduction and Polyhydric Alcohol Oxidation, *ACS Applied Energy Materials* 1 (2018) 5779-5786.

[23] Z. Pan, Y. Bi, L. An, Mathematical modeling of direct ethylene glycol fuel cells incorporating the effect of the competitive adsorption, *Applied Thermal Engineering* 147 (2019) 1115-1124.

[24] L. An, T.S. Zhao, S.Y. Shen, Q.X. Wu, R. Chen, Performance of a direct ethylene glycol fuel cell with an anion-exchange membrane, *International Journal of Hydrogen Energy* 35 (2010) 4329-4335.

[25] L. An, L. Zeng, T.S. Zhao, An alkaline direct ethylene glycol fuel cell with an alkali-doped polybenzimidazole membrane, *International Journal*

of Hydrogen Energy 38 (2013) 10602-10606.

[26] C.-Y. Wen, Y.-S. Lin, C.-H. Lu, T.-W. Luo, Thermal management of a proton exchange membrane fuel cell stack with pyrolytic graphite sheets and fans combined, *International Journal of Hydrogen Energy* 36 (2011) 6082-6089.

[27] L. An, T. Zhao, X. Yan, X. Zhou, P. Tan, The dual role of hydrogen peroxide in fuel cells, *Science Bulletin* 60 (2015) 55-64.

[28] E.H. Yu, U. Krewer, K. Scott, Principles and Materials Aspects of Direct Alkaline Alcohol Fuel Cells, *Energies* 3 (2010).

[29] G.F. McLean, T. Niet, S. Prince-Richard, N. Djilali, An assessment of alkaline fuel cell technology, *International Journal of Hydrogen Energy* 27 (2002) 507-526.

[30] L. An, T.S. Zhao, Z.H. Chai, L. Zeng, P. Tan, Modeling of the mixed potential in hydrogen peroxide-based fuel cells, *International Journal of Hydrogen Energy* 39 (2014) 7407-7416.

[31] L. An, C.Y. Jung, Transport phenomena in direct borohydride fuel cells, *Applied Energy* 205 (2017) 1270-1282.

[32] S. Fukuzumi, Y.J.C. Yamada, Hydrogen peroxide used as a solar fuel in one-compartment fuel cells, *ChemElectroChem* 3 (2016) 1978-1989.

[33] Z. Pan, B. Huang, L. An, Performance of a hybrid direct ethylene glycol fuel cell, *International Journal of Energy Research* 43 (2019) 2583-2591.

[34] W. Chen, W. Yuan, G. Ye, F. Han, Y. Tang, Utilization and positive effects of produced CO₂ on the performance of a passive direct methanol fuel cell with a composite anode structure, *International Journal of*

Hydrogen Energy 42 (2017) 15613-15622.

[35] L. An, T.S. Zhao, R. Chen, Q.X. Wu, A novel direct ethanol fuel cell with high power density, *Journal of Power Sources* 196 (2011) 6219-6222.

[36] L. An, T.S. Zhao, Performance of an alkaline-acid direct ethanol fuel cell, *International Journal of Hydrogen Energy* 36 (2011) 9994-9999.

[37] R. Chen, T.S. Zhao, Porous current collectors for passive direct methanol fuel cells, *Electrochimica Acta* 52 (2007) 4317-4324.

[38] R. Chen, T.S. Zhao, Performance characterization of passive direct methanol fuel cells, *Journal of Power Sources* 167 (2007) 455-460.

[39] T.S. Zhao, R. Chen, W.W. Yang, C. Xu, Small direct methanol fuel cells with passive supply of reactants, *Journal of Power Sources* 191 (2009) 185-202.

[40] J.G. Liu, T.S. Zhao, R. Chen, C.W. Wong, The effect of methanol concentration on the performance of a passive DMFC, *Electrochemistry Communications* 7 (2005) 288-294.

[41] A. Marchionni, M. Bevilacqua, C. Bianchini, Y.-X. Chen, J. Filippi, P. Fornasiero, A. Lavacchi, H. Miller, L. Wang, F. Vizza, Electrooxidation of Ethylene Glycol and Glycerol on Pd-(Ni-Zn)/C Anodes in Direct Alcohol Fuel Cells, *ChemSusChem* 6 (2013) 518-528.

[42] G.H. Miley, N. Luo, J. Mather, R. Burton, G. Hawkins, L. Gu, E. Byrd, R. Gimlin, P.J. Shrestha, G. Benavides, J. Laystrom, D. Carroll, Direct NaBH₄/H₂O₂ fuel cells, *Journal of Power Sources* 165 (2007) 509-516.

[43] B. Bae, B.K. Kho, T.-H. Lim, I.-H. Oh, S.-A. Hong, H.Y. Ha, Performance evaluation of passive DMFC single cells, *Journal of Power Sources* 158 (2006) 1256-1261.

-
- [44] J.G. Liu, T.S. Zhao, Z.X. Liang, R. Chen, Effect of membrane thickness on the performance and efficiency of passive direct methanol fuel cells, *Journal of Power Sources* 153 (2006) 61-67.
- [45] Y. Yu, X. Yang, Y. Zhao, X. Zhang, L. An, M. Huang, G. Chen, R. Zhang, Engineering the Band Gap States of the Rutile TiO₂(110) Surface by Modulating the Active Heteroatom, *Angewandte Chemie International Edition* 57 (2018) 8550-8554.
- [46] Y.S. Li, T.S. Zhao, Z.X. Liang, Performance of alkaline electrolyte-membrane-based direct ethanol fuel cells, *Journal of Power Sources* 187 (2009) 387-392.
- [47] R.K. Raman, N.A. Choudhury, A.K. Shukla, A High Output Voltage Direct Borohydride Fuel Cell, *Electrochemical and Solid-State Letters* 7 (2004) A488.
- [48] Y.S. Li, T.S. Zhao, A high-performance integrated electrode for anion-exchange membrane direct ethanol fuel cells, *International Journal of Hydrogen Energy* 36 (2011) 7707-7713.

Figures

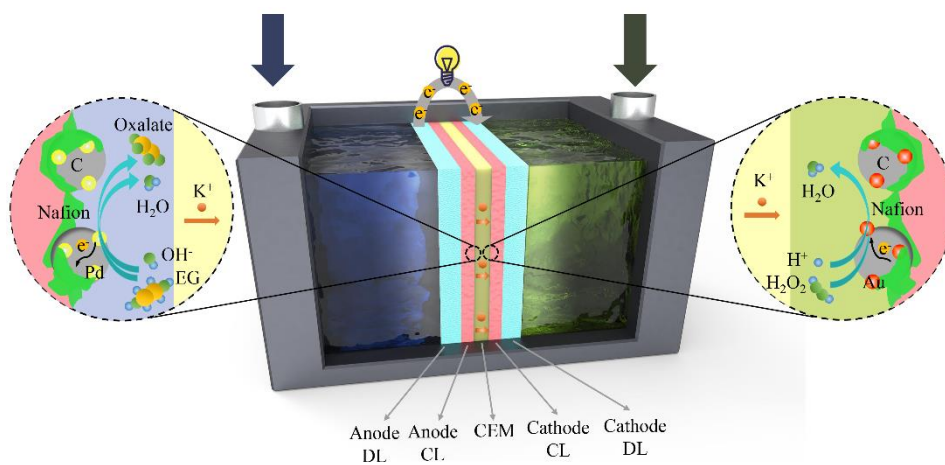


Figure 5.1 Working principle of a passive DEGFC.

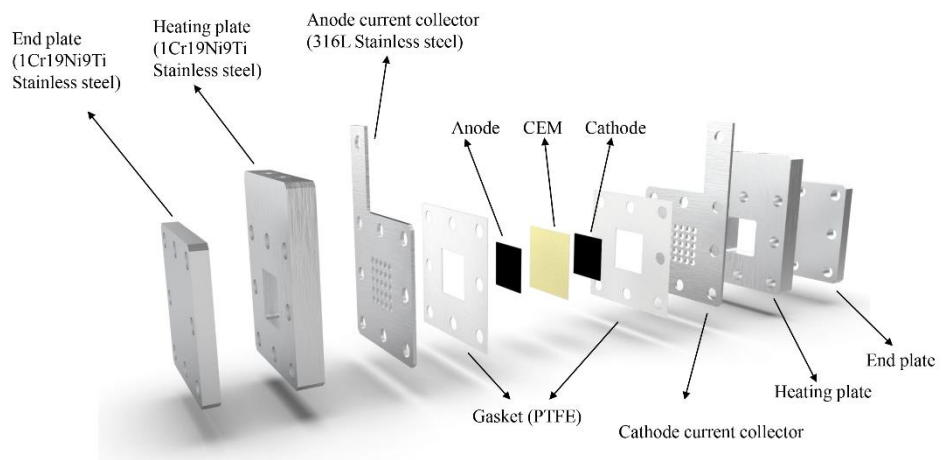


Figure 5.2 Schematic illustration of a passive DEGFC.

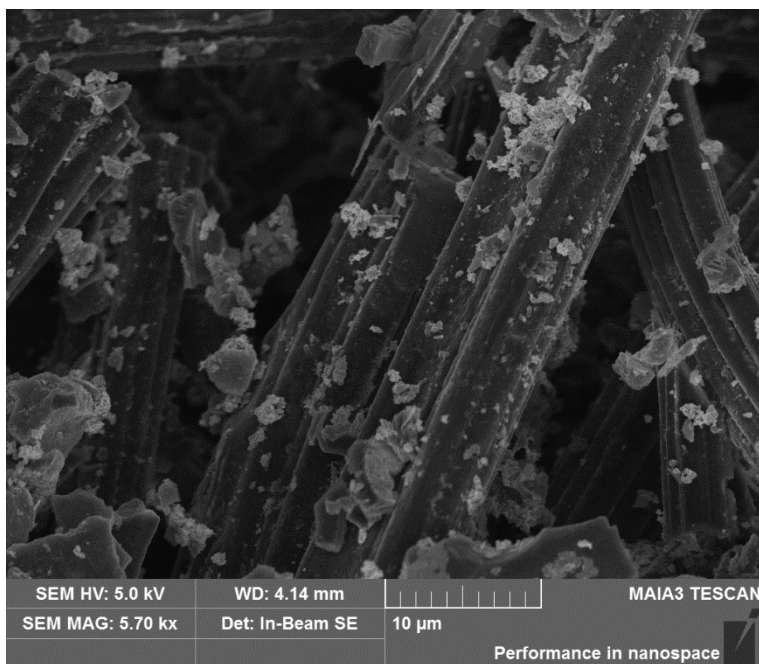


Figure 5.3 SEM images of the catalyst layer of anode.

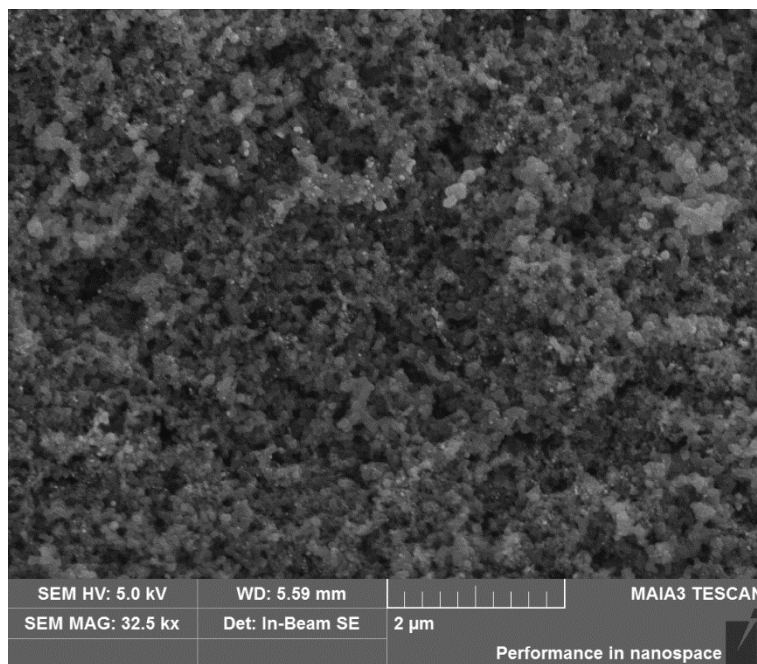


Figure 5.4 SEM images of the catalyst layer of cathode.

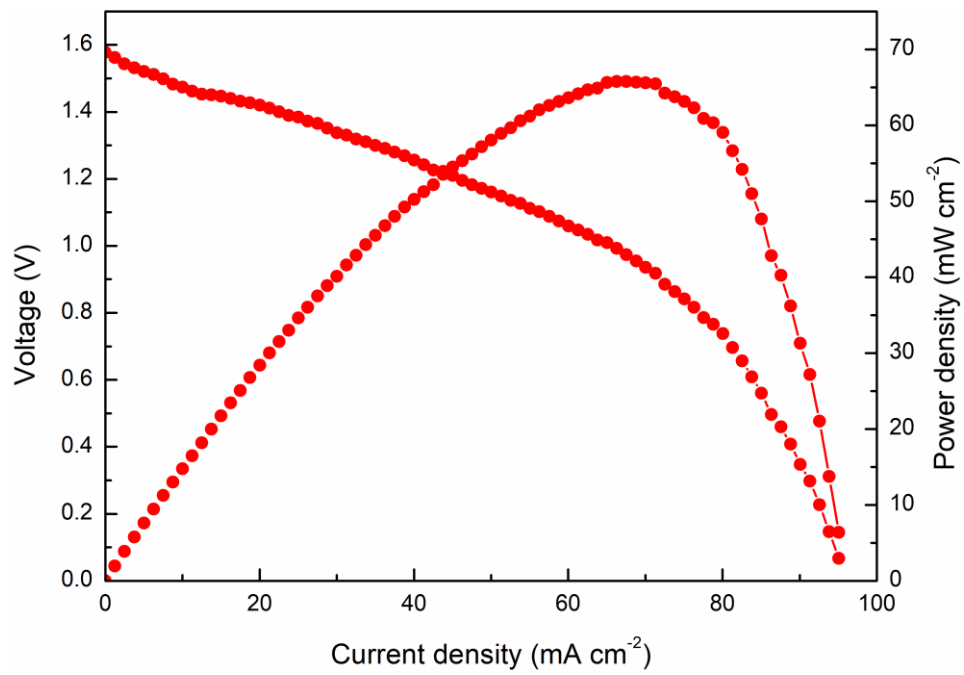


Figure 5.5 General performance of the passive DEGFC.

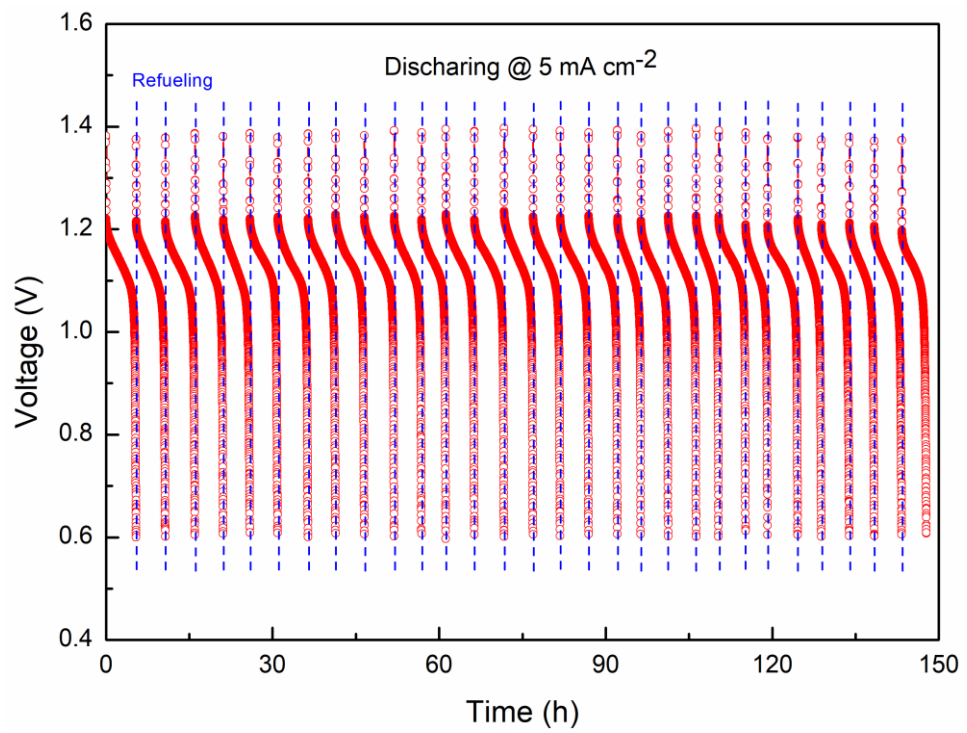


Figure 5.6 Long-term durability of the passive fuel cell.

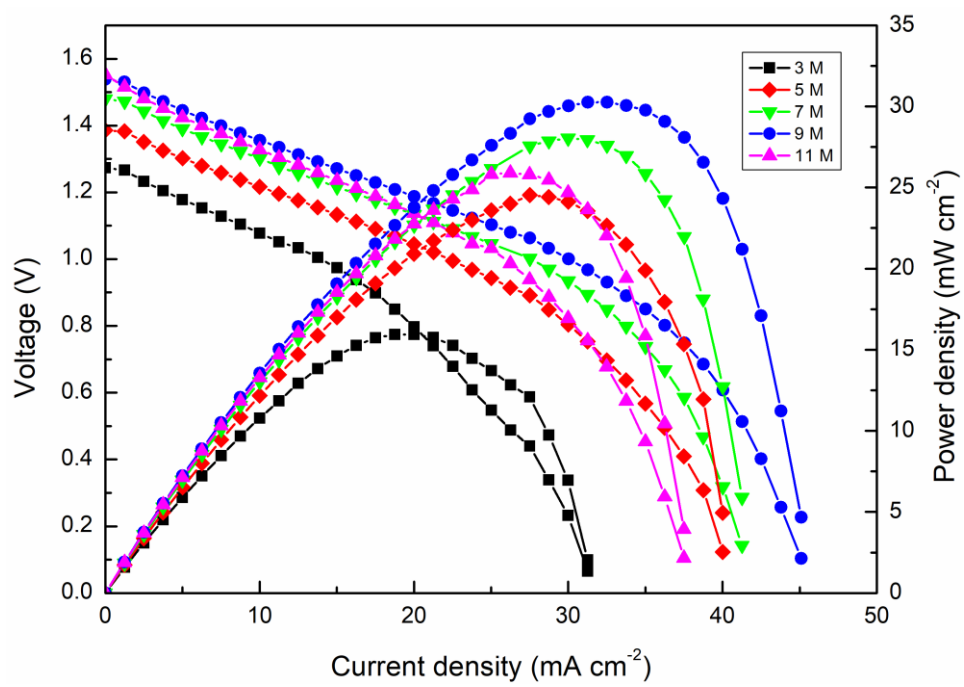


Figure 5.7 Effect of the KOH concentration on the cell performance.

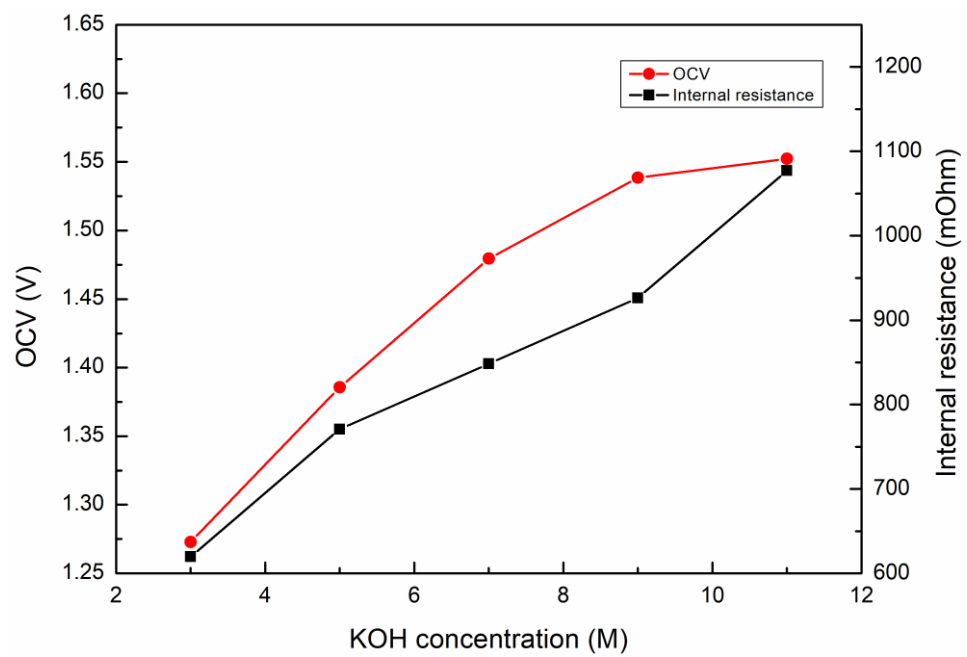


Figure 5.8 Effect of the KOH concentration on the OCV and internal resistance.

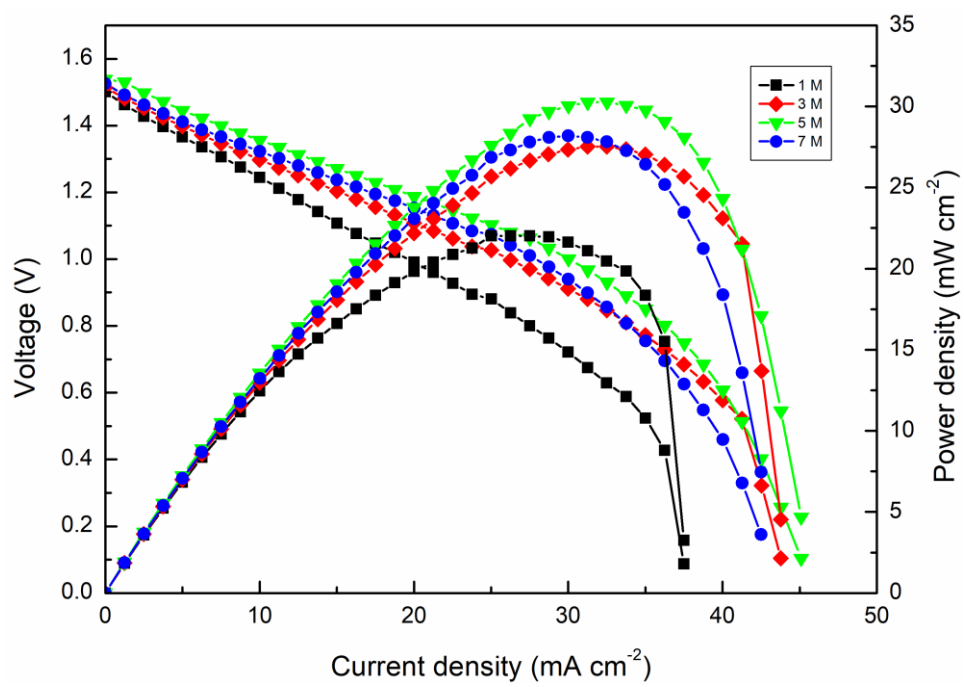


Figure 5.9 Effect of the EG concentration on the cell performance.

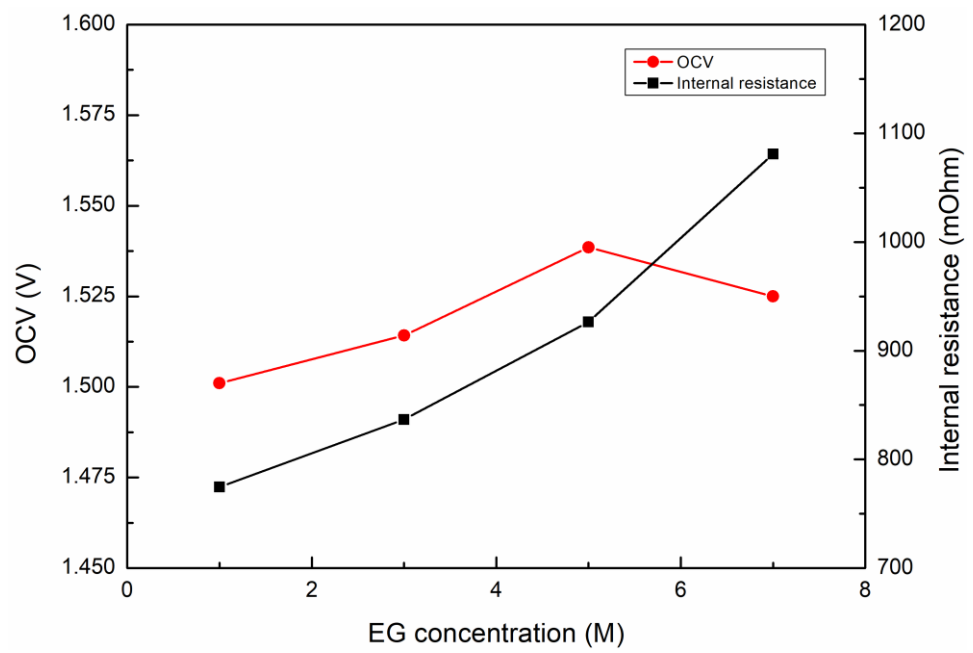


Figure 5.10 Effect of the EG concentration on the OCV and internal resistance.

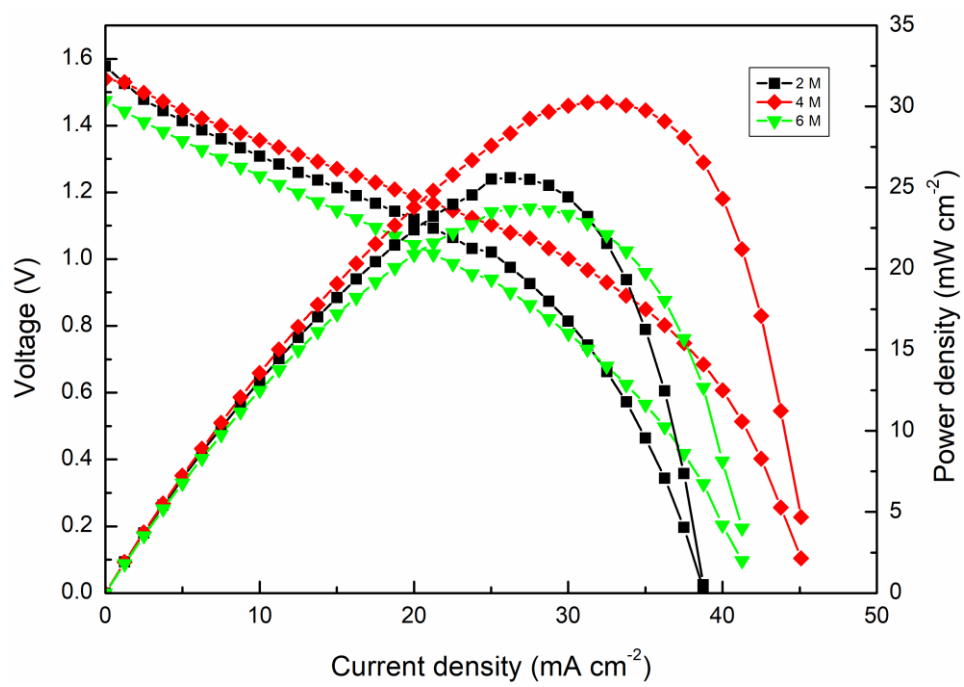


Figure 5.11 Effect of the H₂O₂ concentration on the cell performance.

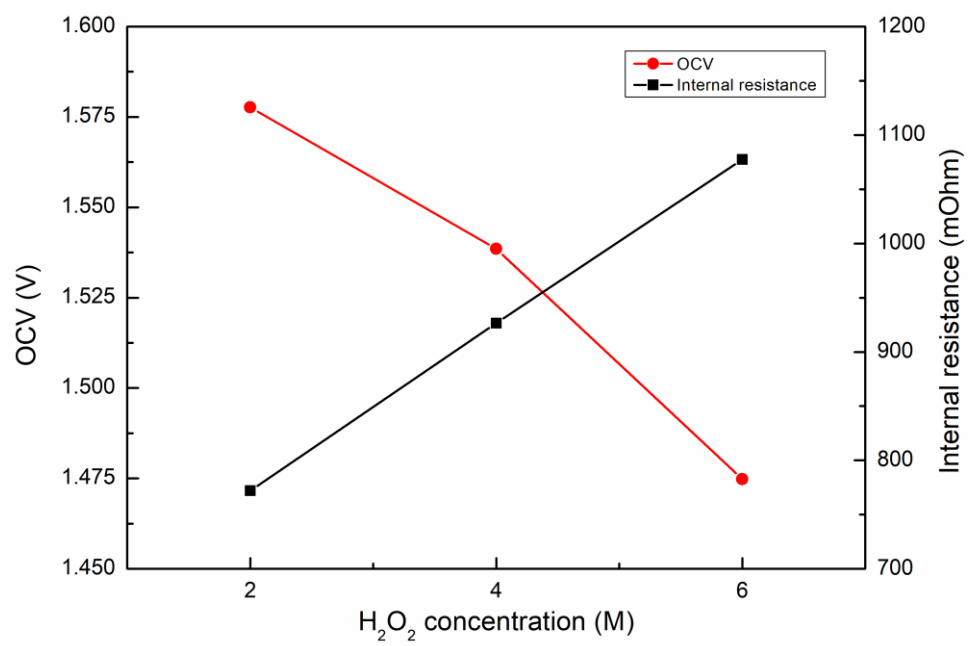


Figure 5.12 Effect of the H₂O₂ concentration on the OCV and internal resistance.

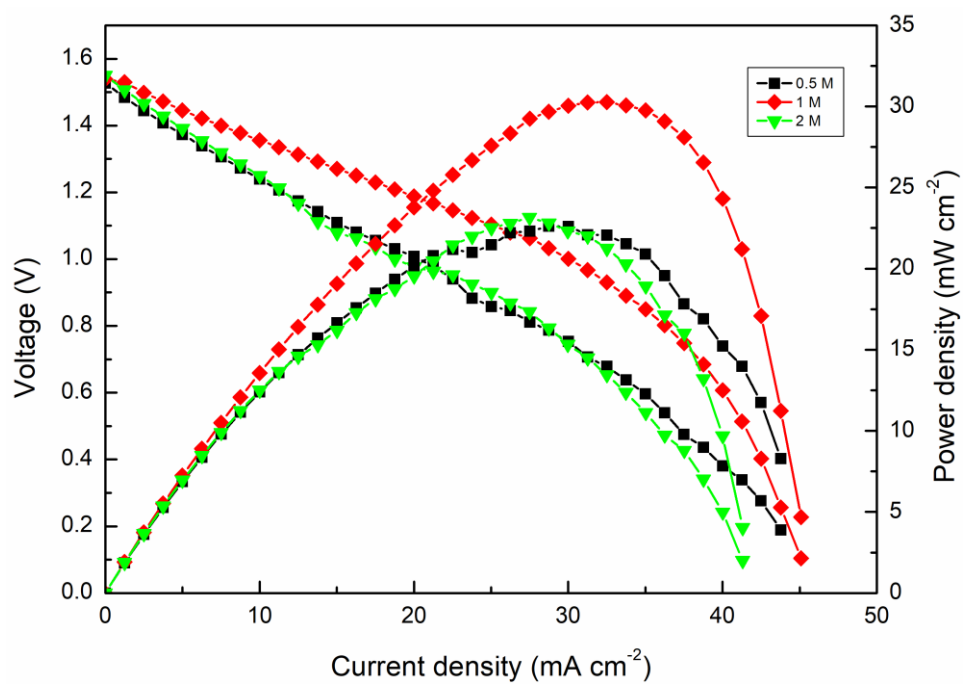


Figure 5.13 Effect of the H₂SO₄ concentration on the cell performance.

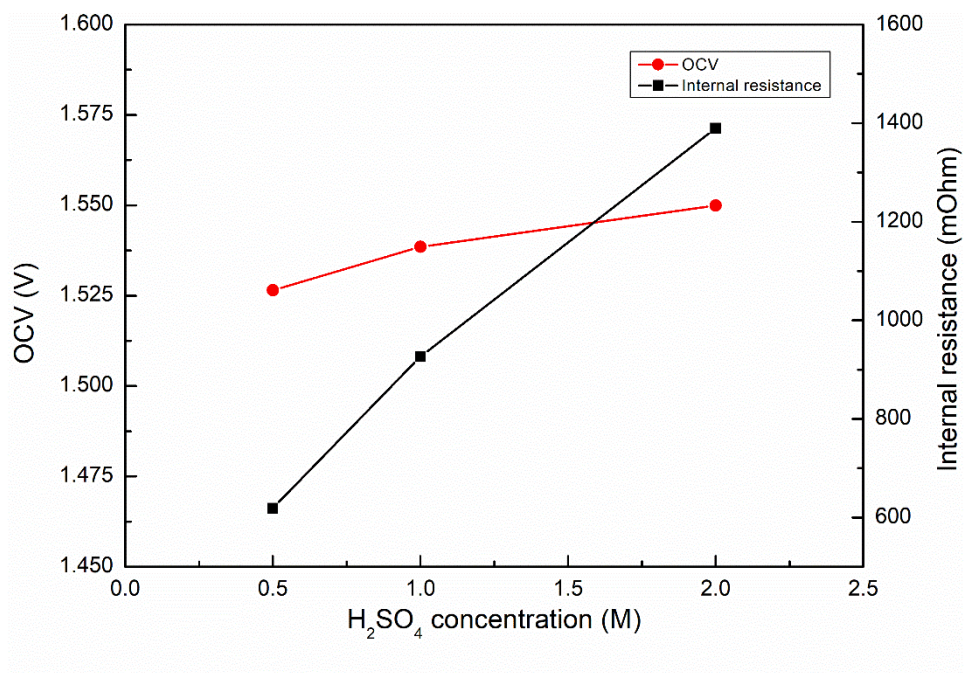


Figure 5.14 Effect of the H₂SO₄ concentration on the OCV and internal resistance.

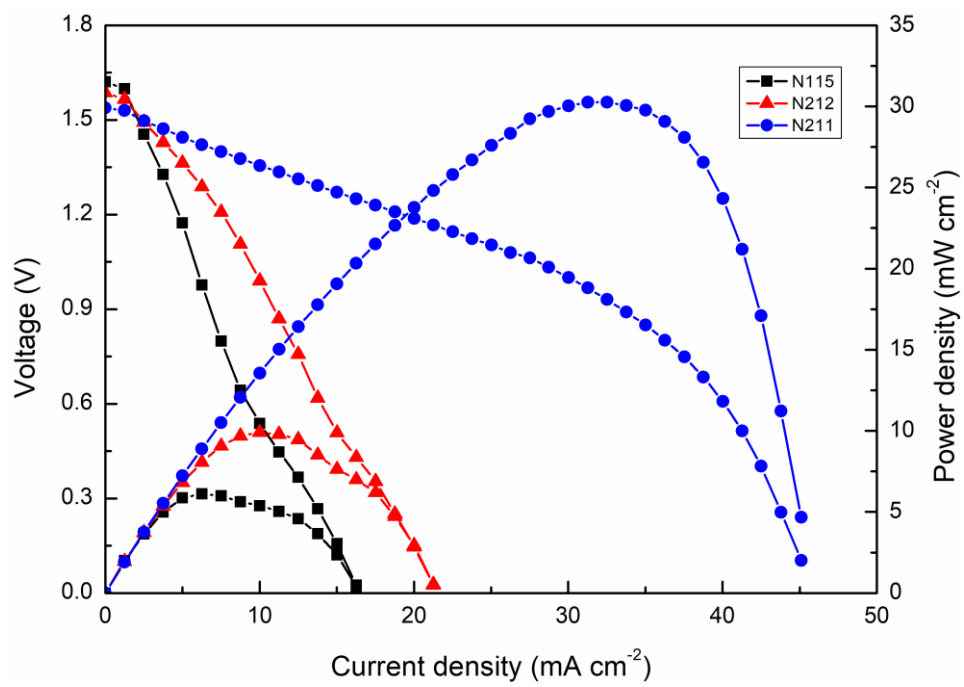


Figure 5.15 Effect of the membrane thickness on the cell performance.

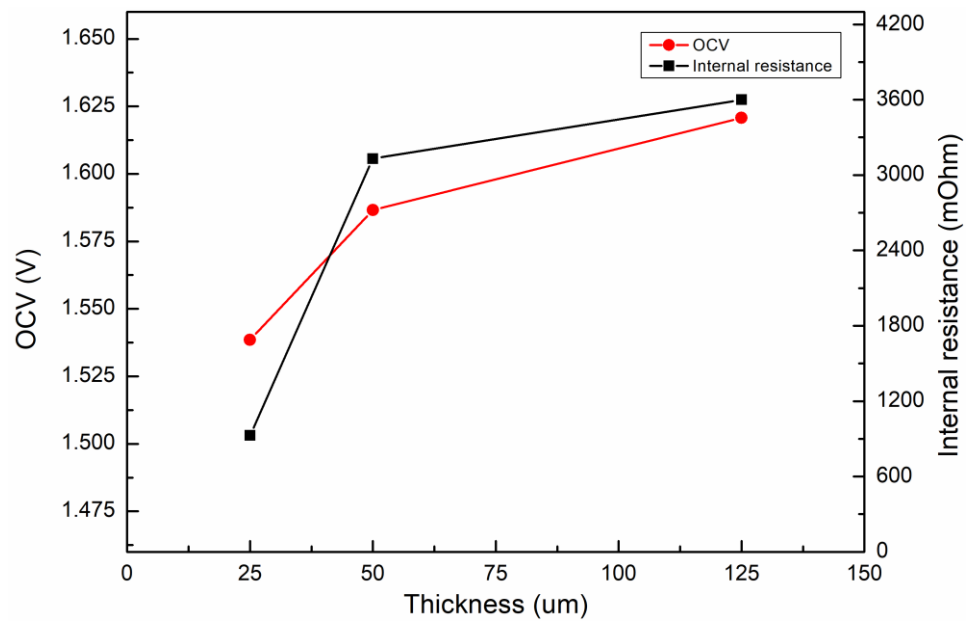


Figure 5.16 Effect of the membrane thickness on the OCV and internal resistance.

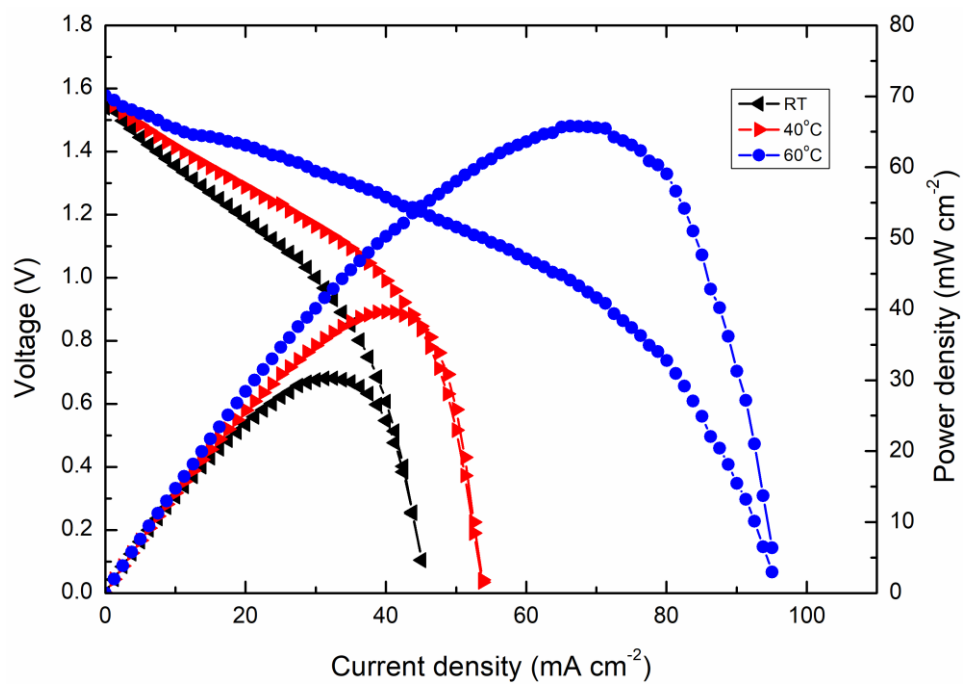


Figure 5.17 Effect of the operating temperature on the cell performance.

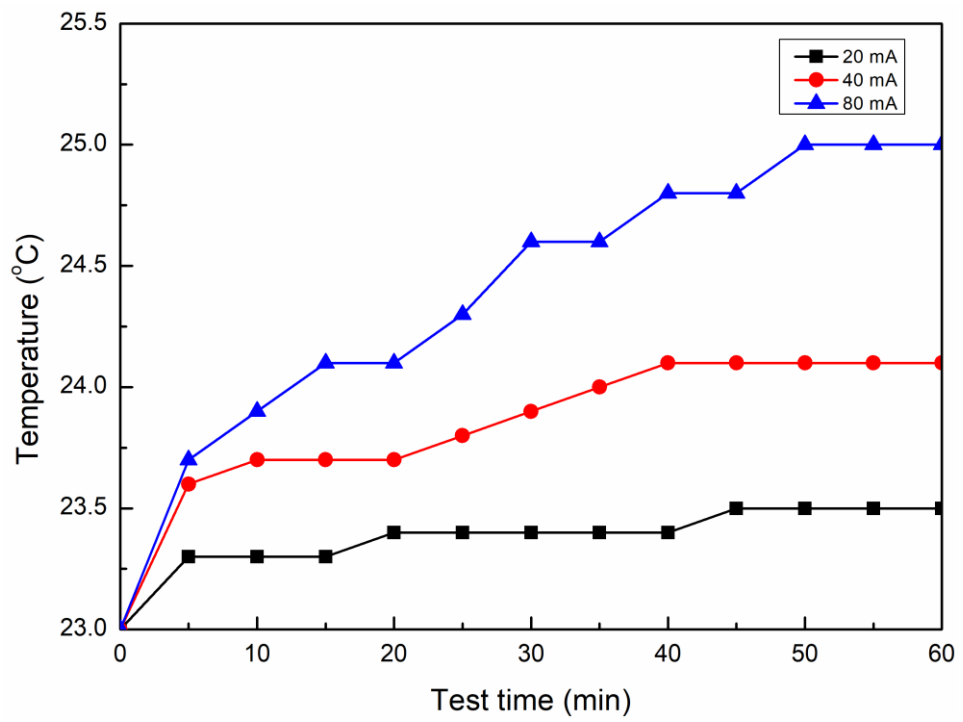


Figure 5.18 Transient cell temperature behaviors with constant current discharging.

Chapter 6 Lab-scale demonstration of a stack

Abstract

A passive direct ethylene glycol fuel cell stack is developed and tested, in which each single cell consists of an alkaline Pd-based anode, an acid Au-based cathode, and a cation exchange membrane. This passive stack design eliminates the gas blowers/compressors for the air supply, external liquid pumps for the liquid fuel supply, or any other auxiliary devices. Hence, the passive design reduces both volume and weight of the stack comparing to the active fuel cell stack, thus both volumetric energy density and specific energy density are much improved. In this study, an alkalized ethylene glycol aqueous solution is used as fuel and an acidified hydrogen peroxide aqueous solution is used as oxidant, respectively. As a result, the theoretical voltage of this fuel cell stack is increased from 2.18 V to 4.94 V comparing to the design using the air, which shows a promising potential for practical applications. Experimentally, at the optimal reactant-feeding concentrations of 5.0 M EG and 9.0 M KOH as anolyte and 4.0 M H₂O₂ and 1.0 M H₂SO₄ as catholyte, this passive stack yields an open-circuit voltage of 3.0 V, a maximum current of 860 mA, and a peak power of 1178 mW at room temperature, which exhibits a two-time higher peak power density (24.5 mW cm⁻²) than a passive stack using the same type of fuel but the air as oxidant (12 mW cm⁻²). The impressive improvement can be ascribed to the faster hydrogen peroxide reduction reaction due to its two-electron transfer process rather than a four-electron process. In addition, the effects of feeding concentrations in both anolyte and catholyte on the stack

performance are studied. Finally, the present passive stack is applied to power an electric fan for around 3 hours under the mimetic underwater circumstance, demonstrating that this passive stack is a promising power source for airtight situations, such as underwater and outer space.

Keywords: Direct ethylene glycol fuel cells; Passive fuel cells; Fuel cell stack; Hydrogen peroxide; Feeding concentrations; Underwater operation

6.1. Introduction

Direct liquid fuel cells (DLFCs) that use liquid alcohols as fuel, e.g. methanol, ethanol, and ethylene glycol (EG), to replace gaseous hydrogen have been regarded as one of the most promising power generation technologies for portable electronics [1-5]. In spite of the general superiorities of fuel cells, such as simple design, high energy conversion efficiency, low emissions as well as quick refueling [4, 6], the DLFCs exhibits a broader range of advantages including mature production, easy transportation, and convenient handling of liquid fuels comparing to hydrogen fuel cells [7-11]. Among various liquid fuels, EG has received considerable interests because of the electron transfer rate as high as 80%, the boiling point of 198°C, and the theoretical energy capacity of 4.8 Ah mL⁻¹, which is a promising fuel for electronic devices [12, 13]. In addition, the toxicity of EG is low and it can be produced by hydration of ethylene oxide (EO) efficiently [14]. Therefore, direct ethylene glycol fuel cells (DEGFCs) have attracted ever-increasing attention, particularly these fuel cells using anion exchange membranes (AEMs) due to the both enhanced anodic and cathodic kinetics [15-18]. AEMs and cation exchange membranes (CEMs) are classified by the charge type of fixed functional groups, which can selectively allow the passage of oppositely charged ions (counter-ions), while obstruct similarly charged ions (co-ions) [19]. An et al. [20] compared the AEM and CEM in direct ethanol fuel cells (DEFCs). It was found that the AEM possessed the higher ionic conductivity and mechanical property, but the worse thermal stability. In addition, the CEM

showed the lower ionic conductivity, but acceptable thermal stability, mechanical property, and species permeability. There is no significant difference in the fuel cell performance between the AEM and CEM at low operating temperatures ($<60^{\circ}\text{C}$), but the CEM-DEFC can operate stably at high operating temperatures (typically 90°C).

In the past decade, numerous effects have been made on performance improvement, catalyst development, and system innovations [21-28]. An et al. [21] developed and tested an alkaline DEGFC using an AEM, which exhibited a peak power density of 67 mW cm^{-2} at 60°C . The outstanding performance was ascribed to the alkaline environment, which much enhances the kinetics of both the oxygen reduction reaction (ORR) and ethylene glycol oxidation reaction (EGOR). Considering the poor stability of AEM at high temperatures, generally over 60°C , they replaced the AEM with an alkali-doped polybenzimidazole in an alkaline DEGFC, which allows the operation of the fuel cell at higher temperatures (90°C). As a result, it was found that a higher peak power density of 112 mW cm^{-2} was achieved at 90°C [22]. To improve the activity of the catalyst toward EGOR, Feng et al. [23] reported networked Pt-Pb nanowires (NWs), which was synthesized via a large-scalable wet-chemical approach. The electrocatalyst showed a 3D networked structure with rich defects/steps. To further promote the cell performance and extend the application situations to underwater and outer space, Pan et al. [29] reported that an open-circuit voltage (OCV) of 1.41 V and a peak power density of 80.9 mW cm^{-2} at 60°C were achieved by replacing the oxygen with hydrogen peroxide in the

DEGFC. This type of DEGFC boosted the OCV by 62.1% and the peak power density by 20.8%, as well as eliminated the requirement of air from the ambient environment. Using the acidified hydrogen peroxide rather than the oxygen or air in the cathode as the oxidant has been tested in fuel cells running on various fuels such as formate [30], propanol, and glycerol [31]. Li [30] found that the AEM direct formate-peroxide fuel cell showed a more stable cell voltage than the AEM direct ethanol fuel cell in a conceptual half-hour constant-current discharge. Chino et al. [31] reported that the split pH environment improved the thermodynamics of the fuel cell by creating a large potential difference between electrodes. However, the decomposition of H_2O_2 and thus generation of O_2 may form a two-phase flow in the cathode flow channel, resulting in the voltage fluctuation, which is not desirable in the practical applications. Meanwhile, it creates a large transport resistance of H_2O_2 from the cathode flow channel to the cathode CL, which may lead to the H_2O_2 in the cathode CL at a starving state, thus the cathodic reaction kinetics is sluggish [32].

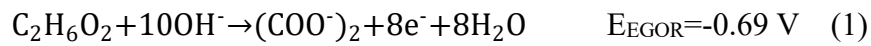
Moreover, to meet the voltage requirement of electronics in practice, a fuel cell stack rather than a single cell is used, which is constituted by cells connected in series. Cremers et al. [33] developed an active AEM-DEGFC stack using the air as oxidant. When the feeding rates were 12 mL min^{-1} on the anode and 800 sccm on the cathode, the fuel cell stack showed a peak power density of 44 mW cm^{-2} at 50°C . Although the performance is promising, the active operation mode needs auxiliary equipment such as liquid pumps and gas compressors, leading to a more complicated and

heavier system [34, 35]. To meet the demand for portable electronic devices, the active operation mode can be replaced by a passive way, which makes the reactants store in the reservoirs and transport to the catalyst layer mainly via diffusion, driven by the concentration gradient [36]. It should be mentioned that the delivery of reactants at the passive operation mode in the porous electrode is slower than the active one does, which is attributed to the fact that an additional driving force of convection for the delivery of reactants exists at the active operation mode. Hence, the passive fuel cell performance is generally lower than the active fuel cell does at the same operation conditions. Pan et al. [37] developed a passive DEFC with hydrogen peroxide as oxidant. This fuel cell exhibited peak power densities of 30.3 and 65.8 mW cm⁻² at 23 and 60°C, respectively. Marchionni et al. [38] synthesized Pd-(Ni-Zn)/C catalyst, which was Pd nanoparticles supported on a Ni-Zn phase, and adopted it as the anode catalyst in a passive DEFC. It was found that the peak power density increased from 12 mW cm⁻² to 24 mW cm⁻² at 25°C when the Pd-(Ni-Zn)/C replaced the Pd/C. Fashedemi et al. [39] prepared Pd-based ternary core-shell (FeCo@Fe@Pd) nanocatalyst using multi-walled carbon nanotubes bearing carboxylic (MWCNT-COOH) as supporting platform and compared its performance with the Pd/MWCNT-COOH in a passive DEFC. It was reported that the running time of the fuel cell using the FeCo@Fe@Pd/MWCNT-COOH-based anode was around 4.7 h at a discharging current density of 20 mA cm⁻², which was higher than the Pd/MWCNT-COOH-based anode did (3.3 h).

In this study, being motivated by the practical needs for reducing the design complexity of the fuel cell system as well as the high voltage requirement of electronics in practice, we designed, fabricated, and tested a passive DEGFC stack, constituted by two single cells, using hydrogen peroxide as oxidant, which avoids the use of liquid pumps and gas compressors as well as possesses a promising theoretical OCV of 4.94 V. As a result of the simpler structure, the specific energy density and volumetric energy density are increased, and the design complexity is reduced significantly. Moreover, the replacement of the oxygen provided from the environment by the hydrogen peroxide in the proposed fuel cell stack is in favor of allowing the fuel cell stack to be air-independent power sources for underwater and outer space applications. Although it is attractive, the H_2O_2 is not stable and will be decomposed to oxygen and water, thus the produced oxygen will reduce the electrochemical surface area (ECSA) and block the channels for reactant delivery, to which future research attention can be paid. The effects of feeding concentrations on the fuel cell stack performance are investigated. When the fuel cell stack is operated at the optimal reactant-feeding concentrations of 5.0 M EG and 9.0 M KOH as anolyte and 4.0 M H_2O_2 and 1.0 M H_2SO_4 as catholyte, it exhibits an actual OCV of 3.0 V, a maximum current of 860 mA, and a peak power of 1178 mW at room temperature. It is found that the whole running time of the fan powered by this passive fuel cell stack was 2 hours and 36 minutes underwater, which was similar to the that in the natural circumstance, demonstrating that this passive fuel cell stack is a promising power source for airtight situations.

6.2. Working principle

As depicted in Figure 6.1, the passive stack is constituted by two single cells connected in series, which are named as cell 1 and cell 2. The single cell is symmetrically constructed. From the anode to the cathode, the components are the anode diffusion layer (DL), the anode catalyst layer (CL), the CEM, the cathode CL, and the cathode DL in sequence. In cell 1, the anolyte diffuses from the anode reservoir to the anode CL driven by the concentration gradient, where EGOR occurs and oxalate, electrons and water are produced as shown in Eq. (1) [12]:



The electrons produced by the EGOR of cell 1 are transported from the anode to the cathode of cell 2 through the external circuit. At the same time, H_2O_2 and protons in the cathode reservoir of cell 2 are transported through the cathode DL to the CL and react with coming electrons to produce water, which is known as the hydrogen peroxide reduction reaction (HPRR) [40]:



Meanwhile, the EGOR occurs in the anode of cell 2 and the electrons produced are transported through the external circuit to the cathode of cell 1. The HPRR is induced in the cathode of cell 1 when receiving the electrons from the anode of cell 2. In both cell 1 and cell 2, the potassium ions transport from the anode to the cathode to complete the internal ionic circuit. The overall reaction is obtained by combining the EGOR and HPRR, which achieves a significantly high theoretical voltage of 2.47 V for a single cell [37]:



6.3. Experiments

6.3.1. Preparation of membrane electrode assembly

The membrane electrode assembly (MEA) is the key component in the passive stack. Two pairs of home-made anodes and cathodes with an active area of 3.0 cm × 8.0 cm are used in the two single cells and the pretreated Nafion 211 (30 μm in the dry state) is selected as the CEM due to the smaller thickness. The Pd-based anode could be fabricated by the method in the open literature [41]. The preparation of the catalyst ink was mixing the ethanol, 5 wt.% Nafion (Fuel Cell Store, USA), and 30 wt. % Pd/C (Sigma-Aldrich Co., USA). Afterwards, the mixed ink underwent an ultrasonic treatment in the ultrasonic oscillating instrument for 30 minutes. Then the catalyst ink was coated on the carbon cloth (Hesen, China) by a spraying method until the catalyst loading reached 1.0 mg_{Pd} cm⁻². Similarly, 60 wt. % Au/C (Premetek Co., USA) was mixed with 15 wt. % Nafion and ethanol to prepare the cathode catalyst ink, which was then sprayed on the carbon cloth by the same method, and the catalyst loading of the catalyst was 2.75 mg_{Au} cm⁻². In terms of the preparation of CEMs, the membranes were cut to an area of 4.0 cm × 9.0 cm so that it can fully cover the electrode, which were then immersed in the 2.5 M KOH solution. After one-hour immersion at 80°C, DI water was used to wash the membrane for three times and the membrane was kept in DI water for further assembly.

6.3.2. Fuel cell setup and instrumentation

As depicted in Figure 6.2, the stack consists of two pairs of MEAs, three

endplates, four reservoirs, four current collectors, and assorted screws. In case of corrosion by the acid and alkaline environments, 1Cr18Ni9Ti stainless steel and 316L stainless steel were chosen as the materials of endplates and current collectors, respectively. The electrolyte reservoir was designed to be transparent by using polymethyl methacrylate (PMMA) with a hole drilled on the top so that the process of anolyte/catholyte injection is visible. Polytetrafluoroethylene (PTFE) gaskets were added between each layer of the stack to prevent the leakage. The two single cells were connected in series and the electrode arrangement of these two single cells were opposite to avoid the formation of internal fuel cell and self-discharging. The polarization curve and internal resistance of the passive fuel cell stack were tested by using Arbin BT2000 (Arbin instrument Inc.).

6.4. Results and discussion

6.4.1. General performance

Figure 6.3 shows the results of the polarization test and the power of the passive stack at room temperature with 5.0 M EG and 9.0 M KOH as anolyte and 4.0 M H₂O₂ and 1.0 M H₂SO₄ as catholyte. It is demonstrated that the passive stack outputs an OCV of 3.0 V, a maximum current of 860 mA, and a peak power of 1178 mW. In a previous study [42], when EG was used as fuel in the anode and O₂ was used as oxidant in the cathode, the passive single cell achieved an OCV of 0.7 V and a peak power density of 12 mW cm⁻². The passive stack in this study exhibits an OCV (3.0 V) four times higher than 0.7 V and a peak power density (24.5 mW cm⁻²) twice higher than 12 mW cm⁻². The performance elevation of this passive stack is

mainly ascribed to the superior nature of HPRR comparing to ORR. The two-electron-transfer process of HPRR is more beneficial to the fuel cell performance due to the enhancement of reaction kinetics and a higher theoretical voltage comparing to the four-electron-transfer process of ORR [43]. However, the practical OCV of the stack (3.0 V) is significantly lower than the theoretical OCV (4.94 V). In general, the theoretical OCV can hardly achieve due to the presence of the activation loss, which is caused by the slowness of the reactions taking place on the surface of the electrodes as well as the poor reversibility of anodic and cathodic reactions. Hence, a proportion of the voltage generated is sacrificed to drive the chemical reaction that transfers the electrons to or from the electrode [44]. From this perspective, four methods can be adopted to reduce the activation loss, which are raising the fuel cell operating temperature, using more effective catalysts, increasing the roughness of the electrode, and increasing the reactant concentrations appropriately [45]. In addition, the large OCV loss is associated with the H_2O_2 as well. The H_2O_2 in the cathode is supposed to be used as oxidant, nonetheless, the H_2O_2 also can be oxidized, which establishes of an internal H_2O_2 -based fuel cell and causes the mixed potential in the cathode [37]. Moreover, the H_2O_2 is not stable and will be decomposed to oxygen and water. The produced oxygen gas results in two disadvantages. On one hand, the active sites on the catalyst particle may be covered by oxygen, reducing the electrochemical surface area. On the other hand, oxygen in the porous DL and CL will block the pathways for the reactant transport.

The consistency of the individual cell was investigated by monitoring the voltage of cell 1 and cell 2 at different current densities. As shown in Figure 6.4, the voltage of the two cells exhibited a good consistency over the whole current region. However, it can be observed that the voltage of cell 1 decreased slightly faster than cell 2 with increasing current, which was ascribed to the higher internal resistance of cell 1. The good conformance of individual cell consistency reflects a high degree of reproducibility achieved by the appropriate electrode manufacturing process [46], which predicts a promising future for the mass production in practical applications. Meanwhile, the transient OCV behavior of the stack was investigated. The cell stack was first discharged completely and rested for 20 minutes, and the OCV was recorded and shown in Figure 6.5. The OCV of the stack increased rapidly in the first 5 minutes and stabilized at around 2.8 V subsequently. The OCV of this passive stack did not experience a decrease after reaching the maximum value during the rest period, which is different from some other types of fuel cell, such as the direct methanol fuel cells (DMFCs) and DEFCs [47]. This performance improvement is ascribed to the fact that the Au catalyst is inactive to EG, thus the mixed potential problem in the cathode is eliminated, which leads to the stable OCV during the rest period.

Moreover, the constant discharging behavior of this stack was studied. As shown in Figure 6.6, when the discharging process was conducted at a constant current of 150 mA, the stack was operated with a stable voltage around 2.5 V for about 160 minutes, presenting a stable and satisfactory

performance. In addition, the cost of this passive fuel cell stack can be obtained by summing up the cost of all the components. The unit prices of the anode catalyst, cathode catalyst, CEM, and DL are $\$42.7 \text{ g}^{-1}$, $\$136 \text{ g}^{-1}$, $\$0.07 \text{ cm}^{-2}$, and $\$0.11 \text{ cm}^{-2}$, respectively. Based on the usage of materials in the electrode fabrication, the anode catalyst costs around $\$8.59$, the cathode catalyst is around $\$35.90$, the CEMs are about $\$4.86$, the DLs are about $\$16.32$, and the fixers are about $\$5.10$. Hence, taking the peak power of 1.178 W achieved by this passive fuel cell stack into consideration, the cost normalized by power output of this passive fuel cell stack is about $\$60.08 \text{ W}^{-1}$. Comparing to the cost of an active DMFC stack, which is $\$43.19 \text{ W}^{-1}$ [48], the cost of this passive fuel cell stack is higher, which is attributed to the high cathode catalyst loading. All the results show that the passive stack is a promising candidate to be further studied for future application.

6.4.2. Effect of the EG concentration

The effect of the EG concentration on the passive stack performance was studied as shown in Figs. 4 (a) and (b). In addition to the variations EG concentrations from 1.0 M to 7.0 M , the concentrations of KOH , H_2O_2 , and H_2SO_4 were fixed at 9.0 M , 4.0 M and 1.0 M , respectively. Meanwhile, the operating temperature was room temperature, and a pretreated Nafion 211 membrane was used as the cation exchange membrane. Figure 6.7 presents the polarization curves of the stack with different concentrations of EG. The peak power increased at first and then decreased with the increasing concentrations of EG from 1.0 M to 7.0 M , and the maximum value of the peak power reached 1178 mW with 5.0 M EG. At the same time, the values

of the maximum current showed a large variation. The maximum current was 480 mA with 1.0 M EG. Then, it increased to around 860 mA when the concentration of EG was increased to 3.0 M and 5.0 M. However, with EG concentration further increasing to 7.0 M, the maximum current decreased to 590 mA. Moreover, as presented in Figure 6.8, the OCV increased from 2.89 V to 3.00 V with concentration of EG increasing from 1.0 M to 5.0 M. However, the OCV was reduced to 2.85 V at a EG concentration of 7.0 M. These observations of stack performance with different concentrations of EG can be explained by these reasons. When the EG concentration varies from 1.0 M to 5.0 M, the diffusion of EG is promoted due to the increasing concentration gradient of EG, which results in an elevation of EG concentration on the anode CL from the starvation state to the sufficient state. Therefore, the OCV is elevated with the increasing EG concentration from 1.0 M to 5.0 M. This explanation is also validated by the sharp decrease of voltage and power at the high current region of 480 mA with 1.0 M EG, which is caused by the severe concentration loss due to the fuel shortage. However, when the EG concentration was increased to 3.0 M and 5.0 M, the concentration losses at high current region became less severe. When the concentration of EG was further increased to 7.0 M, the stack performance experienced a significant degradation ascribed to three possible reasons. Firstly, competitive adsorption between EG and OH^- on the active sites occurs with a high EG concentration. When the concentration of EG is 7.0 M, the active sites on the anode CL are taken up by the EG, which hinders the adsorption of OH^- and results in a lower

kinetics of EGOR. The sharp decrease of cell voltage with 7.0 M EG at a high current region of 590 mA is caused by the severe concentration loss due to the OH^- shortage, which validates the above explanation. Secondly, the crossover of EG becomes severer with a higher EG concentration. Although the EG permeated to the cathode cannot produce the mixed potential due the fact that Au is not sensitive to EG, a portion of active sites on the cathode CL is occupied by the EG. The reaction kinetics of HPRR is negatively affected, which is reflected by the decreased OCV of the cell stack with EG concentration increasing from 5.0 M to 7.0 M as shown in Figure 6.8. Lastly, the viscosity of anolyte increases as EG concentration increases. The transportation of the reactants and charges is hindered, which results in a larger internal resistance and an elevated ohmic loss as shown in Figure 6.8. In summary, the passive stack outputs the maximum OCV, current, and power of 3.0 V, 860 mA, and 1178 mW, respectively, at an EG concentration of 5.0 M when other operating conditions are constant.

6.4.3. Effect of the KOH concentration

Figure 6.9 shows the effect of the KOH concentration on the stack performance with EG, H_2O_2 , and H_2SO_4 concentrations fixed at 5.0, 4.0, and 1.0 M accordingly. It can be observed that the OCV increased from 2.68V to 3.06V with OH^- concentration increasing from 5.0 M to 11.0 M. In terms of a specific catalyst, the kinetics of EGOR is dominated by the local concentrations of species in the anode CL. At an EG concentration of 5.0 M, a higher OH^- feeding concentration will result in enhanced OH^- transportation from the anode reservoir to the anode CL where a starvation

state of OH^- is transferred to a sufficient state. Therefore, the EGOR kinetics is enhanced through this process, which leads to a gradually increasing OCV as presented in Figure 6.10. However, the gradient of the OCV curve in Figure 6.10 was smaller, indicating that further increasing the OH^- concentration had little contribution to the enhancement of OCV. This can be explained that the adsorption of OH^- has almost been saturated at the concentration of 9.0 M, thus limited OH^- is able to be adsorbed on the active sites. It can be obtained that the peak power of 1178 mW was reached at 9.0 M as presented in Figure 6.9, while the performance would degrade with either higher or lower OH^- concentration. Generally, the electrochemical kinetics and the species transport in the anode largely depend on the alkalinity of the anode. It can be observed from Figure 6.10 that the internal resistance enlarged from 285 mOhm to 316 mOhm when OH^- concentration increased from 5.0 M to 9.0 M. The performance is still improved because the compensation of positive effect of facilitated EGOR kinetics on stack performance for the increased ohmic loss is adequate. When further increasing the OH^- concentration, the internal resistance increasing to 331 mOhm led to a larger ohmic loss. In addition, the active sites will be fully occupied by OH^- , hence the EGOR kinetics is reduced and the concentration loss is promoted. In conclusion, the performance of the passive stack improves with OH^- concentration increasing from 5.0 M to 9.0 M, then declines with OH^- concentration increasing from 9.0 M to 11.0 M.

6.4.4. Effect of the H_2O_2 concentration

The H_2O_2 used in the cathode acts as the oxidant for the passive stack, and its concentration plays a crucial role on the stack performance. As shown in Figs. 6 (a) and (b), the effect of H_2O_2 concentration on stack performance was investigated with a constant H_2SO_4 concentration at 1.0 M. In Figure 6.11, it could be seen from the polarization curves with different H_2O_2 concentrations that the stack performance was improved as the H_2O_2 concentration was first elevated from 2.0 M to 4.0 M, then degraded with H_2O_2 concentration further increasing to 6.0 M. The stack voltage in the whole current region increased first and then decreased with the increasing concentration of H_2O_2 and the maximum current also conformed to the same trend. The best performance was obtained when the concentration of H_2O_2 was 4.0 M with a highest power of 1178 mW and a maximum current of 860 mA. Figure 6.12 shows that the OCV of the stack experienced an increase from 2.92 V to 3.00 V with H_2O_2 concentration increasing from 2.0 M to 4.0 M, and then decreasing to 2.79 V as H_2O_2 concentration further reached 4.0 M. Meanwhile, the internal resistance of the stack enlarged from 331 mOhm to 368 mOhm with the increased concentration of H_2O_2 . The above observations can be explained as follows. As shown in Figure 6.11, the significant concentration loss at high current range with the H_2O_2 concentration of 2.0 M reveals the fact that the local concentration of H_2O_2 on cathode CL is in a deficient state. As the concentration of H_2O_2 increases from 2.0 M to 4.0 M, the diffusion of H_2O_2 to the CL is promoted and the concentration of H_2O_2 on the CL is transferred from a deficient state to a sufficient state. Meanwhile, the kinetics of HPRR is much improved. Thus,

the OCV of the stack increases in this process as presented in Figure 6.12, and the stack performance is improved. However, with the H_2O_2 concentration further increasing to 6.0 M, the OCV decreases and the stack performance degrades as well. This phenomenon can be attributed to three aspects. Firstly, the excessively high concentration of H_2O_2 leads to the competitive adsorption between H_2O_2 and H^+ on the active sites of cathode CL. The adsorption of H^+ becomes insufficient and the kinetics of HPRR becomes lower, which is also reflected by the sharp decrease of the stack voltage in high current region. Secondly, with a higher H_2O_2 concentration, the self-decomposition of H_2O_2 becomes severer, which produces a larger number of gaseous products in the cathode. The gas bubbles presented in the electrolyte reservoir may impede the transport of H_2O_2 and H_2SO_4 to the cathode CL and leads to an increasing internal resistance of the stack as presented in Figure 6.12. Last but not least, the crossover of H_2O_2 from the cathode to anode is severer with a higher concentration. At the same time, the transport of EG and KOH in the anode may also be influenced by the gaseous products produced by the self-decomposition of the H_2O_2 in the anode, which produces negative impact on the stack performance as well.

6.4.5. Effect of the H_2SO_4 concentration

Figure 6.13 presents the effect of the H_2SO_4 concentration on the passive stack performance with EG, H_2O_2 , and KOH concentrations fixed at 5.0, 4.0, and 9.0 M, respectively. It can be observed that the OCV increased from 2.85 V to 3.01 V with H_2SO_4 concentration increasing from 0.5 M to 1.0 M and decreased from 3.01 V to 2.86 V with H_2SO_4 concentration

further increasing from 1.0 M to 2.0 M. This phenomenon can be accounted as follows. With H₂SO₄ concentration increasing from 0.5 M to 1.0 M, the increasing voltage is resulted from the enhanced transportation of H⁺ which weakens the concentration loss of H⁺ [49]. However, further increasing H₂SO₄ concentration to 2.0 M did not lead to a better performance. One reason is that the redundant H₂SO₄ have taken up numerous active sites, which results in shortage of H₂O₂ in the CL. Then a higher H₂O₂ concentration loss is caused and the voltage degrades. Another reason is that the viscosity of catholyte is enlarged due to the increasing H₂SO₄ concentration. Meanwhile, the internal resistance rises when H₂SO₄ concentration increases as shown in Figure 6.14, which then causes severer ohmic loss. Therefore, the passive stack has the best performance with H₂SO₄ concentration at 1.0 M.

In summary, the reasons why the fuel cell performance will drop at higher feeding-concentrations of reactants can be concluded as follows: (1) the competitive adsorption between the reactants on active sites results in the lowered reaction kinetics and the increased concentration loss; (2) the viscosity of electrolyte becomes larger, impeding the transportation of reactants and charges; and (3) the hindered delivery of reactants leads to a larger internal resistance and an increased ohmic loss.

6.4.6. Demonstration of the stack to power an underwater fan

As mentioned, one advantage of the passive stack using hydrogen oxide is the feasibility to be a power source for underwater and outer space applications where the air is insufficient. Therefore, this superiority is

emphasized by comparing the capacity of the passive stack powering an electric fan with different oxidants, i.e., hydrogen peroxide and air, under different working circumstances, i.e., normal environment and mimetic underwater environment. The fuel cell stack is operated with 5.0 M EG and 9.0 M KOH as anolyte and 4.0 M H₂O₂ and 1.0 M H₂SO₄ as catholyte at room temperature. The capacity is verified by the running time of the fan, whose power rating and revolutions per minute are 1.8 W and 20000 rpm, respectively. Under the normal environment, after the connection of the anode and cathode of the stack and the fan by wires, the fan could not run when the passive stack used the ambient air as oxidant. This is because that the Au based cathode is not able to catalyze the ORR effectively, thus the power output is unable to drive the fan. On the contrary, when the hydrogen peroxide was used, the fan rotated at a high speed. To present the continuous output ability of the passive stack, a stopwatch was used to measure how long the fan would run until the fan gradually slowed down and completely stopped. It can be observed from Figure 6.15 that the whole running time was 2 hours and 52 minutes, indicating that the passive stack possesses the potential for practical applications. As shown in Figure 6.16, to further imitate the underwater environment without air supply, an airtight condition was created by a sealed box within the stack and fan, which was placed in a larger box full of water. It is found that the whole running time of the fan was 2 hours and 36 minutes underwater, which was similar to the result in the natural circumstance. The satisfactory performance under the underwater condition demonstrates that the passive stack is an applicable

power source and has the potential for future application in relevant fields.

6.5. Summary

In this study, a passive direct ethylene glycol fuel cell stack is proposed, fabricated, and tested. The effect of feeding species concentrations on the stack performance is studied. The results indicate that the peak power of this passive stack is 1178 mW at room temperature with the optimal reactant-feeding concentrations of 5.0 M EG and 9.0 M KOH as anolyte and 4.0 M H₂O₂ and 1.0 M H₂SO₄ as catholyte. The achieved peak power density is twice as high as that of a passive cell using ethylene glycol as fuel and air as oxidant. The impressive improvement results from the faster hydrogen peroxide reduction reaction due to its two-electron-transfer process rather than the four-electron-transfer process. In addition, the individual cell in the passive stack exhibits a good consistency over the whole current region, indicating a high degree of reproducibility achieved by the appropriate electrode manufacturing process. Moreover, to demonstrate the passive stack to be a promising power source under special situations, such as underwater and outer space, the passive stack is applied to power an electric fan under the mimetic underwater environment. It is demonstrated that the whole running time of the electric fan is 2 hours and 36 minutes with hydrogen peroxide as oxidant, while the air is used as oxidant, the electric fan is unable to run, suggesting that this passive stack can be applied in situations where air is insufficient.

6.6. References

- [1] Z.F. Pan, L. An, T.S. Zhao, Z.K. Tang, Advances and challenges in alkaline anion exchange membrane fuel cells, *Progress in Energy and Combustion Science* 66 (2018) 141-175.
- [2] Q.X. Wu, Z.F. Pan, L. An, Recent advances in alkali-doped polybenzimidazole membranes for fuel cell applications, *Renewable and Sustainable Energy Reviews* 89 (2018) 168-183.
- [3] Z.F. Pan, L. An, C.Y. Wen, Recent advances in fuel cells based propulsion systems for unmanned aerial vehicles, *Applied Energy* 240 (2019) 473-485.
- [4] Y. Li, Y. Feng, X. Sun, Y. He, A Sodium-Ion-Conducting Direct Formate Fuel Cell: Generating Electricity and Producing Base, *Angewandte Chemie International Edition* 56 (2017) 5734-5737.
- [5] B. Huang, Z. Pan, X. Su, L. An, Tin-based materials as versatile anodes for alkali (earth)-ion batteries, *Journal of Power Sources* 395 (2018) 41-59.
- [6] S. Rousseau, C. Coutanceau, C. Lamy, J.M. L éger, Direct ethanol fuel cell (DEFC): Electrical performances and reaction products distribution under operating conditions with different platinum-based anodes, *Journal of Power Sources* 158 (2006) 18-24.
- [7] Y. Li, X. Sun, Y. Feng, Hydroxide Self-Feeding High-Temperature Alkaline Direct Formate Fuel Cells, *ChemSusChem* 10 (2017) 2135-2139.
- [8] T.S. Zhao, C. Xu, R. Chen, W.W. Yang, Mass transport phenomena in direct methanol fuel cells, *Progress in Energy and Combustion Science* 35 (2009) 275-292.

-
- [9] L. An, T.S. Zhao, Transport phenomena in alkaline direct ethanol fuel cells for sustainable energy production, *Journal of Power Sources* 341 (2017) 199-211.
- [10] Y. Li, Y. Feng, X. Sun, Insight into Interface Behaviors to Build Phase-Boundary-Matched Na-Ion Direct Liquid Fuel Cells, *ACS Sustainable Chemistry & Engineering* 6 (2018) 12827-12834.
- [11] V. Livshits, M. Philosoph, E. Peled, Direct ethylene glycol fuel-cell stack—study of oxidation intermediate products, *Journal of Power Sources* 178 (2008) 687-691.
- [12] L. An, R. Chen, Recent progress in alkaline direct ethylene glycol fuel cells for sustainable energy production, *Journal of Power Sources* 329 (2016) 484-501.
- [13] A. Serov, C. Kwak, Recent achievements in direct ethylene glycol fuel cells (DEGFC), *Applied Catalysis B: Environmental* 97 (2010) 1-12.
- [14] H. Yue, Y. Zhao, X. Ma, J. Gong, Ethylene glycol: properties, synthesis, and applications, *Chemical Society Reviews* 41 (2012) 4218-4244.
- [15] J. Qi, N. Benipal, C. Liang, W. Li, PdAg/CNT catalyzed alcohol oxidation reaction for high-performance anion exchange membrane direct alcohol fuel cell (alcohol=methanol, ethanol, ethylene glycol and glycerol), *Applied Catalysis B: Environmental* 199 (2016) 494-503.
- [16] R. Kannan, A.R. Kim, J.S. Kim, D.J. Yoo, 3D graphene-mixed metal oxide-supported carbonpalladium quantum dot nanoarchitectures – A facile bifunctional electrocatalyst for direct ethylene glycol fuel cells and oxygen

evolution reactions, *International Journal of Hydrogen Energy* 41 (2016) 18033-18043.

[17] O.O. Fashedemi, H.A. Miller, A. Marchionni, F. Vizza, K.I. Ozoemena, Electro-oxidation of ethylene glycol and glycerol at palladium-decorated FeCo@Fe core-shell nanocatalysts for alkaline direct alcohol fuel cells: functionalized MWCNT supports and impact on product selectivity, *Journal of Materials Chemistry A* 3 (2015) 7145-7156.

[18] Z.F. Pan, R. Chen, L. An, Y.S. Li, Alkaline anion exchange membrane fuel cells for cogeneration of electricity and valuable chemicals, *Journal of Power Sources* 365 (2017) 430-445.

[19] T. Luo, S. Abdu, M. Wessling, Selectivity of ion exchange membranes: A review, *Journal of membrane science* 555 (2018) 429-454.

[20] L. An, T. Zhao, Q. Wu, L. Zeng, Comparison of different types of membrane in alkaline direct ethanol fuel cells, *International Journal of Hydrogen Energy* 37 (2012) 14536-14542.

[21] L. An, T.S. Zhao, S.Y. Shen, Q.X. Wu, R. Chen, Performance of a direct ethylene glycol fuel cell with an anion-exchange membrane, *International Journal of Hydrogen Energy* 35 (2010) 4329-4335.

[22] L. An, L. Zeng, T.S. Zhao, An alkaline direct ethylene glycol fuel cell with an alkali-doped polybenzimidazole membrane, *International Journal of Hydrogen Energy* 38 (2013) 10602-10606.

[23] Y. Feng, L. Bu, S. Guo, J. Guo, X. Huang, 3D Platinum-Lead Nanowire Networks as Highly Efficient Ethylene Glycol Oxidation Electrocatalysts, *Small* 12 (2016) 4464-4470.

-
- [24] Z. Pan, Y. Bi, L. An, Mathematical modeling of direct ethylene glycol fuel cells incorporating the effect of the competitive adsorption, *Applied Thermal Engineering* 147 (2019) 1115-1124.
- [25] E. Peled, V. Livshits, T. Duvdevani, High-power direct ethylene glycol fuel cell (DEGFC) based on nanoporous proton-conducting membrane (NP-PCM), *Journal of Power Sources* 106 (2002) 245-248.
- [26] Y.-C. Shi, J.-J. Feng, X.-X. Lin, L. Zhang, J. Yuan, Q.-L. Zhang, A.-J. Wang, One-step hydrothermal synthesis of three-dimensional nitrogen-doped reduced graphene oxide hydrogels anchored PtPd alloyed nanoparticles for ethylene glycol oxidation and hydrogen evolution reactions, *Electrochimica Acta* 293 (2019) 504-513.
- [27] Z.-N. Yu, Z. Zhang, Z.-S. Lv, M.-T. Liu, L. Zhang, A.-J. Wang, L.-Y. Jiang, J.-J. Feng, Platinum₆₉-cobalt₃₁ alloyed nanosheet nanoassemblies as advanced bifunctional electrocatalysts for boosting ethylene glycol oxidation and oxygen reduction, *Journal of Colloid and Interface Science* 525 (2018) 216-224.
- [28] X.-Y. Huang, A.-J. Wang, X.-F. Zhang, L. Zhang, J.-J. Feng, One-step synthesis of PtCu alloyed nanocages with highly open structures as bifunctional electrocatalysts for oxygen reduction and polyhydric alcohol oxidation, *ACS Applied Energy Materials* 1 (2018) 5779-5786.
- [29] Z. Pan, B. Huang, L. An, Performance of a hybrid direct ethylene glycol fuel cell, *International Journal of Energy Research* 43 (2019) 2583-2591.

-
- [30] Y. Li, A liquid-electrolyte-free anion-exchange membrane direct formate-peroxide fuel cell, *International Journal of Hydrogen Energy* 41 (2016) 3600-3604.
- [31] I. Chino, K. Hendrix, A. Keramati, O. Muneeb, J.L. Haan, A split pH direct liquid fuel cell powered by propanol or glycerol, *Applied Energy* 251 (2019) 113323.
- [32] T. Zhao, C. Xu, R. Chen, W. Yang, Mass transport phenomena in direct methanol fuel cells, *Progress in Energy and Combustion Science* 35 (2009) 275-292.
- [33] C. Cremers, A. Niedergesäß, F. Jung, D. Müller, J. Tübke, Development of an Alkaline Anion Exchange Membrane Direct Ethylene Glycol Fuel Cell Stack, *ECS Transactions* 41 (2011) 1987-1996.
- [34] J.P. Pereira, D.S. Falcão, V.B. Oliveira, A.M.F.R. Pinto, Performance of a passive direct ethanol fuel cell, *Journal of Power Sources* 256 (2014) 14-19.
- [35] Y.S. Li, T.S. Zhao, A passive anion-exchange membrane direct ethanol fuel cell stack and its applications, *International Journal of Hydrogen Energy* 41 (2016) 20336-20342.
- [36] S.S. Munjewar, S.B. Thombre, R.K. Mallick, Approaches to overcome the barrier issues of passive direct methanol fuel cell – Review, *Renewable and Sustainable Energy Reviews* 67 (2017) 1087-1104.
- [37] Z. Pan, Y. Bi, L. An, Performance characteristics of a passive direct ethylene glycol fuel cell with hydrogen peroxide as oxidant, *Applied Energy* 250 (2019) 846-854.

-
- [38] A. Marchionni, M. Bevilacqua, C. Bianchini, Y.X. Chen, J. Filippi, P. Fornasiero, A. Lavacchi, H. Miller, L. Wang, F. Vizza, Electrooxidation of Ethylene Glycol and Glycerol on Pd-(Ni-Zn)/C Anodes in Direct Alcohol Fuel Cells, *ChemSusChem* 6 (2013) 518-528.
- [39] O.O. Fashedemi, H.A. Miller, A. Marchionni, F. Vizza, K.I. Ozoemena, Electro-oxidation of ethylene glycol and glycerol at palladium-decorated FeCo@ Fe core-shell nanocatalysts for alkaline direct alcohol fuel cells: functionalized MWCNT supports and impact on product selectivity, *Journal of Materials Chemistry A* 3 (2015) 7145-7156.
- [40] L. An, T. Zhao, R. Chen, Q. Wu, A novel direct ethanol fuel cell with high power density, *Journal of Power Sources* 196 (2011) 6219-6222.
- [41] L. An, T.S. Zhao, Performance of an alkaline-acid direct ethanol fuel cell, *International Journal of Hydrogen Energy* 36 (2011) 9994-9999.
- [42] A. Marchionni, M. Bevilacqua, C. Bianchini, Y.-X. Chen, J. Filippi, P. Fornasiero, A. Lavacchi, H. Miller, L. Wang, F. Vizza, Electrooxidation of Ethylene Glycol and Glycerol on Pd-(Ni-Zn)/C Anodes in Direct Alcohol Fuel Cells, *ChemSusChem* 6 (2013) 518-528.
- [43] G.H. Miley, N. Luo, J. Mather, R. Burton, G. Hawkins, L. Gu, E. Byrd, R. Gimlin, P.J. Shrestha, G. Benavides, J. Laystrom, D. Carroll, Direct NaBH₄/H₂O₂ fuel cells, *Journal of Power Sources* 165 (2007) 509-516.
- [44] D. Noren, M. Hoffman, Clarifying the Butler-Volmer equation and related approximations for calculating activation losses in solid oxide fuel cell models, *Journal of Power Sources* 152 (2005) 175-181.

-
- [45] J. Larminie, A. Dicks, M.S. McDonald, Fuel cell systems explained, J. Wiley Chichester, UK, 2003.
- [46] T.R. Ralph, G.A. Hards, J.E. Keating, S.A. Campbell, D.P. Wilkinson, M. Davis, J. St-Pierre, M.C. Johnson, Low Cost Electrodes for Proton Exchange Membrane Fuel Cells: Performance in Single Cells and Ballard Stacks, *Journal of The Electrochemical Society* 144 (1997) 3845-3857.
- [47] S.S. Pethaiah, J. Arunkumar, M. Ramos, A. Al-Jumaily, N. Manivannan, The impact of anode design on fuel crossover of direct ethanol fuel cell, *Bulletin of Materials Science* 39 (2016) 273-278.
- [48] M. Sgroi, F. Zedde, O. Barbera, A. Stassi, D. Sebastián, F. Lufrano, V. Baglio, A. Aricò, J. Bonde, M. Schuster, Cost analysis of direct methanol fuel cell stacks for mass production, *Energies* 9 (2016) 1008.
- [49] R.K. Raman, N.A. Choudhury, A.K. Shukla, A High Output Voltage Direct Borohydride Fuel Cell, *Electrochemical and Solid-State Letters* 7 (2004) A488-A491.

Figures

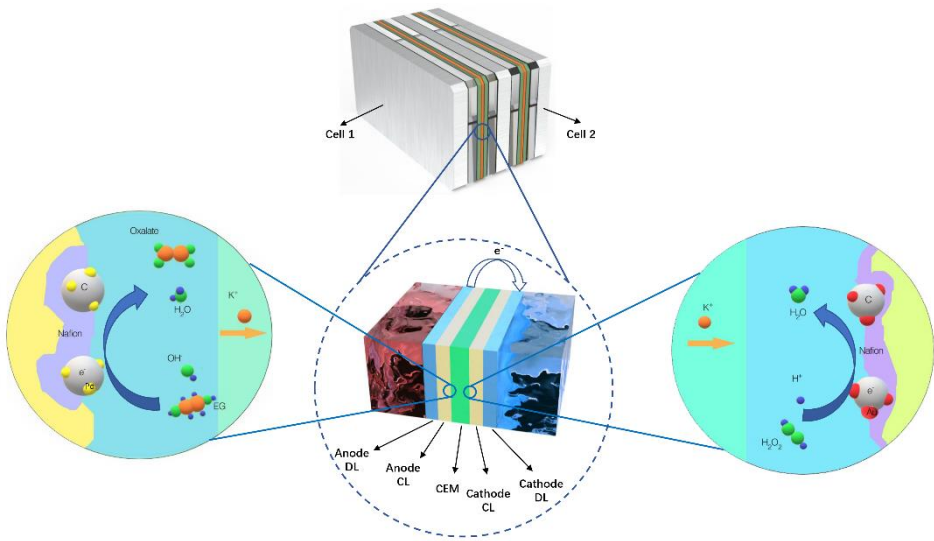


Figure 6.1 Working principle of a passive DEGFC stack.

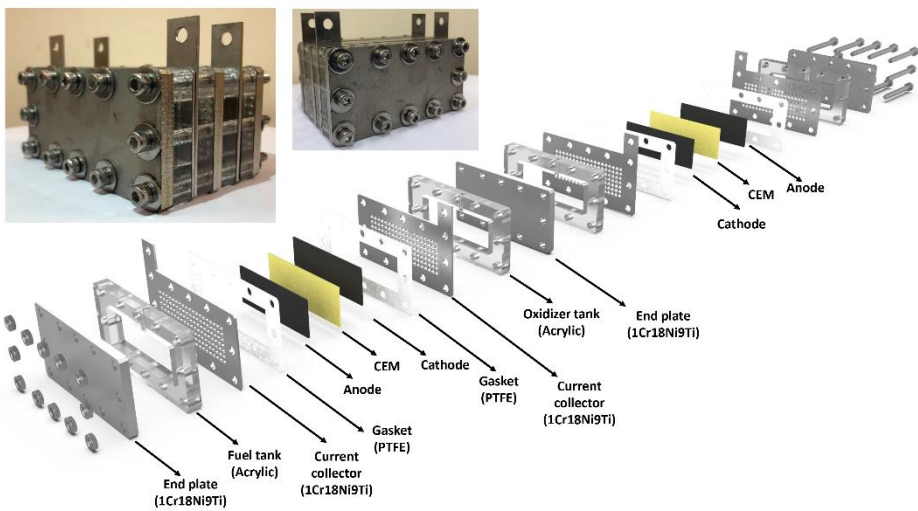


Figure 6.2 Schematic illustration of a passive DEGFC stack.

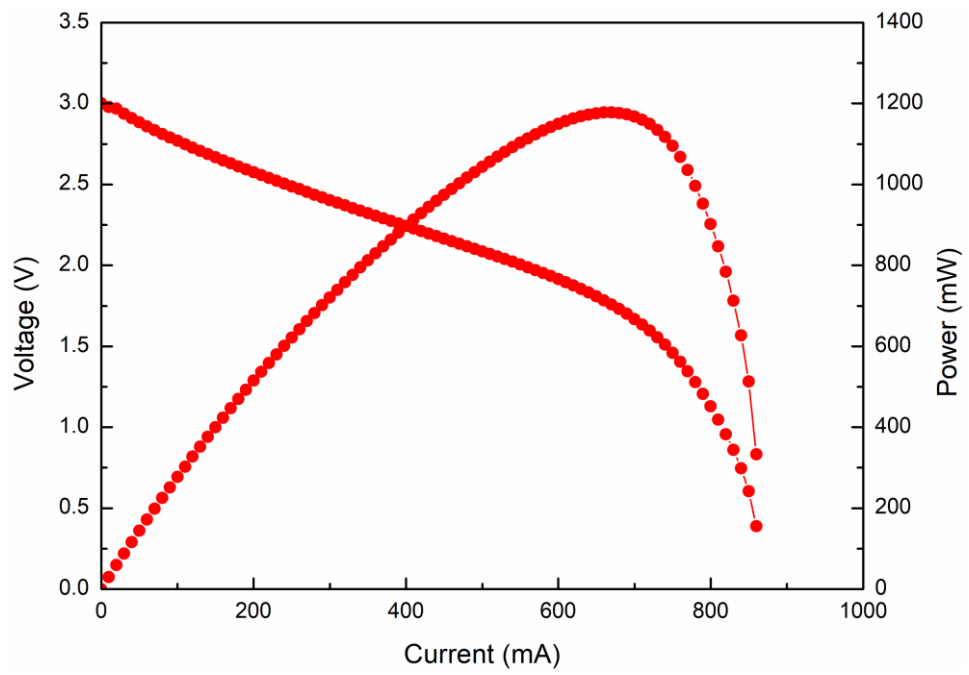


Figure 6.3 General Performance of the passive stack.

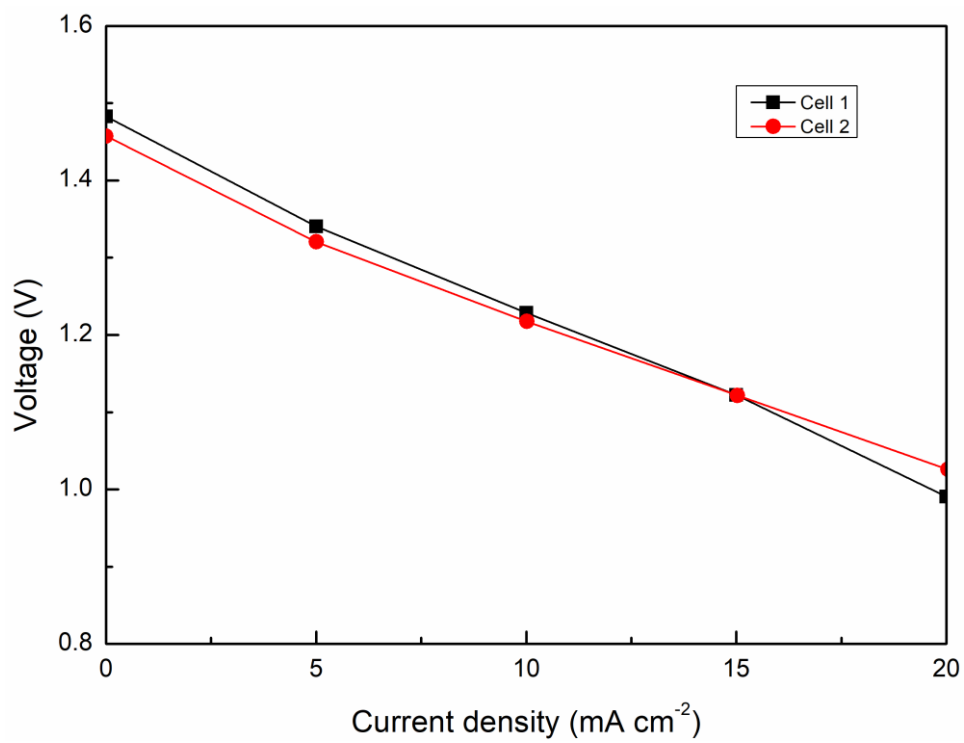


Figure 6.4 The consistency of the individual cell.

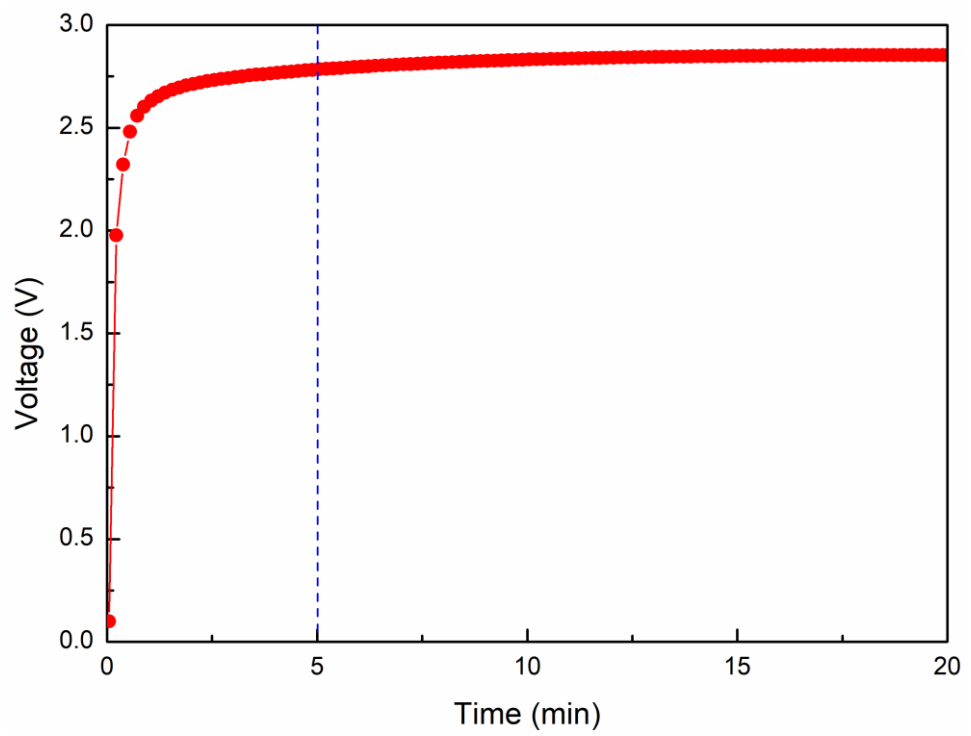


Figure 6.5 Transient OCV behavior of the passive stack.

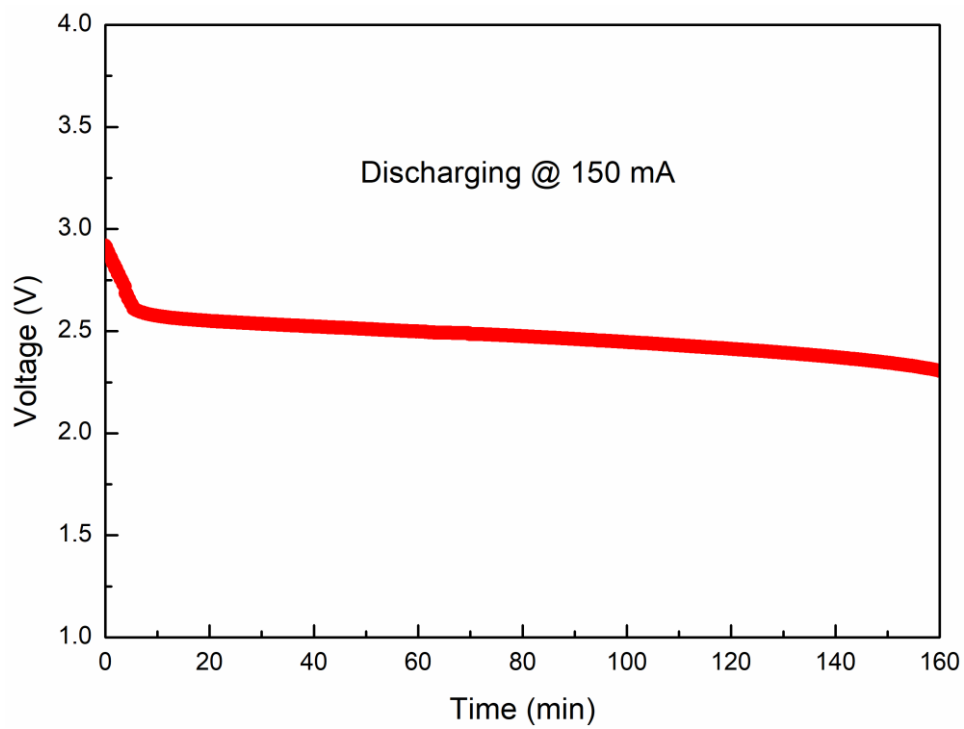


Figure 6.6 Transient discharging behavior of the passive stack.

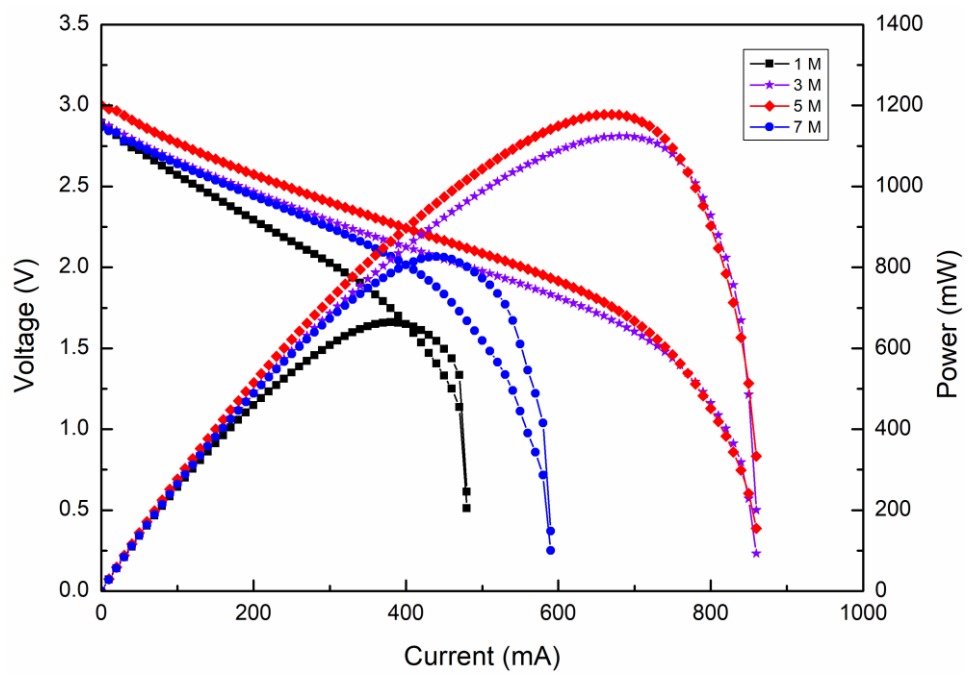


Figure 6.7 Effect of the EG concentration on the stack performance.

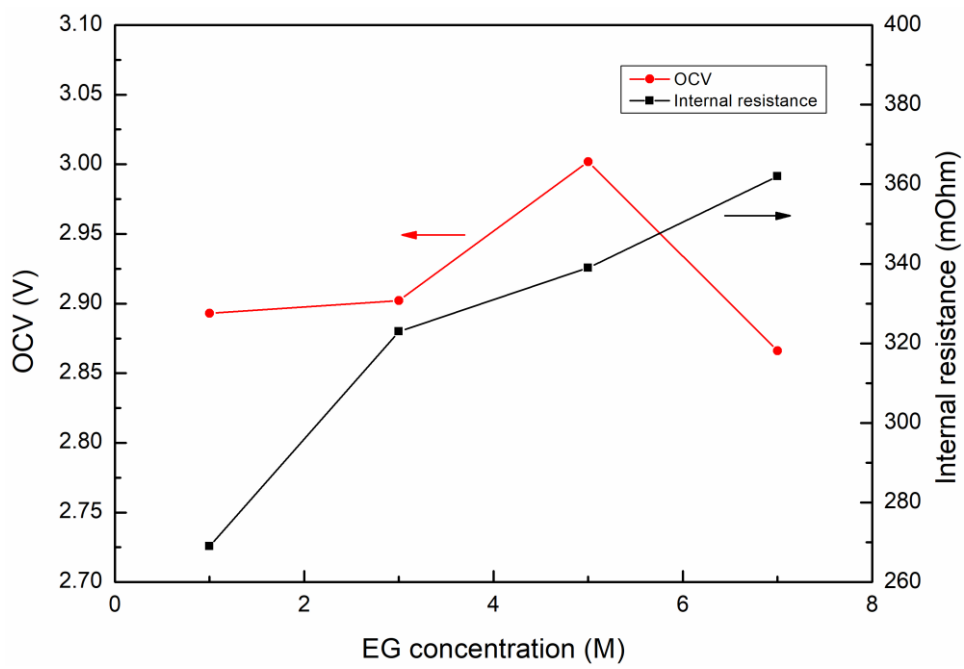


Figure 6.8 Effect of the EG concentration on the OCV and internal resistance.

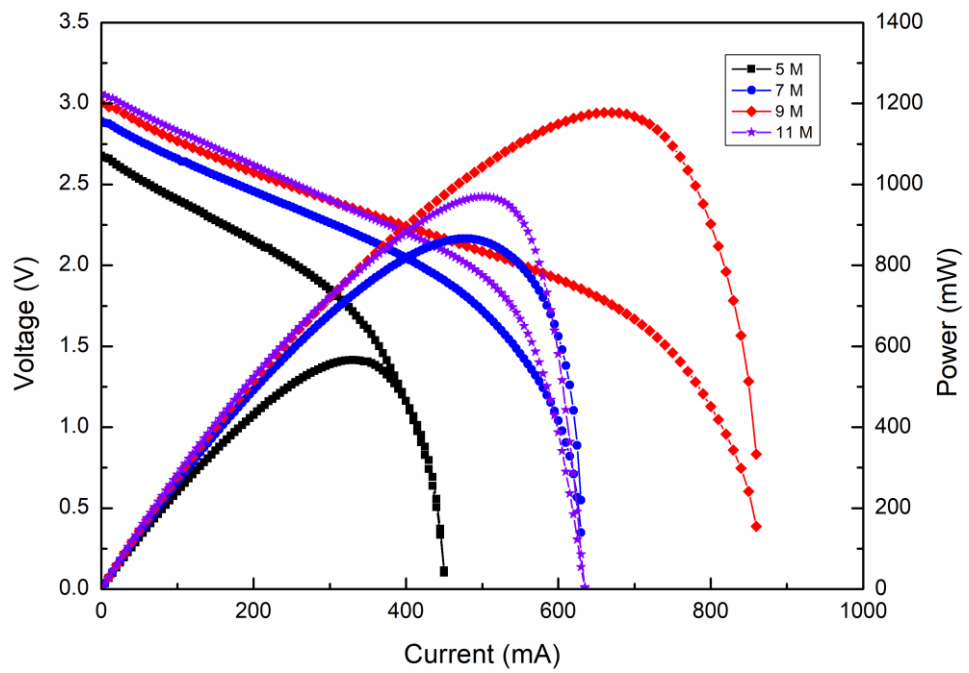


Figure 6.9 Effect of the KOH concentration on the stack performance.

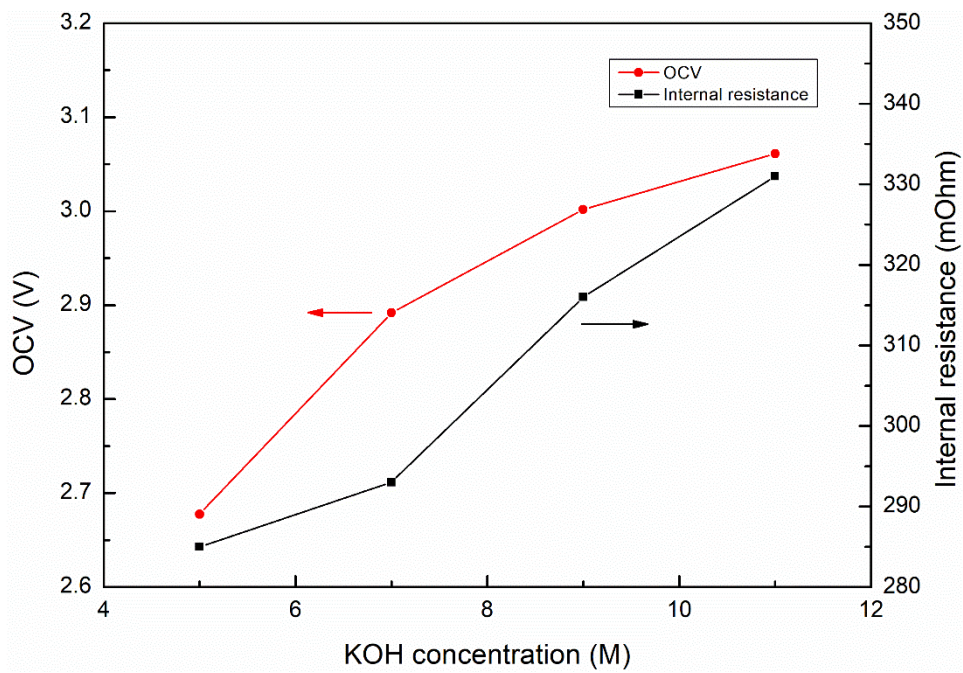


Figure 6.10 Effect of the KOH concentration on the OCV and internal resistance.

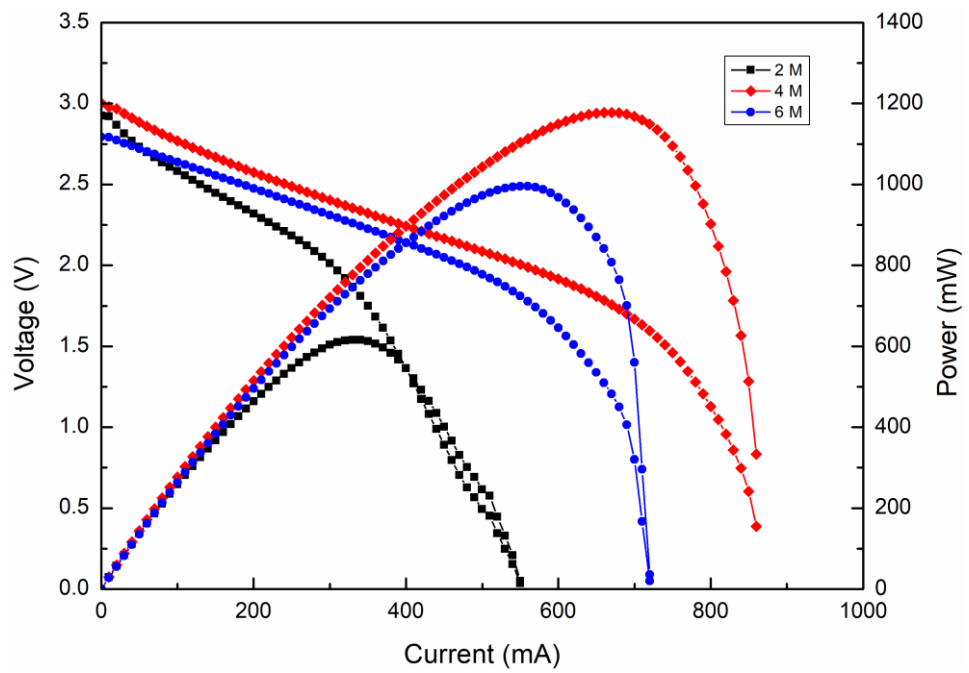


Figure 6.11 Effect of the H₂O₂ concentration on the stack performance.

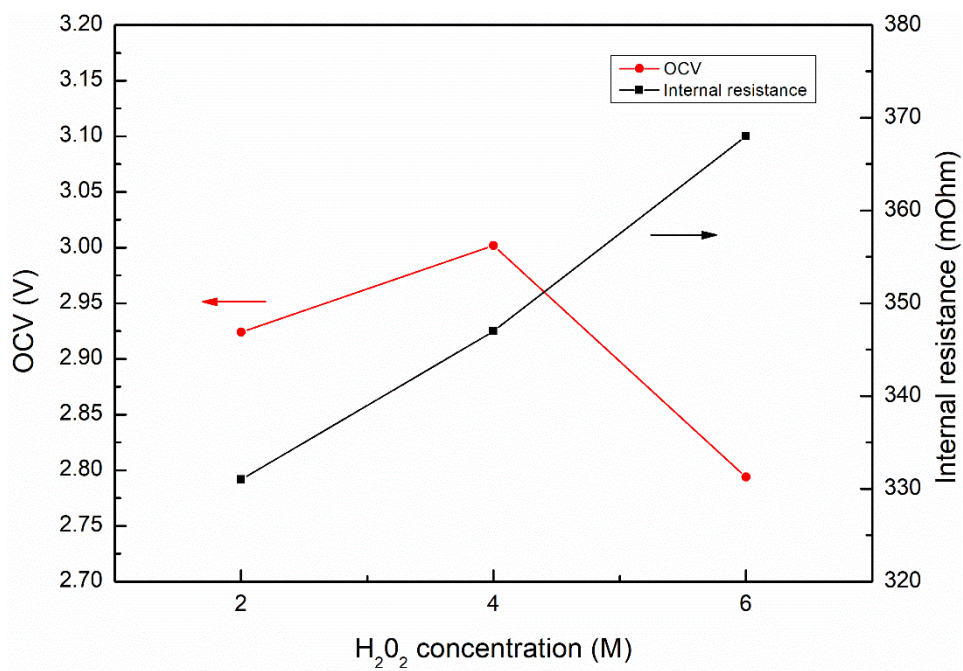


Figure 6.12 Effect of the H₂O₂ concentration on the OCV and internal resistance.

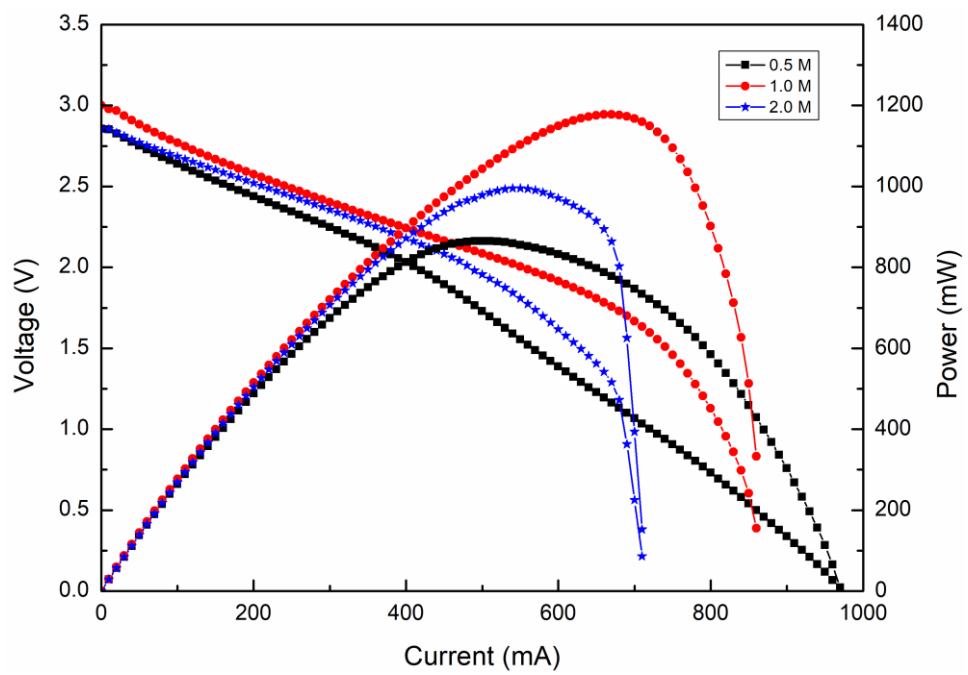


Figure 6.13 Effect of the H₂SO₄ concentration on the stack performance.

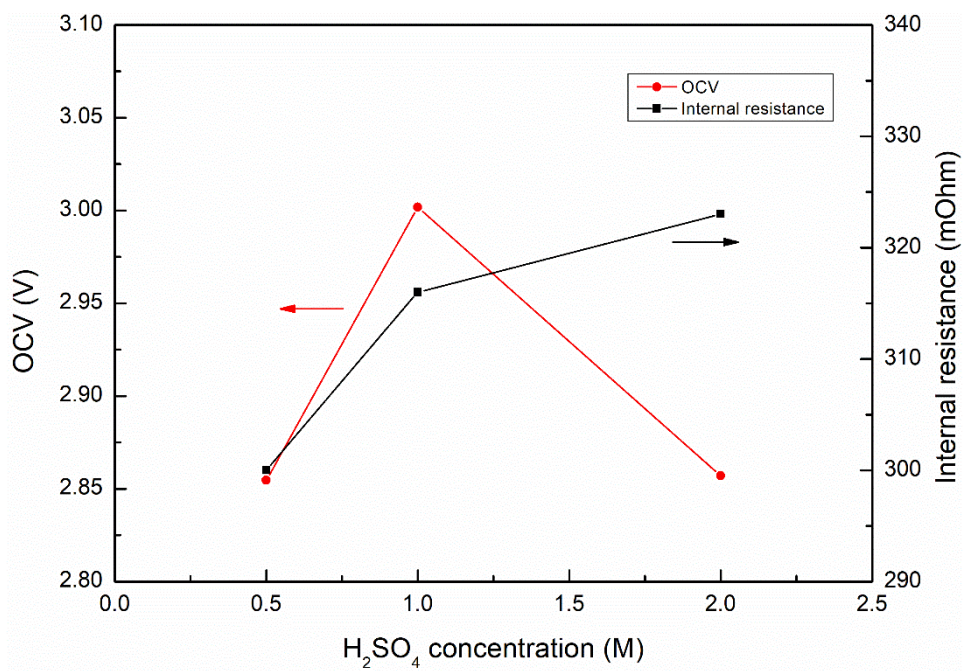


Figure 6.14 Effect of the H₂SO₄ concentration on the OCV and internal resistance.

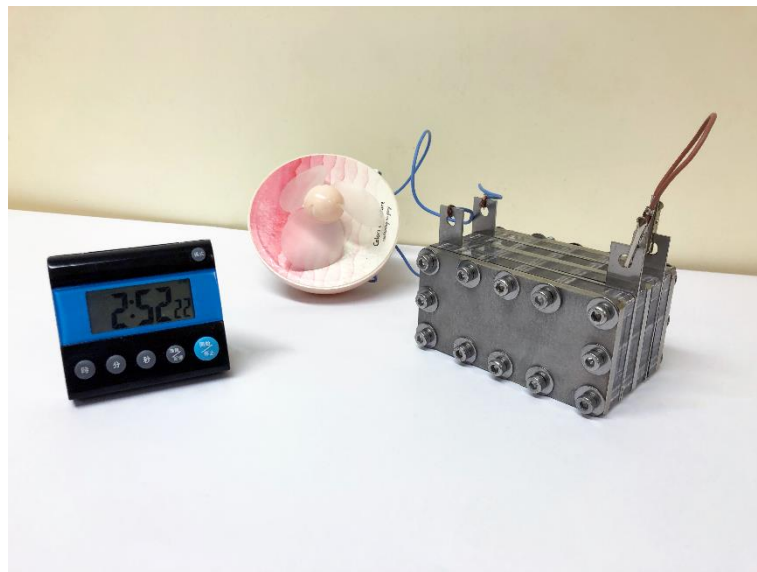


Figure 6.15 Running time of the fan powered by the passive stack under the ambient environment.

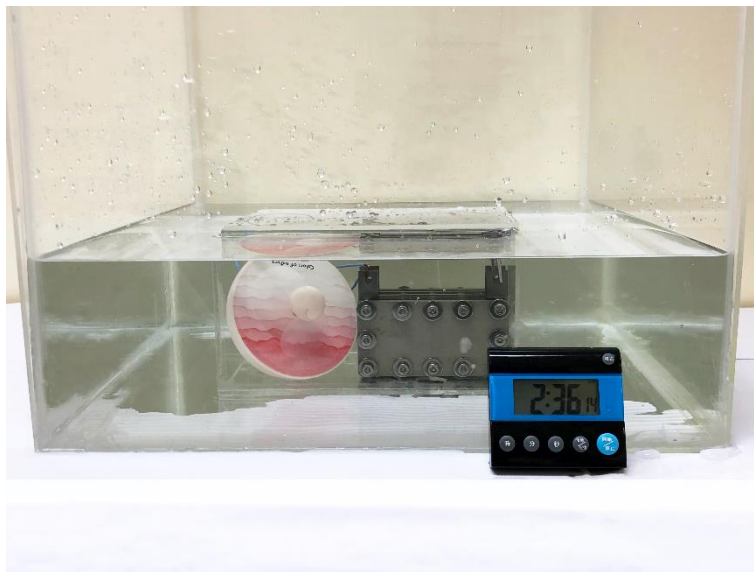


Figure 6.16 Running time of the fan powered by the passive stack under the imitated underwater environment.

Chapter 7 Mathematical modeling of direct ethylene glycol fuel cells

Abstract

In this work, a one-dimensional mathematical model for a direct ethylene glycol fuel cell using hydrogen peroxide as oxidant is developed. This model considers the ethylene glycol crossover and the competitive adsorption between ethylene glycol molecules and hydroxyl ions at reaction sites, in addition to mass/charge transport and electrochemical reactions. In addition, the complicated co-existence of the hydrogen peroxide reduction reaction, the hydrogen peroxide oxidation reaction, and the oxygen reduction reaction in the cathode is also considered in this model. The mathematical model under the consideration of the above-mentioned physicochemical processes exhibits a good agreement with experimental results. In addition, the effects of various operating and electrode structural parameters on the cell performance are examined, including concentrations of various species, the exchange current density and the thickness of diffusion layer. The numerical results exhibit that the cell performance improves with the increasing concentrations of hydrogen peroxide and sulfuric acid. As for the ethylene glycol and hydroxyl ions, increasing the concentrations makes contribution to higher performance, while the cell performance experiences a degradation at a high current density region due to the remarkable ohmic loss. The model also shows that increasing both the anode and cathode exchange current density leads to an improved cell

performance, which indicates the significance of developing novel catalyst with superior catalytic activity. Moreover, the effect of the structural design parameters of the anode and cathode diffusion layer is also investigated, and the results show that increasing thickness of diffusion layers has a negative effect on the cell performance.

Keywords: Direct ethylene glycol fuel cell; Hydrogen peroxide; Mathematical modeling; Mass transport; Competitive adsorption; Fuel crossover

Nomenclature

| | |
|-------|---|
| C | Concentration (mol m^{-3}) |
| D | Diffusivity ($\text{m}^2 \text{s}^{-1}$) |
| E^0 | Standard potential (V) |
| E | Potential (V) |
| F | Faraday's constant (A s mol^{-1}) |
| i_0 | Exchange current density (A m^{-2}) |
| j | Current density (A m^{-2}) |
| K | Rate constant ($\text{mol m}^{-2} \text{s}^{-1}$) |
| k | Mass transfer coefficient (m s^{-1}) |
| n | Number of electrons transferred |
| N | Species flux ($\text{mol m}^2 \text{s}^{-1}$) |
| R | Internal resistance (Ω) |
| s | Stoichiometric coefficient |
| V | Cell voltage (V) |
| v | Superficial velocity (m s^{-1}) |

Greek

| | |
|---------------|-----------------------------|
| α | Transfer coefficient |
| ε | Porosity of diffusion layer |
| δ | Bulk radius (m) |
| γ | Reaction order |
| η_a | Anode polarization (V) |
| η_c | Cathode polarization (V) |
| θ | Coverage on the catalyst |

Superscripts and subscripts

| | |
|------------------------|--------------------------------------|
| a | Anode |
| ADL | Anode diffusion layer |
| ACL | Anode catalyst layer |
| c | Cathode |
| CCL | Cathode catalyst layer |
| CDL | Cathode diffusion layer |
| EGOR | Ethylene glycol oxidation reaction |
| EG | Ethylene glycol |
| eff | Effective |
| F | Feeding |
| HPRR | Hydrogen peroxide reduction reaction |
| HPOR | Hydrogen peroxide oxidation reaction |
| H_2O_2 | Hydrogen peroxide |
| H^+ | Proton |
| i | Different species |
| M | Membrane |
| OH^- | Hydroxyl ion |
| ORR | Oxygen reduction reaction |
| O_2 | Oxygen |
| ref | Reference |
| R | Reactant |
| S | Catalyst surface |

7.1. Introduction

Direct alcohol fuel cells (DAFCs) have received ever-increasing attention as a propitious power source, primarily due to their high efficiency, simple design, quick refueling as well as low emissions [1-5]. Among various alcohol fuels, small molecule and short-chain alcohols, e.g., methanol and ethanol, are regarded as promising fuel candidates, because the rate of oxidation reaction is higher than that of large molecule and long-chain alcohols [6-9]. Although promising, direct methanol fuel cells (DMFCs) suffer from the severe performance decline derived from the serious methanol crossover and poisonousness of derivative to the catalyst [6]. In addition, direct ethanol fuel cells (DEFCs) exhibit a low electron transfer rate (33%) due to the hardly broken C-C bond at low temperatures (generally < 60°C) [10, 11]. Recently, direct ethylene glycol fuel cells (DEGFCs) running on ethylene glycol (EG), which are regarded as an alternative DAFC, have attracted great attention for mobile, stationary, and portable applications, which is attributed to its intrinsic superiorities, including high theoretical energy capacity (4.8 Ah mL⁻¹), high boiling point (198°C), and high electron transfer rate (80%) [12-16]. In addition, using hydrogen peroxide as oxidant in the cathode to replace the air or pure oxygen has been extensively studied [17-19]. The use of liquid hydrogen peroxide brings about the following advantages: (1) a substantial increase in the theoretical voltage; (2) low activation loss of the reduction reaction due to two-electron transfer; and (3) no water flooding problem [20]. Moreover, hydrogen peroxide is more favorable in air shortage situations,

e.g., outer space and underwater. For instance, Pan et al. [19] developed a hybrid DEFC using hydrogen peroxide as oxidant yielding an open-circuit voltage (OCV) of 1.41 V and a peak power density of 80.9 mW cm⁻² at 60°C. It was reported that the hybrid DEFC boosted the OCV by 62.1% and the peak power density by 20.8% comparing to the same cell using oxygen.

In general, the fuel cell performance relies on various parameters, including the materials and electrode structures, species concentrations, as well as operating temperature [21-23]. However, investigating the effect of each parameter on cell performance via experimental approach is quite cost-ineffective and time-consuming. Thus, mathematical modeling, which is regarded as an economical and powerful tool, is essential for the detailed study and optimization of operating parameters of fuel cells, so that the performance can be maximized [24]. Jiao et al. [25] presented an excellent work on water transport in polymer electrolyte membrane fuel cells (PEMFCs) and comprehensively reviewed different models adopted for different purposes in water transport in PEMFCs. Bahrami et al. [26] proposed a one-dimensional, isothermal, single-phase model to investigate the mass transport in a DEFC, but the addition of alkali was not taken into consideration. Recently, Guo et al. [27] developed a transient two-dimensional multi-phase model for passive vapor-feed DMFC fed with neat methanol to investigate the mass transport processes with different cell designs and operation conditions. Xie et al. [28] further studied the effects of open ratio, carbon dioxide exit length, micro-porous layer (MPL) and

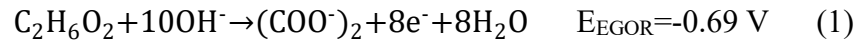
porous layer's hydrophobicity on the cell performance. Wang et al. [29] developed a quasi-2D transient model of proton exchange membrane fuel cell with anode recirculation. Huo et al. [30] investigated the effect of various operating pressures on the water transfer mechanism in an alkaline electrolyte membrane fuel cell and studied the effect of operating behavior on the cell performance both experimentally test and analytically.

It should be mentioned that the addition of alkali in the anode can improve the electrochemical kinetics of the EG oxidation reaction (EGOR), but the anode becomes a complex cation-anion co-existing compartment, which makes the physicochemical processes in the fuel cell system more complicated, including mass transport, electron transport, ion transport, as well as electrochemical reactions [31]. Meanwhile, the involvement of hydrogen peroxide and acid in the cathode also entangles the physicochemical processes. On one hand, the mass transport, electron transport, and ion transport are more convoluted, which is similar to the situation in the anode. On the other hand, not only the hydrogen peroxide reduction reaction (HPRR) takes place in the cathode, but the hydrogen peroxide oxidation reaction (HPOR) also occurs simultaneously. Moreover, the oxygen derived from the HPOR also can participate in reduction reactions. Therefore, there are two reduction reactions and an oxidation reaction existing in the cathode, which may spontaneously establish an internal hydrogen peroxide fuel cell. To our best knowledge, there is no attempt to mathematically investigate the alkaline DEGFC with hydrogen peroxide as oxidant. In this work, a comprehensive one-dimensional steady-

state isothermal mathematical model is developed to extensively investigate the operating parameters and electrode designs on the cell performance.

7.2. Model development

As depicted in Figure 7.1, the DEGFC consists of the anode/cathode flow fields (FFs), the anode/cathode diffusion layers (DLs), the anode/cathode catalyst layers (CLs), and a cation exchange membrane (CEM). In the anode, the anolyte containing EG and NaOH transports from the anode FF through the anode DL to the anode CL, where the EG reacts with hydroxyl ions to produce electrons, oxalate and water. The EGOR reaction is shown as follows [11]:



The electrons produced on the anode are transported through the external circuit to the cathode, where the HPRR occurs according to [32]:



Meanwhile, the sodium ions are transported from the anode to cathode through the membrane, which forms the internal ionic circuit. Consequently, the overall reaction of the passive DEGFC can be obtained by combining EGOR on the anode and HPRR on the cathode as follows:



In the present work, the model equations are defined in one direction (x-axis) through the anode, CEM, and cathode. To simplify the complicated processes, the following assumptions and simplifications are made:

(1) The fuel cell is assumed to operate under steady-state and isothermal conditions.

(2) The mass/charge transport through the cathode DL is assumed to be a diffusion-predominated process, while both diffusion and convection are considered in the anode DL.

(3) The CLs are too thin so that they are treated as interfaces.

(4) The competitive adsorption on the active sites is assumed to be concentration-dependent.

(5) The EG transporting through the membrane is completely oxidized in the cathode so that the EG concentration in cathode CL is zero.

(6) The hydroxyl-ion crossover, hydrogen peroxide crossover, and oxygen crossover through the membrane are ignored.

7.2.1. Anode

7.2.1.1. Mass transport

In the anode DL, where no chemical reaction occurs, the species flux (N_i^{ADL}) remains constant. The flux expression is developed based on the work of Pathak and Basu [33] and can be presented as:

$$N_i^{ADL} = \frac{C_i^F e^{v^{ADL}/k_i^{ADL}} - C_i^{ACL}}{e^{v^{ADL}/k_i^{ADL}} - 1} v^{ADL} \quad (4)$$

where C_i^F is the feeding concentration (i : EG, OH⁻), $v^{ADL} = k_w \Delta P / \mu_w l_{ADL}$ is the superficial velocity of water in the anode DL, $k_i^{ADL} = D_i^{ADL,eff} / l_d$ is the mass transfer coefficient in the anode DL, and C^{ACL} is the species concentration in the anode CL. The D_i^{eff} is given by [34]:

$$D_i^{eff} = \varepsilon^{3/2} D_i \quad (5)$$

where ε is the porosity of the anode DL, and the D_i is free-space diffusivity of species (i : EG, OH⁻). In the anode CL, since the mass transport is

considered to be diffusion-predominated, the flux (N_i^S) can be obtained based on Fick's law:

$$N_i^S = -D_i^{eff} \frac{C_i^{ACL} - C_i^S}{\delta_{ACL}} \quad (6)$$

where C_i^{ACL} is the species concentration in the anode CL, the C_i^S is the species concentration on the catalyst, and δ_{ACL} is the radius of the bulk. Through the membrane, the EG crossover (N_i^M) is in the same way as it transports through DL. Hence, it is given by:

$$N_i^M = \frac{C_i^{ACL} e^{v^M/k^M}}{e^{v^M/k^M} - 1} v^M \quad (7)$$

where $v^M = k_w \Delta P / \mu_w l_M$ is the superficial velocity of water in membrane, $k^M = D^{M,eff} / l_M$ is the mass transfer coefficient in membrane. It is believed that the electrochemical reactions take place at the active sites on the catalyst, which implies that the actual reactant concentration participating in the EGOR does not equal to the species concentration on the catalyst surface. In other words, for a specific active site, the actual reactant concentration mainly depending on the species concentration on the catalyst surface is the result of the competitive adsorption between EG and OH^- . It is clear that the reactant with higher concentration is more likely to be adsorbed on the active sites, thus the assumption that the competitive adsorption on the active sites is concentration-dependent is made. Based on this assumption, the actual reactant concentration can be given by:

$$C_{EG}^R = \frac{C_{EG}^S}{C_{EG}^S + C_{OH^-}^S} C_{EG}^S \quad (8)$$

$$C_{OH^-}^R = \frac{C_{OH^-}^S}{C_{EG}^S + C_{OH^-}^S} C_{OH^-}^S \quad (9)$$

where C_i^R is the actual reactant concentration at the active sites (i : EG , OH), and C_i^S is the reactant concentration on the catalyst surface.

7.2.1.2. Electrochemical kinetics

The EGOR is a multi-step and multi-pathway electrochemical process; therefore, its reaction mechanism has not been completely understood yet. Herein, a Tafel-form electrochemical model for the EGOR incorporating the mass transport effect is adopted:

$$j_a = i_{0,a} \left(\frac{C_{EG}^R}{C_{EG}^{ref}} \right)^{\gamma_a^{EG}} \left(\frac{C_{OH^-}^R}{C_{OH^-}^{ref}} \right)^{\gamma_a^{OH^-}} \exp\left(\frac{\alpha_a F}{RT} \eta_a\right) \quad (10)$$

$$\gamma_a^{EG} \begin{cases} 0 & C_{EG}^R > C_{EG}^{ref} \\ 1 & C_{EG}^R \leq C_{EG}^{ref} \end{cases} \quad (11)$$

$$\gamma_a^{OH^-} \begin{cases} 0 & C_{OH^-}^R > C_{OH^-}^{ref} \\ 1 & C_{OH^-}^R \leq C_{OH^-}^{ref} \end{cases} \quad (12)$$

where C_i^R is the reactant concentration on the active sites, C_i^{ref} is the reference reactant concentration, and γ is the reaction order related to the species concentration. When the concentration is higher than a reference value, it is zero. Otherwise, it is one.

7.2.2. Cathode

In the cathode, the formation for the mass/charge transport and electrochemical reactions is based on our previous work [17]. Briefly, the species flux in the cathode DL (N_i^{CDL}) can be described according to:

$$N_i^{CDL} = -D_i^{eff} \frac{dC_i^F}{dx} \quad (13)$$

where C_i^F is the feeding concentration (i : H_2O_2 , H^+). The superficial current density j_c can be defined by three respective current densities, which are

j_{HPRR} derived from HPRR, j_{HPOR} derived from HPOR, as well as j_{ORR} derived from oxygen reduction reaction (ORR):

$$\begin{aligned}
j_c &= j_{\text{HPRR}} + j_{\text{ORR}} - j_{\text{HPOR}} \\
&= i_{0,\text{HPRR}} \left(\frac{C_{\text{H}_2\text{O}_2}^{\text{CL}}}{C_{\text{H}_2\text{O}_2}^{\text{ref}}} \right)^{\gamma_{\text{HPRR}}^{\text{H}_2\text{O}_2}} \left(\frac{C_{\text{H}^+}^{\text{CL}}}{C_{\text{H}^+}^{\text{ref}}} \right)^{\gamma_{\text{HPRR}}^{\text{H}^+}} \exp \left[\frac{\alpha_{\text{HPRR}} F}{RT} (E_{\text{HPRR}}^0 \right. \\
&\quad \left. - E_{\text{mixed}}) \right] \\
&\quad + i_{0,\text{ORR}} \left(\frac{C_{\text{O}_2}^{\text{CL}}}{C_{\text{O}_2}^{\text{ref}}} \right)^{\gamma_{\text{ORR}}^{\text{O}_2}} \left(\frac{C_{\text{H}^+}^{\text{CL}}}{C_{\text{H}^+}^{\text{ref}}} \right)^{\gamma_{\text{ORR}}^{\text{H}^+}} \exp \left[\frac{\alpha_{\text{ORR}} F}{RT} (E_{\text{ORR}}^0 \right. \\
&\quad \left. - E_{\text{mixed}}) \right] - n_{\text{HPOR}} F k \exp \left[\frac{\alpha_{\text{HPOR}} F}{RT} (E_{\text{mixed}} \right. \\
&\quad \left. - E_{\text{HPOR}}^0) \right] \theta_{\text{H}_2\text{O}_2}
\end{aligned} \tag{14}$$

$$\gamma_{\text{HPRR}}^{\text{H}_2\text{O}_2} \begin{cases} 0 & C_{\text{H}_2\text{O}_2}^{\text{CL}} > C_{\text{H}_2\text{O}_2}^{\text{ref}} \\ 1 & C_{\text{H}_2\text{O}_2}^{\text{CL}} \leq C_{\text{H}_2\text{O}_2}^{\text{ref}} \end{cases} \tag{15}$$

$$\gamma_{\text{HPRR}}^{\text{H}^+} \begin{cases} 0 & C_{\text{H}^+}^{\text{CL}} > C_{\text{H}^+}^{\text{ref}} \\ 1 & C_{\text{H}^+}^{\text{CL}} \leq C_{\text{H}^+}^{\text{ref}} \end{cases} \tag{16}$$

$$\gamma_{\text{ORR}}^{\text{O}_2} \begin{cases} 0 & C_{\text{O}_2}^{\text{CL}} > C_{\text{O}_2}^{\text{ref}} \\ 1 & C_{\text{O}_2}^{\text{CL}} \leq C_{\text{O}_2}^{\text{ref}} \end{cases} \tag{17}$$

$$\gamma_{\text{ORR}}^{\text{H}^+} \begin{cases} 0 & C_{\text{H}^+}^{\text{CL}} > C_{\text{H}^+}^{\text{ref}} \\ 1 & C_{\text{H}^+}^{\text{CL}} \leq C_{\text{H}^+}^{\text{ref}} \end{cases} \tag{18}$$

where $i_{0,\text{HPRR}}$ is the exchange current density of HPRR, $i_{0,\text{ORR}}$ is the exchange current density of ORR, C_i^{CL} is the reactant concentration on the cathode CL, C_i^{ref} is the reference reactant concentration, γ is the reaction order based on the concentration of different species, E^0 is the theoretical

potential, k is the rate constant, α is the transfer coefficient, $\theta_{H_2O_2}$ is the coverage of H_2O_2 on the catalyst, E_{mixed} is the mixed potential.

7.2.3. Boundary conditions

In the anode,

$$x = x_1: C_i = C_i^F \quad (i: EG, OH^-) \quad (19)$$

$$x = x_2: N_i^S = \frac{i_{cell} S_i}{n_a F} \quad (i: EG, OH^-) \quad (20)$$

Through the membrane,

$$x = x_3: C_{i, x3} = C_{i, x2} \quad (i: EG, OH^-) \quad (21)$$

$$x = x_4: C_{i, x4} = 0 \quad (i: EG) \quad (22)$$

In the cathode,

$$x = x_5: N_{H_2O_2} = \frac{S_{HPRR}^{H_2O_2} j_{HPRR}}{n_{HPRR} F} + \frac{S_{HPOR}^{H_2O_2} j_{HPOR}}{n_{HPOR} F} \quad (23)$$

$$N_{H^+} = \frac{S_{HPRR}^{H^+} j_{HPRR}}{n_{HPRR} F} + \frac{S_{ORR}^{H^+} j_{ORR}}{n_{ORR} F} - \frac{S_{HPOR}^{H^+} j_{HPOR}}{n_{HPOR} F} \quad (24)$$

$$N_{O_2} = \frac{S_{ORR}^{O_2} j_{ORR}}{n_{ORR} F} - \frac{S_{HPOR}^{O_2} j_{HPOR}}{n_{HPOR} F} \quad (25)$$

$$x = x_6: C_i = C_i^F \quad (i: H_2O_2, H^+) \quad (26)$$

where s is the stoichiometric coefficient, and n is the number of electrons transferred.

7.2.4. Cell voltage

The cell voltage can be determined by Equation (27):

$$V_{cell} = E_c^0 - E_a^0 - \eta_a - \eta_c - i_{cell} R_{internal} \quad (27)$$

where η_a is the anode polarization, η_c is the cathode polarization, and $R_{internal}$ is the overall internal resistance, which is measured by experiment. The physicochemical, operating, structural, and transport parameters are shown

in Tables 1–4, respectively. In addition, above equations are numerically solved by using Matlab.

7.3. Experiments

The home-made fuel cell was composed of a Pd-based anode, a cation exchange membrane, and a gold-based cathode. The anode electrode was prepared by spraying the catalyst ink (1.0 mg cm^{-2} Pd/C and 5 wt. % Nafion) onto a piece of carbon cloth with an active area of $1.0 \text{ cm} \times 1.0 \text{ cm}$. The cathode electrode was made by spraying the catalyst ink (2.66 mg cm^{-2} Au/C and 15 wt. % Nafion) onto a piece of carbon cloth with the same active area. The membrane electrode assembly (MEA) was fixed between an anode plate and a cathode plate, both of which are made of 316 L stainless steel plates with serpentine flow fields. The polarization curves were measured by an Arbin BT2000 (Arbin Instrument Inc.) and the internal resistance was measured by the built-in function of the Arbin BT2000.

7.4. Results and discussion

7.4.1. Model validation

As shown in Figure 7.2, the comparison between the numerical results of the polarization curves under various EG concentrations, i.e. 0.5 M, 1.0 M, and 2.0 M, and the experimental results are made. The experimental results were obtained with a home-made fuel cell. The experimental results were collected when the home-made cell was running with a mixed solution of 7.0 M NaOH and EG as the fuel and a mixed solution of 4.0 M H_2O_2 and 1.0 M H_2SO_4 as the oxidant at 60°C . It is shown that the predicted cell

performance is in good agreement with the experimental data. In the following sections, the voltage losses as well as the effects of species concentrations, electrocatalyst activities, and electrode structures on the cell performance will be presented.

7.4.2. Voltage loss

As shown in Figure 7.3, anode polarization, ohmic polarization, and cathode polarization are demonstrated, all of which result in the voltage loss between the theoretical cell voltage and the practical cell voltage. In general, both the anode and the cathode are suffering from activation polarization and concentration polarization derived from electrochemical loss and transport loss, respectively [46]. Meanwhile, the ohmic polarization derived from internal resistance also occurs. It is seen that the cathode polarization is the severest voltage loss among the anode polarization, ohmic polarization, and cathode polarization, indicating that research attention should be paid to the cathode so that the cathode polarization can be substantially reduced. In brief, the spectacular cathode polarization can be attributed to the spontaneous establishment of an internal hydrogen peroxide-based fuel cells due to hydrogen peroxide self-decomposition. Therefore, to synthesize an appropriate and efficient electrocatalyst for the direct reduction of hydrogen peroxide is the future direction. In addition, the ohmic polarization is negligible in the low current density region but becomes notable in the high current density region.

7.4.3. Effect of the EG concentration

Particularly, the species concentrations exhibit significant effects on the cell

performance when the fuel cell design is determined. Figure 7.4 displays the effect of EG concentration on the cell performance. When the EG concentration increases from 0.5 M to 2.0 M, the OCV increases with the EG concentration. It is because a higher EG concentration will result in the more EG adsorbed on the active sites on the catalyst due to the enhanced mass transport of EG, which is evidenced by the Figure 7.6. Hence, the electrochemical kinetics of the EGOR is enhanced and the concentration loss is reduced because of the higher EG concentration, which is consistent with results from Figure 7.5 that the anode potential under 2.0-M operation is much lower than that under 0.5-M operation under open-circuit condition. It can be seen that the cell with 0.5 M EG supply yields the poorest performance among three EG concentrations. It can be explained that the cell is at starve state under 0.5-M operation due to the relatively low EG concentration on the active sites, as shown in Figure 7.6. Hence, the insufficient EG supply leads to the largest anode polarization, which is evident in Figure 7.5. At around the limiting current region, the EG concentration reaches nearly zero and the anode polarization exponentially increases, resulting in the rapid voltage degradation. When the EG concentration increases to 1.0 M, the cell performance experiences a remarkable promotion in both the OCV and limiting current density. It is attributed to more abundant EG adsorbed on active sites as well as the mitigatory anode polarization comparing to the 0.5-M operation. When the EG concentration further increases from 1.0 M to 2.0 M, the cell performance under 2.0-M operation is superior than that under 1.0-M

operation at a low current density region ($< 1000 \text{ A m}^{-2}$), while it is inferior at medium and high current density regions ($> 1000 \text{ A m}^{-2}$). This observation can be explained as follows. At the low current density region, the anode polarization under 2.0-M operation is lower than that under 1.0-M operation and ohmic polarization shows negligible effect on the cell performance. As a result, the positive effect on the cell performance derived from low anode polarization is stronger than the negative effect derived from the high internal resistance, so that the overall performance under 2.0-M operation is better than that under 1.0-M operation at the low current density region. However, the ohmic polarization becomes notable at the high current density region due to the linear relation between the ohmic polarization and the current density. Hence, at the high current density region, the positive effect on the cell performance derived from low anode polarization is not able to compensate the remarkable negative effect derived from the ohmic polarization. As a result, the overall performance under 2.0 M operation is worse than that under 1.0 M operation at the high current density region.

7.4.4. Effect of the NaOH concentration

It has been realized that the addition of alkali in the anolyte can elevate the cell performance significantly, indicating that the NaOH concentration is an important parameter. Hence, the effect of NaOH concentration on the cell performance is studied and the results are presented in Figure 7.7. It is found that the OCV increases with the NaOH concentration increasing from 1.0 M to 7.0 M as expected. It is attributed to the fast transport of OH^- to the

active sites with higher feeding concentration, so that the OH^- concentration on the active sites is higher, as evidenced in Figure 7.9. As a consequence, the anode polarization at open-circuit state is lower due to the faster EGOR kinetics as well as the limited concentration loss, as depicted in Figure 7.8. After the cell is discharging, the cell under 1.0 M operation shows the worst performance. The reason for this phenomenon is the relatively low OH^- concentration on the active sites, as shown in Figure 7.9. Hence, the cell undergoes severe concentration loss, which causes the rapid voltage to decline in the range of 600 to 800 A m^{-2} . When further increasing the OH^- concentration, the cell performances under 3.0-M, 5.0-M, and 7.0-M operation are similar at the current density range of 0 to 1600 A m^{-2} . The cell performance under 3.0-M operation exhibits an obvious degradation, which is attributed to the conspicuously increased anode overpotential, as presented in Figure 7.8. Figure 7.9 indicates that the OH^- concentration reaches nearly zero at the current density higher than 2000 A m^{-2} , accounting for the notable anode overpotential due to the presence of the serious concentration loss. It is seen from Figures 7.8 and 7.9 that the anode polarizations under 5.0-M and 7.0-M operation do not show huge difference, and the OH^- concentrations on the active sites both are sufficient. However, the performance under 7.0-M operation is inferior comparing to that under 5.0-M operation at high current densities. This is because the ohmic loss will play a non-negligible role in the cell performance. As the internal resistance increases with the OH^- concentration, the large ohmic loss results in the performance degradation

7.4.5. Effect of the H₂O₂ concentration

In this type of fuel cell, hydrogen peroxide is used as oxidant in the cathode to replace the oxygen or air. Hence, the H₂O₂ concentration is bound to an important parameter, which possesses critical effect on the cell performance. Figure 7.10 exhibits the polarization curves with various H₂O₂ feeding concentration. It is found that the OCV increases when the H₂O₂ concentration is elevated from 1.0 M to 4.0 M, which can be ascribed to the lower cathode overpotential with higher H₂O₂ concentration, as evidenced in Figure 7.11. It should be noted that higher H₂O₂ concentration results in the higher cathode potential (around 0.85 V), but the cathode potential is still far below the theoretical cathode potential (1.78 V). The significant performance loss is because of the spontaneous establishment of an internal hydrogen peroxide fuel cell in the cathode bringing about the tremendous mixed potential. The cell performance increases with the H₂O₂ concentration as well. This observation can be explained as follows. On one hand, the transport of H₂O₂ will be facilitated when the H₂O₂ concentration becomes higher, so that the H₂O₂ concentration is higher at the active sites. On the other hand, the electrochemical kinetics of HPRR will be enhanced when the H₂O₂ concentration becomes higher, which can be confirmed by Figure 7.11. For instance, at 1500 A m⁻², the cathode potentials under 1.0-M, 2.0-M, and 4.0-M operations are 0.17 V, 0.35 V, and 0.56 V, respectively. The huge cathode overpotential under 1.0-M operation plays the dominant role in the rapid voltage decline.

7.4.6. Effect of the H₂SO₄ concentration

Since H^+ ion is a necessary reactant in the HPRR process, the H^+ concentration is certain to have effect on the cell performance. The effects of H^+ concentration on the cell performance and the cathode potential are shown in Figures 7.12 and 7.13, respectively. It is seen from Figure 7.12 that the OCV increases with the H^+ concentration increasing from 0.5 M to 2.0 M, which can be attributed to the lower cathode overpotential with higher H^+ concentration, as evidenced in Figure 7.13. After the cell is discharging, the cell performance is increasing with the H^+ concentration as well. This phenomenon can be explained as follows. On one hand, the delivery of H^+ ions to the cathode CL will be elevated when the H^+ concentration increases, resulting in that the H^+ concentration is higher on the active sites. On the other hand, the electrochemical kinetics of HPRR will be enhanced when the H^+ concentration is higher, which can be confirmed by Figure 7.13. For instance, at 1000 A m^{-2} , the cathode potentials under 0.5-M, 1.0-M, and 2.0-M operation are 0.29 V, 0.48 V, and 0.69 V, respectively. The prominent cathode overpotential under 0.5-M operation is believed to play the dominant role in the rapid voltage degradation.

7.4.7. Effect of the exchange current density

For a given cell structure and a fixed operating condition, the cell performance mainly depends on the electrocatalytic activity of the anode and cathode catalysts, respectively. Generally, the exchange current density

reflects the electrocatalytic activity of the catalyst. The effects of the anode exchange current density on the cell performance and the anode potential are demonstrated in Figures 7.14 and 7.15. It is indicated from the Figure 7.14 that the OCV increases with the anode exchange current density increasing from 1 to 100 A m⁻². In addition, the cell with higher anode exchange current density yields the superior performance over the whole current density range as well. The promotion is mainly attributed to the dramatic anode overpotential reduction, as shown in Figure 7.15. The similar observation can be obtained when the cathode exchange current density increases. The higher cathode exchange current density results in higher OCV and superior cell performance over the whole current density range, as shown in Figures 7.16 and 7.17. The improvement is also attributed to the significant cathode overpotential reduction. As a consequence, it is extremely critical to develop novel catalyst with high electrocatalytic activity towards EGOR and HPRR processes.

7.4.8. Effect of the diffusion layer thickness

As the anode DL provides the channels for the EG and NaOH delivery, the anode DL thickness will affect the EG and NaOH transport process, and thus the cell performance. Therefore, the cell performance with different anode DL thickness is studied, and the results are depicted in Figure 7.18. The cell performance decreases along with the increased anode DL thickness from 500 to 2000 μm over the whole current density range. This trend can be ascribed to the fact that a thicker anode DL will increase the transfer length in the anode DL, thus the mass-transport resistance is

enhanced simultaneously as expected. Therefore, for a given anolyte, less reactants are able to reach the active sites to participate in the EGOR process, resulting in the enlarged anode overpotential, as demonstrated in Figure 7.19. In addition, it is also difficult for the products to remove from the cell, which is disadvantageous for achieving a satisfactory cell performance. Hence, the cell voltage experiences an obvious degradation when the anode DL thickness increases. As for the cathode DL thickness, the results from Figures 7.20 and 7.21 show that the increase in the cathode DL thickness will increase the cathode overpotential, and thus decrease the cell voltage, which is similar to the anode DL thickness. It is worth mentioning that the DL also serves as a CL supporter. Too thin will result in the insufficient support for the CL, thus it is difficult to achieve the desired catalyst loading. In addition, the coated catalyst may suffer from severe loss with the cell operation due to the weak interaction between the catalyst particles and the DL. Hence, it is necessary to take all the parameters into consideration in practical application so that the diffusion layer thickness can be determined.

7.5. Summary

A one-dimensional mathematical model for the DEGFC with hydrogen peroxide as oxidant is developed. Various physicochemical processes are involved in this fuel cell, including mass/charge transport and several electrochemical reactions. These processes are taken into consideration in the model, and the model results show a good agreement with the experimental data. The voltage loss is investigated first, and the results

show that the cathode polarization exhibits the severest voltage loss, which can be attributed to the internal hydrogen peroxide-based fuel cell in cathode. Meanwhile, the effects of operating conditions and electrode structural parameters are investigated. The results show that the cell performance improves initially with the increasing concentration of EG and OH⁻, while undergoing a decline at the high current density region, which might be attributed to the enhanced ohmic loss. In addition, the cell performance increases over the whole current density region with increasing hydrogen peroxide and H⁺ concentrations. Meanwhile, the numerical results exhibit that the cell performance is elevated when the anode exchange current density or the cathode exchange current density is increasing from 1 to 100 A m⁻², which emphasizes the significance of developing novel catalyst with superior catalytic activity. Moreover, the effect of the structural parameter of anode and cathode DL on the cell performance is investigated, including the thickness of both anode and cathode DL. As shown by the numerical results, the increase of DL thickness in both anode and cathode has a negative effect on the cell performance. The resistance of mass-transport increases with when the DL becomes thicker, and influences both the delivery of reactants and the removal of reaction products. Future research attention will be mainly paid to developing more precise and advanced theory for the effect of the competitive adsorption on reaction kinetics.

7.6. References

- [1] C. Lamy, A. Lima, V. LeRhun, F. Delime, C. Coutanceau, J.-M. Léger, Recent advances in the development of direct alcohol fuel cells (DAFC), *Journal of Power Sources* 105 (2002) 283-296.
- [2] C. Bianchini, P.K. Shen, Palladium-based electrocatalysts for alcohol oxidation in half cells and in direct alcohol fuel cells, *Chemical Reviews* 109 (2009) 4183-4206.
- [3] E. Antolini, E. Gonzalez, Alkaline direct alcohol fuel cells, *Journal of Power Sources* 195 (2010) 3431-3450.
- [4] D. Sebastian, A. Serov, I. Matanovic, K. Artyushkova, P. Atanassov, A. Aricò, V. Baglio, Insights on the extraordinary tolerance to alcohols of Fe-NC cathode catalysts in highly performing direct alcohol fuel cells, *Nano Energy* 34 (2017) 195-204.
- [5] L. An, T.S. Zhao, *Anion exchange membrane fuel cells: Principles, Materials and Systems*, Springer International Publishing, Cham, Switzerland, 2018.
- [6] X. Chen, T. Li, J. Shen, Z. Hu, From structures, packaging to application: a system-level review for micro direct methanol fuel cell, *Renewable and Sustainable Energy Reviews* 80 (2017) 669-678.
- [7] S.S. Munjewar, S.B. Thombre, R.K. Mallick, Approaches to overcome the barrier issues of passive direct methanol fuel cell–Review, *Renewable and Sustainable Energy Reviews* 67 (2017) 1087-1104.
- [8] A. Chamaani, N. Chawla, M. Safa, B. El-Zahab, One-Dimensional Glass Micro-Fillers in Gel Polymer Electrolytes for Li-O₂ Battery

Applications, *Electrochimica Acta* 235 (2017) 56-63.

[9] L. An, T. Zhao, Y. Li, Carbon-neutral sustainable energy technology: direct ethanol fuel cells, *Renewable and Sustainable Energy Reviews* 50 (2015) 1462-1468.

[10] Z.F. Pan, R. Chen, L. An, Y.S. Li, Alkaline anion exchange membrane fuel cells for cogeneration of electricity and valuable chemicals, *Journal of Power Sources* 365 (2017) 430-445.

[11] L. An, R. Chen, Recent progress in alkaline direct ethylene glycol fuel cells for sustainable energy production, *Journal of Power Sources* 329 (2016) 484-501.

[12] H. Yue, Y. Zhao, X. Ma, J. Gong, Ethylene glycol: properties, synthesis, and applications, *Chemical Society Reviews* 41 (2012) 4218-4244.

[13] A. Serov, C. Kwak, Recent achievements in direct ethylene glycol fuel cells (DEGFC), *Applied Catalysis B: Environmental* 97 (2010) 1-12.

[14] C. Cremers, A. Niedergesäß, F. Jung, D. Müller, J. Tübke, Development of an alkaline anion exchange membrane direct ethylene glycol fuel cell stack, *ECS Transactions* 41 (2011) 1987-1996.

[15] L. Xin, Z. Zhang, J. Qi, D. Chadderdon, W. Li, Electrocatalytic oxidation of ethylene glycol (EG) on supported Pt and Au catalysts in alkaline media: Reaction pathway investigation in three-electrode cell and fuel cell reactors, *Applied Catalysis B: Environmental* 125 (2012) 85-94.

[16] O.O. Fashedemi, H.A. Miller, A. Marchionni, F. Vizza, K.I. Ozoemena, Electro-oxidation of ethylene glycol and glycerol at palladium-decorated FeCo@ Fe core-shell nanocatalysts for alkaline direct alcohol fuel cells:

functionalized MWCNT supports and impact on product selectivity, *Journal of Materials Chemistry A* 3 (2015) 7145-7156.

[17] L. An, T. Zhao, Z. Chai, L. Zeng, P. Tan, Modeling of the mixed potential in hydrogen peroxide-based fuel cells, *International Journal of Hydrogen Energy* 39 (2014) 7407-7416.

[18] L. An, C. Jung, Transport phenomena in direct borohydride fuel cells, *Applied Energy* 205 (2017) 1270-1282.

[19] Z.F. Pan, B. Huang, L. An, Performance of a hybrid direct ethylene glycol fuel cell, *International Journal of Energy Research* (2018).

[20] S. Fukuzumi, Y. Yamada, Hydrogen Peroxide used as a Solar Fuel in One-Compartment Fuel Cells, *ChemElectroChem* 3 (2016) 1978-1989.

[21] X. Yan, P. Gao, G. Zhao, L. Shi, J. Xu, T. Zhao, Transport of highly concentrated fuel in direct methanol fuel cells, *Applied Thermal Engineering* 126 (2017) 290-295.

[22] B. Wang, Y. Zhou, Q. Du, Y. Yin, K. Jiao, Transient investigation of passive alkaline membrane direct methanol fuel cell, *Applied Thermal Engineering* 100 (2016) 1245-1258.

[23] Y. Yu, X. Yang, Y. Zhao, X. Zhang, L. An, M. Huang, G. Chen, R. Zhang, Engineering the Band Gap States of the Rutile TiO₂ (110) Surface by Modulating the Active Heteroatom, *Angewandte Chemie* (2018).

[24] G. Zhang, K. Jiao, Multi-phase models for water and thermal management of proton exchange membrane fuel cell: A review, *Journal of Power Sources* 391 (2018) 120-133.

[25] K. Jiao, X. Li, Water transport in polymer electrolyte membrane fuel

-
- cells, *Progress in Energy and Combustion Science* 37 (2011) 221-291.
- [26] H. Bahrami, A. Faghri, Multi-layer membrane model for mass transport in a direct ethanol fuel cell using an alkaline anion exchange membrane, *Journal of Power Sources* 218 (2012) 286-296.
- [27] T. Guo, J. Sun, J. Zhang, H. Deng, X. Xie, K. Jiao, X. Huang, Transient analysis of passive vapor-feed DMFC fed with neat methanol, *International Journal of Hydrogen Energy* 42 (2017) 3222-3239.
- [28] X. Xie, H. Yu, H. Deng, G. Zhang, T. Guo, J. Sun, K. Jiao, Modeling of passive vapor feed alkaline membrane direct methanol fuel cell, *Applied Thermal Engineering* 131 (2018) 920-932.
- [29] B. Wang, K. Wu, Z. Yang, K. Jiao, A quasi-2D transient model of proton exchange membrane fuel cell with anode recirculation, *Energy Conversion and Management* 171 (2018) 1463-1475.
- [30] S. Huo, J. Zhou, T. Wang, R. Chen, K. Jiao, Experimental and analytical analysis of polarization and water transport behaviors of hydrogen alkaline membrane fuel cell, *Journal of Power Sources* 382 (2018) 1-12.
- [31] M.Z. Yu, S. Zhou, Y. Liu, Z.Y. Wang, T. Zhou, J.J. Zhao, Z.B. Zhao, J.S. Qiu, Long life rechargeable Li-O₂ batteries enabled by enhanced charge transfer in nanocable-like Fe@N-doped carbon nanotube catalyst, *Science China-Materials* 60 (2017) 415-426.
- [32] L. An, T. Zhao, R. Chen, Q. Wu, A novel direct ethanol fuel cell with high power density, *Journal of Power Sources* 196 (2011) 6219-6222.
- [33] R. Pathak, S. Basu, Mathematical modeling and experimental

verification of direct glucose anion exchange membrane fuel cell, *Electrochimica Acta* 113 (2013) 42-53.

[34] R. Chen, T. Zhao, Mathematical modeling of a passive-feed DMFC with heat transfer effect, *Journal of Power Sources* 152 (2005) 122-130.

[35] J.P. Hoare, Oxygen Overvoltage Measurements on Bright Platinum in Acid Solutions II Bright Platinum in Stabilized Acid Solutions, *Journal of The Electrochemical Society* 112 (1965) 608-611.

[36] I. Katsounaros, W.B. Schneider, J.C. Meier, U. Benedikt, P.U. Biedermann, A.A. Auer, K.J. Mayrhofer, Hydrogen peroxide electrochemistry on platinum: towards understanding the oxygen reduction reaction mechanism, *Physical Chemistry Chemical Physics* 14 (2012) 7384-7391.

[37] S. Huo, J. Zhou, T. Wang, R. Chen, K. Jiao, Experimental and analytical analysis of polarization and water transport behaviors of hydrogen alkaline membrane fuel cell, *Journal of Power Sources* 382 (2018) 1-12.

[38] N. Bussayajarn, D.A. Harrington, S. Therdthianwong, A. Therdthianwong, N. Djilali, The cathodic polarization prediction of H₂/H₂O₂ fuel cells by using EIS spectra, *Paper A 12* (2004).

[39] S.B. Hall, E.A. Khudaish, A.L. Hart, Electrochemical oxidation of hydrogen peroxide at platinum electrodes. Part 1. An adsorption-controlled mechanism, *Electrochimica Acta* 43 (1998) 579-588.

[40] L. An, Z. Chai, L. Zeng, P. Tan, T. Zhao, Mathematical modeling of alkaline direct ethanol fuel cells, *International Journal of Hydrogen Energy*

38 (2013) 14067-14075.

[41] C. Xu, T. Zhao, Q. Ye, Effect of anode backing layer on the cell performance of a direct methanol fuel cell, *Electrochimica Acta* 51 (2006) 5524-5531.

[42] G. Ternström, A. Sjöstrand, G. Aly, Å. Jernqvist, Mutual diffusion coefficients of water+ ethylene glycol and water+ glycerol mixtures, *Journal of Chemical & Engineering Data* 41 (1996) 876-879.

[43] G.H. Miley, E.D. Byrd, in: Excerpt from the proceedings of the COMSOL users conference, 2006.

[44] J. Newman, K.E. Thomas-Alyea, *Electrochemical systems*, John Wiley & Sons, 2012.

[45] W. Yang, T. Zhao, A two-dimensional, two-phase mass transport model for liquid-feed DMFCs, *Electrochimica Acta* 52 (2007) 6125-6140.

[46] Z.F. Pan, L. An, T.S. Zhao, Z.K. Tang, Advances and challenges in alkaline anion exchange membrane fuel cells, *Progress in Energy and Combustion Science* 66 (2018) 141-175.

Figures

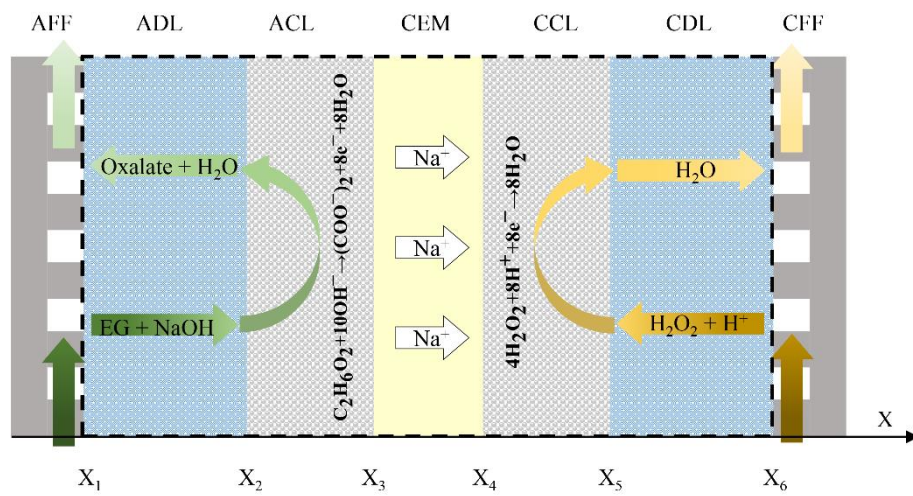


Figure 7.1 Schematic of a DEGFC and the coordinate system.

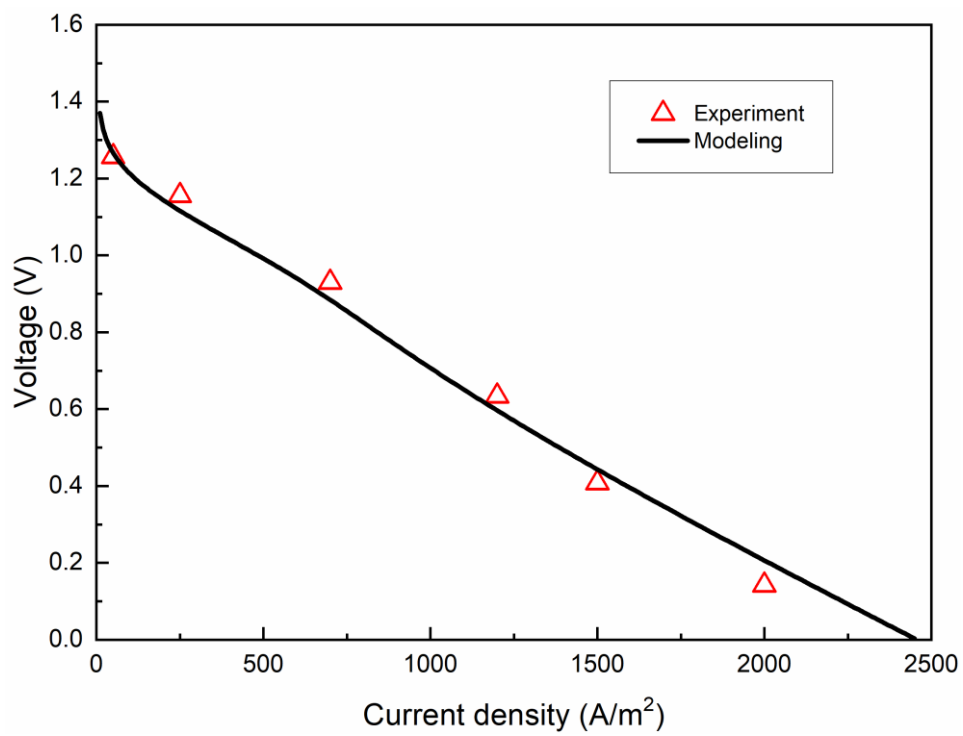


Figure 7.2 Validation made between numerical results and experimental data.

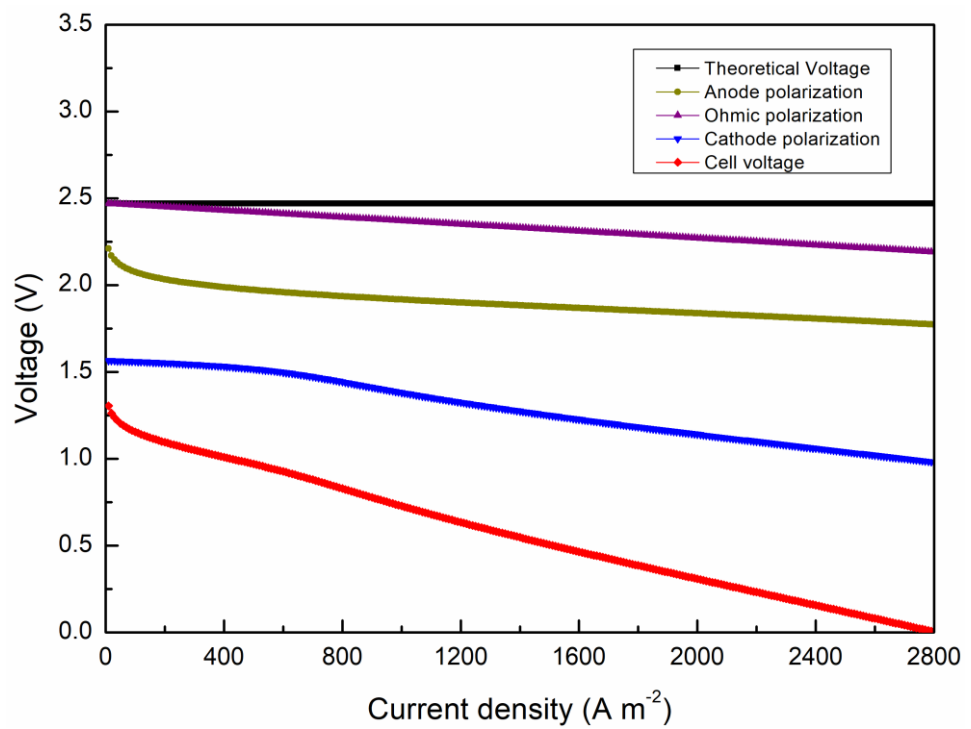


Figure 7.3 Specific polarizations and overall voltage loss with the current density.

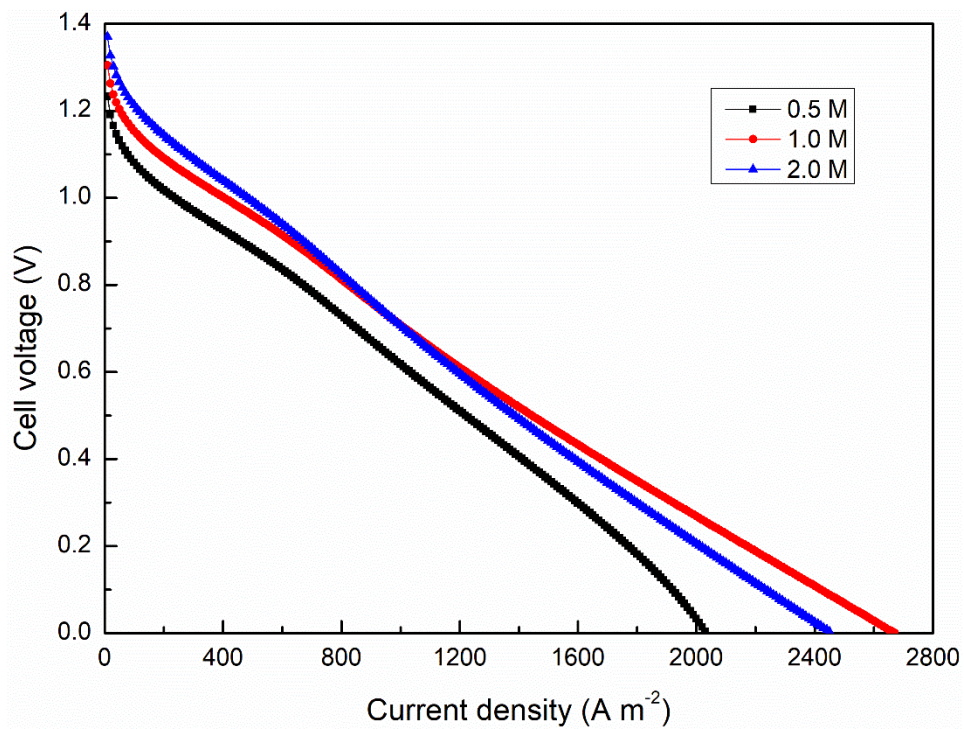


Figure 7.4 Effect of the EG concentration on the polarization curves.

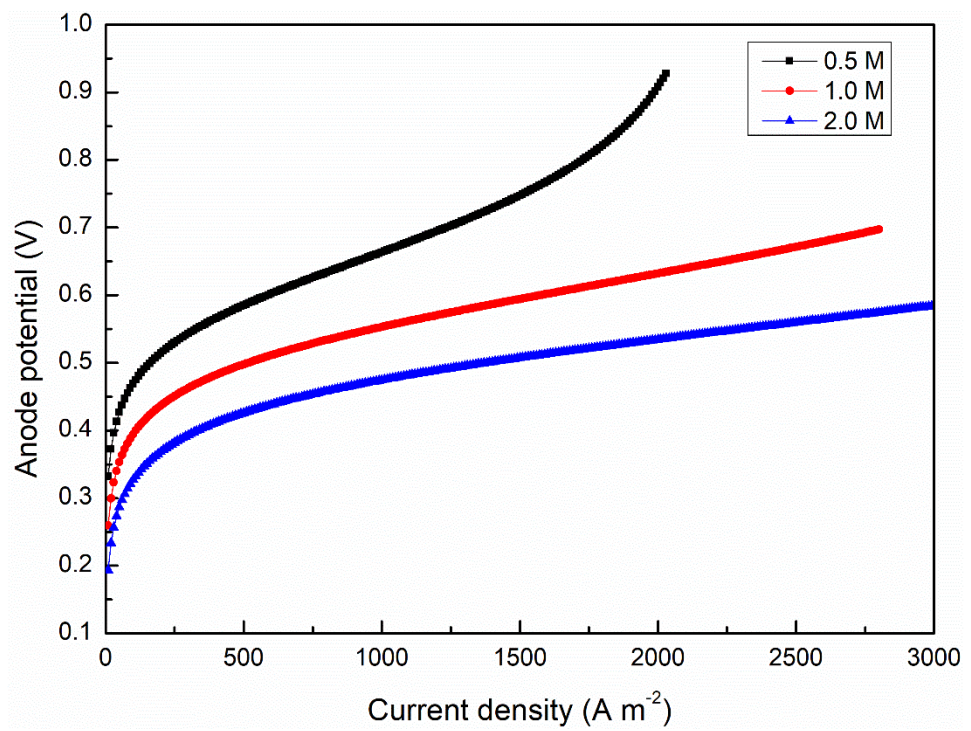


Figure 7.5 Effect of the EG concentration on the anode overpotentials.

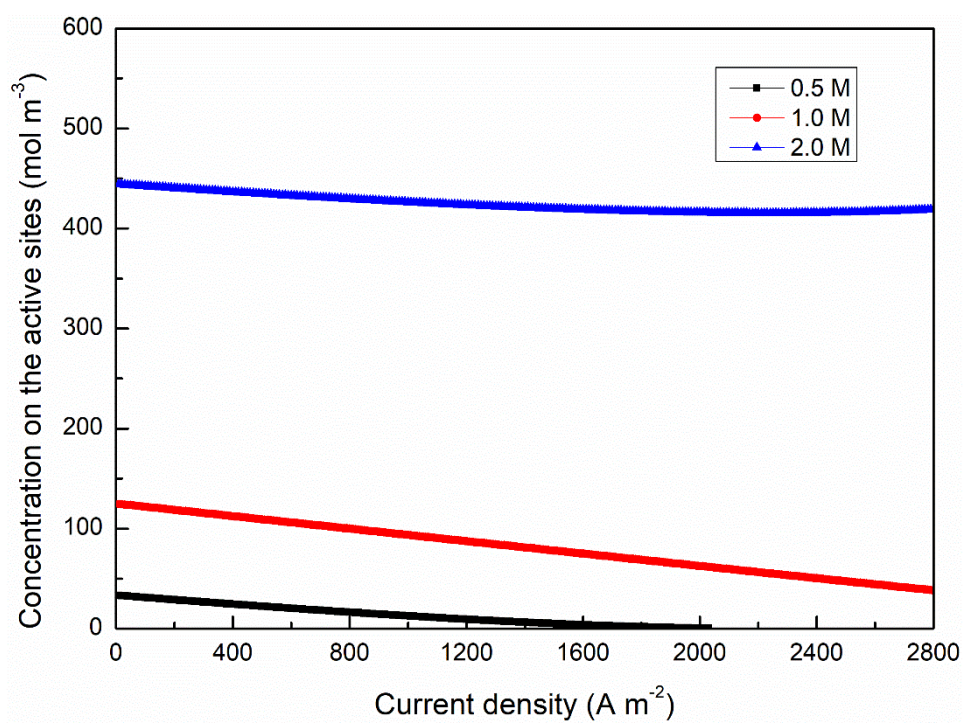


Figure 7.6 Effect of the EG concentration on the concentration on the active sites.

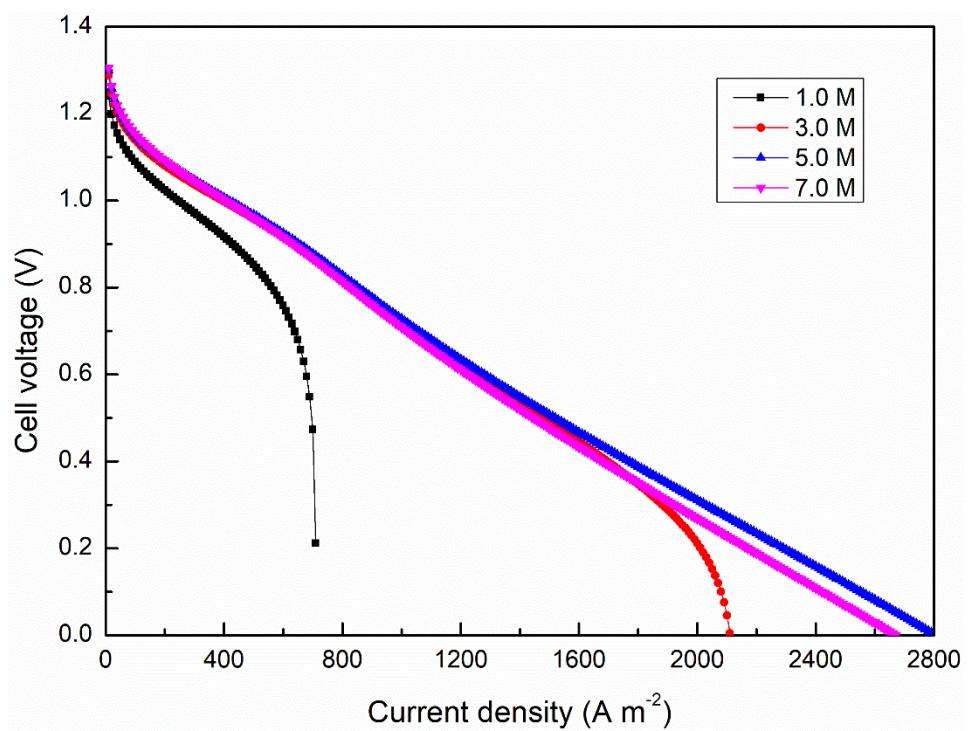


Figure 7.7 Effect of the hydroxyl ion concentration on the polarization curves.

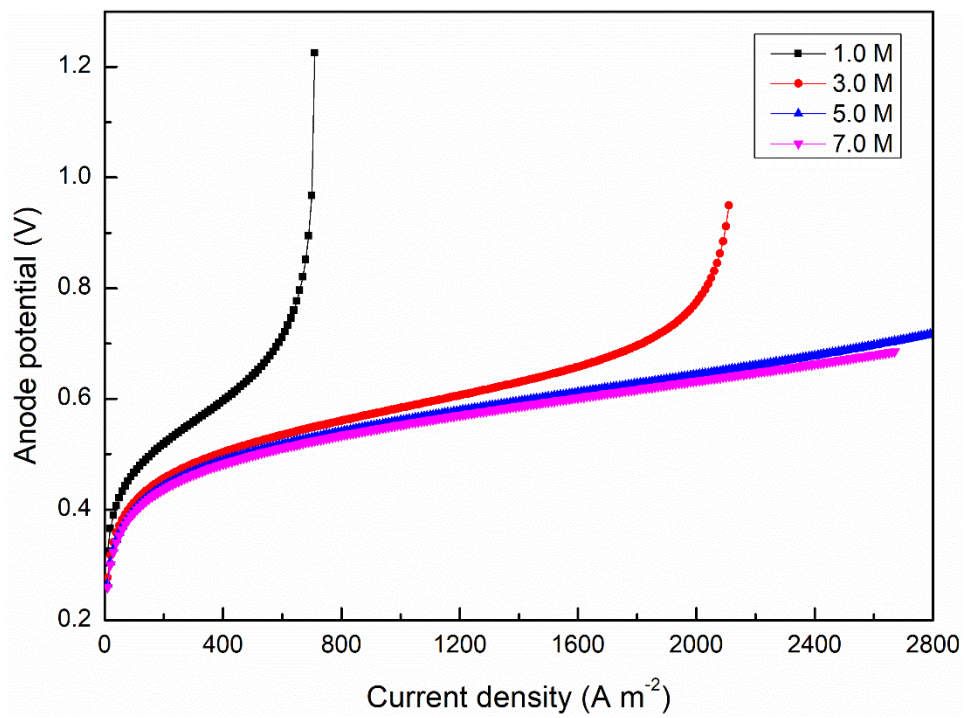


Figure 7.8 Effect of the hydroxyl ion concentration on the anode overpotentials.

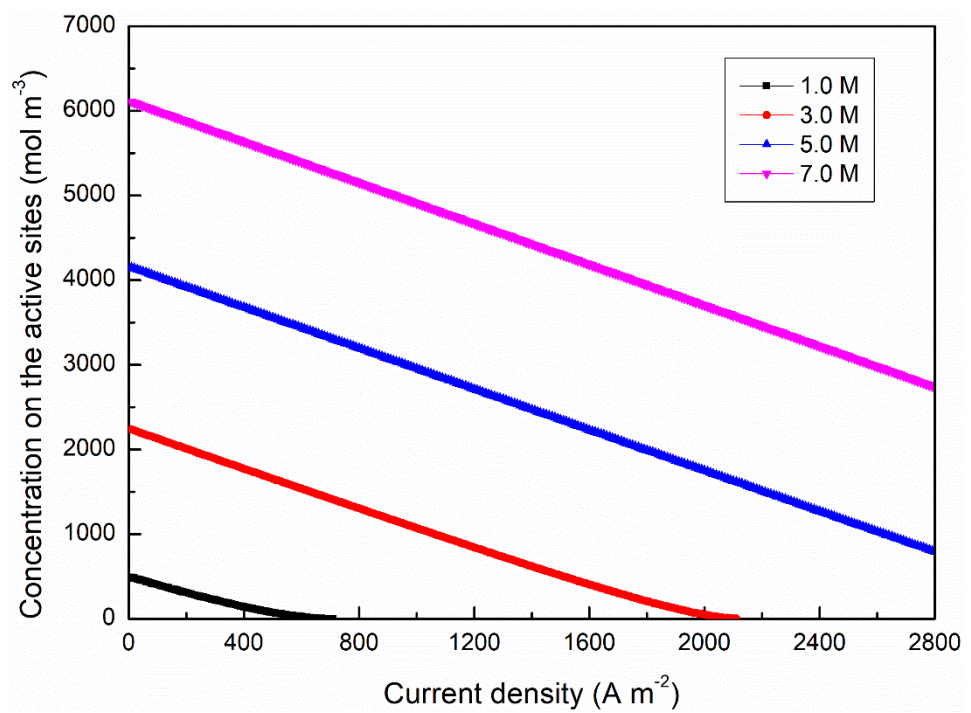


Figure 7.9 Effect of the hydroxyl ion concentration on the concentration on the active sites.

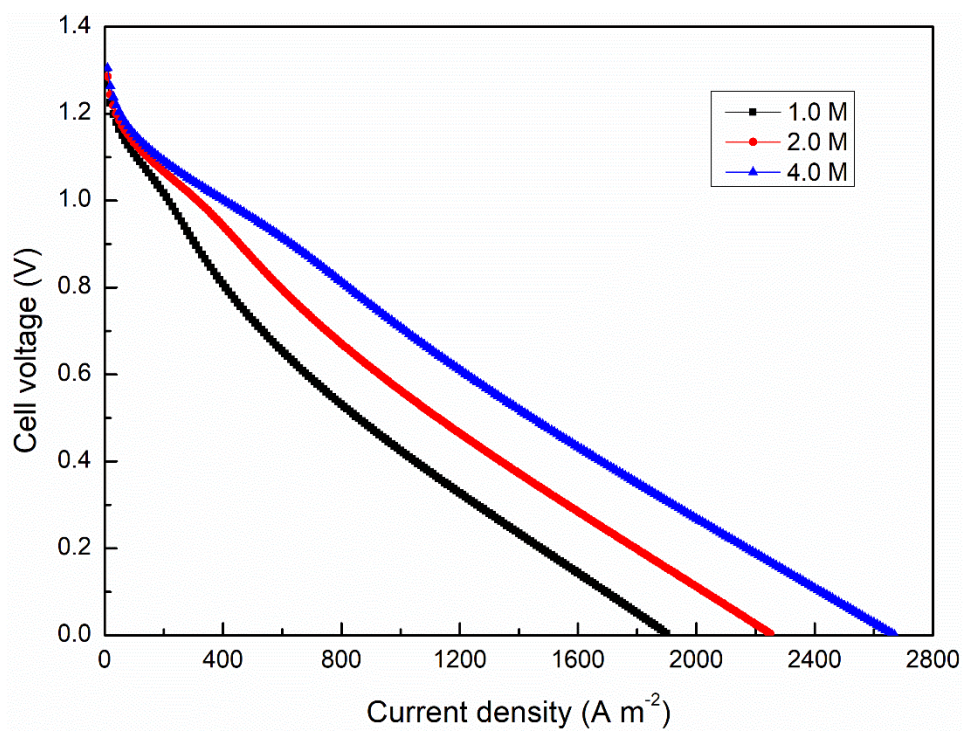


Figure 7.10 Effect of the hydrogen peroxide concentration on the polarization curves.

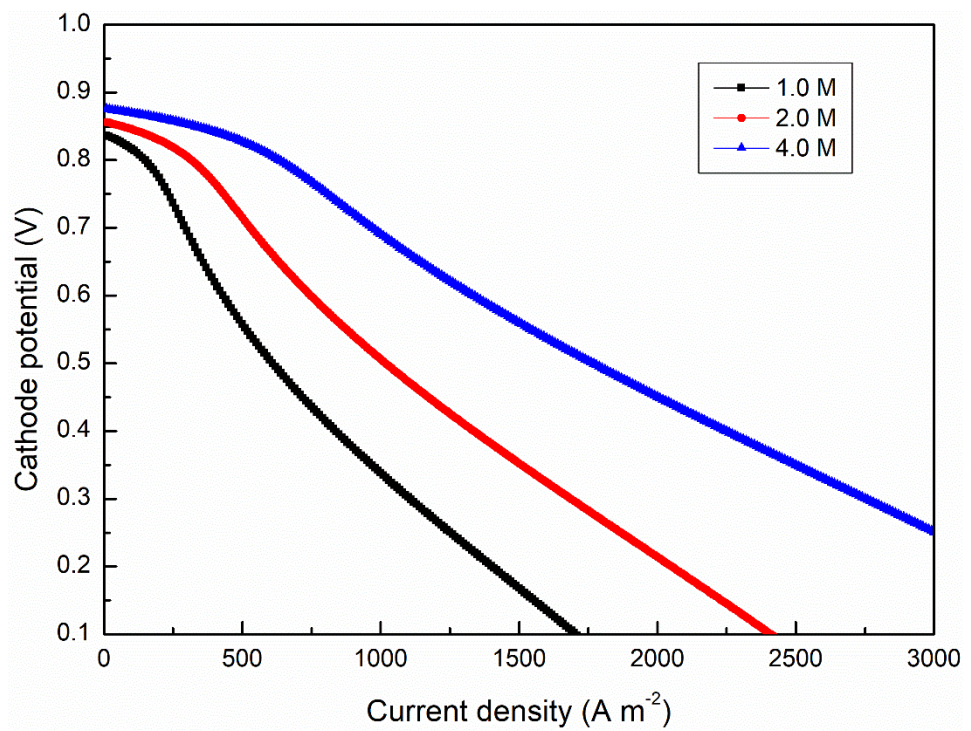


Figure 7.11 Effect of the hydrogen peroxide concentration on the cathode overpotentials.

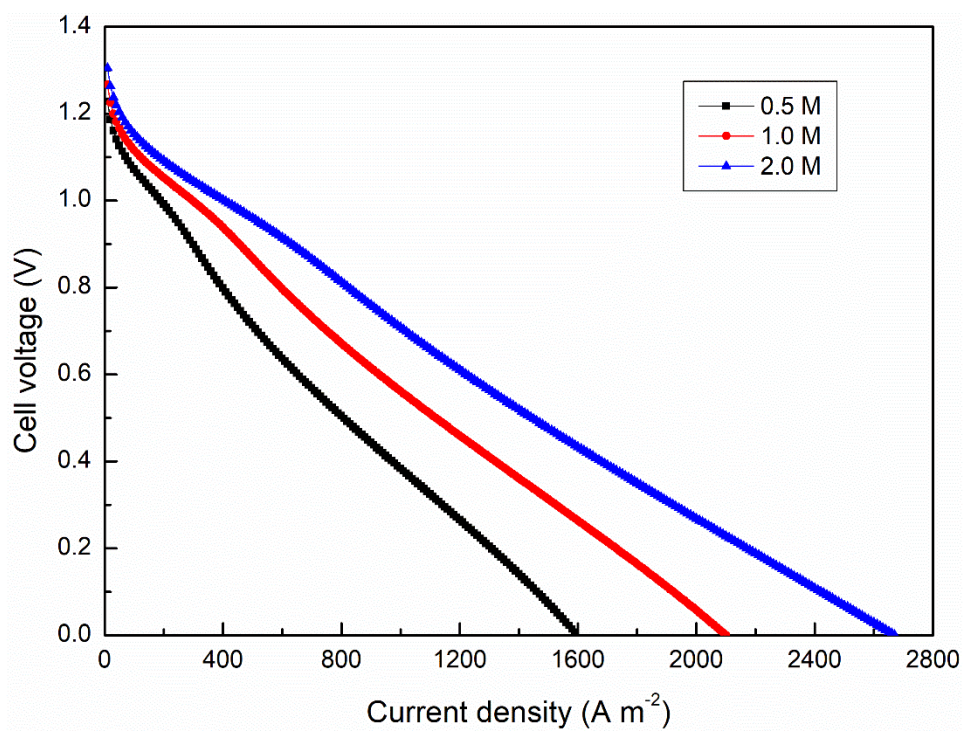


Figure 7.12 Effect of the H⁺ concentration on the polarization curves.

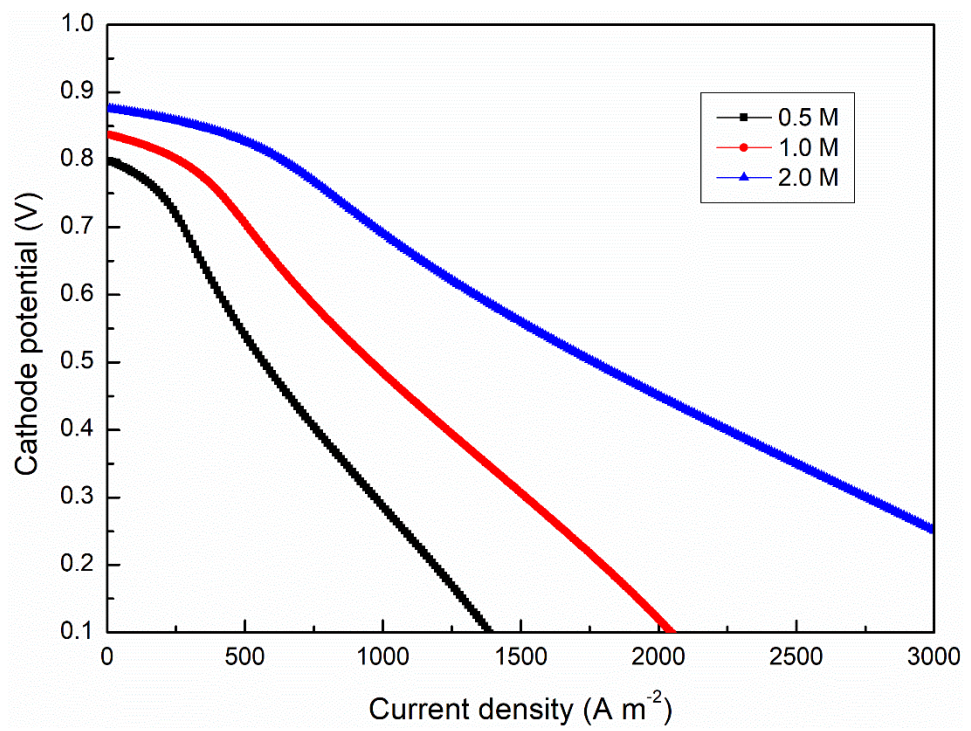


Figure 7.13 Effect of the H⁺ concentration on the cathode overpotentials.

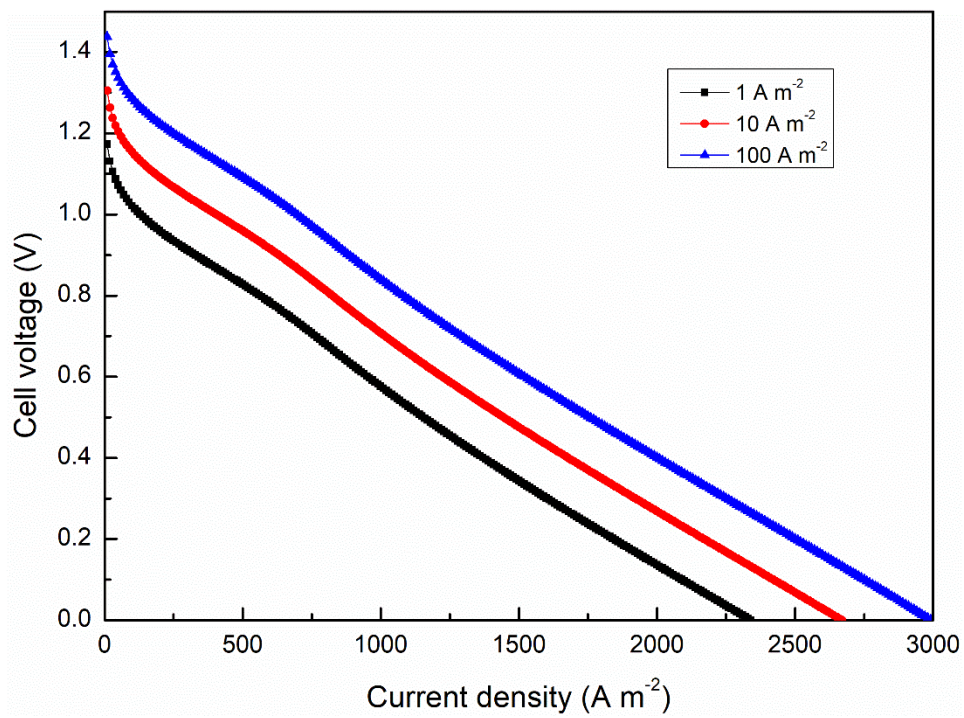


Figure 7.14 Effect of the anode exchange current density on the polarization curves.

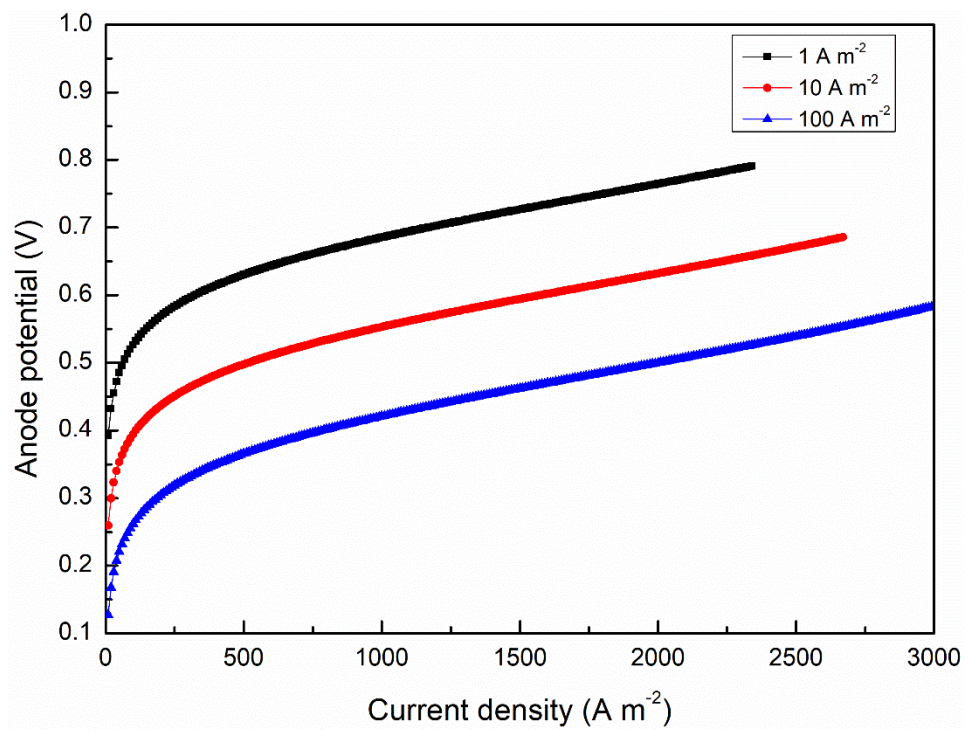


Figure 7.15 Effect of the anode exchange current density on the anode overpotentials.

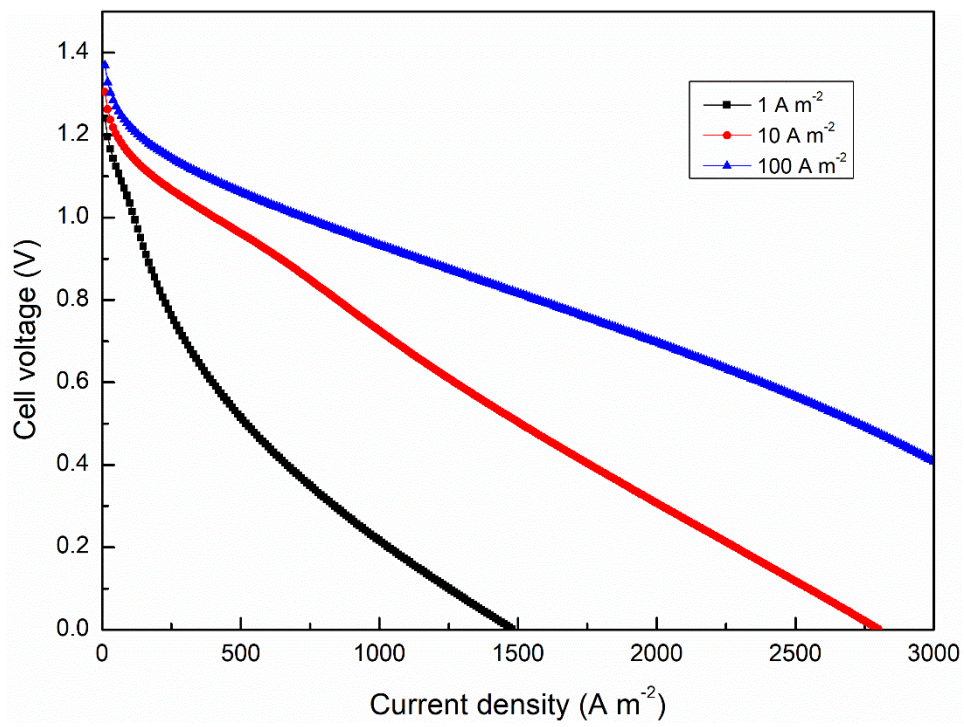


Figure 7.16 Effect of the cathode exchange current density on the polarization curves.

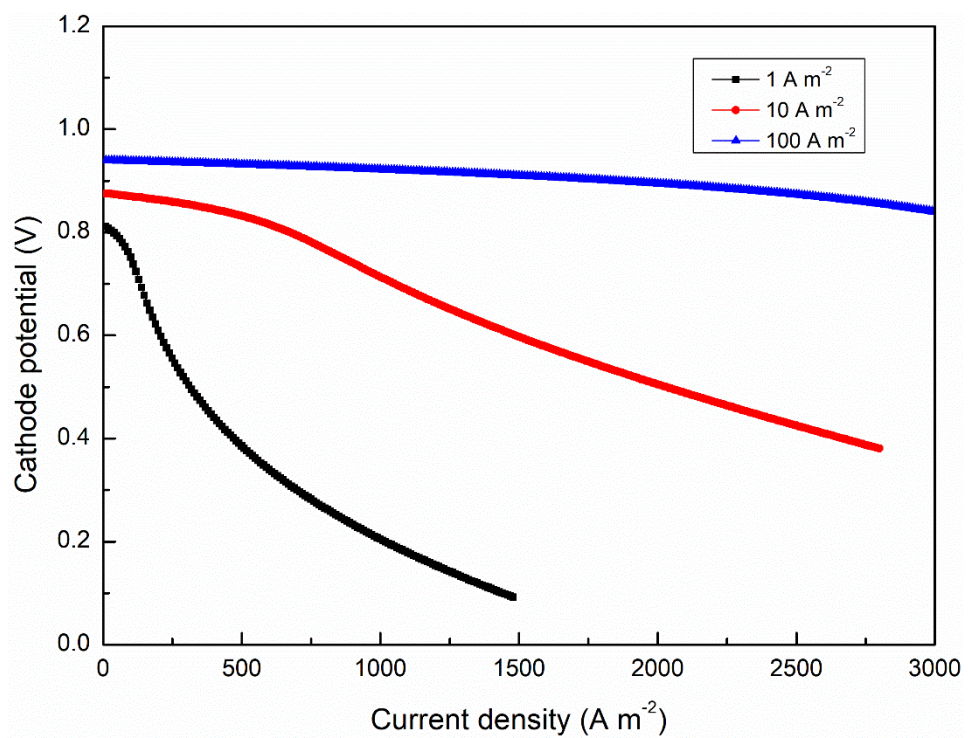


Figure 7.17 Effect of the cathode exchange current density on the cathode overpotentials.

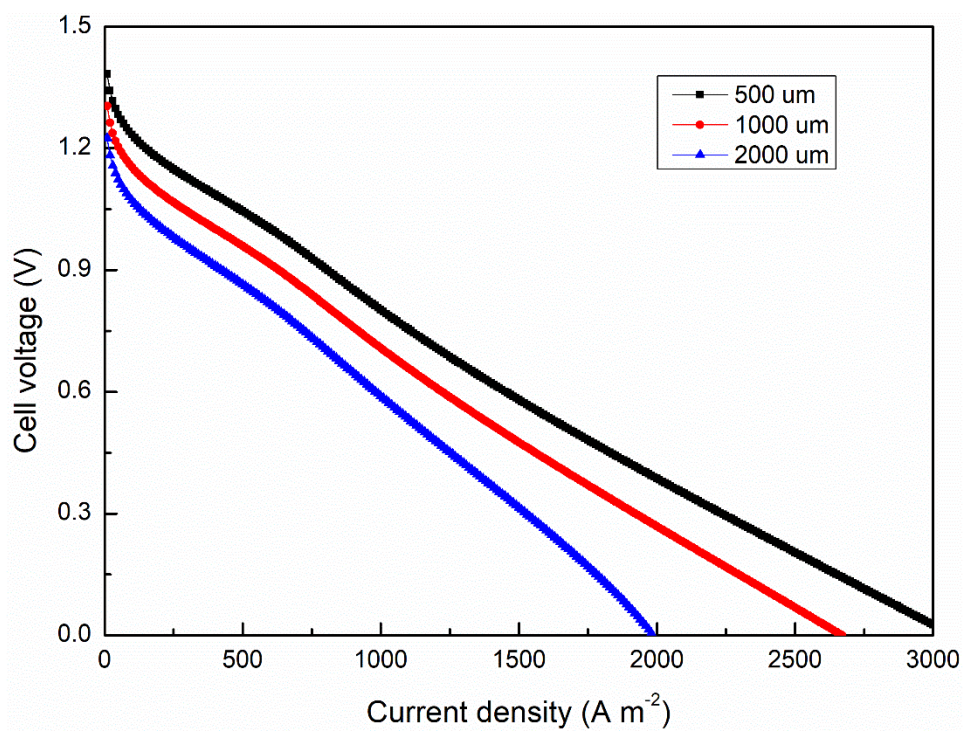


Figure 7.18 Effect of the anode DL thickness on the polarization curves.

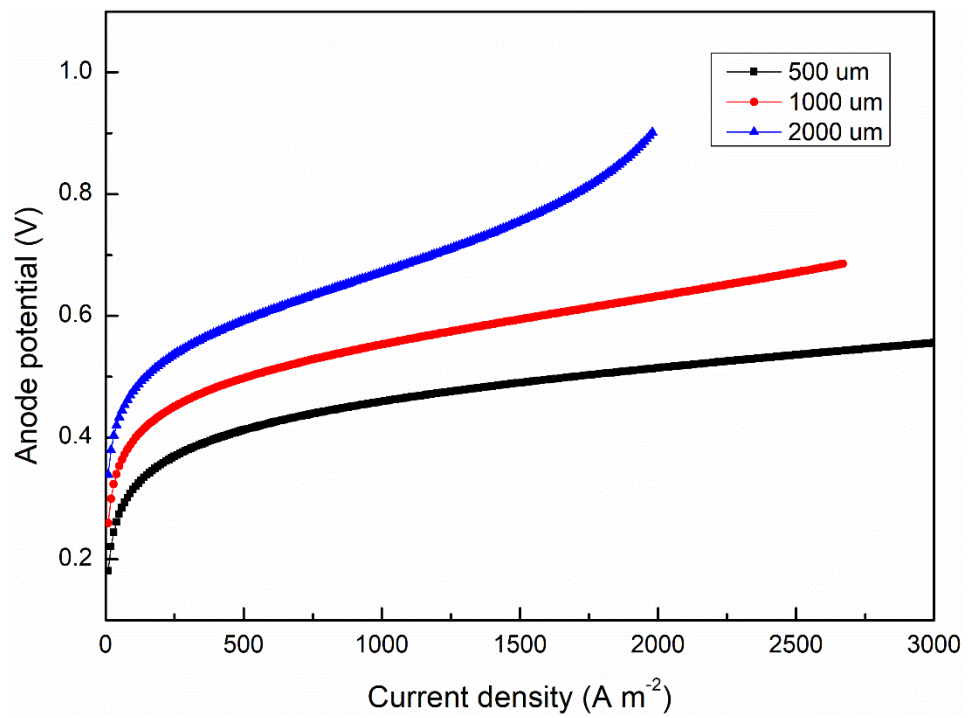


Figure 7.19 Effect of the anode DL thickness on the anode overpotentials.

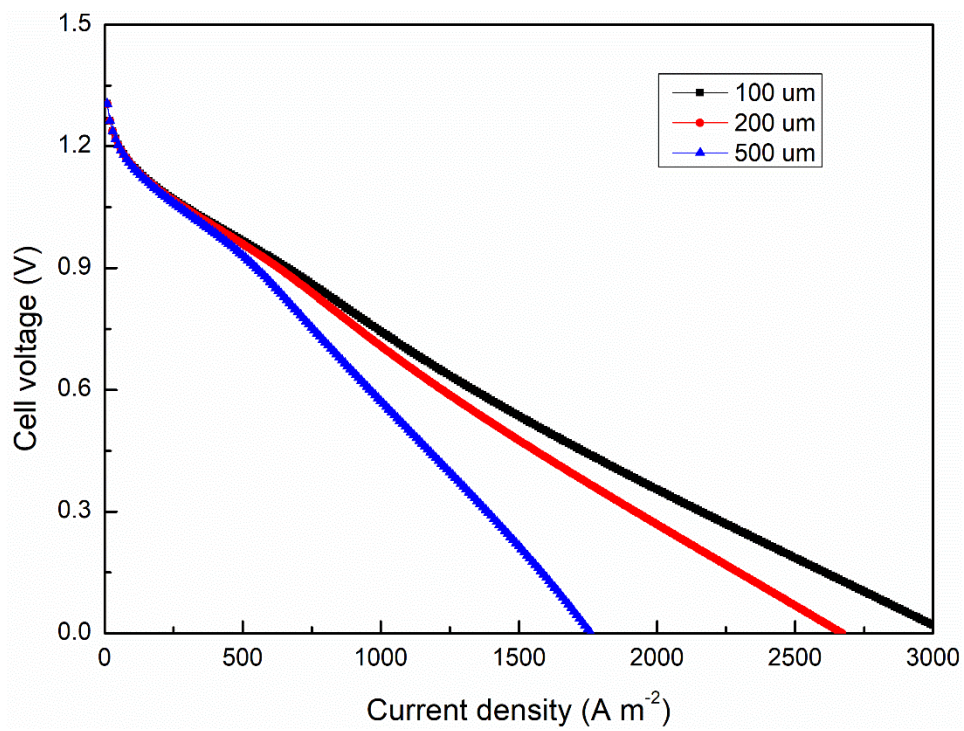


Figure 7.20 Effect of the cathode DL thickness on the polarization curves.

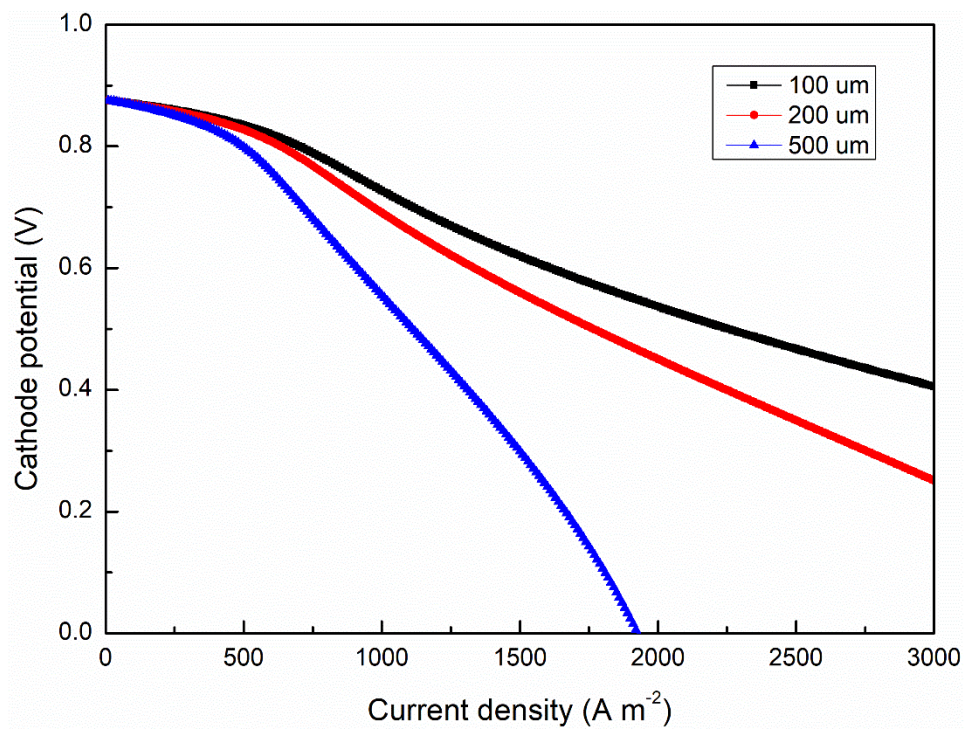


Figure 7.21 Effect of the cathode DL thickness on the cathode overpotentials.

Table

Table 7-1 Physicochemical parameters.

| Physicochemical parameters | | | | |
|--|-----------------|-----------------------|-------------------------------------|-----------|
| Parameter | Symbol | Value | Unit | Reference |
| Anode standard potential | E_a^0 | -0.69 | V | [11] |
| Anode transfer coefficient | α_a | 0.5 | - | Assumed |
| Anode exchange current density | $i_{0,a}$ | 10 | A m ⁻² | Assumed |
| Number of anode transferred electrons | n_a | 8 | - | |
| Hydraulic permeability | k_w | 1.0×10^{-14} | m ² | [33] |
| Viscosity of water | μ_w | 0.000899 | Pa s | [33] |
| Pressure difference | ΔP | 1200 | Pa | [33] |
| Standard potential (HPRR) | E_{HPRR}^0 | 1.78 | V | [32] |
| Standard potential (HPOR) | E_{HPOR}^0 | 0.69 | V | [35] |
| Standard potential (ORR) | E_{ORR}^0 | 1.23 | V | [36] |
| Transfer coefficient (HPRR) | α_{HPRR} | 0.13 | - | Assumed |
| Transfer coefficient (HPOR) | α_{HPOR} | 0.9 | - | Assumed |
| Transfer coefficient (ORR) | α_{ORR} | 0.5 | - | [37] |
| Exchange current density (HPRR) | $i_{0,HPRR}$ | 10 | A m ⁻² | [38] |
| Exchange current density (ORR) | $i_{0,ORR}$ | 44 | A m ⁻² | [34] |
| Universal gas constant | R | 8.314 | J mol ⁻¹ K ⁻¹ | |
| Faraday's constant | F | 96485.3 | A s mol ⁻¹ | |
| Number of transferred electrons (HPRR) | n_{HPRR} | 2 | - | |
| Number of transferred electrons (HPOR) | n_{HPOR} | 2 | - | |
| Number of transferred electrons (ORR) | n_{ORR} | 4 | - | |
| Rate constant | k_2 | 1.01×10^{-3} | mol m ⁻² s ⁻¹ | [39] |

Table 7-2 Operating parameters.

| Operating parameters | | | | |
|--|--------------------|--------|---------------------|-----------|
| Parameter | Symbol | Value | Unit | Reference |
| Operating temperature | T | 333.15 | K | |
| Feeding concentration (O ₂) | $C_{O_2}^F$ | 0 | mol m ⁻³ | Assumed |
| Reference concentration (EG) | C_{EG}^{ref} | 1000 | mol m ⁻³ | Assumed |
| Reference concentration (OH ⁻) | $C_{OH^-}^{ref}$ | 7000 | mol m ⁻³ | Assumed |
| Reference concentration (H ₂ O ₂) | $C_{H_2O_2}^{ref}$ | 4000 | mol m ⁻³ | [32] |
| Reference concentration (H ⁺) | $C_{H^+}^{ref}$ | 2000 | mol m ⁻³ | [32] |
| Reference concentration (O ₂) | $C_{O_2}^{ref}$ | 36.573 | mol m ⁻³ | [34] |

Table 7-3 Structural parameters.

| Structural parameters | | | | |
|-----------------------|---------------------|----------------------|------|-----------|
| Parameter | Symbol | Value | Unit | Reference |
| Anode DL porosity | ε_{ADL} | 0.95 | - | [40] |
| Anode DL thickness | l_{ADL} | 1.0×10^{-3} | m | [40] |
| Anode CL porosity | ε_{ACL} | 0.6 | - | [33] |
| Anode CL thickness | l_{ACL} | 2.0×10^{-5} | m | [33] |
| Anode CL bulk radius | δ_{ACL} | 2.0×10^{-6} | m | [40] |
| Membrane thickness | l_M | 5.0×10^{-5} | m | Measured |
| Cathode DL porosity | ε_{CDL} | 0.73 | - | [41] |
| Cathode DL thickness | l_{CDL} | 2.0×10^{-4} | m | [40] |

Table 7-4 Mass/charge transport parameters.

| Mass/charge transport parameters | | | | |
|--|--------------|-----------------------|--------------|-----------|
| Parameter | Symbol | Value | Unit | Reference |
| Diffusivity of OH ⁻ | D_{OH^-} | 5.26×10^{-9} | $m^2 s^{-1}$ | [40] |
| Diffusivity of EG | D_{EG} | 2.0×10^{-9} | $m^2 s^{-1}$ | [42] |
| Diffusivity of H ₂ O ₂ | $D_{H_2O_2}$ | 3.47×10^{-9} | $m^2 s^{-1}$ | [43] |
| Diffusivity of H ⁺ | D_{H^+} | 9.31×10^{-9} | $m^2 s^{-1}$ | [44] |
| Diffusivity of O ₂ | D_{O_2} | 3.03×10^{-9} | $m^2 s^{-1}$ | [45] |

Chapter 8 Conclusions and future work

8.1. Conclusions

Direct ethylene glycol fuel cells (DEGFCs), a clean and efficient power generation technology, have attracted great research interest as a promising power source, primarily because of excellent properties of ethylene glycol, including high energy density and ease of transportation, storage as well as handling. This thesis has conducted experimental and numerical investigations on this technology, and the detailed procedures and results obtained during the study have been addressed in chapters 2 to 7. Salient results are summarized as follows:

- i) A cost-effective poly(vinylidene fluoride-co-hexafluoropropylene) (PVDF-HFP) is adopted as electrode binder, which tends to form a porous structure and adhere the catalyst nanoparticles onto the nickel foam skeleton but not to isolate the catalyst nanoparticles, achieving a higher effective active area. Meanwhile, it contains more amorphous domains capable of trapping a large amount of liquid electrolyte, creating more effective active sites. At the electrode level, the electrochemical surface areas of the three electrodes using PVDF-HFP, Nafion, and PTFE are 24.10, 18.62, and 16.44 m² g⁻¹, respectively. At the cell level, using the PVDF-HFP-based electrode exhibits the best performance with an open-circuit voltage (OCV) of 1.47 V, a maximum current density of 300 mA cm⁻², and a peak power density of 120.0 mW cm⁻² at 60°C, which shows an improvement of 13.7% and

58.1%, respectively, comparing to the fuel cell performance achieved by using Nafion and PTFE as the electrode binder.

- ii) An active fuel cell using ethylene glycol (EG) as fuel and hydrogen peroxide as oxidant is designed, fabricated, and tested, which theoretically offers a theoretical voltage as high as 2.47 V. This active fuel cell can experimentally output an OCV of 1.41 V and a peak power density of 80.9 mW cm^{-2} at 60°C , which is 20.8% higher than that of using oxygen (67 mW cm^{-2}). The performance improvement is mainly attributed to the faster kinetics of the two-electron-transfer hydrogen peroxide reduction reaction.
- iii) A passive fuel cell using EG as fuel and hydrogen peroxide as oxidant is demonstrated, which avoids the usage of auxiliary devices. Although the passive fuel cell generates a lower power density than does an active one, it is more structurally compact, no parasitic loss in power, and can be operated under ambient conditions, making it a suitable candidate for powering portable electronic devices. It is found that this passive fuel cell yields an OCV of 1.58 V and peak power densities of 30.3 mW cm^{-2} and 65.8 mW cm^{-2} at 23°C and 60°C , respectively, showing an impressive improvement comparing to a passive air-based fuel cell, which is more than two times higher in the OCV (0.7 V) and more than five times higher in the peak power density (12 mW cm^{-2}).
- iv) A passive fuel cell stack consisting of two single cells is developed to examine the feasibility of this fuel cell technology in practical applications and then demonstrated to power an electric fan in

underwater condition. This passive fuel cell stack exhibits an actual OCV of 3.0 V, a maximum current of 860 mA, and a peak power of 1178 mW at room temperature. The individual cell in the passive stack exhibits a good consistency over the whole current region, indicating a high degree of reproducibility achieved by the appropriate electrode manufacturing and cell assembly processes. Moreover, the running time (per refueling) of an electric fan powered by this passive stack is 2 hours and 36 minutes in underwater condition, demonstrating that this passive fuel cell stack is a promising power source for airtight situations, such as underwater and outer space.

- v) A mathematical model is developed to give the in-depth insights of physical and chemical processes occurring in this fuel cell, which incorporates mass/charge transport and electrochemical reactions. Previous models treat the local concentration as the actual reactant concentration participating in the electrochemical reaction, suggesting that EG molecules and OH^- ions are completely adsorbed on active sites. For a specific active site, however, the reactant with a higher local concentration is more likely to be adsorbed, which may lead to active sites fully occupied. The other with a lower local concentration cannot be further adsorbed, hindering the electrochemical reaction. As such, the fuel cell performance is significantly affected by the fuel solution composition and their transport characteristics. By considering the competitive adsorption of reactants on active sites, the present model accurately predicts the voltage losses, electrode potentials, local

concentrations, and thus fuel cell performance under various operating and structural design parameters.

8.2. Future work

The three-dimensional electrode has greatly improved the mass transport and active sites, and the PVDF-HFP has significantly reduced the cost. The effects of the reactant supply method and operating conditions on the fuel cell performance have been revealed. A lab-scale demonstration has been presented to show the application potential of this fuel cell at air-tight situations. There is some future work that will be done:

- i) The noble metal-based electrocatalysts greatly increase the cost of the electrode fabrication, hindering this technology worldwide commercialization. Efficient non-noble metal-based electrocatalysts will be developed to effectively reduce the cost.
- ii) On the cathode, the hydrogen peroxide will spontaneously decompose to oxygen and water. The generated oxygen will cover the active sites in the cathode catalyst layer, hindering the hydrogen peroxide transporting to the active sites. The structure of cathode will be designed to facilitate the removal of oxygen.
- iii) The stable operation of fuel cell under cold environment is a crucial requirement. Considering another function of EG, an antifreeze agent, the successful operation of the DEGFC at low temperatures (generally $< -20^{\circ}\text{C}$) will be demonstrated, and it will be tested as a power source for smart phone at cold environment.

Appendix I Publications during PhD study at The Hong Kong Polytechnic University

Journal papers

1. **Z.F. Pan**, L. An, T.S. Zhao, Z.K. Tang, “Advances and challenges in alkaline anion exchange membrane fuel cells”, *Prog. Energy Combust. Sci.* **66** (2018) 141-175. **(ESI highly cited paper and Hot paper)**
2. **Z.F. Pan**, Y.D. Bi, L. An, “A cost-effective and chemically stable electrode binder for alkaline-acid direct ethylene glycol fuel cells”, *Applied Energy* **258** (2020) 114060.
3. **Z.F. Pan**, Y.D. Bi, L. An, “Performance characteristics of a passive direct ethylene glycol fuel cell with hydrogen peroxide as oxidant”, *Applied Energy* **250** (2019) 846-854.
4. **Z.F. Pan**, L. An, C.Y. Wen, “Recent advances in fuel cells based propulsion systems for unmanned aerial vehicles”, *Applied Energy* **240** (2019) 473-485. **(ESI highly cited paper)**
5. **Z.F. Pan**, H.R. Zhuang, Y.D. Bi, L. An, “A direct ethylene glycol fuel cell stack as air-independent power sources for underwater and outer space applications”, *J. Power Sources* **437** (2019) 226944.
6. **Z.F. Pan**, R. Chen, L. An, Y.S. Li, “Alkaline anion exchange membrane fuel cells for cogeneration of electricity and valuable chemicals”, *J. Power Sources* **365** (2017) 430-445.

-
7. **Z.F. Pan**, Y.D. Bi, L. An, “Mathematical modeling of direct ethylene glycol fuel cells incorporating the effect of the competitive adsorption”, *Applied Thermal Engineering* **147** (2019) 1115-1124.
 8. **Z.F. Pan**, B. Huang, L. An, “Performance of a hybrid direct ethylene glycol fuel cell”, *Int. J. Energy Research* **43** (2019) 2583-2591.
 9. Q.F. Liu[†], **Z.F. Pan**[†], E.D. Wang, L. An, G.Q. Sun, “Aqueous Metal-Air Batteries: Fundamentals and Applications”, *Energy Storage Materials* **27** (2020) 478-505. [†] Co-first author.

Book chapter

1. **Z.F. Pan**, L. An, “Removal of Heavy Metal from Wastewater Using Ion Exchange Membranes”, *Applications of Ion Exchange Materials in the Environment* (2019) 25-46 Springer, Cham.